

**SYNTHESIS, CHARACTERIZATION AND
EVALUATION OF ANTI-CANCER ACTIVITIES OF
SOME GOLD COMPLEXES WITH DIAMINE,
PHOSPHINE AND DITHIOCARBAMATE LIGANDS**

BY

SAID SALMAN AL-JAROUDI

A Dissertation Presented to the
FACULTY OF THE COLLEGE OF GRADUATE STUDIES
KING FAHD UNIVERSITY OF PETROLEUM & MINERALS
DHAHRAN, SAUDI ARABIA

In Partial Fulfillment of the
Requirements for the Degree of

DOCTOR OF PHILOSOPHY

In

CHEMISTRY

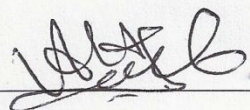
September 2014

KING FAHD UNIVERSITY OF PETROLEUM & MINERALS

DHAHRAN- 31261, SAUDI ARABIA

DEANSHIP OF GRADUATE STUDIES

This thesis, written by **SAID SALMAN AL-JAROUDI** under the direction his thesis advisor and approved by his thesis committee, has been presented and accepted by the Dean of Graduate Studies, in partial fulfillment of the requirements for the degree of **DOCTOR OF PHILOSOPHY IN CHEMISTRY.**



Dr. Anvarhusein A. Isab
(Advisor)



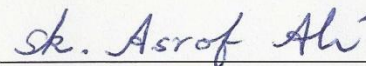
Dr. Abdulaziz A. Al-Al-Saadi.
Department Chairman



Dr. Mohammed I. M. Wazeer
(Member)




Dr. Salam A. Zummo
Dean of Graduate Studies



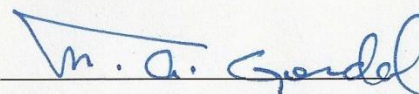
Dr. Shaik Asraf Ali
(Member)

30/10/14

Date



Dr. Mohammed B. Fettouhi
(Member)



Dr. Mohammad A. Gondal
(Member)

©SAID SALMAN AL-JAROUDI

2014

This work is dedicated to my research advisors, honorable teachers,
sincere friends and souls of my beloved parents (late)
who encouraged me for better pursuits in life.

ACKNOWLEDGMENTS

Above all, all glory be to God, my creator in which all things are possible. All praises are for Allah Subhanahu Wataala (SBW), who bestowed me with all His blessings to accomplish this work. All compliments and the blessings of Allah are upon Prophet Muhammad sallallahu alaihi wallah wasallam.

I would like to thank KFUPM for financial support as well as providing a conducive academic and research environment. I am thankful to the Chairman, Dr. Abdullah Jafar Al-Hamdan for providing access to all possible research facilities in the Chemistry Department. Also, I would like to thank Saudi Aramco for giving me this great chance to complete my Ph.D. degree. Undertaking this Ph.D. has been a truly life-changing experience for me and it would not have been possible to do without Saudi Aramco support.

First and foremost with deep sense of gratitude and appreciation, I would like to thank my dissertation advisor Professor Dr. Anvarhusein A. Isab, for his versatile and learned guidance during the research work. It has been an honor to be one of his PhD students. His generous cooperation, erudite suggestions, invigorating encouragement and patience, have persisted a source of inspiration for me.

Besides my advisor, I would like to thank the rest of my thesis committee: Professor Dr. M. I. Wazeer, Professor Dr. Ali S. Asrof, Professor Dr. Mohammad A. Gondal and Dr. Mohammed B. Fettouhi, for their encouragement, insightful comments, motivation, enthusiasm, and immense knowledge.

I am very grateful to Professor Dr. M. I. Wazeer as co-advisor for helping me in interpretation of NMR data, writing manuscripts for publications and practical learning on NMR instruments.

I am highly obliged by Associate Professor Dr. M. B. Fettouhi for X-ray single crystal determination of metal complexes, conceptual understanding of Advanced Inorganic Chemistry and scientific writing of PhD dissertation. My sincere acknowledgment goes to Dr. M. Altaf for his usual and highly support in X-ray crystallography characterization.

I am greatly beholden to Dr. Hassan A. Al-Muallem for his encouragement and great academic support and input and personal kind. I am also grateful to all faculty and staff members for their kind and cheerful cooperation

I am thankful to M. Arab for guiding me through his NMR expertise, Bahauddin for providing synthesis facilities, Ayman Al-Majid for elemental analysis and Mansour Al-Zaki for IR and UV-Vis analysis during this research work.

I would like to express my greatest gratitude to my parents for their continuous du'aa and support. I must not forget here my family members, my sisters and my brothers, Last, but certainly not least, I must acknowledge with tremendous and deep thanks my Wife and Gids for their cooperation and prayers for my studies.

(Said Salman Al-Jaroudi)

TABLE OF CONTENTS

ACKNOWLEDGMENTS	V
TABLE OF CONTENTS.....	VII
LIST OF TABLES.....	XIII
LIST OF FIGURES.....	XVII
LIST OF ABBREVIATIONS.....	XXIV
ABSTRACT.....	XXVII
ملخص الرسالة.....	XXIX
1 CHAPTER INTRODUCTION	1
1.1 Current Status of the Problem	8
1.2 Aim of the Present Research	10
2 CHAPTER LITERATURE REVIEW	13
3 CHAPTER 3 OBJECTIVES	31
3.1 Synthesis of Dithiocarbamate Ligands	31
3.1.1 Synthesis of Ammonium Dithiocarbamate	31
3.1.2 Synthesis of 2-Cyclohexanaminium dithiocarbamate	33
3.1.3 Synthesis of 2-Mercaptobenzimidazole	34
3.2 Synthesis of Chlorido(phosphane)gold(I) Complexes	34
3.3 Synthesis of Dichlorido(1,2-diaminocyclohexane)gold(III) Chloride Complexes.....	35
3.4 Synthesis of Azanechlorido(1,2-Diaminocyclohexane)gold(III) Chloride Complexes	36
3.5 Synthesis of Diazane(1,2-diaminocyclohexane)gold(III) Chloride Complexes.....	37

3.6	Synthesis of Bis(1,2-Diaminocyclohexane)gold(III)Chloride Complexes	38
3.7	Synthesis of 1,2-Diaminocyclohexane(ethylenediamine)gold(III) Chloride Complexes	40
3.8	Synthesis of 1,2-Diaminocyclohexane(propylenediamine)gold(III) Chloride Complexes	41
3.9	Synthesis of Ammoniumdithiocarbamatodichloridogold(III) Chloride Complexes	42
3.10	Synthesis of Dichlorido(2-cyclohexanaminiumdithiocarbamato)gold(III) Chloride Complexes .	44
3.11	Synthesis of Mixed-LigandDithiocarbamatophosphane gold(I) Complexes.....	45
3.12	Synthesis of Mixed-Ligand 5-Methyl-2-mercaptobenzimidazolo(phosphane)gold(I) Complexes	46
3.13	Synthesis of Mixed-Ligand Substituted 2-mercaptobenzimidazolo(trimethylphosphane)gold(I) Complexes.....	46
3.14	Synthesis of Mixed-Ligand4-Nitro-2-mercaptobenzimidazolo(phosphane)gold(I) Complexes ..	47
3.15	Synthesis of Mixed-Ligand 5-Nitro-2-mercaptobenzimidazolo(phosphane)gold(I) Complexes..	48
3.16	Synthesis of Substituted 2-Mercaptobenzimidazolo1,3-Bis(2,6-di-isopropylphenyl)imidazol-2-ylidene Gold(I) Complexes.....	49
3.17	Synthesis of Dinuclear2-MBI{1,3-bis(diphenylphosphino)methane}gold(I)Complexes	49
3.18	Characterization of GoldComplexes.....	50
3.19	Structural Analysis of GoldComplexes	50
3.20	Study of Anticancer Properties of Gold Complexes.....	51
3.21	Study of Electrochemical Properties of Gold Complexes.....	51
4	CHAPTER EXPERIMENTAL	52
4.1	Chemicals	52
4.2	Cell Lines	53
4.3	Synthesis of Dithiocarbamate Ligands	53
4.3.1	Synthesis of AmmoniumdithiocarbamateLigands.....	53
4.3.2	Synthesis of 2-Cyclohexanaminium Dithiocarbamate Ligands	54
4.3.3	Synthesis of 2-Mercaptobenzimidazole Ligands	55

4.4	Synthesis of Chlorido(phosphane)gold(I) Precursor Complexes	56
4.5	Synthesis of Dichlorido(1,2-diaminocyclohexane)gold(III) Chloride Complexes.....	57
4.6	Synthesis of Azanechlorido(1,2-Diaminocyclohexane)gold(III) Chloride Complexes.	59
4.7	Synthesis of Diazane(1,2-diaminocyclohexane)gold(III) Chloride Complexes.....	60
4.8	Synthesis of Bis(1,2-Diaminocyclohexane)gold(III) Chloride Complexes	61
4.9	Synthesis of 1,2-Diaminocyclohexane(ethylenediamine)gold(III) Chloride Complexes.	62
4.10	Synthesis of 1,2-Diaminocyclohexane(propylenediamine)gold(III) Chloride Complexes.	63
4.11	Synthesis of Ammoniumdithiocarbamatodichloridogold(III) Chloride Complexes.	64
4.12	Synthesis of Dichlorido(2-cyclohexanaminiumdithiocarbamato)gold(III) Chloride Complexes .	67
4.13	Synthesis of Mixed-Ligand Dithiocarbamatophosphanegold(I) Complexe.	68
4.14	Synthesis of Mixed-Ligand 5-Methyl-2-mercaptobenzimidazolo(phosphane)gold(I) Complexes.	72
4.15	Synthesis of Substituted2-mercaptobenzimidazolo(trimethylphosphane)gold(I) Complexes. ..	73
4.16	Synthesis of Mixed-Ligand 4-Nitro-2-mercaptobenzimidazolo(phosphane)gold(I) Complexes..	74
4.17	Synthesis of Mixed-Ligand 5-Nitro-2-Mercaptobenzimidazolophosphanegold(I) Complexes....	75
4.18	Synthesis of Substituted 2-Mercaptobenzimidazolo{1,3-Bis(2,6-di-isopropylphenyl)imidazol-2-ylidene}gold(I) Complexes.	76
4.19	Synthesis of Dinuclear2-MBI{1,3-bis(Diphenylphosphino)methane}gold(I) Complexes	77
4.20	Spectroscopic Characterization.....	78
4.20.1	Elemental Analysis	78
4.20.2	Mid-IR and Far-IR studies	78
4.20.3	UV-Vis Studies	79
4.20.4	Solution NMR Measurements	79
4.20.5	Solid State NMR Measurements.....	80
4.20.6	NMR Studies for StabilityDetermination	80
4.21	X-ray Structure Determination	81

4.22	Computational Study.....	82
4.23	Electrochemistry.....	82
4.24	Anticancer Properties.....	83
4.24.1	Assessment of Cell Proliferation	83
4.24.2	<i>in vitro</i> Cytotoxic assay for Cisplatin Sensitive Prostate (PC3) and Cisplatin Resistance Gastric (SGC7901) Cells.....	84
4.24.3	Assay For Inhibitory Effect Complexes (1-129) on Prostate (PC3) and Gastric (SCG7901) Cancer Cells.....	85
5	CHAPTER RESULTS AND DISCUSSION	87
5.1	Gold(III) 1,2-Diaminocyclohexane dichlorido Complexes.....	87
5.1.1	MID-IR and Far-IR Spectroscopic Studies	87
5.1.2	UV-Vis Studies	88
5.1.3	Solution NMR Studies.....	89
5.1.4	Solid State NMR	94
5.1.5	Crystal structure of complexes (36) and (37)	96
5.1.6	Effect of Complexes (36)-(38) on cell proliferation	100
5.1.7	Conclusion	108
5.2	Gold(III) Complexes of Bis(1,2-Diaminocyclohexane) Ligands	109
5.2.1	Mid and Far-IR Spectroscopic Studies	110
5.2.2	Solution NMR Characterization	111
5.2.3	Solid State NMR Characterization.....	116
5.2.4	X-ray Crystal Structure of Complexes (45) and (46).....	118
5.2.5	UV-Vis Spectra.....	125
5.2.6	Stability Studies of Gold(III) Compounds (45)-(47).....	128
5.2.7	Electrochemistry of Gold(III) Compounds (36-38) and (45-47)	130
5.2.8	Anticancer Activity of [(1,2-DACH) ₂ Au(III)]Cl ₃ (45-47) on PC3 and SGC7901 Cancer Cell Lines..	133

5.2.9	Conclusion	143
5.3	Mixed-Ligand 1,2-Diaminocyclohexane(ethylenediamine)gold(III) Chloride Complexes	143
5.3.1	Electronic spectra	144
5.3.2	Mid and Far-IR Spectroscopic Studies	146
5.3.3	Solution NMR Characterization	148
5.3.4	Solid-State NMR	151
5.3.5	Computational Study.....	152
5.3.6	NMR Profiles Stability Study.....	156
5.3.7	Electrochemical Studies of Compounds 48-50.	159
5.3.8	Effect of Compounds (48), (49) and (50) on Cell Proliferation	162
5.3.9	Conclusion	172
5.4	Mixed-Ligand Diaminocyclohexane(propylenediamine)gold(III) Chloride Complexes.....	173
5.4.1	Electronic Spectra.....	173
5.4.2	Mid and Far-IR spectroscopic studies	175
5.4.3	Solution NMR characterization.....	177
5.4.4	Solid-state NMR	182
5.4.5	Computational Study.....	183
5.4.6	Crystal Structure of [(<i>cis</i> -1 <i>S</i> ,2 <i>R</i> -DACH)Au(<i>pn</i>)]Cl ₃	185
5.4.7	NMR Profiles Stability Study.....	189
5.4.8	Electrochemical Studies of Compounds 51-53.	193
5.4.9	Effect of Compounds (51), (52) and (53) on Cell Proliferation	195
5.4.10	Conclusion	203
5.5	Crystal Structure of Compound [Me ₃ PAu(DMDT)] (70)	203
6	CHAPTER SUMMARY AND CONCLUSIONS	208
6.1	Future Studies	210

APPENDIX A -LIST OF PUBLICATIONS.....	211
APPENDIX B -CONFERENCE PRESENTATIONS.....	212
REFERENCES.....	213

LIST OF TABLES

Table 4.1 Melting point and Elemental analysis of ammonium dithiocarbamate ligands.....	54
Table 4.2 Melting point and elemental analysis of 2-cyclohexanaminium dithiocarbamate ligands.....	55
Table 4.3 Melting point and elemental analysis of substituted 2-mercaptobenzimidazole ligands.....	56
Table 4.4 Melting point and elemental analysis of chloridophosphanegold(I) complexes ...	57
Table 4.5 Melting point and elemental analysis of dichlorido(1,2-diaminocyclohexane)gold(III) chloride complexes.....	58
Table 4.6 Elemental analysis of azanechlorido(1,2-diaminocyclohexane)gold(III) chloride complexes	59
Table 4.7 Elemental analysis of diazane(1,2-diaminocyclohexane)gold(III) chloride complexes	60
Table 4.8 Melting point and elemental analysis of bis(1,2-DACH)gold(III) chloride complexes	61
Table 4.9 Melting point and elemental analysis of 1,2-diaminocyclohexane(ethylenediamine)gold(III)chloride complexes	63
Table 4.10 Melting point and elemental analysis of 1,2-diaminocyclohexane(propylenediamine)gold(III)chloride complexes	64
Table 4.11 Elemental analysis of ammoniumdithiocarbamatodichloridogold(III) chloride complexes	65
Table 4.12 IR frequencies, ν (cm^{-1}) for ammoniumdithiocarbamatodichloridogold(III) chloride complexes	66
Table 4.13 Far-IR frequencies, ν (cm^{-1}) for ammoniumdithiocarbamatodichloridogold(III) chloride complexes.....	66
Table 4.14 ^{13}C NMR chemical shifts of free ligands and ammoniumdithiocarbamatodichloridogold(III) chloride complexes in D_2O	66
Table 4.15 Melting point and elemental analysis of dichlorido(2-cyclohexanaminiumdithiocarbamato)gold(III) chloride complexes.....	67
Table 4.16 Elemental analysis of dithiocarbamatotrialkylphosphanegold(I) complexes	69
Table 4.17 Mid-IR frequencies, ν (cm^{-1}) for dithiocarbamatotrialkylphosphanegold(I)complexes.....	70
Table 4.18 Far-IR frequencies, ν (cm^{-1}) for dithiocarbamatotrialkylphosphanegold(I)complexes.....	70
Table 4.19 ^{13}C NMR chemical shifts of precursor complexes and dithiocarbamatotrialkylphosphanegold(I) complexes in CDCl_3	71
Table 4.20 ^{31}P NMR chemical shifts of precursor complexes and dithiocarbamatotrialkylphosphanegold(I)complexes in CDCl_3	71
Table 4.21 Melting point and elemental analysis of 5-methyl-2-mercaptobenzimidazolo(phosphane)gold(I) complexes	72

Table 4.22 Melting point and elemental analysis of substituted 2-mercaptobenzimidazolotrimethylphosphane-gold(I) complexes	74
Table 4.23 Melting point and elemental analysis of 4-nitro-2-mercaptobenzimidazolotrialkylphosphane-gold(I) complexes	75
Table 4.24 Melting point and elemental analysis of 5-NO ₂ -2-mercaptobenzimidazolophosphane-gold(I) complexes	76
Table 4.25 Melting point and elemental analysis of 2-mercaptobenzimidazolo(IPr)gold(I) complexes	77
Table 4.26 Melting point and elemental analysis of Dinuclear 2-MBI{1,3-bis(Diphenylphosphino)methane}gold(I) complexes	78
Table 5.1 IR frequencies, $\nu(\text{cm}^{-1})$ for [(1,2-DACH)Au(III)Cl ₂]Cl complexes	88
Table 5.2 Far-IR frequencies, $\nu(\text{cm}^{-1})$ for [(1,2-DACH)Au(III)Cl ₂]Cl complexes.....	88
Table 5.3 UV-Vis spectra λ_{max} for [(1,2-DACH)Au(III)Cl ₂]Cl complexes.....	89
Table 5.4 ¹ H NMR chemical shifts of free ligands and [(1,2-DACH)Au(III)Cl ₂]Cl complexes in CD ₃ OD	90
Table 5.5 ¹³ C NMR chemical shifts of free ligands and [(1,2-DACH)Au(III)Cl ₂]Cl complexes in CD ₃ OD.....	90
Table 5.6 Solid ¹³ C NMR chemical shifts of [(1,2-DACH)Au(III)Cl ₂]Cl complexes.....	94
Table 5.7 Crystal and structure refinement data for compounds (36) and (37).....	97
Table 5.8 Selected bond lengths (Å) and bond angles (o) for compounds (36) and (37).....	98
Table 5.9 Effect of compound (36) on PC3 cell line and SGC-7901 cell line (mean, SD) after incubation for 24h and 72h.....	101
Table 5.10 Cytotoxicity of the compound [cis-(1,2-DACH)Au(III)Cl ₂]Cl (36) toward different tumor cell lines. The data were collected after 72h exposure to compound.....	102
Table 5.11 Mid-IR frequencies, $\nu(\text{cm}^{-1})$ for [(1,2-DACH) ₂ Au(III)]Cl ₃ complexes.....	111
Table 5.12 Far-IR frequencies, $\nu(\text{cm}^{-1})$ for [(1,2-DACH) ₂ Au(III)]Cl ₃ complexes	111
Table 5.13 ¹ H NMR chemical shifts of free ligands and corresponding [(1,2-DACH) ₂ Au(III)]Cl ₃ complexes in D ₂ O	112
Table 5.14 Solution ¹³ C NMR chemical shifts of free ligands and corresponding [(1,2-DACH) ₂ Au(III)]Cl ₃ complexes in D ₂ O	113
Table 5.15 Solid state ¹³ C NMR chemical shifts of free ligands and corresponding [(1,2-DACH) ₂ Au(III)]Cl ₃ (45-47) complexes	117
Table 5.16 Crystal and structure refinement data for compounds (45) and (46).....	121
Table 5.17 Selected bond lengths (Å) and bond angles (o) for compounds (45) and (46)..	122
Table 5.18 λ_{max} values for [(1,2-DACH) ₂ Au(III)]Cl ₃ (45-47) complexes obtained from UV-Vis spectra.....	125
Table 5.19 Peak potential values (vs ENH) for reduction of compounds [Au(1,2-DACH)Cl ₂]Cl and [Au(1,2-DACH) ₂]Cl ₃	131

Table 5.20 <i>in vitro</i> cytotoxicity data of compounds [(1,2-DACH) ₂ Au(III)]Cl ₃ (45-47) for 72 h exposure on PC3 and SGC7901 cancer cell lines	135
Table 5.21 UV-Vis spectra λ_{\max} for complexes (48)-(50) dissolved in the reference physiological buffer solution.	146
Table 5.22 Mid-IR frequencies, $\nu(\text{cm}^{-1})$ for 1,2-cyclohexanediamine(ethylenediamine)Au(III) chloride complexes.....	147
Table 5.23 Far-IR frequencies, $\nu(\text{cm}^{-1})$ for 1,2-cyclohexanediamine(ethylenediamine)Au(III) chloride complexes.....	148
Table 5.24 ¹ H NMR chemical shifts of free ligands and 1,2-cyclohexanediamine(ethylenediamine)Au(III) chloride complexes in D ₂ O.....	149
Table 5.25 ¹³ C NMR chemical shifts of free ligands and 1,2-cyclohexanediamine(ethylenediamine)Au(III) chloride complexes in D ₂ O.....	150
Table 5.26 Solid ¹³ C NMR chemical shifts of free ligands and 1,2-cyclohexanediamine(ethylenediamine)Au(III) chloride complexes.....	152
Table 5.27 Calculated bond lengths and bond angles of the [(1,2-DACH)(en)Au(III)] ³⁺ complex in its four possible conformations	153
Table 5.28 Relative energies (kcal/mol) of the four possible conformations of [(1,2-DACH)(en)Au(III)] ³⁺ complexes.....	154
Table 5.29 Peak potential values (vs ENH) for reduction of the gold(III) complexes (48-50) in the buffered aqueous solution processes at the platinum electrode.....	160
Table 5.30 Effect of compounds 48, 49 and 50 on cell/proliferation and cell cycle of PC3 cell line and SGC-7901 cell line (Mean, SD) after incubation for 24 h and 72 h.....	163
Table 5.31 IC ₅₀ Cytotoxicity values of the complexes towards different tumor cell lines. The data were collected after 72 h exposure to compound (48-50).....	171
Table 5.32 UV-Vis spectra λ_{\max} for complexes of [(diaminocyclohexane)(ethylenediamine)Au(III)]chloride dissolved in the reference physiological buffer solution.	174
Table 5.33 Mid IR frequencies, $\nu(\text{cm}^{-1})$ for 1,2-cyclohexanediamine(1,3-Propylenediamine)Au(III) chloride complexes.	176
Table 5.34 Far-IR frequencies, $\nu(\text{cm}^{-1})$ for 1,2-cyclohexanediamine(1,3-Propylenediamine)Au(III) chloride complexes.	177
Table 5.35 ¹ H NMR chemical shifts of free ligands and cyclohexanediamine propylenediamine Au(III) complexes in D ₂ O.....	178
Table 5.36 ¹³ C NMR chemical shifts of free ligands and cyclohexanediaminepropylenediamine Au(III) complexes in D ₂ O.....	179
Table 5.37 Solid ¹³ C NMR chemical shifts of free ligands and (1,2-DACH)Au(III)(pn) complexes.	183
Table 5.38 Relative energies (kcal/mol) of the four possible conformations of the [(DACH)Au(pn)] ³⁺ complex.....	185

Table 5.39 Crystallographic data for [(cis-1 <i>S</i> ,2 <i>R</i> -DACH)Au(pn)]Cl ₃ (51).....	186
Table 5.40 Selected bond distances and bond angles for [(cis-1 <i>S</i> ,2 <i>R</i> - DACH)Au(pn)]Cl ₃ (51)	187
Table 5.41 Peak Potential values (vs ENH) for reduction of the present gold(III) complexes in the buffered aqueous solution processes at the platinum electrode	193
Table 5.42 IC ₅₀ Cytotoxicity values of the complexes towards different tumor cell lines. The data were collected after 72 h exposure to compound (51), (52) and (53) .	195
Table 5.43 Summary of crystal data and details of the structure refinement for compound (70).....	205
Table 5.44 Selected bond lengths and bond angles in compound (70).....	207

LIST OF FIGURES

Figure 1.1 Structures of some anticancer platinum compounds	2
Figure 1.2 Structures of some gold-based drugs.....	3
Figure 1.3 Structures of potential anticancer gold(I) complexes containing phosphine and heterocyclic compounds.....	5
Figure 1.4 Structures of potential anticancer gold(I) complexes containing phosphine and thioamides compounds.....	5
Figure 1.5 Chemical structures of gold(III) dithiocarbamate complexes	7
Figure 2.1. Schematic representation of how cisplatin is activated and subsequently bind to DNA.....	16
Figure 2.2 Structure of [(damp)AuCl ₂].....	17
Figure 2.3 Structure of Au-Naph-1 complex	18
Figure 2.4 Structure of gold phosphole complex GoPI	19
Figure 2.5 Schematic drawing of Au(I) complexes with multiple phosphine ligands.....	20
Figure 2.6 Structures of various bioactive gold(I) species	22
Figure 2.7 Schematic drawings of gold(III) complexes with Au-N bond	24
Figure 2.8 Schematic drawing of gold(III) porphyrin 1acomplex with Au-N bond.....	25
Figure 2.9 Schematic drawings of caffeine-based gold(I) N-heterocyclic carbenes complexes	26
Figure 2.10 Schematic drawings of gold(I) carbene complexes.....	27
Figure 3.1 Structures of ammonium dithiocarbamate ligands	32
Figure 3.2 Structures 2-cyclohexanaminium dithiocarbamate ligands.....	33
Figure 3.3 Structures of 2-mercaptobenzimidazole ligands	34
Figure 3.4 Structures of phosphane gold(I) chloride complexes	35
Figure 3.5 Structures of dichlorido 1,2-diaminocyclohexane gold(III) chloride complexes..	36
Figure 3.6 Structures of azane chlorido 1,2-diaminocyclohexane gold(III) chloride complexes	37
Figure 3.7 Structures of diazane 1,2-diaminocyclohexane gold(III) chloride complexes.....	38
Figure 3.8 Predicted structure of the synthesized bis(1,2-diaminocyclohexane)gold(III) chloride complexes	39
Figure 3.9 Predicted chemical structure of 1,2-diaminocyclohexane(ethylenediamine)gold(III)chloride complexes	40
Figure 3.10 Predicted chemical structure of 1,2-diaminocyclohexane(propylenediamine)gold(III) chloride complexes	41
Figure 3.11 Chemical structure of ammoniumdithiocarbamato(dichlorido)gold(III) chloride complexes	43
Figure 3.12 Chemical structure of dichlorido(2-cyclohexanaminiumdithiocarbamato)gold(III)chloride complexes.....	44
Figure 3.13 Chemical structure of dithiocarbamato(trialkylphosphane)gold(I) complexes ..	45

Figure 3.14 Chemical structure of 5-methyl-2-mercaptobenzimidazolo(phosphane)gold(I)complexes	46
Figure 3.15 Chemical structure of 5-methyl-2-mercaptobenzimidazolo(phosphane)gold(I)complexes	47
Figure 3.16 Chemical structure of 4-nitro-2-mercaptobenzimidazolo(phosphane)gold(I)complexes	48
Figure 3.17 Chemical structure of 5-nitro-2-mercaptobenzimidazolo(phosphane)gold(I)complexes	48
Figure 3.18 Chemical structure of IPr(2-mercaptobenzimidazolo)gold(I) complexes	49
Figure 3.19 Chemical structure of dinuclear2-MBI{1,3-bis(diphenylphosphino)methane} gold(I)complexes	50
Figure 4.1 X-ray structure of (Ph) ₃ PAu(I)(5-Me-2-MBI) (96)	73
Figure 5.1 The 500-MHz ¹ H solution NMR spectrum of [(1,2-DACH)Au(III)Cl ₂]Cl complexes	92
Figure 5.2 The 125.65-MHz ¹³ C{ ¹ H} solution NMR spectrum of[(1,2-DACH)Au(III)Cl ₂]Cl complexes	93
Figure 5.3 Solid state ¹³ C{ ¹ H} NMR spectra of complexes 36 & 37	95
Figure 5.4 X-ray structure of [cis-(1,2-DACH)Au(III)Cl ₂]Cl (36)	99
Figure 5.5 Molecular packing in [cis-(1,2-DACH)Au(III)Cl ₂]Cl (36)	99
Figure 5.6 X-ray structure of compound [trans-(1,2-DACH)Au(III)Cl ₂]Cl (37)	100
Figure 5.7 Effect of <i>cis</i> -(±)1,2-(DACH)-gold(III)complex on cell growth in (A) PC-3 and (B) SGC-7901 cells. The cells were treated with 10 μM for 1 day and 3 days. The anti-proliferative effect was measured by MTT assay. Results were expressed as the mean, SD. *P<0.05	102
Figure 5. 8 Effect of <i>trans</i> -(±)1,2-(DACH)-gold(III) complex on cell growth in (A) PC-3 and (B) SGC-7901 cells. The cells were treated with 10 μM for 1 day and 3 days. The anti-proliferative effect was measured by MTT assay. Results were expressed as the mean, SD. *P<0.05	103
Figure 5.9 Effect of (<i>S,S</i>)-(+)-1,2-(DACH)-gold(III) complex on cell growth in (A) PC-3 and (B) SGC-7901 cells. The cells were treated with 10 μM for 1 day and 3 days. The anti-proliferative effect was measured by MTT assay. Results were expressed as the mean, SD. *P<0.05	104
Figure 5.10 Effect of <i>cis</i> -(±)-1,2-(DACH)-gold complex on cell growth in (A) PC-3 and (B) SGC-7901 cells. The cells were treated with various concentrations for 24 h. The anti-proliferative effect was measured by MTT assay. Results were expressed as the mean, SD. *P<0.05	105
Figure 5.11 Effect of <i>trans</i> -(±)-1,2-(DACH)-gold complex on cell growth in (A) PC-3 and (B) SGC-7901 cells. The cells were treated with various concentrations for 24 h. The anti-proliferative effect was measured by MTT assay. Results were expressed as the mean, SD. *P<0.05	106

Figure 5.12 Effect of (<i>S,S</i>)-(+)-1,2-(DACH)-gold(III) complex on cell growth in (A) PC-3 and (B) SGC-7901 cells. The cells were treated with various concentrations for 24 h. The anti-proliferative effect was measured by MTT assay. Results were expressed as the mean, SD. *P<0.05.....	107
Figure 5.13 Effect of compounds 37 and 36 on cell growth in (A) PC-3 and (B) SGC-7901 cells. The cells were treated with 10 μ M for day 1, day2 and day 3. The anti-proliferative effect was measured by MTT assay. Results were expressed as the mean, SD. *P<0.05	108
Figure 5.14 The 500-MHz ^1H solution NMR spectra of [(1,2-DACH) $_2$ Au(III)]Cl $_3$ (45-47) complexes	114
Figure 5.15 The 500-MHz ^1H solution NMR spectra of [(1,2-DACH) $_2$ Au(III)]Cl $_3$ (45-47) complexes	116
Figure 5.16 Solid state $^{13}\text{C}\{^1\text{H}\}$ NMR spectrum of complex [(<i>cis</i> -1,2-DACH) $_2$ Au(III)]Cl $_3$ (45).....	117
Figure 5.17 Solution $^{13}\text{C}\{^1\text{H}\}$ NMR spectra of compound (46) (a), co-crystal of mono- and bis(<i>trans</i> -DACH)gold(III) (b) and mono- <i>trans</i> -(DACH)gold(III) (c)	119
Figure 5.18 X-ray molecular structure of compound[(<i>cis</i> -1,2-DACH) $_2$ Au(III)]Cl $_3$ (45) ...	123
Figure 5.19 X-ray molecular structures of the two components of co-crystal [(<i>trans</i> -1,2-DACH) $_2$ Au(III)]Cl $_3$ (46).....	124
Figure 5.20 Hydrogen bonding network in compound[(<i>cis</i> -1,2-DACH) $_2$ Au(III)]Cl $_3$ (45) .	124
Figure 5.21 UV-Vis spectra of [(1,2-DACH) $_2$ Au(III)]Cl $_3$ (45-47) complexes, followed by dissolution in the buffer solution (a) just after mixing and (b) after 3 days at 37 $^\circ\text{C}$	127
Figure 5.22 ^1H NMR spectra of compound (46) in D $_2$ O (a) just after mixing and (b) after 3 days.	128
Figure 5.23 Solution $^{13}\text{C}\{^1\text{H}\}$ NMR spectra of [(<i>trans</i> -1,2-DACH) $_2$ Au(III)]Cl $_3$ (46) in D $_2$ O (a) after mixing and (b) after 3 days.	129
Figure 5.24 ^1H NMR spectra of [(<i>trans</i> -1,2-DACH) $_2$ Au(III)]Cl $_3$ (46) in (DMSO/D $_2$ O, 3:1) (a) just after mixing and (b) after 3 days.....	129
Figure 5.25 Solution $^{13}\text{C}\{^1\text{H}\}$ NMR spectra of [(<i>trans</i> -1,2-DACH) $_2$ Au(III)]Cl $_3$ (46) in (DMSO/D $_2$ O, 3:1) (a) after mixing and (b) after 3 days.	130
Figure 5.26 Cyclic voltammetric curves of the compounds (45-47) and their corresponding mono-DACH gold(III) compounds (36-38). Curve labeled with (a) is corresponding to the bis-DACH, while, (b) corresponding to mono-DACH	132
Figure 5.27 Time dependent inhibitory effect of 10 μ M [{ <i>cis</i> -1,2-(DACH)} $_2$ Au]Cl $_3$ on growth of (A) PC3 and (B) SGC7901 cells for 1 day and 3 days using MTT assay. Results were expressed as the mean, SD. *P<0.05	136

Figure 5.28 Time dependent inhibitory effect of 10 μM [$\{\text{trans}-(\pm)\text{-1,2-}(\text{DACH})\}_2\text{Au}\}\text{Cl}_3$ on growth of (A) PC3 and (B) SGC7901 cells for 1 day and 3 days using MTT assay. Results were expressed as the mean, SD. * $P < 0.05$...	137
Figure 5.29 Time dependent inhibitory effect of 10 μM [$\{(1S,2S)\text{-}(+)\text{-}(\text{DACH})\}_2\text{Au}\}\text{Cl}_3$ on growth of (A) PC3 and (B) SGC7901 cells for 1 day and 3 days using MTT assay. Results were expressed as the mean, SD. $P < 0.05$	138
Figure 5.30 Effect of [$\{\text{cis}\text{-1,2-}(\text{DACH})\}_2\text{Au}\}\text{Cl}_3$ complex on cell growth in (A) PC-3 and (B) SGC-7901 cells. The cells were treated with various concentrations for 24 h. The anti-proliferative effect was measured by MTT assay. Results were expressed as the mean, SD. $P < 0.05$	139
Figure 5.31 Effect of [$\{\text{trans}-(\pm)\text{-1,2-}(\text{DACH})\}_2\text{Au}\}\text{Cl}_3$ complex on cell growth in (A) PC-3 and (B) SGC-7901 cells. The cells were treated with various concentrations for 24 h. The anti-proliferative effect was measured by MTT assay. Results were expressed as the mean, SD. * $P < 0.05$	140
Figure 5.32 Effect of [$\{(1S,2S)\text{-}(+)\text{-}(\text{DACH})\}_2\text{Au}\}\text{Cl}_3$ complex on cell growth in (A) PC-3 and (B) SGC-7901 cells. The cells were treated with various concentrations for 24 h. The anti-proliferative effect was measured by MTT assay. Results were expressed as the mean, SD. * $P < 0.05$	141
Figure 5.33 Comparative time dependent inhibitory effects for 10 μM of compounds (45-47) on growth of (A) PC3 and (B) SGC7901 cells for day 1, day 2 and day 3 using MTT. Results were expressed as the mean, SD. * $P < 0.05$	142
Figure 5.34 Time effect on electronic spectra of complexes (48)-(50) following dissolution in the buffer solution at mixing (a) and after 7 days (b) at 37 $^\circ\text{C}$	146
Figure 5.35 The 500-MHz ^1H solution NMR spectrum of [$(1S,2S)\text{-}(+)\text{-}(\text{DACH})\text{Au}(\text{en})\}\text{Cl}_3$ complex.....	150
Figure 5.36 The 125.65-MHz $^{13}\text{C}\{^1\text{H}\}$ solution NMR spectrum of [$(1S,2S)\text{-}(+)\text{-}(\text{DACH})\text{Au}(\text{en})\}\text{Cl}_3$ complex.....	151
Figure 5.37 Optimized geometries of [$(1,2\text{-DACH})\text{Au}(\text{III})(\text{en})\}^{+3}$, obtained at the B3LYP/LanL2DZ level of theory using GAUSSIAN09 W	156
Figure 5.38 The 500-MHz ^1H solution NMR spectra of [$\text{cis}\text{-1,2-}(\text{DACH})\text{Au}(\text{en})\}\text{Cl}_3$ complex in D_2O at mixing (a) and after 7 days (b).....	157
Figure 5.39 The 125.65-MHz $^{13}\text{C}\{^1\text{H}\}$ solution NMR spectra of [$\text{Cis}\text{-1,2-}(\text{DACH})\text{Au}(\text{en})\}\text{Cl}_3$ complex in D_2O at mixing (a) and after 7 days (b).....	158
Figure 5.40 The 500-MHz ^1H solution NMR spectra of [$(1S,2S)\text{-}(+)\text{-}(\text{DACH})\text{Au}(\text{en})\}\text{Cl}_3$ complex in $\text{D}_2\text{O}/\text{DMSO}$ at mixing (a) and after 7 days (b)	158
Figure 5.41 The 125.65-MHz $^{13}\text{C}\{^1\text{H}\}$ solution NMR spectra of [$(1S,2S)\text{-}(+)\text{-}(\text{DACH})\text{Au}(\text{en})\}\text{Cl}_3$ complex in ($\text{DMSO}/\text{D}_2\text{O}$, 1:2) at mixing (a) and after 7 days (b).....	159
Figure 5. 42 Cyclic voltammograms of compound 48, 49 and 50 in the phosphate buffer at platinum electrode.....	161

Figure 5.43 Effect of [<i>cis</i> -1,2-(DACH)gold(III)(en)]Cl ₃ complex on cell growth in (A) PC3 and (B) SGC7901 cells. The cells were treated with 10 μM for 1 day and 3 days. The anti-proliferative effect was measured by MTT assay. Results were expressed as the mean, SD. *P<0.05.....	164
Figure 5.44 Effect of [<i>trans</i> -(±)-1,2-(DACH)gold(III)(en)]Cl ₃ complex on cell growth in (A) PC-3 and (B) SGC-7901 cells. The cells were treated with 10 μM for 1 day and 3 days. The anti-proliferative effect was measured by MTT assay. Results were expressed as the mean, SD. *P < 0.05.....	165
Figure 5.45 Effect of [(<i>S,S</i>)-(+)-1,2-(DACH)gold(III)(en)]Cl ₃ complex on cell growth in (A) PC-3 and (B) SGC-7901 cells. The cells were treated with 10 μM for 1 day and 3 days. The anti-proliferative effect was measured by MTT assay. Results were expressed as the mean, SD. *P < 0.05.....	166
Figure 5.46 Effect of [<i>cis</i> -1,2-(DACH)gold(III)(en)]Cl ₃ complex on cell growth in (A) PC-3 and (B) SGC-7901 cells. The cells were treated with various concentrations for 24 h. The anti-proliferative effect was measured by MTT assay. Results were expressed as the mean, SD. *P < 0.05	167
Figure 5. 47 Effect of [<i>trans</i> -(±)-1,2-(DACH)gold(III)(en)]Cl ₃ complex on cell growth in (A) PC-3 and (B) SGC-7901 cells. The cells were treated with various concentrations for 24 h. The anti-proliferative effect was measured by MTT assay. Results were expressed as the mean, SD. *P < 0.05	168
Figure 5.48 Effect of [(<i>S,S</i>)-(+)-1,2-(DACH)gold(III)(en)]Cl ₃ complex on cell growth in (A) PC-3 and (B) SGC-7901 cells. The cells were treated with various concentrations for 24 h. The anti-proliferative effect was measured by MTT assay. Results were expressed as the mean, SD. *P < 0.05	169
Figure 5. 49 Effect of compounds (48-50) on cell growth in (A) PC-3 and (B) SGC-7901 cells. The cells were treated with 10 μM for day 1 and day 3. The anti-proliferative effect was measured by MTT assay. Results were expressed as the mean, SD. *P < 0.05	170
Figure 5. 50 Electronic spectra with time of 1,2-diaminocyclohexane(propylenediamine)gold(III) chloride complexes following dissolution in the buffer solution at mixing (a) and after 7 days (b) at 37 °C.....	175
Figure 5.51 The 500-MHz ¹ H solution state NMR spectrum of [(1 <i>S</i> ,2 <i>S</i>)-(+)-(DACH)Au(pn)]Cl ₃ complex.....	179
Figure 5.52 The 500-MHz ¹ H solution state NMR spectrum of [<i>cis</i> -1,2-(DACH)Au(pn)]Cl ₃ complex.....	180
Figure 5.53 The 125.65-MHz ¹³ C{ ¹ H} solution state NMR spectrum of [(1 <i>S</i> ,2 <i>S</i>)-(+)-1,2-(DACH)Au(pn)]Cl ₃ complex.....	181
Figure 5.54 The 125.65-MHz ¹³ C{ ¹ H} solution state NMR spectrum of [<i>cis</i> -1,2-(DACH)Au(pn)]Cl ₃ complex.....	182

Figure 5.55 Optimized geometries of [(1,2-DACH)Au(III)(pn)]Cl ₃ , obtained at the B3LYP/LanL2DZ level of theory using GAUSSIAN09 W	184
Figure 5.56 X-ray structure of [(<i>cis</i> -1 <i>S</i> ,2 <i>R</i> -DACH)Au(pn)]Cl ₃ (51).....	186
Figure 5.57 View of the hydrogen bonded network of[(<i>cis</i> -1 <i>S</i> ,2 <i>R</i> -DACH)Au(pn)]Cl ₃ (51) along plane c-axis of the unit cell. Blue dotted lines show hydrogen bonds between different functional groups of molecules.....	189
Figure 5.58 The 500-MHz ¹ H solution state NMR spectrum of [(1 <i>S</i> ,2 <i>S</i>)-(+)-1,2-(DACH)Au(pn)]Cl ₃ complex in D ₂ O at mixing (a) and after 7 days (b).....	191
Figure 5.59 The 125.65-MHz ¹³ C{ ¹ H} solution state NMR spectrum of [(1 <i>S</i> ,2 <i>S</i>)-(+)-1,2-(DACH)Au(pn)]Cl ₃ complex in D ₂ O at mixing (a) and after 7 days (b).	191
Figure 5.60 The 500-MHz ¹ H solution state NMR spectrum of [(1 <i>S</i> ,2 <i>S</i>)-(+)-1,2-(DACH)Au(pn)]Cl ₃ complex in D ₂ O/DMSO at mixing (a) and after 7 days (b).....	192
Figure 5.61 The 125.65-MHz ¹³ C{ ¹ H} solution state NMR spectrum of [(1 <i>S</i> ,2 <i>S</i>)-(+)-1,2-(DACH)Au(pn)]Cl ₃ complex in (DMSO/D ₂ O, 1:2) at mixing (a) and after 7 days (b).....	192
Figure 5.62 Cyclic voltammograms of compound 48, 49 and 50 in the phosphate buffer at platinum electrode.....	194
Figure 5.63 Effect of <i>cis</i> -1,2-(DACH)gold(III)(pn)complex (51) on cell growth in (A) PC-3 and (B) SGC-7901 cells. The cells were treated with 10 μM for 1 day and 3 days. The anti-proliferative effect was measured by MTT assay. Results were expressed as the mean, SD. *P<0.05.....	196
Figure 5.64 Effect of <i>trans</i> -(±)-1,2-(DACH)gold(III)(pn)complex (52) on cell growth in (A) PC-3 and (B) SGC-7901 cells. The cells were treated with 10 μM for 1 day and 3 days. The anti-proliferative effect was measured by MTT assay. Results were expressed as the mean, SD. *P<0.05.....	197
Figure 5.65 Effect of (<i>S,S</i>)-(+)-1,2-(DACH)gold(III)(pn) complex (53) on cell growth in (A) PC-3 and (B) SGC-7901 cells. The cells were treated with 10 μM for 1 day and 3 days. The anti-proliferative effect was measured by MTT assay. Results were expressed as the mean, SD. *P<0.05.....	198
Figure 5.66 Effect of <i>cis</i> -1,2-(DACH)gold(pn) complex (51) on cell growth in (A) PC-3 and (B) SGC-7901 cells. The cells were treated with various concentrations for 24 h. The anti-proliferative effect was measured by MTT assay. Results were expressed as the mean, SD. *P<0.05.....	199
Figure 5.67 Effect of <i>trans</i> -(±)-1,2-(DACH)gold(pn) complex (52) on cell growth in (A) PC-3 and (B) SGC-7901 cells. The cells were treated with various concentrations for 24 h. The anti-proliferative effect was measured by MTT assay. Results were expressed as the mean, SD. *P<0.05	200
Figure 5.68 Effect of (<i>S,S</i>)-(+)-1,2-(DACH)gold(III)(pn) complex (53) on cell growth in (A) PC-3 and (B) SGC-7901 cells. The cells were treated with various	

concentrations for 24 h. The anti-proliferative effect was measured by MTT assay. Results were expressed as the mean, SD. *P<0.05	201
Figure 5.69 Effect of compounds (51-53) and on cell growth in (A) PC-3 and (B) SGC-7901 cells. The cells were treated with 10 μ M for day 1, day2 and day 3. The anti-proliferative effect was measured by MTT assay. Results were expressed as the mean, SD. *P<0.05	202
Figure 5.70A view of the molecular structure of complex (70), with partial atom labelling scheme and displacement ellipsoids are drawn at 50% probability level.	205
Figure 5.71 View of the crystal packing diagram of compound (70) along plane c-axis of the unit cell. Blue and red dotted lines show short contacts between different functional groups of molecules.	205

LIST OF ABBREVIATIONS

ATCC	American Type Culture Collection
B3LYP	Becke, 3-parameter, Lee-Yang-Parr
<i>bn</i>	Butylenediamine
CCL	Chronic lymphocytic leukemia
CPMAS	Cross Polarization Magic Angle Spinning
Cyclam	1,4,8,11-Tetraazacyclotetradecane
CV	Cyclic voltammetry
D.P.	Decomposition Point
Dach	1,2-Diaminocyclohexane
DFT	Density Functional Theory
DMEM	Dulbecco's Modified Eagle Medium
DMSO	Dimethyl sulfoxide
DNA	Deoxyribonucleic acid
DTC	Dithiocarbamate
DEDT	Diethyldithiocarbamate
DMDT	Dimethyldithiocarbamate
<i>E. coli</i>	<i>Escherichia Coli</i>
EA	Elemental Analysis
ECACC	European Collection of Cell Cultures
ELISA	Enzyme-linked immune-sorbent assay
<i>en</i>	Ethylenediamine
Et ₃ PAuSATg	<i>Auranofin</i>
FDA	Food and Drug Administration (USA)
<i>F.Streptococcus</i>	<i>Fetal Streptococcus</i>
Far-IR	Far-Infrared
FBS	Fetal Bovine Serum

FID	Free Induction Decay
Gly	Glycine
HBA	Host Bus Adapter
His	L-Histidine
HPC	Heterotrotrpic Plate Counts
IC ₅₀	Half maximal inhibitory concentration
IPr	1,3-bis(2,6-di-isopropylphenyl)imidazol-2-ylidene)
LANL2DZ	Los Alamos National Laboratory 2 double ζ
LMCT	Ligand-to-Metal Charge Transfer
LUMO	Lowest Unoccupied Molecular Orbitals
M.P.	Melting Point
MAS	Magic Spinning Angle
MBI	Mercaptobenzimidazole
MIR	Mid-Infrared
MTCC	Microbial Type Culture Collection (India)
MTT	Methylthiazol tetrazolium (assay)
N,N'-Et ₂ -en	N,N'-di-ethyl-ethylenediamine
N,N'-Et ₂ -pn	N,N'-di-ethyl-propylenediamine
N,N'-iPr ₂ -en	N,N'-di-iso-propyl-ethylenediamine
N,N'-Pr ₂ -en	N,N'-di-propyl-ethylenediamine
N,N'-Me ₂ -en	N,N'-di-methyl-ethylenediamine
N-Et-en	N-ethyl-ethylenediamine
N-i-Pr-en	N-iso-propyl-ethylenediamine
N-Me-en	N-methyl-ethylenediamine
N-Et-pn	N- ethyl-propylenediamine
NMR	Nuclear Magnetic Resonance
ORTEP	Oak Ridge Thermal Ellipsoid Plot Program

<i>P. aeruginosa</i>	<i>Pseudomonas aeruginosa</i>
PC3	Prostate Cancer 3(human cell line)
Phen	Phenanthroline
<i>pn</i>	Propylenediamine
PPh ₃	Triphenylphosphine
RPMI	Roswell Park Memorial Institute (medium)
<i>S. aureus</i>	<i>Staphylococcus aureus</i>
<i>S. typhi</i>	<i>Salmonella typhi</i>
SD	Standard Deviation
SGC7901	Gastric Cancer 7901 (human cell line)
Terpy	Terpyridine
TMS	Tetramethylsilane
UV	Ultra violet
Vis	Visible

ABSTRACT

Full Name : Said Salman Al-Jaroudi
Thesis Title : Synthesis, characterization and evaluation of anti-cancer activities of some gold complexes with diamine, phosphine and dithiocarbamate ligands
Major Field : Chemistry
Date of Degree : June 2014

Since the discovery of anticancer properties of cisplatin and its introduction in the clinical practice that was in 1978, a large number of coordination compounds of platinum and other metals have been investigated for their anticancer potency. In recent years, gold complexes have demonstrated a great potential for the design and development of new anticancer agents. In view of this potential, we prepared several gold(III) complexes and evaluated their antitumor properties.

In this dissertation, series of gold(III) and gold(I) complexes are reported using various ligands such as diamine, phosphine, dithiocarbamate and mercaptobenzimidazole.

The synthesized complexes were characterized using elemental analysis, various spectroscopic techniques including UV-Vis, FTIR spectroscopy, solution and solid-state NMR measurements; and X-ray crystallography. The data of CHN analysis supports the formation of the synthesized compounds. The blue shift in N-H stretching frequency in mid-FTIR and the presence of $\nu(\text{Au-N})$ in far-FTIR showed the coordination of $-\text{NH}_2$ group in 1,2-cyclohexane (1,2-DACH) with Au(III) center *via* nitrogen donor atoms. The solid-state ^{13}C NMR chemical shift shows that ligands are strongly bound to the gold(III) and gold (I) center. UV-Vis spectra also indicate that the gold center in gold(III) compounds remains in the 3+ oxidation state. The molecular structures of some complexes were determined by X-ray diffraction method. The X-ray crystallographic data reveals that the cyclohexyl ring of 1,2-DACH attains a chair conformation. The coordination geometry around the gold(III) and gold(I) ions is pseudo-square planar and linear, respectively, as indicated by X-ray crystallography analysis. The stability of the

complexes was checked by UV-Vis spectroscopy and NMR measurements. The electrochemical behavior of the complexes was also investigated through cyclic voltammetry.

Spectroscopic data was essentially evaluated by comparing with calculated data from the built and optimized structure by GAUSSIAN 09 at the RB3LYP level with LanL2DZ bases set. The computational study shows that the gold(III) adopts distorted square planar geometry.

The potential of new complexes as anticancer agents was investigated by measuring *in vitro* cytotoxicity in terms of IC₅₀ and inhibitory effect on growth of human prostate (PC3) and gastric (SGC7901) cancer cell lines. According to the biological assays, all (1,2-DACH) gold(III) chloride complexes are promising candidates as anti-cancer agents with [bis-(*cis*-1,2-DACH)₂Au(III)]Cl₃ is the most active agent. Some of our complexes show *in vitro* comparable and higher cytotoxicity to cisplatin.

ملخص الرسالة

الاسم الكامل: سعيد سلمان الجارودي

عنوان الرسالة: تصنيع و توصيف سلسلة جديدة من معقدات الذهب و تقييم سميتها ضد مجموعة من الخلايا السرطانية

التخصص: الكيمياء

تاريخ الدرجة العلمية: 9\6\1435 الموافق ل 10\6\2014

منذ إكتشاف السمة المميزة لخصائص (cisplatin) المضادة للسرطان , فإنه قد تم البحث في عدد كبير من مركبات البلاتين التساهمية وغيرها من المعادن لدراسة إمكانية إستخدامها كمضاد للسرطان. خلال السنوات الحالية أظهرت معقدات الذهب إمكانات كبيرة في تصميم وتطوير عوامل مضادة للسرطان. إدراكا لهذه الامكانات قمنا بتحضير عدد من معقدات الذهب وتقييم خصائصها المضادة للأورام.

في هذه الاطروحة تم توثيق سلسلة جديدة من معقدات الذهب (I) و (III): ثنائي امينات , فوسفين , ثنائي ثيوكراميت و مركبتو بنزو ايمدازول.

لقد تم توصيف المعقدات بعد ذلك باستخدام جهاز تحليل العناصر وجهاز مطيافية الاشعة تحت الحمراء وجهاز الرنين النووي المغناطيسي الخاص بالسوائل والحالة الصلبة. نتائج جهازي الرنين النووي المغناطيسي ومطيافية الاشعة تحت الحمراء تظهر رابطة تناسقية لكلايات ثنائي أمين مع Au(III) عبر ذرات N المانحة. كما ان جميع التحاليل تؤيد تكوين هذه المعقدات.

لقد تم تقييم النتائج المطيافية بمقارنتها مع النتائج المحسوبة من الاشكال المبنية المحسنة باستخدام GAUSSIAN 09 على مستوى RB3LYP مع مجموعة قواعد LanL2DZ. الدراسة الحسابية تظهر أن Au (III) يعتمد شكل هندسي مربع مستوي مشوه.

لقد تم تقييم قدرة خصائص معقدات عنصر الذهب (III) المضادة للسرطان في المختبر على خطوط خلايا سرطان البروستات PC3 والمعدة SGC7901. بشكل عام جميع المعقدات اظهرت خصائص جيدة للمقاومة ضد خلايا السرطان المستخدمة في الدراسة. لقد وجد أن معقد $[\text{bis}-(\text{cis}-1,2\text{-DACH})_2\text{Au(III)}]\text{Cl}_3$ العامل الاكثر سمية للخلايا السرطانية وبفاعلية تضاهي وتتفوق في بعض الحالات العقار المستخدم طبيا لخلايا سرطان المعدة SGC7901 ، cisplatin. وقد أظهرت النتائج تقارب في سمية الخلايا مع cisplatin. الدراسة المخبرية لسمية الخلايا لمعقدات Au(III)-ثنائي امينات و في بعض من معقداتنا أظهر سمية خلوية مخبريا مقارنة لعقار cisplatin.

CHAPTER 1

INTRODUCTION

Cancer is one of the diseases that contribute to the high mortality rate globally which is one of the major public health problems worldwide. Annually, an estimated 10 million people worldwide are diagnosed with cancer, while approximately 6.2 million die from this disease [1,2]. One area that has gained prominence is the use of inorganic compounds as anticancer drugs. Since the serendipitous discovery of *cis*-diaminedichloroplatinum(II) (cisplatin) by Rosenberg and co-workers in 1965 [3] (Figure 1.1(a)) and its introduction in the clinical practice was in 1978 [4]. Cisplatin is one of the most effective drugs in the treatment of testicular, ovarian, bladder, head and neck cancers [5]. The discovery of the anticancer properties of cisplatin opened up new prospects in the exploitation of metal-based chemotherapeutics to struggle cancer.

Despite the success of treating certain kinds of cancers with cisplatin there are several side effects, as well as the occurrence of intrinsic and acquired resistances, which limit the organotropic profile of the drug [6]. Some of the reasons that lead to this acquired resistance include reduced cellular uptake and deactivation of cisplatin by thiol containing biomolecules, such as glutathione [7]. This has generated continues interest in the development of not only platinum complexes but also other platinum group metal-based complexes which could be less toxic and exhibit no cross-resistance in tumor cells as cisplatin. As a result, this led to the discovery of interesting second-generation

platinum(II) antitumour complexes that carry ‘non-leaving’ ligands other than ammonia. More than 3000 platinum analogues of cisplatin have been synthesized but only few have made it to the clinical stages [8]. Examples include carboplatin (Figure 1.1b), AMD-473 (Figure 1.1c) and oxaliplatin (Figure 1.1d). Carboplatin displays similar activities with cisplatin but also exhibits bone-marrow toxicity [9-10]. On the other hand, AMD-473 showed promising *in-vitro* activity against cisplatin resistant A2780cisR cells [9-11].

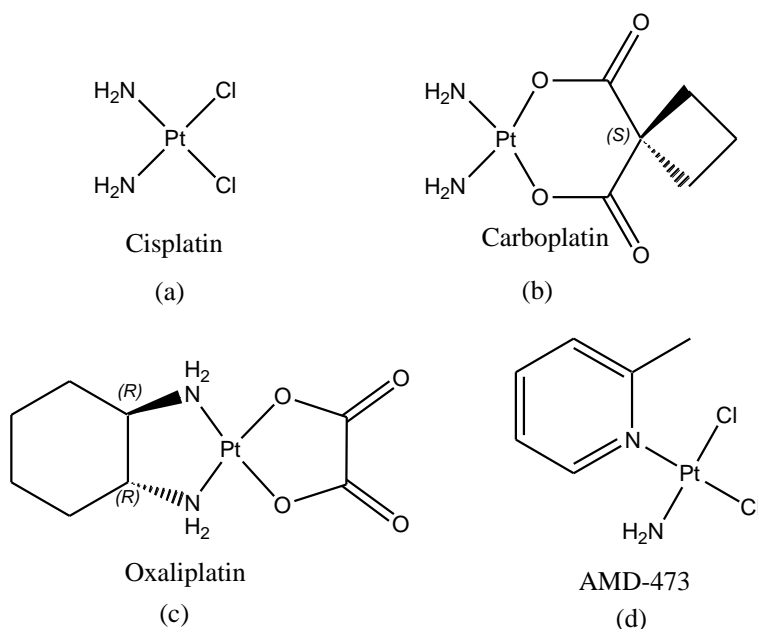


Figure 1.1 Structures of some anticancer platinum compounds

Among the non-platinum transition metal complexes tested so far, gold complexes have demonstrated a great promise for the design and development of anticancer agents. Chrysotherapy, the use of gold compounds in medicine, refers to the fact that gold compounds, usually gold thiolates, are used clinically in the alleviation of the symptoms associated with rheumatoid arthritis. Representations of some of the commonly used compounds used in this context are shown in Fig. 1.2. Aurothioglucose (solganol), which

is neutral, and the charged species aurothiomalate (myocrysin), aurothiosulphate (sanocrysin), aurothiopropyl sulphonate (allocrysin) and monomeric, neutral gold(I) species, triethylphosphinegold(I) tetraacetatothioglucose (auranofin) all have been successfully used over many years for the treatment of rheumatoid arthritis [12-15]. For instance, first comprehensive study of auranofin and auranofin analogues was published in 1986 [16]. In this study the *invitro* cytotoxicity of 62 gold compounds against both B16 melanoma and P388 leukemia cells was examined. The conclusion of this work was that a wide variety of phosphine-gold(I)-thiolates display significant cytotoxicity. In terms of a possible structure/activity relationship several trends were apparent that the presence of a phosphine ligand was important to demonstrated significant cytotoxicity.

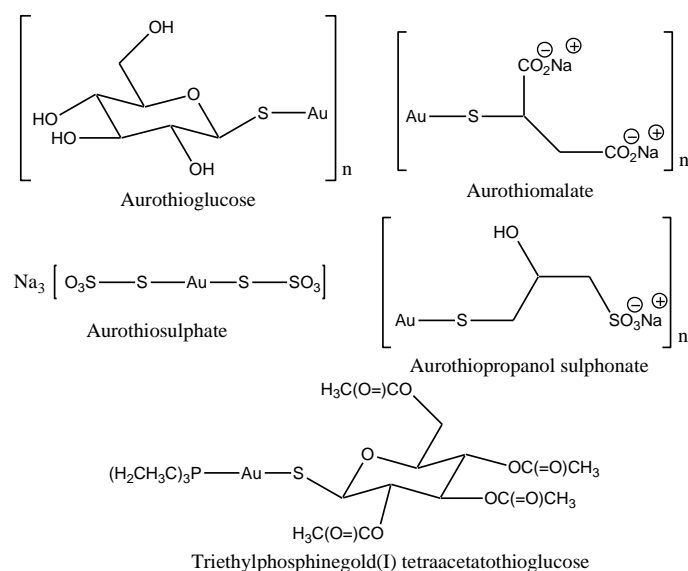


Figure 1.2 Structures of some gold-based drugs

Gold compounds are attracting growing attention within the scientific community as potential anticancer agents. Indeed, following the success of platinum based anticancer complexes, several other metal compounds have been prepared and evaluated as experimental anticancer agents in the course of last two decades [17,18]. For instance,

gold(I) and gold(III) are among the tested classes of metal-based agents which have been given great attention [19]. Gold complexes have recently gained considerable attention as a class of compounds with different pharmacodynamic and kinetic properties than cisplatin [20]. Furthermore, the increasing number of scientific reports in the last decade testifies the important role played by Au(I) and Au(III) complexes in biochemical and chemical research [21-30].

Attention was directed towards gold compounds for two reasons: (1) gold(III) centers are isoelectronic to Pt(II) compounds and adopt square-planar configurations similar to that of cisplatin, and (2) gold(I) compounds are well known pharmaceuticals, some of which are currently being used to treat rheumatoid arthritis. Gold compounds have displayed strong tumor cell growth inhibition effects by a non-cisplatin-like mode of action. Antitumor effects of tetrahedral gold(I) complexes $[\text{Au}(\text{dppe})_2]^+$ and related compounds are ascribed to their delocalized lipophilic cation properties [31–32].

Heterocyclic compounds and their metal complexes display a broad spectrum of pharmacological properties. For instance, preparation and characterization of four novel gold(I) complexes, $[\text{C}_{28}\text{H}_{26}\text{NPS}_2\text{Au}]\text{Cl}$ (Fig. 1.3a), $\text{C}_{14}\text{H}_{20}\text{N}_2\text{OPSAu}$ (Fig. 1.3b) $\text{C}_{26}\text{H}_{20}\text{N}_2\text{OPSAu}$ (Fig. 1.3c) and $[\text{C}_{16}\text{H}_{26}\text{NPS}_2\text{Au}]\text{Cl}$ (Fig. 1.3d) were obtained with 3-benzyl-1,3-thiazolidine-2-thione or 5-phenyl-1,3,4-oxadiazole-2-thione and phosphines [33]. The compounds exhibited more cytotoxic than cisplatin to colon cancer (CT26WT) and metastatic skin melanoma (B16F10) tumor cell lines and presented a high selectivity index.

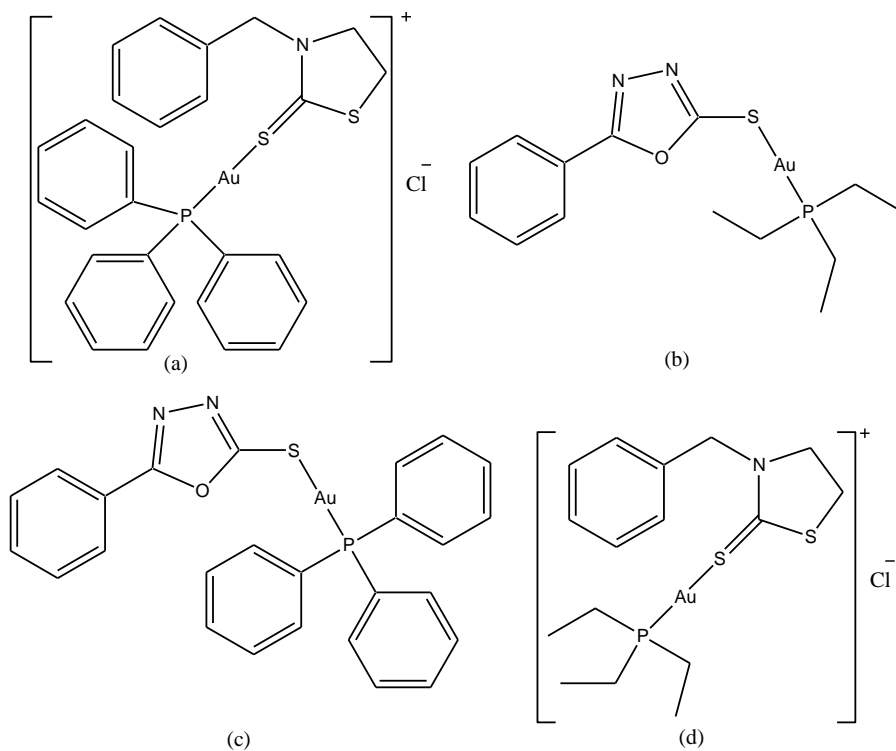


Figure 1.3 Structures of potential anticancer gold(I) complexes containing phosphine and heterocyclic compounds

Kouroulis *et al.* described the *in vitro* activity of a series of gold(I) complexes, [Au(tpp)(mtzd)] (a) and [Au(tpp)(Clmbzt)] (b) as shown in Figure 1.4 against the leiomyosarcoma cancer cell line [34]. These complexes showed significant cytotoxic effects and were found more active than cisplatin to a large extent.

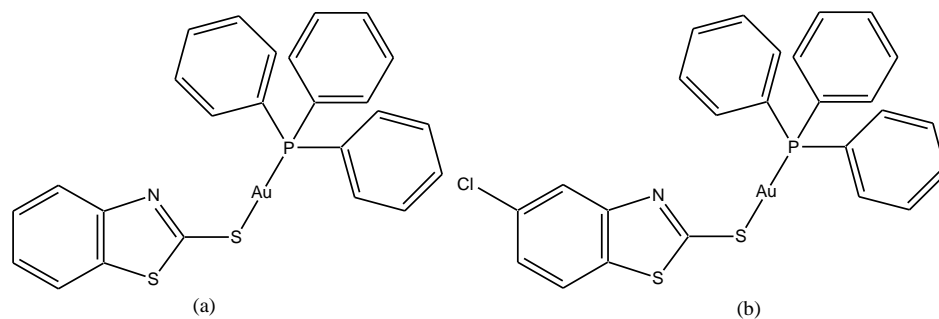


Figure 1.4 Structures of potential anticancer gold(I) complexes containing phosphine and thioamides compounds

Some of gold compounds have been entered clinical trials since a few of them are highly cytotoxic to solid cancer tumors in vitro and in vivo while causing minimal systemic toxicity [35–39]. Most gold(III) compounds display reduced affinity for DNA and it seems reasonable that DNA is neither the primary nor the exclusive target for most gold(III) complexes. Recent studies have proposed different modes of action for these compounds. For instance, gold(III)-porphyrin complexes, known gold-based DNA intercalators, induce intracellular oxidation and apoptosis through both caspase-dependent and -independent mitochondrial pathways [39–41]. Furthermore, gold(III) complexes with dithiocarbamate ligands inhibit thioredoxin reductase activity, generate free radicals, increase ERK1/2 phosphorylation, affecting mitochondrial functions [36,42]. These compounds have also been described to cause a strong inhibition of the proteasome system, via both redox-dependent and -independent processes [43].

Gold(III) compounds have greatly attracted researchers' attention in the last decade for their outstanding cytotoxic actions. It is a metal ion which typically adopts a four-coordinate, square-planar geometry and is therefore expected to mimic the structural and electronic properties of platinum(II). Recent studies have shown that several gold(III) complexes are highly cytotoxic against different tumor cells [44–46], including some which are active even against the cisplatin-resistant cell lines [47–49]. Several lines of evidence suggest that gold(III) compounds produce their antiproliferative effects through innovative and non-conventional modes of action. For instance, the hypothesis that their biological effects are mediated by an antimitochondrial mechanism rather than by direct DNA damage, as it is the case for cisplatin and its analogs, has gained much credit during the last few years [50].

To obtain gold(III) complexes with superior chemotherapeutic index in terms of increased bioavailability, higher cytotoxicity, and lower side effects than cisplatin, Ronconi et al. synthesized new gold(III) dithiocarbamate derivatives with defined coordination geometry [51]the synthesized gold complexes were tested for their *in vitro* cytotoxic activity toward a panel of human tumor cell lines. Remarkably, most of them, in particular gold(III) derivatives of *N,N*-dimethyldithiocarbamate (Compounds (a)&(c); Fig. 1.5) and thylsarcosinedithiocarbamate (Compounds (b)&(d); Fig. 1.5), were shown to be 1–4-fold more cytotoxic than cisplatin and to overcome to a large extent both intrinsic and acquired resistance to cisplatin. The choice of dithiocarbamate ligands was not accidental; they were being evaluated for their efficacy as inhibitors of cisplatin-induced nephrotoxicity without decreasing its antitumor activity [52-54].

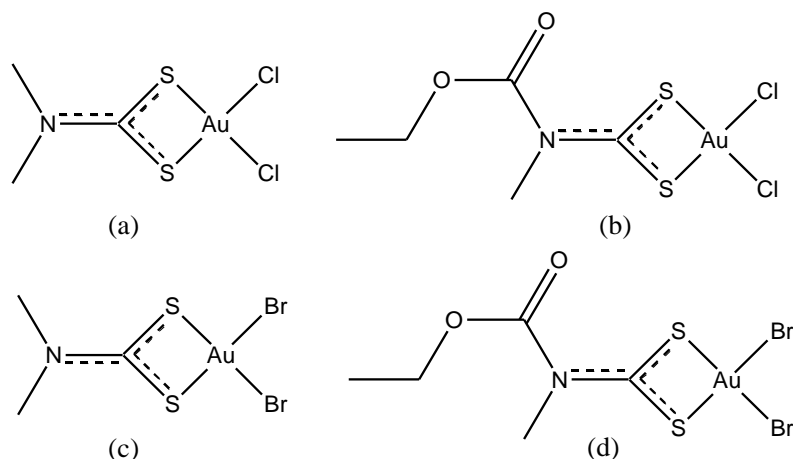


Figure 1.5 Chemical structures of gold(III) dithiocarbamate complexes

In the light of the above mentioned medicinal role of gold compounds, it is important to study the coordination chemistry of gold(III) and gold(I) from the point of view of

designing new drugs as well as to understand the biochemical mechanism of action of the known anticancer complexes.

1.1 Current Status of the Problem

- 1) Cisplatin has been used as an anticancer agent for the last few decades. Unfortunately, they have several major drawbacks. Common problems include cumulative toxicities of nephrotoxicity and cytotoxicity. In addition to the serious side effects, the therapeutic efficacy is also limited by inherent or treatment-induced resistant tumor cells.
- 2) Even though over 28 new platinum(II) compounds have entered human clinical trials, only few of them, carboplatin, oxaliplatin, nedaplatin and lobaplatin, received approval and achieved routine clinical use. However, all these platinum(II) drugs are active in the same range of tumors and are still administered intravenously. As a result, their impact as anticancer drugs is still reduced by the significant side effects, such as gastrointestinal and hematological toxicity, and drug-resistance phenomena.
- 3) Researchers have been focusing on the development and *in vitro* testing of both novel platinum- and other metals-based compounds with the aim of obtaining complexes with higher effectiveness, increased selectivity for tumor tissue, reduced toxicity, wider spectrum of activity, and able to overcome tumor resistance often associated with cisplatin treatment.

- 4) Regardless of the observed side effects, the successes achieved with cisplatin in cancer chemotherapy stimulated search for other coordinated metal complexes as potential anti-cancer agents. For example, metal complexes offer an opportunity for the discovery of new antitumor drugs with truly new mechanisms of action by varying structural features in order to improve the physico-chemical and biological properties.
- 5) Recent advances in this area demonstrated a great promise for the utilization of non-platinum complexes in cancer chemotherapy.
- 6) Our interest in using gold for the development of anticancer agent arises from the fact that this metal has extensively been employed in medicinal inorganic chemistry during the last decades.
- 7) Some gold(III) complexes, isoelectronic with antitumor platinum(II) complexes, have recently been evaluated *in vitro* tests, showing significant cytotoxic effects.
- 8) The increasing number of scientific reports in the last decade testifies the important role played by Au(I) and Au(III) complexes in biochemical and chemical research.
- 9) Auranofin (S-Au(I)- PEt₃) presented an *in vitro* activity similar to or even greater than cisplatin.
- 10) Auranofin and a number of its analogs showed potent cytotoxic activity against melanoma and leukemia cell lines *in vitro* and anti-tumor activity against leukemia *in vivo*. However, these complexes were completely inactive against solid tumors. The main observations from these experiments were that (i) lack of

potency *in vitro* correlates well with lack of anti-tumor activity; (ii) potent cytotoxicity *in vitro* does not necessarily translate into anti-tumor activity *in vivo*; and (iii) *in vivo* anti-tumor activity is generally optimized by ligation of Au(I) with a substituted phosphine.

11) A large number of phosphine complexes (R_3PAuX) have been evaluated and all exhibit *in vitro* potent cytotoxicity against tumor cells.

12) The biological profile of the Au(I)diphosphine complexes exhibited high lipophilicity which allows them to penetrate cells and their high kinetic and thermodynamic stability which prevents unwanted side reactions *in vivo*.

1.2 Aim of the Present Research

(A) Synthesis of Ligands.

- 1) To synthesize various ammonium dithiocarbamate ligands functionalized with ethylenediamine (en), propylenediamine (pn), butylenediamine (bn) and 1,2-diaminocyclohexane (1,2-DACH) and their full chemical characterization.
- 2) To synthesize various substituted benzimidazole-2-thione ligands and their full chemical characterization.

(B) Synthesis of Gold(I) Complexes.

- 1) To synthesize various chlorido phosphane gold(I) complexes of the type $[R_3PAuCl]$.

- 2) To synthesize various phosphane dithiocarbamate gold(I) complexes of the type $[R_3PAu(DTC)]$, where DTC is dithiocarbamate.
- 3) To synthesize various dithiocarbamate bis-(phosphane gold(I)) complexes of the type $[((Au(DTC))_2(DPP))]$, where DTC and DPP are dithiocarbamate and bis-diphenylphosphine, respectively.

(C) Synthesis of Gold(III) Complexes.

- 1) To synthesize various 1,2-diaminocyclohexane chlorido gold(III) chloride complexes of the type $[(DACH)AuCl_2]Cl$, where DACH is 1,2-diaminocyclohexane.
- 2) To synthesize various 2-cyclohexanaminium dithiocarbamate chlorido gold(III) chloride complexes of the type $[(DACH-DTC)AuCl_2]Cl$, where DACH-DTC is 2-cyclohexanaminium dithiocarbamate.
- 3) To synthesize various ammonia 1,2-diaminocyclohexane chlorido gold(III) chloride complexes of the type $[(DACH)Au(NH_3)Cl]Cl_2$, where DACH is 1,2-diaminocyclohexane.
- 4) To synthesize various diammonia 1,2-diaminocyclohexane gold(III) chloride complexes of the type $[(DACH)Au(NH_3)_2]Cl_3$, where DACH is 1,2-diaminocyclohexane.
- 5) To synthesize various bis(1,2-diaminocyclohexane) gold(III) chloride complexes of the type $[(DACH)_2Au]Cl_3$, where DACH is 1,2-diaminocyclohexane.
- 6) To synthesize various mixed-ligand 1,2-diaminocyclohexane ethylenediamine gold(III) chloride complexes of the type

$[(\text{DACH})(\text{en})\text{Au}]\text{Cl}_3$, where DACH and en are 1,2-diaminocyclohexane and ethylenediamine, respectively.

- 7) To synthesize various mixed-ligand 1,2-diaminocyclohexane 1,3-propylenediamine gold(III) chloride complexes of the type $[(\text{DACH})(\text{pn})\text{Au}]\text{Cl}_3$, where DACH and pn are 1,2-diaminocyclohexane and 1,3-propylenediamine, respectively.

All new synthesized compounds were characterized using various analytical and spectroscopic techniques including elemental analysis, UV-Vis and FTIR spectra; and solution as well as solid-state NMR measurements. Also, their structure-activity relationships in tumor models will be examined and evaluated.

The outcome of this research may ultimately, lead to the discovery of new type of anti-cancer agents. If we are successful it will not only benefit the people who suffer from cancer in Kingdom of Saudi Arabia but also the cancer victims of the entire world.

CHAPTER 2

LITERATURE REVIEW

Medical properties of gold have been explored throughout the history of civilization. Even ancient cultures in India and Egypt exploited gold and used it for various medicinal preparations. The earliest therapeutic application of gold can be traced back to 2500 B.C. in China where gold was used to treat smallpox, skin ulcers, and measles [55]. Moreover, at that time, people thought of gold as being immortal and everlasting, and associated gold with longevity. Some cultures still believe in the healing properties of gold. As an illustration, Japanese tradition suggests that thin gold-foils placed into tea, sake and food could be beneficial to human health.

Although gold and gold complexes have historically been used for the treatment of a wide range of ailments, the rational use of gold in medicine began in the early 1920s when gold was clinically tested for its *in vitro* bacteriostatic effect. The first gold complex used for that purpose was gold cyanide, employed by bacteriologist Robert Koch to kill the mycobacteria, the causative agent of tuberculosis [56]. After its initial use for pulmonary tuberculosis, toxicity associated with that treatment was observed, and the treatment was switched to the less toxic gold(I) thiolate complexes. In the early 1930s, the French physician Jacque Forestier introduced the same thiolate complexes for the treatment of rheumatoid arthritis, a condition which he believed was related to tuberculosis [57].

The unintentionally discovery of the anticancer activity of cisplatin was made during an experiment in 1965 [58] which was conducted at Michigan State University by Barnett Rosenberg. He used a platinum electrode to apply an electric field to a colony of *E. coli*, which was observed to inhibit their growth [59]. A detailed investigation into the cause of this effect concluded that the platinum electrode was breaking down to generate platinum-(II) species *in situ*, which was stopping the cells from multiplying. This observation led to the development of *cis*-diamminedichloridoplatinum(II), commonly known as cisplatin, being approved by the American Food and Drugs Administration (FDA) for cancer therapy in December, 1978 [60]. Since that it has become the most widely used anticancer drug, with an estimated 70 % of patients receiving the compound as part of their treatment [61,62].

The accidental discovery of the anticancer properties of cisplatin, its platinum(II) analogues and their wide clinical application in current cancer treatments promoted a great deal of interest in the area of metal-based anticancer agents [63]. Cisplatin exhibits clinical activity against a wide range of different kinds of cancers. It remains one of the most significant anticancer agents in the clinical armamentarium [64]. Whilst the chemotherapeutic success of platinum is undeniable, it is by no means the perfect drug. It is not effective against many common types of cancer, drug resistance is common and it has a deplorable range of side effects, which can include nerve damage, hair loss and nausea. Disappointingly however, the countless clinical candidates in fifty years later, there have only been two more worldwide drug approvals for precious metal-containing anticancer drugs: carboplatin and oxaliplatin, both of which are direct analogues of cisplatin, approved in 1993 and 2002 respectively.

The mode of action of these platinum complexes is known: the chloride or dicarboxylate ligands are hydrolysed within the cell to generate a bis-aqua species, which binds irreversibly to DNA – usually to two adjacent guanine bases [65] and the cell, unable to replicate, defaults to apoptosis (controlled cell death) [66]. Within the extracellular *milieu* the physiological chloride ion concentration is ca. 100 mM, while inside cells it is ca. 4 mM. These conditions facilitate the aquation of cisplatin (Figure 2.1). The aquated species would then easily react with the target molecule, DNA [67,68]. The binding of metal species to DNA is known to occur in two steps, leading to formation of two forms of adducts; intra-strand and inter-strand cross-links. The formation of these adducts then blocks DNA transcription and replication causing repair (NER) pathway that would repair DNA damage [69]. However, DNA damage caused by cisplatin adducts is very poorly repaired in cells. This is due to the fact that it induced intra-strand cross-links serve as binding targets for high-mobility-group proteins (HMG) [70] because of structural similarity between these intra-strand cross-links and the cells to undergo G2 cell-cycle arrest. Under normal circumstances a nucleotide cutting out the distortion in DNA structure, hence inhibiting DNA repair [67,70]

Platinum-containing compounds such as cisplatin, carboplatin and oxaliplatin are widely used in the treatment of a variety of cancers. Newer, second generation platinum compounds like carboplatin and oxaliplatin were designed to improve efficacy particularly against cell lines that demonstrate second pass cisplatin resistance [71]. Tolerance to cisplatin-induced DNA damage has been suggested as a fundamental mechanism of drug resistance [72].

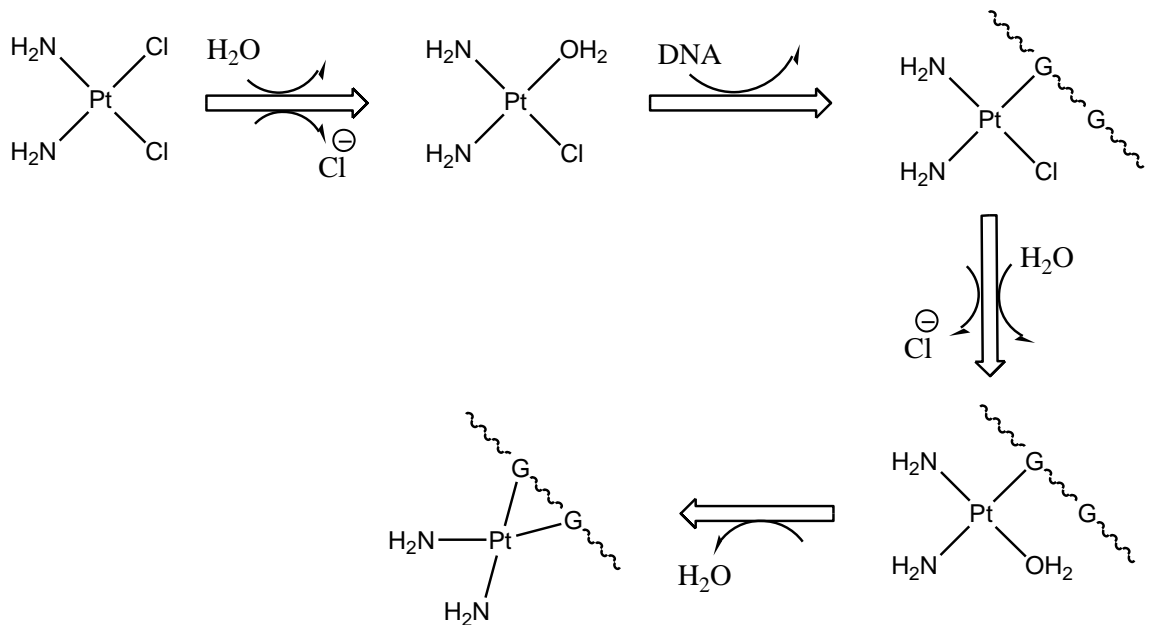


Figure 2.1. Schematic representation of how cisplatin is activated and subsequently bind to DNA

In the early 1980s, the rapidly emergent interest as well as demand has enthused for the design of alternative platinum and non-platinum-based anticancer agents in cancer chemotherapy in order to overcome both intrinsic and acquired resistance in cancer cell lines. Consequently, in recent years the interest in non-platinum metal complexes for cancer chemotherapy has been rapidly growing. Such consideration has further been stimulated by the possibility of developing new agents with a different mode of action and clinical profile from the well-established platinum based metallodrugs [73].

To circumvent the problem of drug-resistance in cisplatin-resistant cells, gold(III)-based complexes have been designed as a potential alternative to cisplatin [74,75]. Gold(III) complexes exhibit iso-electronic and iso-structural features with platinum(II) and have

similar uptake and DNA interference activity [75]. In addition, the higher charge of gold(III) compared to platinum(II) is an added advantage for binding with DNA [76]. Among the several classes of metal complexes that have been taken into consideration as potential anticancer agents starting from the 1980's, only a few investigations have focused on d^8 square planar gold(III) complexes in spite of their stringent similarity to platinum(II) complexes [77-81].

During the 1990s, the gold(III) compounds emerged as potential anticancer agents showing improved stability both in solid and solution phases, lower toxicity and favorable *in-vitro* pharmacological profiles. For example in 1996, Parish, Buckley, reported a series of cytotoxic gold(III) compounds with damp ligands [damp = (dimethylamino)methyl]phenyl] with encouraging results towards the anticancer activity (Figure 2.2)[82]. [(damp)AuCl₂] has been tested in Vitro against a range of microbial strains and several human tumor lines, where it displays differential cytotoxicity similar to that of cisplatin against the ZR-75-1 human tumor xenograft [82].

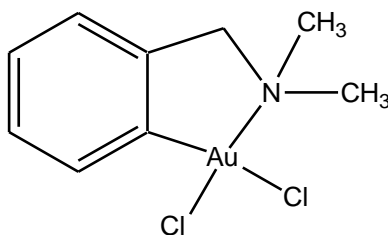


Figure 2.2 Structure of [(damp)AuCl₂]

AuNaphth1 (Figure 2.3) is a gold(I) species, which contains the triethylphosphine moiety of auranofin and a naphthalimide ligand replacing the carbohydrate ligand of auranofin [83]. The drug design strategy for this novel gold complex was motivated by the aim to

replace the auranofin carbohydrate ligand, which is supposedly more relevant for the biodistribution of the compound than for its pharmacodynamic effects, by another bioactive ligand. As bioactive ligand the naphthalimide moiety was chosen based on the promising preclinical results of the naphthalimide class of antitumor drugs [84]. AuNaphth1 displayed promising cell growth inhibiting effects, induced apoptosis and inhibited Thioredoxin reductases (TR, TrxR). Mass spectrometric investigations on a cysteine containing model peptide showed that AuNaphth1 bound covalently to the cysteine residue under loss of its thionaphthalimide ligand, which indicates that the interaction with TrxR might also be based on a covalent binding mechanism.

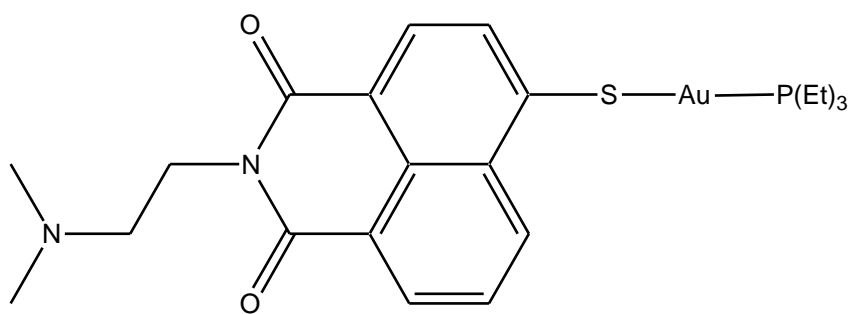


Figure 2.3 Structure of Au-Naphth-1 complex

Exceptional biological properties have also been reported recently for gold phosphole complexes. These gold agents are characterized by a phosphacyclopentadiene ligand attached to the central metal and are potent inhibitors of TrxR and the related glutathione reductase. The complexGoPI (Figure 2.4) shows IC_{50} values for enzyme inhibition in the low nanomolar range and is probably the most potent inhibitor of glutathione reductase reported so far [85,86].

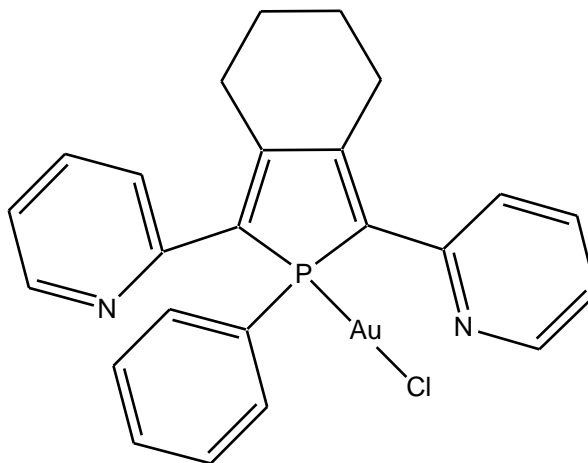


Figure 2.4 Structure of gold phosphole complex GoPI

In this context, $[\text{Au}(\text{dppe})_2]^+$ and its analogues (Figure 2.5) belong to the group of delocalized lipophilic cations (DLCs), which can pass through cellular membranes and accumulate in the mitochondria. Consequently, the lipophilicity of the compounds is a very important parameter in optimizing the biodistribution and activity. Structurally related bidentate phenyl and pyridyl phosphine complexes showed activity against cisplatin-resistant human ovarian cancer cells. Concerning the cytotoxicity the phenyl and 2-pyridyl analogues were superior to the 3- and 4-pyridyl complexes. During exposure to the dinuclear 2-pyridyl derivative SMIV gold was mainly found in the mitochondrial fractions of CH1 cells compared to nuclear and cytosolic fractions highlighting the special role of mitochondria for the antitumor potency of gold compounds. Interestingly, the *in vitro* hepatotoxicity of the complexes correlates with the lipophilicity and cellular uptake of the agents. The authors concluded that complexes with a medium lipophilicity might be optimal for further development [87,88].

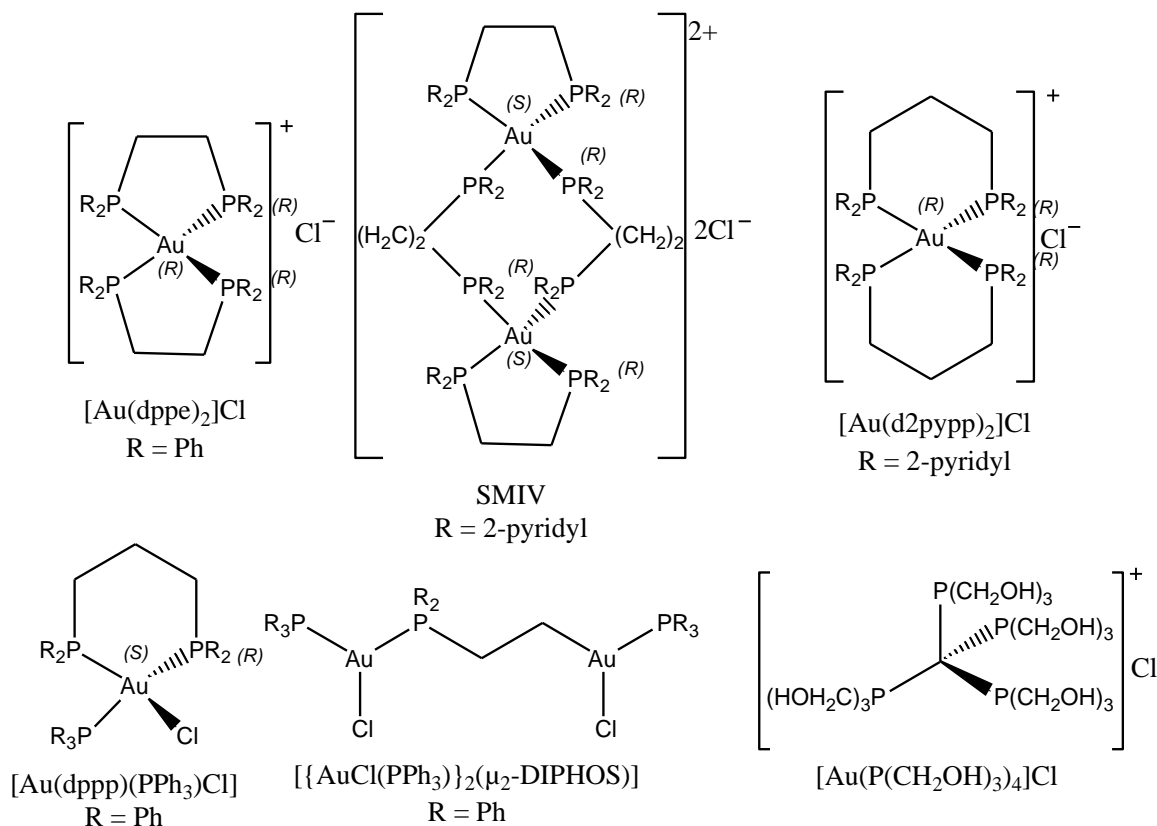


Figure 2.5 Schematic drawing of Au(I) complexes with multiple phosphine ligands

The $[\text{Au}(\text{dppe})_2]^+$ propylene analogue $[\text{Au}(\text{d2pypp})_2]\text{Cl}$ showed selectivity against cancer cells in comparative experiments using normal and cancer breast cells and selectively induced apoptosis in breast cancer cells but not in normal cells. Apoptosis was induced via the mitochondrial pathway involving mitochondrial membrane potential depolarisation, depletion of the glutathione pool and caspase3 and caspase9 activation. The accumulation in the mitochondria was confirmed for the compound. Furthermore, the complex inhibited both thioredoxin and thioredoxin reductase activities [89,91].

The mixed-ligands gold phosphine compound chlorotriphenylphosphine 1,3-bis(diphenylphosphino)propanegold(I) $[\text{Au}(\text{dppp})(\text{PPh}_3)\text{Cl}]$ was investigated in the

national cancer institute (NCI) 60 cell panel screening and showed median Lethal Dose(LC₅₀) values in the low micromolar range in 29 cell lines. The results were most marked in MCF7 breast cancer cells with the LC₅₀ value being below the lowest test concentration used (0.01mM). Unexpectedly, the compound was not active in leukemia cells [91]. Further studies on this agent were performed on a panel of human melanoma cell lines, in which the complex displayed IC₅₀ values in the low micromolar range. An apoptotic response was noted with alterations in the nuclear morphology, loss of mitochondrial membrane potential, cytochrome C and Smac/DIABLO release from mitochondria into cytosol and enhanced caspase9 and caspase3 catalytic activity as well as a decreased expression of antiapoptotic proteins [92]. However, [Au(dppp)(PPh₃)Cl] decomposes in solution under formation of mono and dinuclear complexes making the nature of the pharmacologically active species unclear [93].

The dinuclear cationic complex $[\{AuCl(PPh_3)\}_2(\mu_2-DIPHOS)]$ is the unexpected outcome of a study aiming at developing an ethylene analogue of [Au(dppp)(PPh₃)Cl]. $[\{AuCl(PPh_3)\}_2(\mu_2-DIPHOS)]$ showed activity against JR8, SKMel5 and 2/60 melanoma cell lines, however, it was less effective than [Au(DPPP)(PPh₃)Cl] [93]. Four phosphine ligands at the gold center are realized in tetrakis((trishydroxymethyl)phosphine)gold(I) chloride [Au(P(CH₂OH)₃)₄]Cl. The compound showed excellent activities (with IC₅₀ values in the low nanomolar range!) against prostate cancer, gastrointestinal and colon carcinoma cells and prolonged the G1 phase of the cell cycle. *In vivo* studies in mice confirmed the positive results from the *in vitro* experiments showing a significantly prolonged survival of treated mice compared to the untreated control [94]. These and

preliminary pharmacokinetic data in dogs suggested the further development of the agent in clinical phase I trials [95].

Various other gold(I) species showed promising bioactivities. Some relevant examples are shown in Figure 2.6. IC₅₀ values in the low micromolar range were obtained with triphenylphosphinegold(I) complexes with different sulfanylpropenoate ligands in HeLa and A2780 cells (see [Au(PPh₃)(HCLpspa)] in Figure 2.6 for a relevant example). The free ligands were devoid of activity [96]. The gold(I) 7-azacoumarin species [Au(TS)(PEt₃)] displayed superior cytotoxic effects compared to cisplatin in A2780 cells and was also strongly active in a cisplatin-resistant variant of the cell line [97]. Similar results had been observed with the vitamin K3 derivative [AuPEt₃(K3TSC)], which represents the first gold(I) complex with a thiosemicarbazone ligand [98].

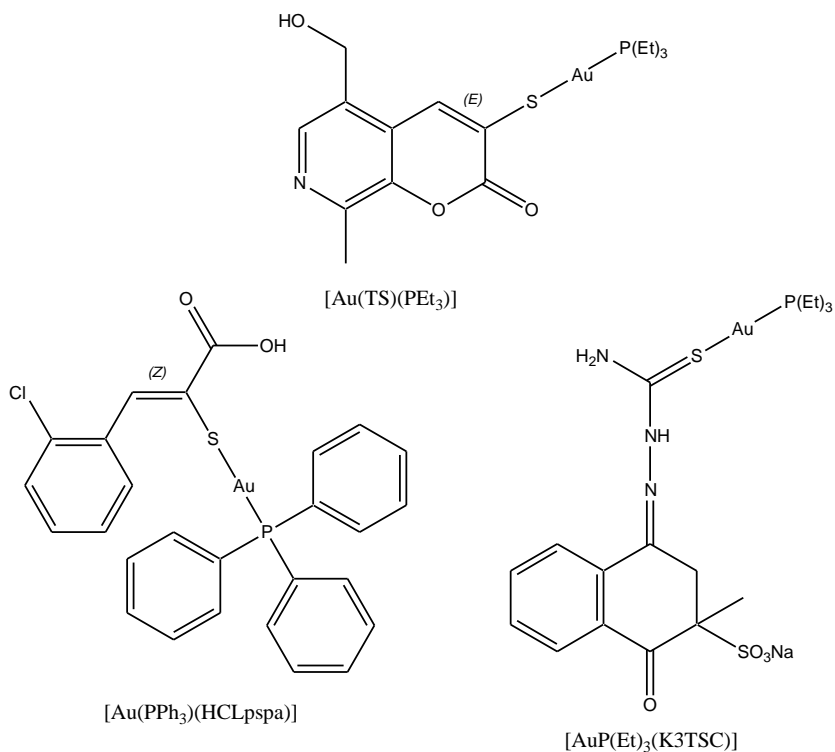


Figure 2.6 Structures of various bioactive gold(I) species

Et₃PAu(S₂CNEt₂) was the most active agent within a series of dithiocarbamate and xanthate complexes in a panel of seven human cancer cell lines [99]. Water soluble cyclodiphosphazane gold(I) complexes exhibited antiproliferative effects in cultured HeLa cells, induced apoptosis and activated the p53 protein [100].

A series of cationic gold complexes with multidentate ligands, namely [Au(phen)Cl₂]Cl, [Au(terpy)Cl]Cl₂, [AuCl(dien)]Cl₂, [Au(cyclam)](ClO₄)₂Cl and [Au(en)₂]Cl₃ (Figure 2.7), showed reasonable stability in physiological like environment. The coordination to the polyamine ligands caused a marked stabilization of gold in the 3+ oxidation state as indicated by measurements of the reduction potentials. The stabilization was less evident for the less basic phenanthrene and terpyridine ligands. With exception of the cyclam species [Au(cyclam)](ClO₄)₂Cl, all complexes exhibited good cytotoxic activities in A2780 human ovarian cancer cells. Furthermore, results obtained in cisplatin-resistant A2780 cells indicated that the compounds might overcome resistance phenomena. The free ligands were also investigated in the same assay. Whereas the free ethylenediamine derived ligands were devoid of any activity, the potency of free phenanthrene and terpyridine was comparable to that of the respective gold(III) complexes making the results of these two compounds difficult to interpret. Overall this study pointed out that the cytotoxicity of the ethylenediamine derived complexes was related to the presence of the gold(III) central atom, the activity was not related to good leaving groups (such as chlorine), no direct correlation of the antiproliferative effects and the reduction potentials was present and the strong stabilization of the gold(III) center led to a loss of activity (as indicated by the results with [Au(cyclam)](ClO₄)₂Cl. For the compounds [Au(phen)Cl₂]Cl and [Au(terpy)Cl]Cl₂, which had also shown good stability under

physiological conditions, an easy reduction was observed in the presence of ascorbate or thiosulfate. This indicates that for these two complexes the release of their toxic ligands upon *in vivo* reduction might be the reason for the bioactivity [101]

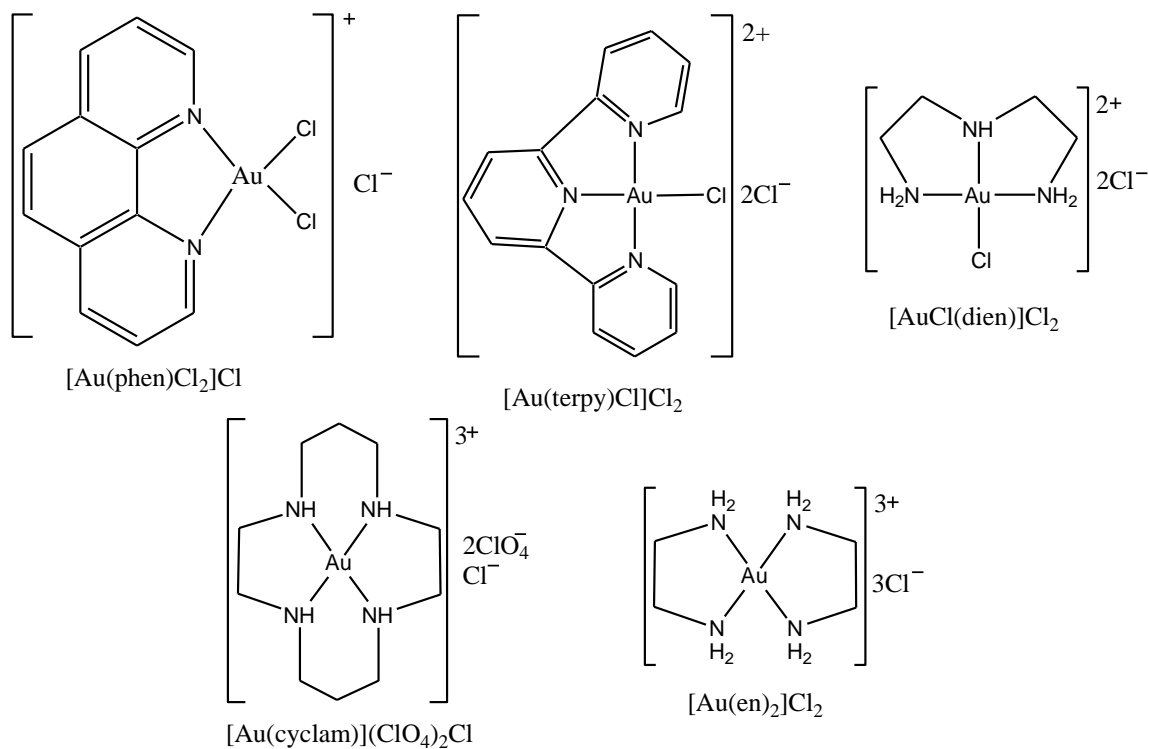


Figure 2.7 Schematic drawings of gold(III) complexes with Au-N bond

Gold(III) tetraarylporphyrins exhibited excellent cytotoxic activities mediated by apoptotic pathways [102]. Detailed pharmacological studies have been performed on gold(III) porphyrin 1a (Figure 2.8). It was found that the apoptosis inducing effects were related to caspase-dependent and caspase-independent mitochondrial pathways including the activation of caspase3 and caspase9. Gold(III) porphyrin 1a treatment led to the release of cytochrome C, which itself activated caspase3 and caspase9 [103]. A proteomic analysis indicated the involvement of multiple pathways and showed that

cellular structure and stress related chaperone proteins, proteins involved in the formation of reactive oxygen species, proteins related to cell proliferation and others were in the altered clusters [104]. The toxicity of the porphyrin complex was not related to phototoxicity, it interacted with the DNA in a non-covalent manner and partly abrogated the cell cycle at G(0)–G(1). The effects on apoptosis and on the cell cycle were dependent [105]. More detailed studies on the mechanisms underlying the induction of apoptosis revealed that the mitogen activated protein kinases p38MAPK and ERK were transiently activated upon exposure to gold(III) porphyrin 1a, multiple phosphotyrosine proteins (namely cytoskeleton and cytoskeleton like proteins, kinase proteins and proteins involved in signal transduction) were involved in apoptosis related to p38MAPK and mitochondrial permeabilisation played an important role [106]. In a rat hepatocellular carcinoma model gold(III) porphyrin 1a significantly prolonged survival but did not lead to a drop down of the body weight of the rats or affected the plasma aspartate aminotransferase level. Furthermore, it induced necrosis and apoptosis in the tumor tissue but not in normal liver tissue [107].

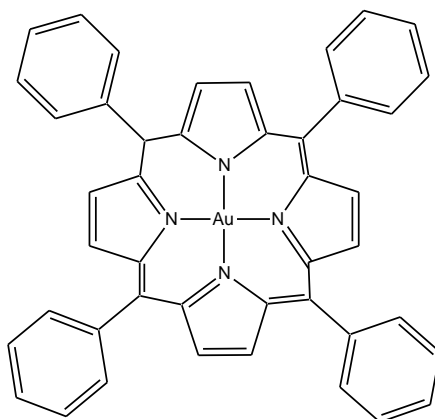


Figure 2.8 Schematic drawing of gold(III) porphyrin 1a complex with Au-N bond

Bertrand *et al.* recently evaluated gold(I) derivatives of new caffeine-based gold(I) NHC complexes based on xanthine ligands (Figure 2.9) for their antiproliferative activities in different cancerous and nontumorigenic cell lines in vitro [108]. The bis-carbene caffeine-based complex $[\text{Au}(\text{MC})_2][\text{BF}_4]$ (4) has shown interesting anticancer properties in vitro against the human ovarian cancer cell line A2780 and its cisplatin resistant variant A2780/R, though it appeared to be poorly toxic in non cancerous HEK-293T cells in vitro, as well as in healthy tissues ex vivo. This latter result is of particular importance for the future development of new metallodrugs with reduced side-effects.

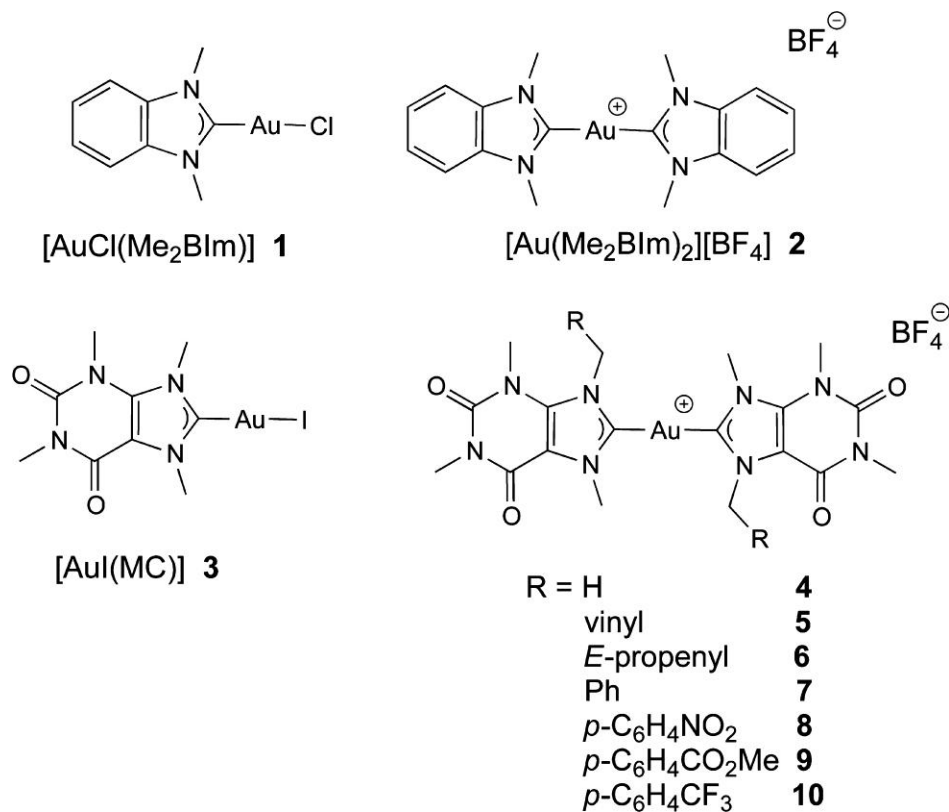


Figure 2.9 Schematic drawings of caffeine-based gold(I) *N*-heterocyclic carbenes complexes

Also, Messori *et al.* described remarkable anticancer properties *in vitro* for two novel gold carbene compounds, namely, chlorido (1-butyl-3-methylimidazole-2-ylidene) gold(I) (1) and bis(1-butyl-3-methyl-imidazole-2-ylidene) gold(I) (2) (Figure 2.10). Both compounds show a high stability in physiological-like media with no evidence of NHC or chloride detachment even over long observation times or upon challenging them with ascorbic acid or GSH. Notably, both complexes manifested similar and very pronounced antiproliferative effects toward the reference cancer cell line A2780; cisplatin resistance was completely overcome [109].

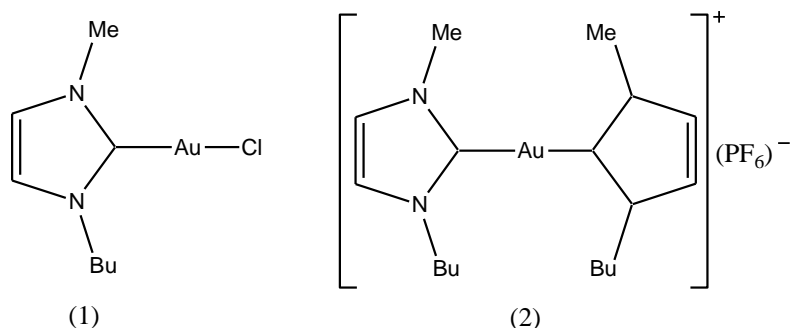


Figure 2.10 Schematic drawings of gold(I) carbene complexes

It is now a quite accepted opinion that the remarkable cytotoxic effects documented for several gold compounds are mainly the consequence of metalation and inactivation of selected crucial proteins [110]. In contrast to the availability of such diverse anticancer agents as mentioned above, gastric and prostate cancer inhibiting gold(III) agents have rarely been explored.

Maiore *et al.* recently evaluated gold(III) derivatives of 2-substituted pyridines for their biological and pharmacological behavior [110]. Palanichamy *et al.* identified four

gold(III) compounds, $[\text{Au}(\text{Phen})\text{Cl}_2]\text{PF}_6$, and its derivatives, exhibiting anticancer activity in both cisplatin sensitive and cisplatin resistant ovarian cancer cells [111]. Gabbiani *et al.* described remarkable anticancer properties *in vitro* for Au(III)bipy and Auoxo6 compounds [112]. Kouodom *et al.* suggested rational design of gold(III)-dithiocarbamate peptidomimetics for the targeted anticancer chemotherapy [113]. Lessa *et al.* reported gold(I) and gold(III) complexes with glyoxaldehyde bis(thiosemicarbazones) as cytotoxic agents against human tumor cell lines and inhibition of thioredoxin reductase activity [114]. In this connection, an attractive strategy has astutely been designed to regulate the chemical and physical behavior of biologically pertinent tetra-coordinate gold(III) complexes. Such concept is executed by inclusion of appropriate bidentate ligands in the well-known gold(III) complexes having anticancer properties.

Dithiocarbamates are versatile ligands capable of forming complexes with most of the elements and able to stabilize transition metals in a variety of oxidation states [115]. This property of stabilizing high oxidation states in metal complexes reflects strong s-bonding characteristic of these ligands. Although the sulphur atoms of dithiocarbamate ligands possess s-donor and n-back-donation characteristics of the same order of magnitude, these ligands have a special feature in that there is an additional n-electron flow from nitrogen to sulphur *via* a planar delocalized π -orbital system. This effect results in strong electron donation and hence a high electron density on the metal leading to its next higher oxidation state [116]. While dithiocarbamate complexes have been known for over a century, with many thousands having been prepared, the vast majority of these contain only simple alkyl substituents such as methyl and ethyl. A developing interest in the area of dithiocarbamate chemistry is the functionalization of the backbone such that new

applications and interactions can be developed. This area is still in its early stages but already interesting potential applications. Dithiocarbamates are a class of metal-chelating, antioxidant compounds with various applications in medicine for the treatment of bacterial and fungal infections, and possible treatment of AIDS [117-119].

It is known that amines react with CS_2 forming dithiocarbamates [120-125]. Recently, Yavari et al. [126] have reported new synthetic strategies to prepare dithiocarbamates due to their large application potential. Dithiocarbamates exhibit numerous biological activities [127-130] and they are used in agriculture [130-132] and as linkers in solid-phase organic synthesis [133-135]. Further, dithiocarbamates are also widely used in medicinal chemistry and they have found application in cancer therapy [136,138].

Gold(III)-dithiocarbamate derivatives have been designed as potential anticancer agents, showing promising and outstanding properties [139,140]. In particular, the choice of dithiocarbamates as ligands was driven by their potential chemoprotective action toward renal toxicity, a major limiting factor in the use of platinum-based therapeutics in the clinic. Strong and irreversible binding of platinum to sulfur-containing biomolecules (including thiol groups of renal enzymes) is believed to alter the conformation of the biomolecules themselves and to lead to substantial changes of their biological functions up to inactivation, thus inducing gastro-, nephro-, and bone marrow toxicity [141–143]. The accurate use and dosing of sodium diethyldithiocarbamate was proved successful in reducing cisplatin nephrotoxicity without decreasing its antitumor properties [144]. On the other hand, the overall nephroprotective benefits were somewhat limited by the acute toxicity profile, especially at neuronal level, exhibited by the free (i.e. not coordinated) dithiocarbamate [145]. Consequently, the design of metal-dithiocarbamate derivatives

has potential owing to the combination of the cytotoxicity of the metal center with the chemoprotective activity of the dithiocarbamate ligand, thus resulting in anticancer agents with high antiproliferative activity as well as reduced toxic side-effects. Moreover, along with the prevention of the intrinsic toxicity of the free dithiocarbamate, in the case of gold(III) complexes the chelating effect of the dithiocarbamate moiety is likely to stabilize the metal center in the +3 oxidation state, thus preventing reduction to gold(I) species or metallic gold (a well-known drawback of gold(III) derivatives often occurring under the normally reducing physiological conditions) [146].

Such optimistic literature reports on Au(III) complexes prompted us to carry out the synthesis of a number of mixed-ligand complexes $[\text{Au}(\text{diamine})\text{Cl}_2]^+$ with thiones such as Imt, Diaz and Diap. Accordingly, we have synthesized mixed ligand gold(III) complexes by using different diamines and thiones. These complexes have been characterized by CHNS analysis, Solid state IR and solid as well as solution NMR spectroscopic methods. Finally, the prepared Au(III)-thione complexes have also been evaluated *in vitro* as cytotoxic agents against C6 glioma cancer cell line.

CHAPTER 3

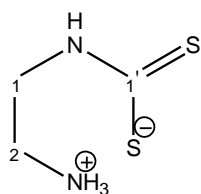
OBJECTIVES

The aim of this research is to synthesize new gold(III) complexes as potential anticancer agents. The main goals of the research work are as follows:

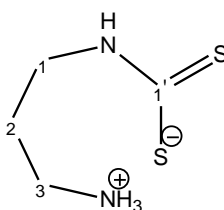
3.1 Synthesis of Dithiocarbamate Ligands

3.1.1 Synthesis of Ammonium Dithiocarbamate

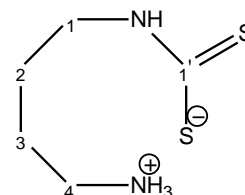
The un-substituted and mono/dialkylsubstituted diamines were used to synthesize the ammonium dithiocarbamate ligands. Their structures are shown in Figure 3.1.



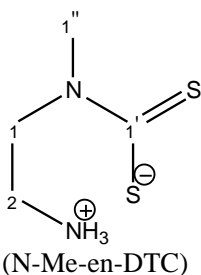
(2-Ammonioethyl)-DTC **(1)**
(en-DTC)



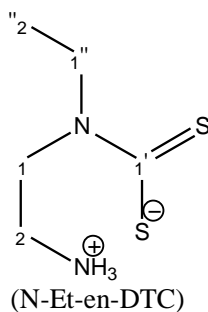
(3-Ammoniopropyl)-DTC **(2)**
(pn-DTC)



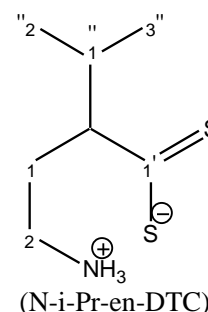
(4-Ammoniobutyl)-DTC **(3)**
(bn-DTC)



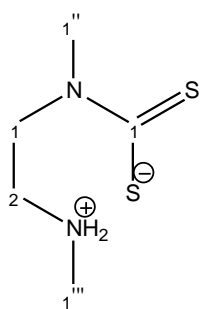
(2-Ammonioethyl)-Methyl-DTC **(4)**



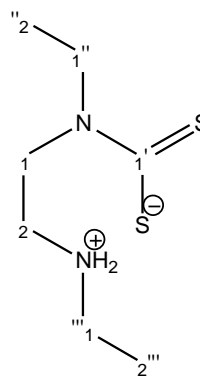
(2-Ammonioethyl)-Ethyl-DTC **(5)**



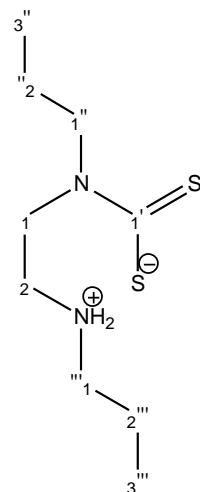
(2-Ammonioethyl)-*iso*-Propyl-DTC **(6)**



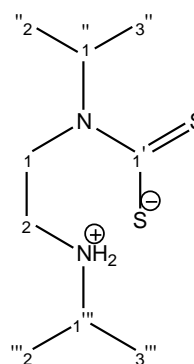
Methyl[2-(methyl ammonio)ethyl]-DTC (**7**)
N,N'-di-Me-en-DTC



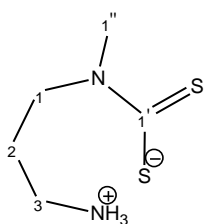
Ethyl[2-(Ethylammonio)ethyl]-DTC (**8**)
N,N'-di-Et-en-DTC



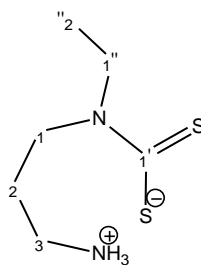
Propyl[2-(Propylammonio)ethyl]-DTC (**9**)
N,N'-di-Pr-en-DTC



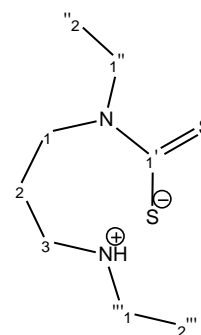
iso-Propyl[2-(*iso*-Propylammonio)ethyl]-DTC (**10**)
N,N'-di-*iso*-Pr-en-DTC



(N-Me-pn-DTC)



(N-Et-pn-DTC)



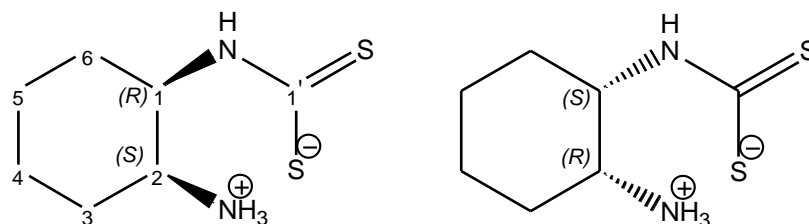
(N,N'-di-Et-pn-DTC)

(3-Ammoniopropyl)Methyl-DTC (**11**) (3-Ammoniopropyl)Ethyl-DTC (**12**) Ethyl[(3-Ethylammonio)Propyl]-DTC (**13**)

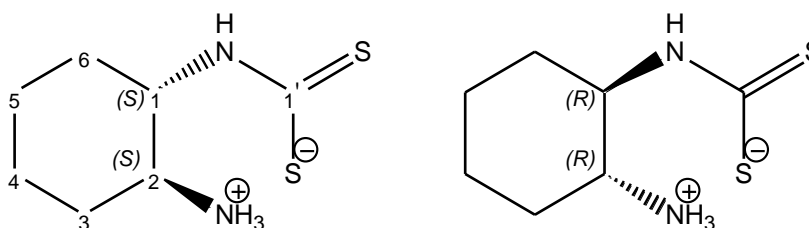
Figure 3.1 Structures of ammonium dithiocarbamate ligands

3.1.2 Synthesis of 2-Cyclohexanaminium dithiocarbamate

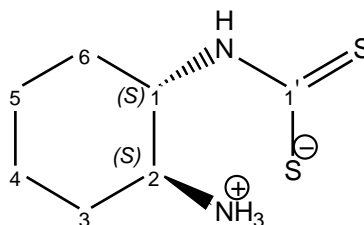
Several of 1,2-Diaminecyclohexane were used to synthesize 2-cyclohexanaminium dithiocarbamate ligands. Their structures are shown in Figure 3.2.



[*Cis*-(1,2)-2-cyclohexanaminium]dithiocarbamate (**14**)
***Cis*-(1,2)-DACH-DTC**

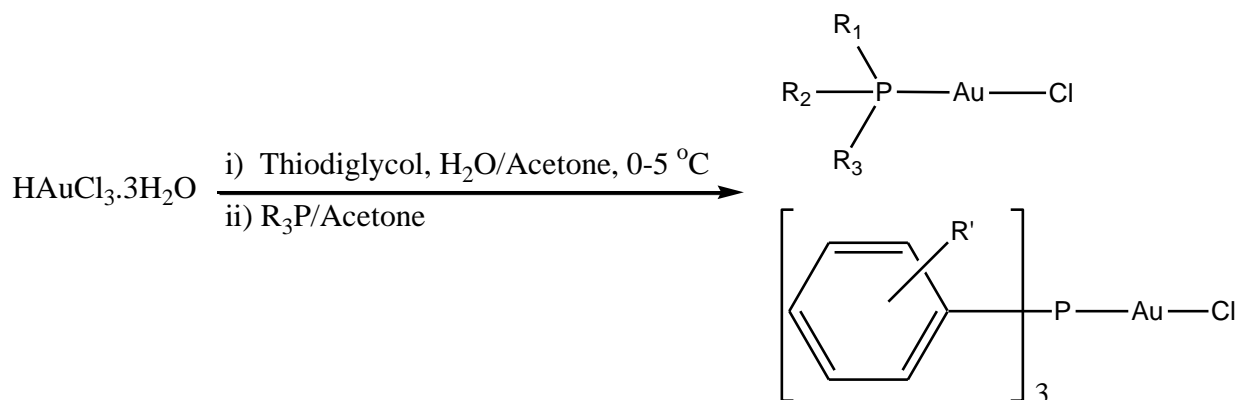


[*Trans*-(1,2)-2-cyclohexanaminium]dithiocarbamate (**15**)
***Trans*-(±)-(1,2)-DACH-DTC**



[*Trans*-(+)-(1*S*,2*S*)-2-cyclohexanaminium]dithiocarbamate (**16**)
[*Trans*-(+)-(1*S*,2*S*)-DACH-DTC

Figure 3.2 Structures 2-cyclohexanaminium dithiocarbamate ligands



Chlorido Phosphane gold(I)

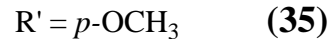
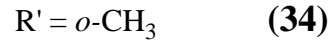
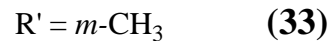
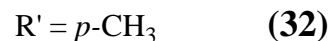
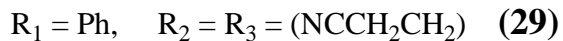
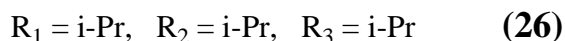
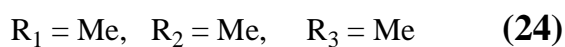
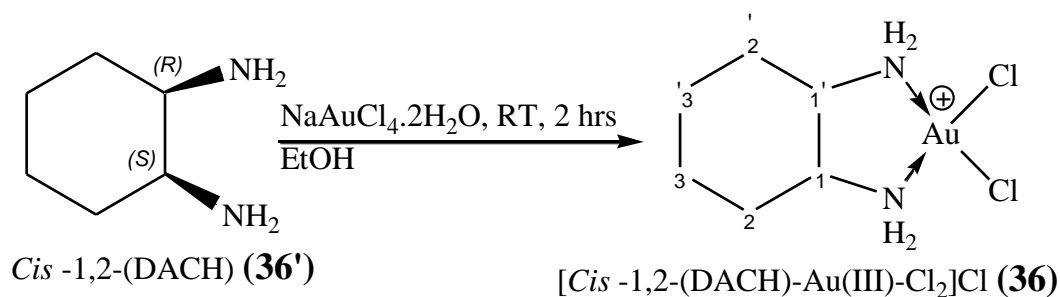


Figure 3.4 Structures of phosphane gold(I) chloride complexes

3.3 Synthesis of Dichlorido(1,2-diaminocyclohexane)gold(III) Chloride Complexes

Various isomers of 1,2-diaminocyclohexane (1,2-DACH) shown in Figure 3.5 were used to synthesize the following dichlorido-1,2-(DACH)gold(III)chloride complexes:



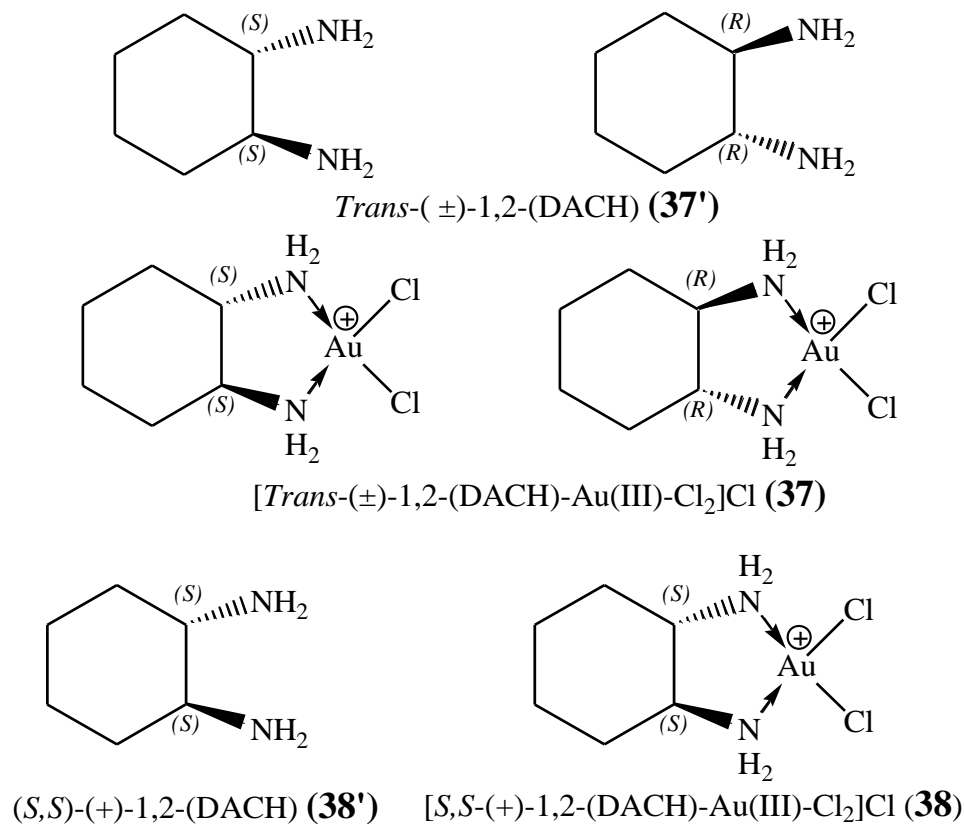


Figure 3.5 Structures of dichlorido-1,2-diaminocyclohexane gold(III) chloride complexes

3.4 Synthesis of Azanechlorido(1,2-Diaminocyclohexane)gold(III) Chloride Complexes

Various 1,2-diaminocyclohexane gold(III) chloride were used to synthesize new azanechlorido(1,2-diaminocyclohexane)gold(III)chloride[1,2-(DACH)Au(III)(NH₃)Cl]Cl₂ complexes as shown in Figure 3.6.

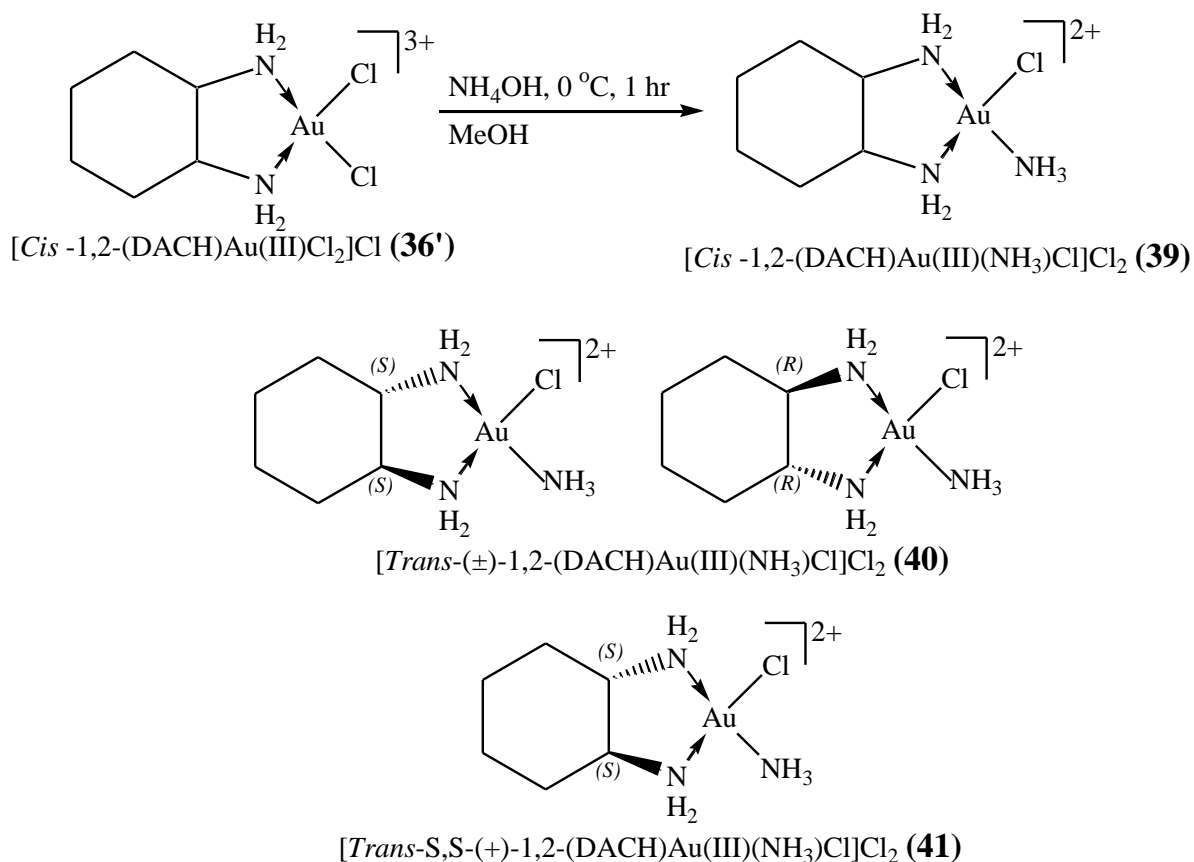


Figure 3.6 Structures of azane chlorido 1,2-diaminocyclohexane gold(III) chloride complexes

3.5 Synthesis of Diazane(1,2-diaminocyclohexane)gold(III) Chloride Complexes

Dichlorido(1,2-diaminocyclohexane)gold(III) chloride were used to synthesize a new diazane(1,2-diaminocyclohexane)gold(III) chloride complexes [1,2-(DACH)Au(III)(NH₃)₂]Cl₃ complexes as shown in Figure 3.7.

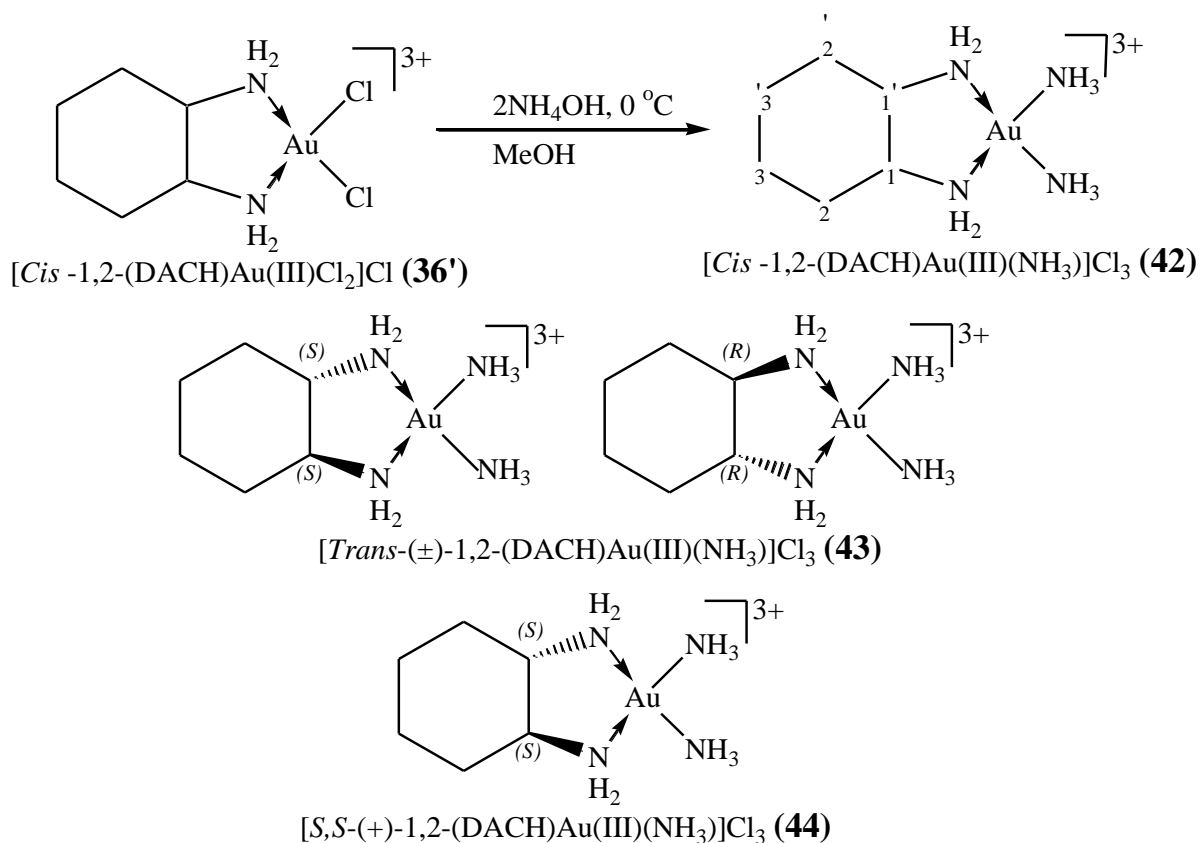
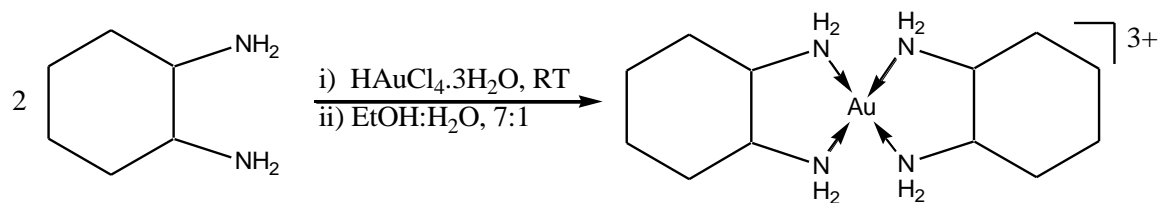
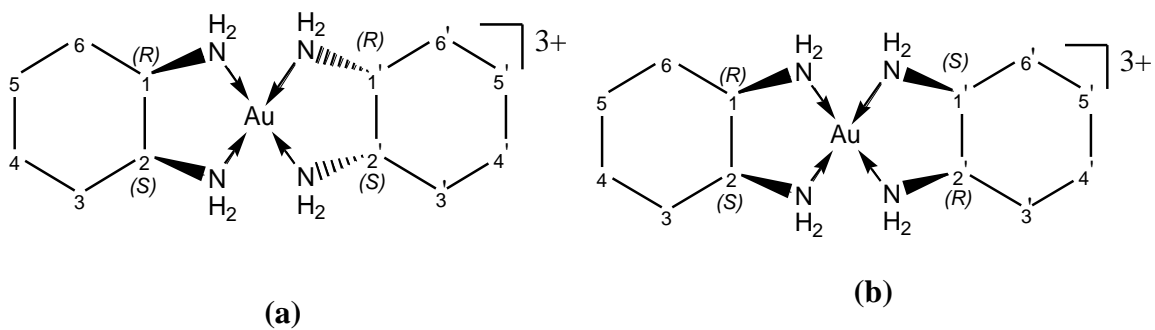


Figure 3.7 Structures of diazane 1,2-diaminocyclohexane gold(III) chloride complexes

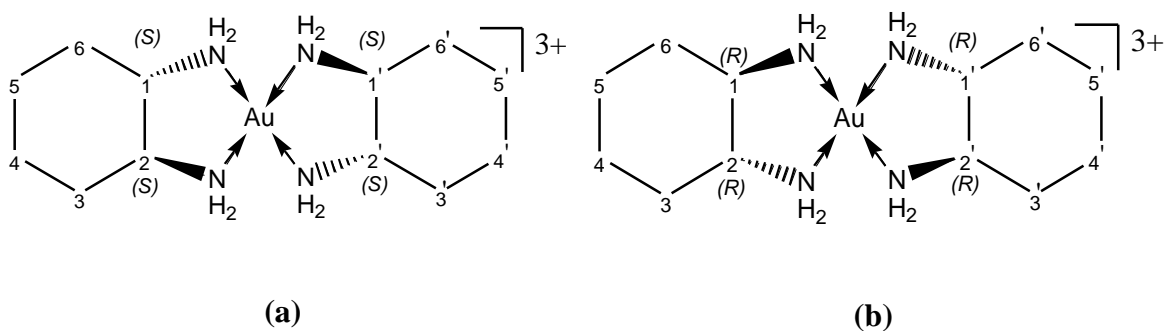
3.6 Synthesis of Bis(1,2-Diaminocyclohexane)gold(III)Chloride Complexes

Various 1,2-diaminocyclohexane were used to synthesize the bis(1,2-diaminocyclohexane)gold(III)chloride complexes as shown in Figure 3.8.





[[*Cis*-1,2-DACH)₂Au(III)]Cl₃ (**45**)



[[*Trans*-(±)-1,2-(DACH)₂Au]Cl₃(**46**)

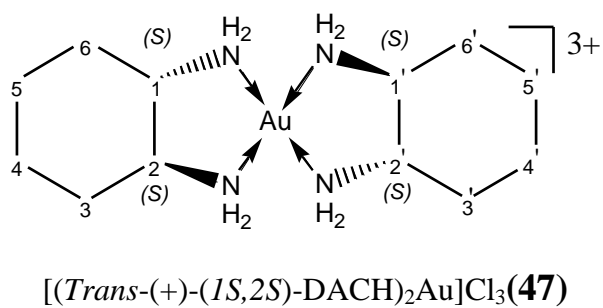
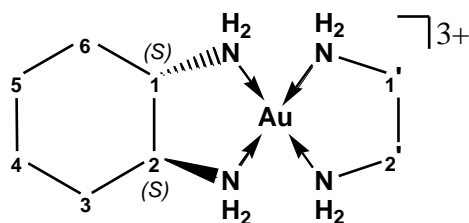
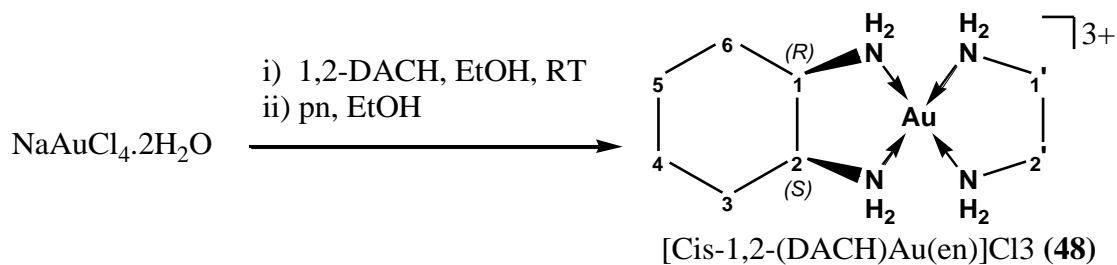


Figure 3.8 Predicted structure of the synthesized bis(1,2-diaminocyclohexane)gold(III) chloride complexes

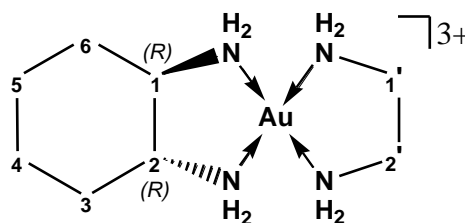
3.7 Synthesis of 1,2-Diaminocyclohexane(ethylenediamine)gold(III)

Chloride Complexes

Various 1,2-diaminocyclohexane, ethylenediamine and $\text{NaAuCl}_4 \cdot 2\text{H}_2\text{O}$ were used to synthesize the 1,2-diaminocyclohexane(ethylenediamine)gold(III) chloride complexes as shown in Figure 3.9.

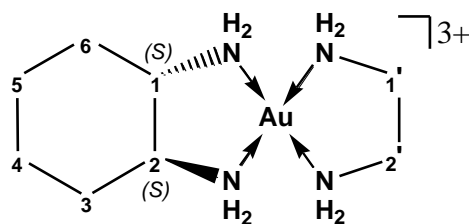


(a)



(b)

[Trans-(±)-1,2-(DACH)Au(en)]Cl₃ (**49**)



[(1S,2S)-(+)-1,2-(DACH)Au(en)]Cl₃ (**50**)

Figure 3.9 Predicted chemical structure of 1,2-diaminocyclohexane(ethylenediamine)gold(III)chloride complexes

3.8 Synthesis of 1,2-Diaminocyclohexane(propylenediamine)gold(III)

Chloride Complexes

Various 1,2-diaminocyclohexane,propylenediamine and $\text{NaAuCl}_4 \cdot 2\text{H}_2\text{O}$ with were used to synthesize the 1,2-diaminocyclohexane(propylenediamine)gold(III) chloride complexes as shown in Figure 3.10.

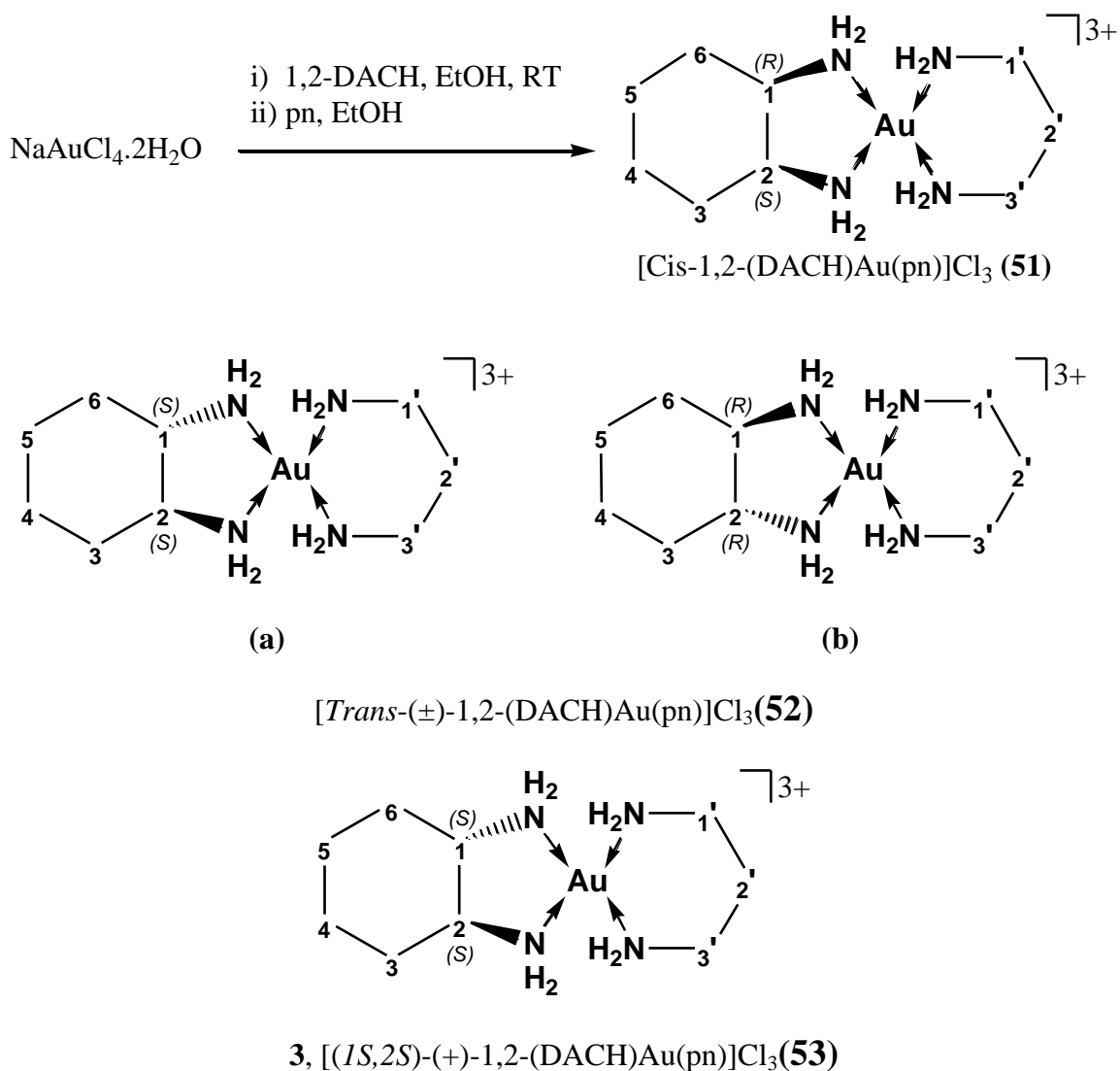
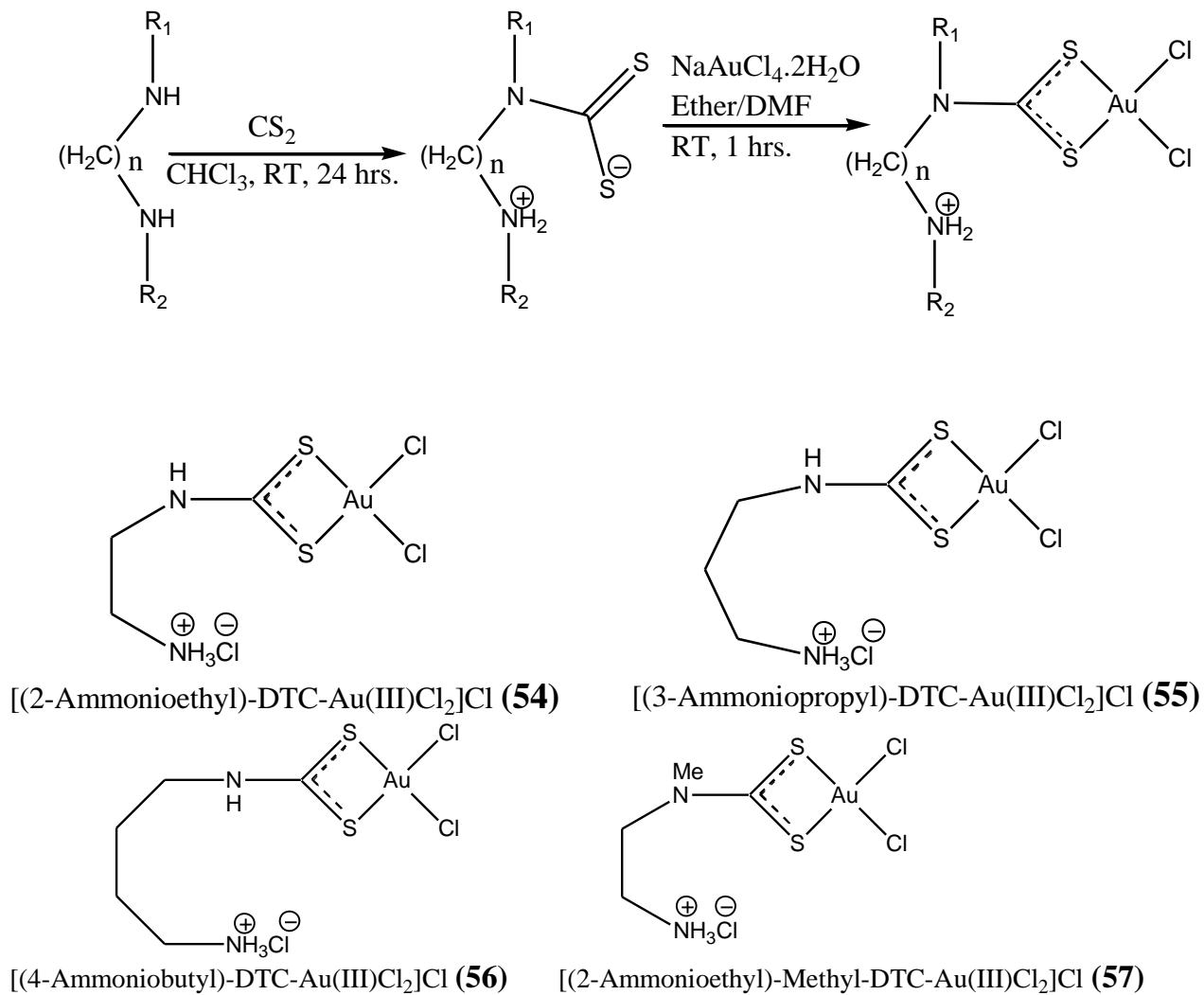


Figure 3.10 Predicted chemical structure of 1,2-diaminocyclohexane(propylenediamine)gold(III) chloride complexes

3.9 Synthesis of Ammoniumdithiocarbamatodichloridogold(III)

Chloride Complexes

Synthesized ammoniumdithiocarbamate ligands were used to synthesize ammoniumdithiocarbamatodichloridogold(III) chloride complexes as shown in Figure 3.11.



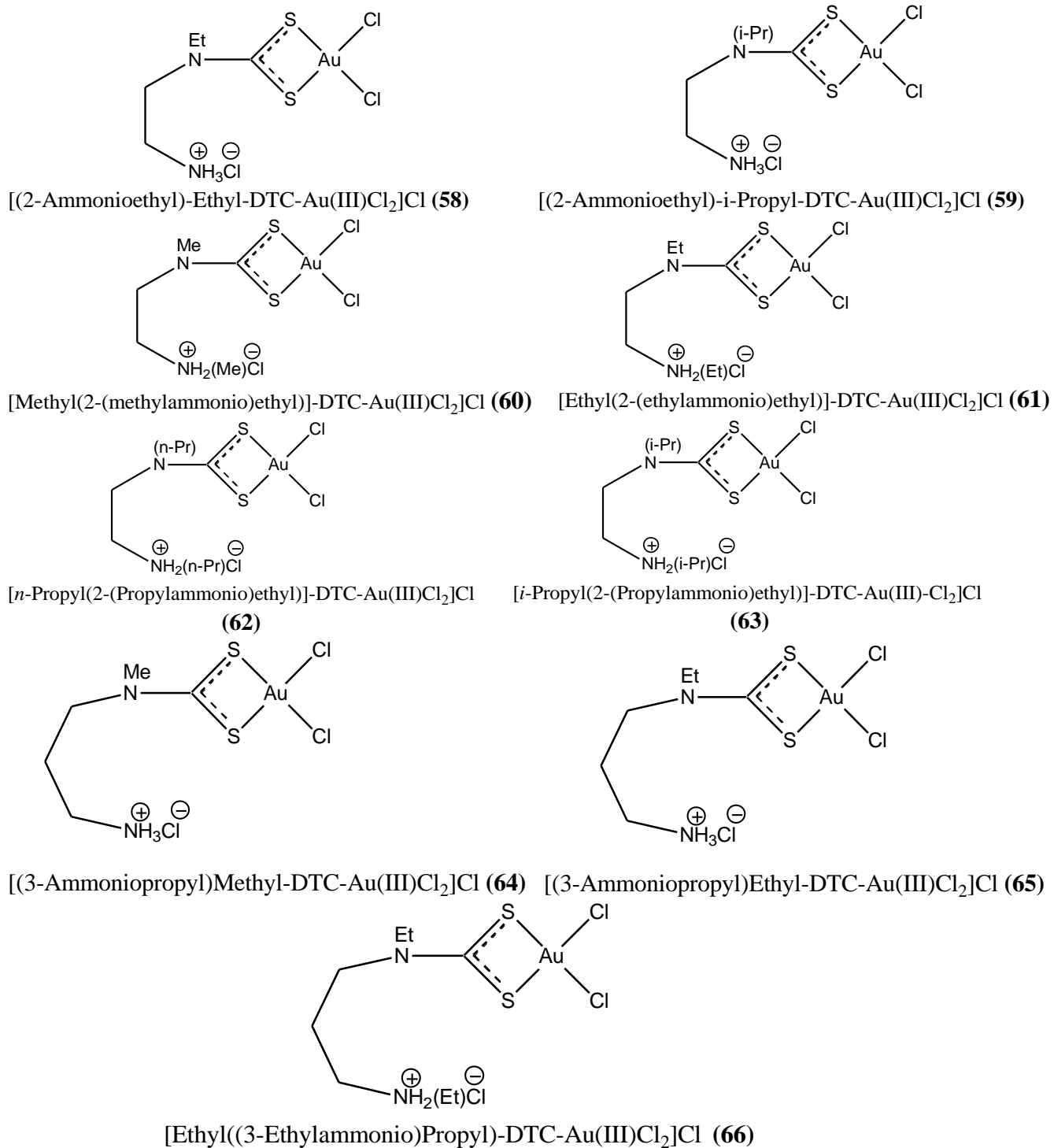
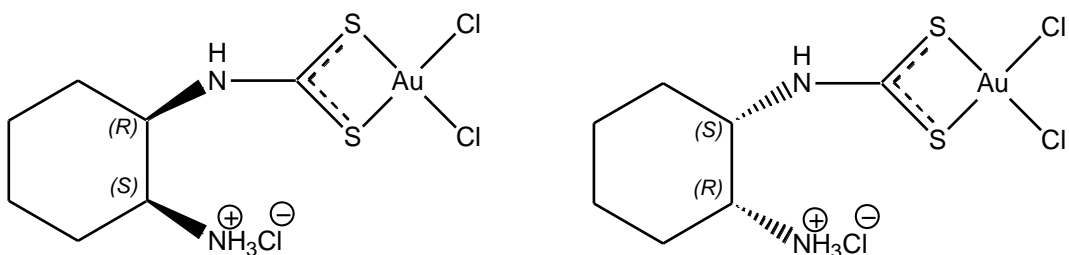


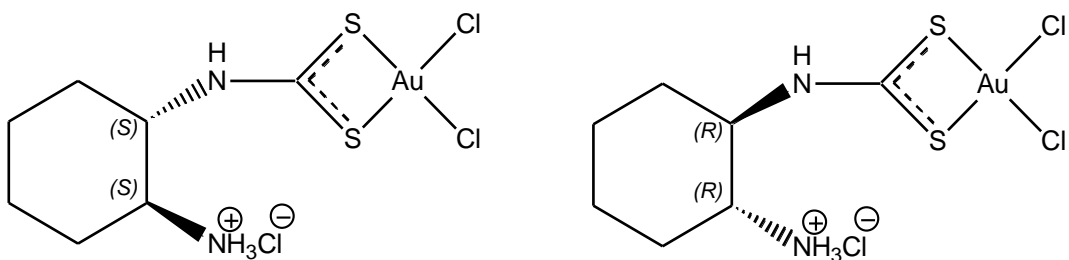
Figure 3.11 Chemical structure of ammoniumdithiocarbamate(dichlorido)gold(III) chloride complexes

3.10 Synthesis of Dichlorido(2-cyclohexanaminiumdithiocarbamato)gold(III) Chloride Complexes

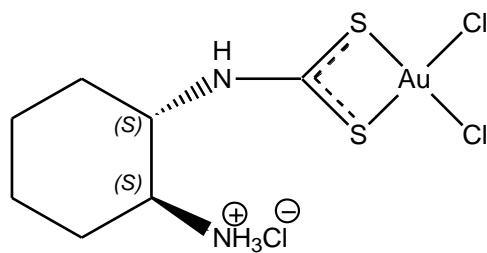
2-Cyclohexanaminium dithiocarbamate ligands were used to synthesize dichlorido(2-cyclohexanaminiumdithiocarbamato)gold(III) chloride complexes as shown in Figure 3.12.



[(*Cis*-(1,2)-2-cyclohexanaminium)-dithiocarbamate gold(III)Cl₂]Cl (**67**)



[(*Trans*-(±)-(1,2)-2-cyclohexanaminium)-dithiocarbamate gold(III)Cl₂]Cl (**68**)



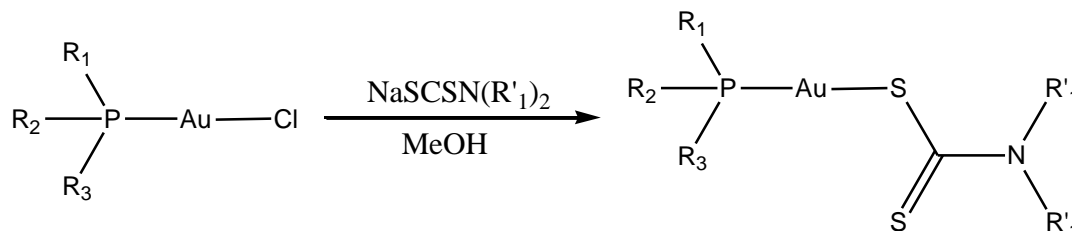
[(*Trans*-(+)-(1*S*,2*S*)-2-cyclohexanaminium)-dithiocarbamate gold(III)Cl₂]Cl (**69**)

Figure 3.12 Chemical structure of dichlorido(2-cyclohexanaminiumdithiocarbamato)gold(III)chloride complexes

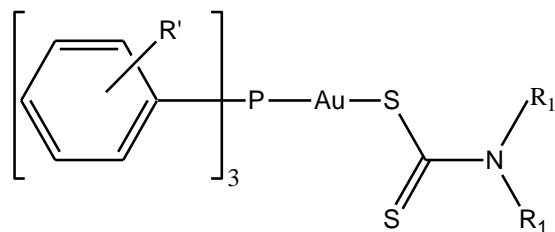
3.11 Synthesis of Mixed-Ligand Dithiocarbamatophosphanegold(I) Complexes

Complexes

Various chloridotrialkylphosphanegold(I) with *n,n'*-di-alkyl-dithiocarbamate were used to synthesize dithiocarbamatophosphanegold(I) complexes as shown in Figure 3.13.



$R_1 = \text{Me}, R_2 = \text{Me}, R_3 = \text{Me},$	$R'_1 = \text{Me}$	(70)
$R_1 = \text{Me}, R_2 = \text{Me}, R_3 = \text{Me},$	$R'_1 = \text{Et}$	(71)
$R_1 = \text{Et}, R_2 = \text{Et}, R_3 = \text{Et},$	$R'_1 = \text{Me}$	(72)
$R_1 = \text{Et}, R_2 = \text{Et}, R_3 = \text{Et},$	$R'_1 = \text{Et}$	(73)
$R_1 = i\text{-Pr}, R_2 = i\text{-Pr}, R_3 = i\text{-Pr},$	$R'_1 = \text{Me}$	(74)
$R_1 = i\text{-Pr}, R_2 = i\text{-Pr}, R_3 = i\text{-Pr},$	$R'_1 = \text{Et}$	(75)
$R_1 = \text{Ph}, R_2 = \text{Ph}, R_3 = \text{Cy},$	$R'_1 = \text{Me}$	(76)
$R_1 = \text{Ph}, R_2 = \text{Ph}, R_3 = \text{Cy},$	$R'_1 = \text{Et}$	(77)
$R_1 = \text{Ph}, R_2 = \text{Ph}, R_3 = \text{Et},$	$R'_1 = \text{Me}$	(78)
$R_1 = \text{Ph}, R_2 = \text{Ph}, R_3 = \text{Et},$	$R'_1 = \text{Et}$	(78)
$R_1 = \text{Ph}, R_2 = R_3 = (\text{NCCH}_2\text{CH}_2),$	$R'_1 = \text{Me}$	(80)
$R_1 = \text{Ph}, R_2 = R_3 = (\text{NCCH}_2\text{CH}_2),$	$R'_1 = \text{Et}$	(81)
$R_1 = R_2 = R_3 = (\text{NCCH}_2\text{CH}_2),$	$R'_1 = \text{Me}$	(82)
$R_1 = R_2 = R_3 = (\text{NCCH}_2\text{CH}_2),$	$R'_1 = \text{Et}$	(83)



$R' = \text{H},$	$R_1 = \text{Me}$	(84)	$R' = m\text{-CH}_3,$	$R_1 = \text{Et}$	(89)
$R' = \text{H},$	$R_1 = \text{Et}$	(85)	$R' = o\text{-CH}_3,$	$R_1 = \text{Me}$	(90)
$R' = p\text{-CH}_3,$	$R_1 = \text{Me}$	(86)	$R' = o\text{-CH}_3,$	$R_1 = \text{Et}$	(91)
$R' = p\text{-CH}_3,$	$R_1 = \text{Et}$	(87)	$R' = p\text{-OCH}_3,$	$R_1 = \text{Me}$	(92)
$R' = m\text{-CH}_3,$	$R_1 = \text{Me}$	(88)	$R' = p\text{-OCH}_3,$	$R_1 = \text{Et}$	(93)

Figure 3.13 Chemical structure of dithiocarbamato(trialkylphosphane)gold(I) complexes

3.12 Synthesis of Mixed-Ligand 5-Methyl-2-mercaptobenzimidazolo(phosphane)gold(I) Complexes

Various chloridophosphanegold(I) with 5-methyl-2-mercaptobenzimidazole were used to synthesize 5-methyl-2-mercaptobenzimidazolo(phosphane)gold(I) complexes as shown in Figure 3.14.

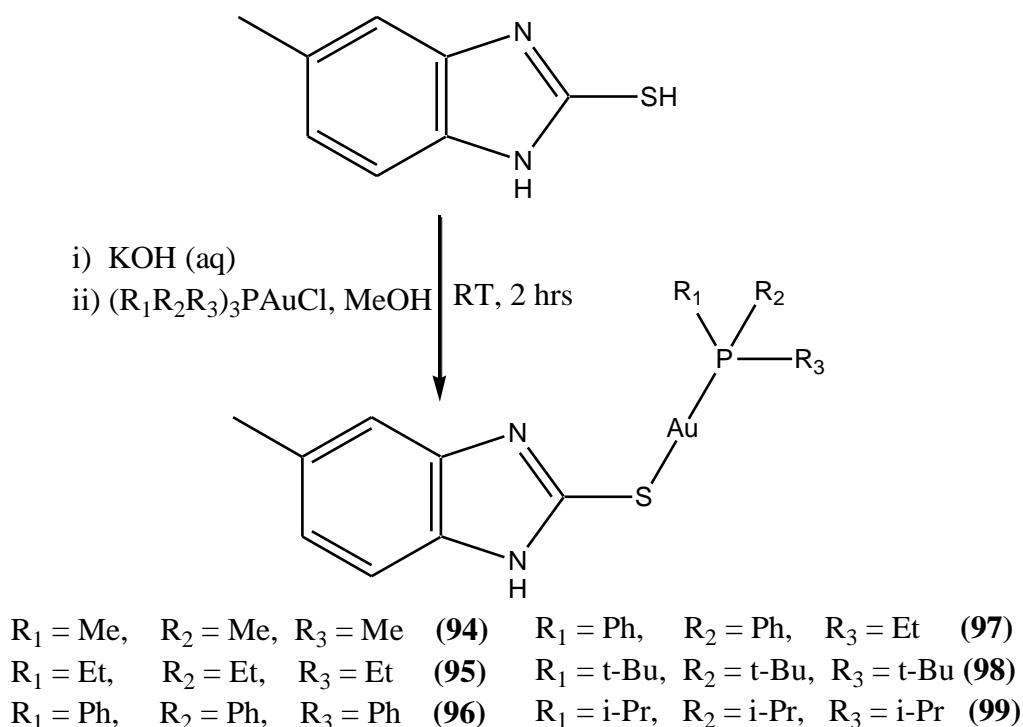


Figure 3.14 Chemical structure of 5-methyl-2-mercaptobenzimidazolo(phosphane)gold(I) complexes

3.13 Synthesis of Mixed-Ligand Substituted 2-mercaptobenzimidazolo(trimethylphosphane)gold(I) Complexes

Various substituted 2-mercaptobenzimidazole with chloridotrimethylphosphanegold(I) were used to synthesize substituted 2-mercaptobenzimidazolo(trimethylphosphane)gold(I) complexes as shown in Figure 3.15.

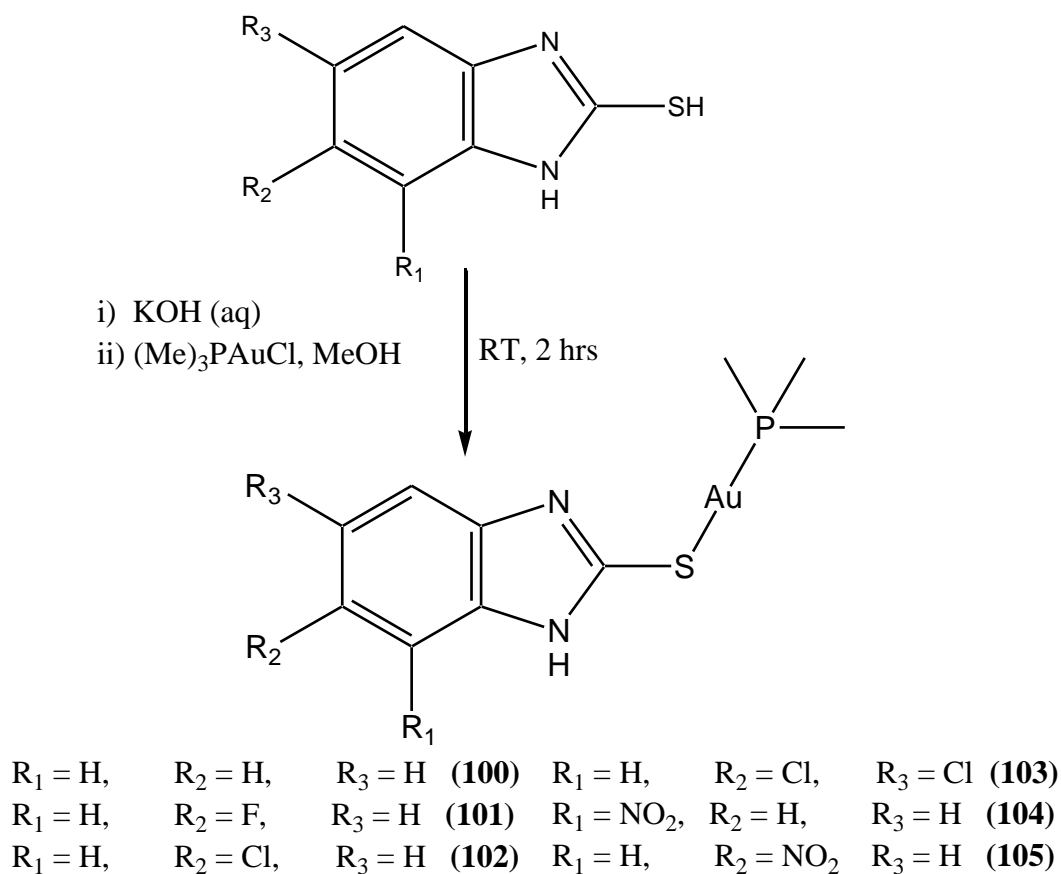


Figure 3.15 Chemical structure of 5-methyl-2-mercaptobenzimidazolo(phosphane)gold(I) complexes

3.14 Synthesis of Mixed-Ligand 4-Nitro-2-mercaptobenzimidazolo(phosphane)gold(I) Complexes

Various chloridophosphanegold(I) with 4-nitro-2-mercaptobenzimidazole were used to synthesize 4-nitro-2-mercaptobenzimidazolo(phosphane)gold(I) complexes as shown in Figure 3.16.

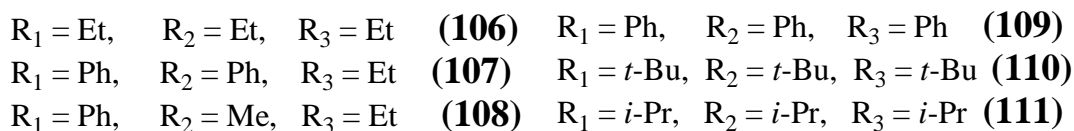
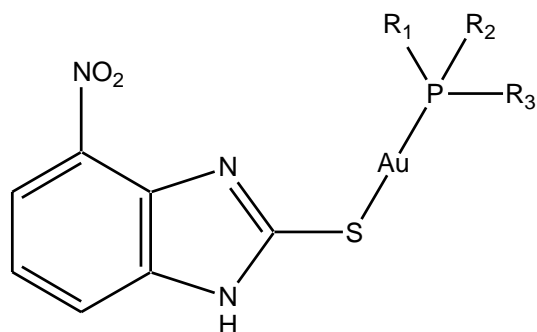


Figure 3.16 Chemical structure of 4-nitro-2-mercaptobenzimidazolo(phosphane)gold(I) complexes

3.15 Synthesis of Mixed-Ligand 5-Nitro-2-mercaptobenzimidazolo(phosphane)gold(I) Complexes

Various chloridophosphanegold(I) with 5-nitro-2-mercaptobenzimidazole were used to synthesize 5-nitro-2-mercaptobenzimidazolo(phosphane)gold(I) complexes as shown in Figure 3.17.

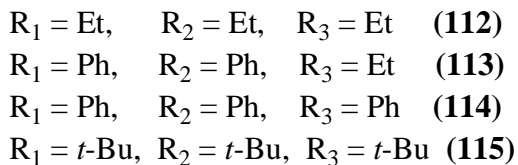
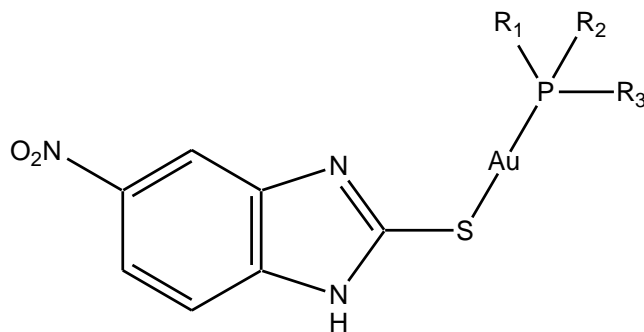


Figure 3.17 Chemical structure of 5-nitro-2-mercaptobenzimidazolo(phosphane)gold(I) complexes

3.16 Synthesis of Substituted 2-Mercaptobenzimidazolo1,3-Bis(2,6-di-isopropylphenyl)imidazol-2-ylidene Gold(I) Complexes

Various substituted 2-mercaptobenzimidazole with chlorido1,3-bis(2,6-di-isopropylphenyl)imidazol-2-ylidene gold(I) were used to synthesize substituted IPr 2-mercaptobenzimidazolo gold(I) (IPr = 1,3-bis(2,6-di-isopropylphenyl)imidazol-2-ylidene) as shown in Figure 3.18.

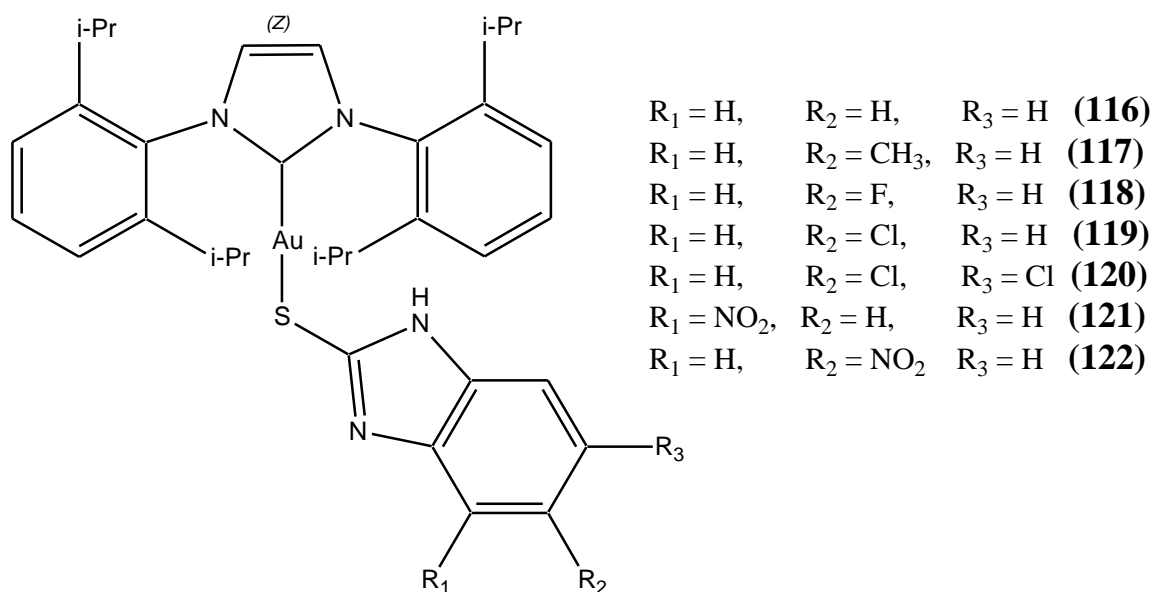


Figure 3.18 Chemical structure of IPr(2-mercaptobenzimidazolo)gold(I) complexes

3.17 Synthesis of Dinuclear2-MBI{1,3-bis(diphenylphosphino)methane}gold(I)Complexes

Various substituted 2-mercaptobenzimidazole with dichlorido1,3-bis(diphenylphosphino)methane gold(I) were used to synthesize dinuclear2-MBI{1,3-bis(diphenylphosphino)methane}gold(I) complexes as shown in Figure 3.19.

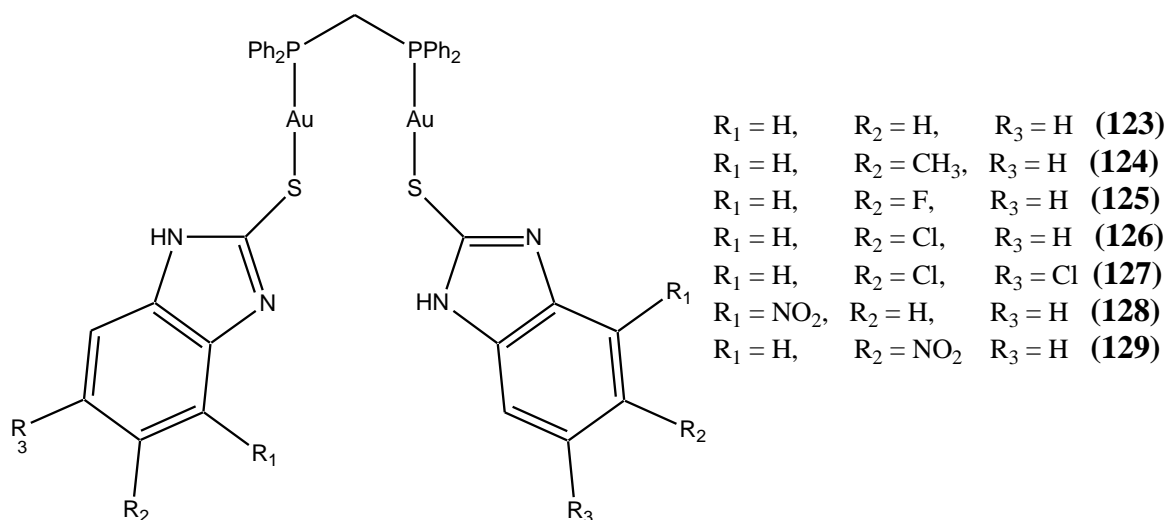


Figure 3.19 Chemical structure of dinuclear2-MBI{1,3-bis(diphenylphosphino)methane}gold(I)complexes

3.18 Characterization of GoldComplexes

The complexes (1)-(129) were characterized by melting point (MP) and elemental analysis techniques.

3.19 Structural Analysis of GoldComplexes

The complexes werethen structurally analyzed by Mid Infrared (MIR), Far Infrared (FIR) and Ultra-Violet (UV)/Visible (Vis) spectroscopic methods; 1H , ^{13}C , ^{15}N solution and ^{13}C solid state Nuclear Magnetic Resonance (NMR) measurements. X-ray crystallography was employed for structure determination of crystalline complexes.

3.20 Study of Anticancer Properties of Gold Complexes

The anticancer properties of gold complexes were studied *in-vitro* against a panel of human cancer cell lines in order to evaluate their potential as possible anticancer agents.

3.21 Study of Electrochemical Properties of Gold Complexes

The cyclic voltammetry behaviors of gold complexes were studied to determine the complexes' reduction potentials in order to evaluate their stabilities.

CHAPTER 4

EXPERIMENTAL

4.1 Chemicals

$\text{HAuCl}_4 \cdot 3\text{H}_2\text{O}$ was obtained from Strem Chemicals Co., while acetone, absolute ethanol, acetonitrile, D_2O and CD_3OD were obtained from Fluka Chemicals Co. 1,2-Diaminoethane, 1,3-Diaminopropane, 1,4-Diaminobutane, N-ethyl-1,2-diaminoethane, N-propyl-1,2-diaminoethane and N-isopropyl-1,2-diaminoethane were purchased from Sigma Aldrich. N,N'-dimethyl-1,2-diaminoethane, N,N'-diethyl-1,2-diaminoethane, N,N'-dipropyl-1,2-diaminoethane and N,N'-diisopropyl-1,2-diaminoethane were obtained from Alfa Aesar.

Imidazole, L-histidine and L-glycine were obtained from Sigma-Aldrich, L- ^{13}C -cysteine and L-methionine were obtained from Isotech, USA. Sodium tetrachloroaurate (III) dihydrate, Imidazolidine-2-thione (Imt), 1,3-Diazinane-2-thione (Diaz), 1,3-Diazipane-2-thione (Diap), Imidazole, were purchased from Sigma-Aldrich.

Potassium cyanide was purchased from Fisher Scientific Co. Potassium thiocyanate was obtained from J. T. Baker Chemicals Co. The ^{15}N label diamines ligands and ^{15}N and ^{13}C label potassium cyanide were obtained from Cambridge Isotope Labs, USA. All other reagents as well as solvents were obtained from Aldrich Chemical Co., and used as received.

4.2 Cell Lines

Human gastric SGC7901 and prostate PC3 cancer cell lines were provided by American Type Culture Collection (ATCC). Cells were cultured in Dulbecco's Modified Eagle Medium (DMEM) supplemented with 10 % Fetal Calf Serum (FCS), penicillin (100 kU L⁻¹) and streptomycin (0.1 g L⁻¹) at 37 °C in a 5 % CO₂-95 % air atmosphere. MTT (3-(4,5-Dimethylthiazol-2-yl)-2,5-diphenyltetrazolium bromide, a yellow tetrazole) was purchased from Sigma Chemical Co, St.Louis, MO, USA.

4.3 Synthesis of Dithiocarbamate Ligands

All reactions were generally carried out using research grade chemicals and solvents. All ligands were subsequently characterized by melting point (MP) and elemental analysis techniques. Elemental analyses were performed on Perkin Elmer Series 11 (CHNS/O), Analyzer 2400. Melting points for complexes were carried out on BÜCHI 510 melting point apparatus.

4.3.1 Synthesis of AmmoniumdithiocarbamateLigands

The synthesis of ammonium dithiocarbamate ligands(1)-(13)were according to a modified literature procedure[147], by dissolving of 30 mmol of un-substituted and mono/dialkylsubstituted diamines in 70 ml of CHCl₃. In a separate beaker, solution of 2.6 g (35 mmol) of CS₂in 10 ml CHCl₃was prepared. The previous solution was added dropwise to the later solution at 0 °C and stirred for overnight at RTcausing precipitation of a white product. This was filtered and washed with CHCl₃(10 mL) and air-dried. The product yield was in the range of 91-95 %

Products were characterized by melting point (M.P.) and elemental analysis as given in Table 4.1 Melting point and Elemental analysis of ammonium dithiocarbamate ligands and their predicted chemical structures are shown in Figure 3.1.

Table 4.1 Melting point and Elemental analysis of ammonium dithiocarbamate ligands

Ligand	M. P. (°C)	Found (Calculated) %			
		%C	%H	%N	%S
(2-Ammonioethyl)-DTC (1)	-	26.12(26.45)	5.93(5.92)	20.47(20.56)	47.12(47.07)
(3-Ammoniopropyl)-DTC (2)	-	31.85(31.97)	6.68(6.71)	18.59(18.64)	42.59(42.68)
(4-Ammoniobutyl)-DTC (3)	-	36.34(36.55)	7.12(7.36)	17.12(17.05)	38.94(39.03)
(2-Ammonioethyl)-Methyl-DTC (4)	142-144	31.87(31.97)	6.62(6.71)	18.59(18.64)	42.75(42.68)
(2-Ammonioethyl)-Ethyl-DTC (5)	138-140	36.39(36.55)	7.41(7.36)	17.12(17.05)	39.12(39.03)
(2-Ammonioethyl)- <i>iso</i> -Propyl-DTC (6)	127-129	40.32(40.41)	7.83(7.91)	15.76(15.71)	36.12(35.96)
Methyl[2-(methylammonio)ethyl]-DTC (7)	149-151	36.37(36.55)	7.42(7.36)	17.09(17.05)	39.11(39.03)
Ethyl[2-(ethylammonio)ethyl]-DTC (8)	139-141	43.64(43.71)	8.43(8.38)	14.43(14.56)	33.19(33.34)
<i>n</i> -Propyl[2-(<i>n</i> -propylammonio)ethyl]-DTC (9)	145-147	48.93(49.05)	9.06(9.15)	12.64(12.71)	29.19(29.10)
<i>iso</i> -Propyl[2-(<i>iso</i> -propylammonio)ethyl]-DTC (10)	139-141	49.12(49.05)	9.11(9.15)	12.77(12.71)	29.16(29.10)
(3-Ammoniopropyl)methyl-DTC (11)	144-146	36.73(36.55)	7.42(7.36)	17.09(17.05)	39.11(39.03)
(3-Ammoniopropyl)ethyl-DTC (12)	135-137	40.37(40.41)	7.95(7.91)	15.67(15.71)	35.84(35.96)
Ethyl[3-(ethylammonio)propyl]-DTC (13)	163-165	46.43(46.56)	8.83(8.79)	13.62(13.57)	31.15(31.08)

4.3.2 Synthesis of 2-Cyclohexanaminium Dithiocarbamate Ligands

The synthesis of 2-cyclohexanaminium dithiocarbamate ligands(**14**)-(16) were according to a modified literature procedure[147], by dissolving of 3.42 g (30 mmol) of (1,2)-diaminocyclohexane in 70 ml of CHCl₃. In a separate beaker, solution of 2.6 g (35 mmol) of CS₂ in 10 ml CHCl₃ was prepared. The previous solution was added dropwise to

the later solution at 0 °C and stirred overnight at RT causing precipitation of a white product. This was filtered and washed with CHCl₃(10 mL) and air-dried. The product yield was in the range of 91-93 %

Products were characterized by elemental analysis as given in Table 4.2 Melting point and elemental analysis of 2-cyclohexanaminium dithiocarbamate ligands and their predicted chemical structures are shown in Figure 3.2.

Table 4.2 Melting point and elemental analysis of 2-cyclohexanaminium dithiocarbamate ligands

Complex	Found (Calculated) %			
	%C	%H	%N	%S
[<i>cis</i> -(1,2)-2-cyclohexanaminium]-DTC (13)	44.22(44.17)	7.46(7.41)	17.75(14.72)	33.75(33.69)
[<i>trans</i> -(±)-(1,2)-2-cyclohexanaminium]-DTC (14)	44.25(44.17)	7.48(7.41)	17.68(14.72)	33.78(33.69)
[<i>trans</i> -(+)-(1,2)-2-cyclohexanaminium]-DTC (15)	44.21(44.17)	7.39(7.41)	17.79(14.72)	33.73(33.69)

4.3.3 Synthesis of 2-Mercaptobenzimidazole Ligands

The synthesis of substituted 2-mercaptobenzimidazole ligands(**17**)-(**23**) were according to a literature procedure[148], by mixing of 15 mmol of substituted-*o*-phenylenediamine and 841 mg (15mmol) of potassium hydroxide with 1.29 g (17mmol) of carbon disulfide in 50 ml of 95% ethanol and 7 ml of water in a 250 ml round bottom flask heated under reflux for 3 hours except complexes (**22**) and (**23**) were refluxed for 24 hrs in presence of Et₃N as a catalyst. Then added 1-1.5 g of charcoal cautiously and the mixture is further heated at the reflux for 10 minutes the charcoal is removed by filtration. The filtrate is heated to 60-70°C, 100 ml of warm water is then added and acidified with dilute acetic acid with good stirring (pH = 4-5). The product separated as glistening colored crystals. The mixture is placed in a refrigerator for overnight to complete the crystallization. The

product is collected on a buckner funnel and dried over night at 40°C. The dried product was recrystallised with ethanol. The product yield was in the range of 90-93 %. Products were characterized by melting point (M.P.) and elemental analysis as given in Table 4.3 Melting point and elemental analysis of Table 4.3 Melting point and elemental analysis of and their predicted chemical structures are shown in Figure 3.3.

Table 4.3 Melting point and elemental analysis of substituted 2-mercaptobenzimidazole ligands

Ligand	M. P. (°C)	Found (Calculated) %			
		%C	%H	%N	%S
2-Mercaptobenzimidazole (17)	303-304	55.72(55.97)	4.09(4.03)	18.53(18.65)	21.29(21.35)
5-Me-2-Mercaptobenzimidazole (18)	294-296	58.25(58.51)	5.05(4.91)	16.98(17.06)	19.48(19.53)
5-F-2-Mercaptobenzimidazole (19)	293-294	49.84(49.99)	3.06(3.00)	16.49(16.66)	19.01(19.07)
5-Cl-2-Mercaptobenzimidazole (20)	308-310	45.22(45.53)	2.81(2.73)	15.05(15.17)	17.28(17.35)
5,6-di-Cl-2-Mercaptobenzimidazole (21)	244-246	38.25(38.37)	1.89(1.84)	12.68(12.79)	14.78(14.64)
5-NO ₂ -2-Mercaptobenzimidazole (22)	283-285	43.01(43.07)	2.62(2.58)	21.48(21.53)	16.33(16.43)
4-NO ₂ -2-Mercaptobenzimidazole (23)	349-351	42.98(43.07)	2.63(2.58)	21.45(21.53)	16.28(16.43)

4.4 Synthesis of Chlorido(phosphane)gold(I) Precursor Complexes

HAuCl₄.3H₂O was reduced by thiodiglycol in aqueous acetone. The solution was cooled to 0-5 °C and added dropwise to a solution of R₃P in acetone. A clear colorless solution resulted; this was stirred for 30 min; then the solvent was concentrated by evaporation at room temperature. The products of chloridophosphanegold(I) complexes (**24**)-(b25) were obtained as a white to cream-colored solid by addition of water and was recrystallized from aqueous methanol and dried overnight in a vacuum at 30 °C [149].The products were in the range 76-93%

Products were characterized by elemental analysis as given in Table 4.4 Melting point and elemental analysis of chloridophosphanegold(I) complexes and their predicted chemical structures are shown in Figure 3.4.

Table 4.4 Melting point and elemental analysis of chloridophosphanegold(I) complexes

Complex	Found (Calculated) %	
	%C	%H
(Me) ₃ PAuCl (24)	11.62(11.68)	2.99(2.94)
(Et) ₃ PAuCl (25)	20.43(20.56)	4.35(4.31)
(<i>i</i> -Pr) ₃ PAuCl (26)	27.42(27.53)	5.47(5.39)
(Ph) ₂ (Cy)PAuCl (27)	43.03(43.17)	4.28(4.23)
(Ph) ₂ (Et)PAuCl (28)	37.52(37.65)	3.43(3.38)
(Ph)(NCCH ₂ CH ₂) ₂ PAuCl (29)	32.02(32.13)	2.97(2.92)
(NCCH ₂ CH ₂) ₃ PAuCl (30)	25.29(25.40)	2.91(2.84)
(Ph) ₃ PAuCl (31)	37.43(37.65)	3.44(3.38)
(<i>p</i> -CH ₃ -Ph) ₃ PAuCl (32)	46.82(46.99)	4.01(3.94)
(<i>m</i> -CH ₃ -Ph) ₃ PAuCl (33)	46.86(46.99)	4.03(3.94)
(<i>o</i> -CH ₃ -Ph) ₃ PAuCl (34)	46.79(46.99)	4.04(3.94)
(<i>p</i> -OCH ₃ -Ph) ₃ PAuCl (35)	42.98(43.13)	3.67(3.62)

4.5 Synthesis of Dichlorido(1,2-diaminocyclohexane)gold(III) Chloride Complexes

Gold(III) complexes of *cis*-1,2-diaminocyclohexane (**36**), *trans*-(±)-1,2-diaminocyclohexane (**37**) and purely optical active isomer of (*S,S*)-(+)-1,2-diaminocyclohexane (**38**) were synthesized by a general method described in literature for similar compounds [150] by dissolving of 199 mg (0.50 mmol) sodium tetrachloroaurate(III) dehydrate NaAuCl₄·2H₂O, in minimum amount of absolute ethanol

at ambient temperature. In a separate beaker, solution of 57 mg (0.50 mmol) of the diaminocyclohexane in least amount of absolute ethanol was prepared, both solutions were mixed (total of 40ml) and stirred for around 30min until clear solution was obtained, which was filtered and concentrated to 10 ml solvent then left for crystallization in the refrigerator. The produced solid was dried under vacuum. The product was in the range of 91–98% yield.

Products were characterized by melting point (M.P.) and elemental analysis as given in Table 4.5 Melting point and elemental analysis of dichlorido(1,2-diaminocyclohexane)gold(III) chloride complexes and their predicted chemical structures are shown in Figure 3.5.

Table 4.5 Melting point and elemental analysis of dichlorido(1,2-diaminocyclohexane)gold(III) chloride complexes

Complex	M. P. (°C)	Found(Calc.)%		
		H	C	N
[<i>cis</i> -1,2-(DACH)Au(III)Cl ₂]Cl (36)	201–206	3.35(3.38)	17.22(17.26)	6.67(6.71)
[<i>trans</i> -(±)-1,2-(DACH)Au(III)Cl ₂]Cl (37)	170 deco.	3.32(3.38)	17.21(17.26)	6.68(6.71)
[(<i>S,S</i>)-(+)-1,2-(DACH)Au(III)Cl ₂]Cl (38)	174 deco.	3.29(3.38)	17.18(17.26)	6.65(6.71)

4.6 Synthesis of Azanechlorido(1,2-Diaminocyclohexane)gold(III)

Chloride Complexes.

Azanechlorido(1,2-diaminocyclohexane)gold(III) chloridewere synthesized by dissolving 209 mg of the correspondingdichlorido 1,2-diaminocyclohexane gold(III) chloride complexes [1,2-(DACH)Au(III)Cl₂]Cl in 15 ml of methanol. Then, the solution was cooled to 0 °C in ice bath and added dropwise to anaqueous solution of ammonium hydroxide [1 eq (0.5 mmol), 8.5 mg of NH₃(aq)] in 5 ml of methanol. The solution is stirred for 30 min under gentle atmospheric nitrogen. Among the addition of the ammonium hydroxide solution, the solution color changed from pale yellow to clear orange color. The orange solution is filtered to remove any apparent insoluble impurities, and the solvent evaporated to obtain orange solid complexes (39)-(41) which were dried overnight in a vacuum.

Products were characterized by elemental analysis as given inTable 4.6 Elemental analysis of azanechlorido(1,2-diaminocyclohexane)gold(III) chloride complexesand their predicted chemical structures are shown in Figure 3.6.

Table 4.6 Elemental analysis of azanechlorido(1,2-diaminocyclohexane)gold(III) chloride complexes

Complex	Found(Calc.)%		
	H	C	N
[<i>cis</i> -1,2-(DACH)Au(III)(NH ₃)Cl]Cl ₂ (39)	3.99(3.94)	16.73(16.58)	9.59(9.67)
[<i>trans</i> -(±)-1,2-(DACH)Au(III)(NH ₃)Cl]Cl ₂ (40)	3.96(3.94)	16.71(16.58)	9.61(9.67)
[(<i>S,S</i>)-(+)-1,2-(DACH)Au(III)(NH ₃)Cl]Cl ₂ (41)	3.91(3.94)	16.50(16.58)	9.64(9.67)

4.7 Synthesis of Diazane(1,2-diaminocyclohexane)gold(III) Chloride Complexes.

Diazane(1,2-diaminocyclohexane)gold(III) chloride complexes (**42-44**) were synthesized by dissolving 209 mg of the corresponding dichlorido 1,2-diaminocyclohexane gold(III) chloride complexes [1,2-(DACH)Au(III)Cl₂]Cl in 15 ml of methanol. Then, the solution was cooled to 0 °C in ice bath and added dropwise to an aqueous solution of ammonium hydroxide [2 eq (1 mmol), 17 mg of NH₃(aq)] in 5 ml of methanol. The solution is stirred for 30 min under gentle atmospheric nitrogen flow. Addition of the ammonium hydroxide solution to the precursor gold complex, the solution color changed from pale yellow to clear orange color. The solution is filtered to remove any apparent insoluble impurities, and the solvent evaporated to obtain orange solid complexes (**42**)-(44) which were dried overnight in vacuum.

Products were characterized by elemental analysis as given in Table 4.7 Elemental analysis of diazane(1,2-diaminocyclohexane)gold(III) chloride complexes and their predicted chemical structures are shown in Figure 3.7.

Table 4.7 Elemental analysis of diazane(1,2-diaminocyclohexane)gold(III) chloride complexes

Complex	Found(Calc.)%		
	H	C	N
[<i>cis</i> -1,2-(DACH)Au(III)(NH ₃) ₂]Cl ₃ (42)	4.51(4.46)	15.83(15.96)	12.54(12.41)
[<i>trans</i> -(±)-1,2-(DACH)Au(III)(NH ₃) ₂]Cl ₃ (43)	4.50(4.46)	15.79(15.96)	12.52(12.41)
[(<i>S,S</i>)-(+)-1,2-(DACH)Au(III)(NH ₃) ₂]Cl ₃ (44)	4.49(4.46)	15.89(15.96)	12.49(12.41)

4.8 Synthesis of Bis(1,2-Diaminocyclohexane)gold(III) Chloride

Complexes

Bis(1,2-DACH)gold(III) chloride complexes of *cis*-1,2-diaminocyclohexane (**45**), *trans*-(±)-1,2-diaminocyclohexane (**46**) and purely optical active isomer of (*S,S*)-(+)-1,2-diaminocyclohexane (**47**) were synthesized by a general method described in literature for similar compounds [151], by dissolving 340 mg (1.0 mmol) chloroauric acid trihydrate $\text{HAuCl}_4 \cdot 3\text{H}_2\text{O}$ in 3ml of water at ambient temperature. In a separate beaker, a solution of 228 mg (2.0 mmol) of the diaminocyclohexane in 2ml of diethyl ether was prepared; both solutions were mixed, gummy yellow precipitate was formed. Then, upon adding 9 ml of aqueous ethanol solution (7:1, EtOH:H₂O) to the latter solution and stirring for around 1 hr, a white precipitate of $[\text{Au}(\text{DACH})_2]\text{Cl}_3$ formed. The product was isolated and dissolved in 1ml of water and recrystallized with addition of 5 ml ethanol. The produced solid was dried under vacuum. The product yield was in the range of 65-70 %. Products were characterized by melting point (M.P.) and elemental analysis as given in Table 4.8 and their predicted chemical structures are shown in Figure 3.8.

Table 4.8 Melting point and elemental analysis of bis(1,2-DACH)gold(III) chloride complexes

Complex	M. P. (°C)	Found(Calc.)%		
		H	C	N
$[(\textit{cis}\text{-}1,2\text{-DACH})_2\text{Au(III)}]\text{Cl}_3$ (45)	203 deco.	5.28(5.31)	27.03(27.11)	10.61(10.54)
$[(\textit{trans}\text{-}(\pm)\text{-}1,2\text{-DACH})_2\text{Au(III)}]\text{Cl}_3$ (46)	180 deco.	5.23(5.31)	26.97(27.11)	10.62(10.54)
$[(1S,2S)\text{-}(+)\text{-DACH})_2\text{Au(III)}]\text{Cl}_3$ (47)	177 deco.	5.25(5.31)	26.99(27.11)	10.65(10.54)

4.9 Synthesis of 1,2-Diaminocyclohexane(ethylenediamine)gold(III)

Chloride Complexes.

The synthesis of mixed-ligand 1,2-Diaminocyclohexane(ethylenediamine)gold(III) complexes(48)-(50) using *cis*-1,2-diaminocyclohexane and ethylenediamine, *trans*-(±)-1,2-diaminocyclohexane and ethylenediamine and purely optical active isomer of (*S,S*)-(+)-1,2-diaminocyclohexane and ethylenediamine were according to a modified literature procedure[150], by dissolving of 398 mg (1.0 mmol) sodium tetrachloroaurate(III) dehydrate $\text{NaAuCl}_4 \cdot 2\text{H}_2\text{O}$ in minimum amount of absolute ethanol at ambient temperature. In a separate beaker, solution of 114 mg (1.00 mmol) of the diaminocyclohexane in least amount of absolute ethanol was prepared, both solutions were mixed dropwise and stirred for around 30 min until a clear solution was obtained, which was then filtered. In a separate beaker, a solution of 120 mg (1.0 mmol) of the ethylenediamine in least amount of absolute ethanol was prepared and added dropwise to the filtrated solution. Then, stirring was continued at RT overnight resulting in white precipitate. The product was separated, dissolved in 2ml of water and filtered through celite pad to remove NaCl. Addition of 100 ml of cold methanol to the filtrate resulted in white solid precipitate which was filtered and washed with cold methanol. The produced solid dried under reduced pressure with P_2O_5 , yielding the corresponding gold complexes with 75–80% yield. Products were characterized by melting point (M.P.) and elemental analysis as given in Table 4.9 and their predicted chemical structures are shown in Figure 3.9.

Table 4.9 Melting point and elemental analysis of 1,2-diaminocyclohexane(ethylenediamine)gold(III)chloride complexes

Complex	M. P. (°C)	Found(Calc.)%		
		H	C	N
[(<i>cis</i> -1,2-DACH)Au(III)(en)]Cl ₃ (48)	161-163	6.57(6.64)	22.26(22.59)	13.05(13.17)
[(<i>trans</i> -(±)-1,2- DACH)Au(III)(en)]Cl ₃ (49)	175-178	6.59(6.64)	22.32(22.59)	13.01(13.17)
[(1 <i>S</i> ,2 <i>S</i>)-(+)- DACH)Au(III)(en)]Cl ₃ (50)	176-178	6.60(6.64)	22.48(22.59)	13.03(13.17)

4.10 Synthesis of 1,2-Diaminocyclohexane(propylenediamine)gold(III) Chloride Complexes.

The synthesis of mixed ligandgold complexes of *cis*-1,2-diaminocyclohexane and 1,3-propylenediamine (**51**), *trans*-(±)-1,2-diaminocyclohexane and 1,3-propylenediamine (**52**) and purely optical active isomer of (*S,S*)-(+)-1,2-diaminocyclohexane and 1,3-propylenediamine (**53**) were according to modified literature procedure [150], by dissolving of 398 mg (1.00 mmol) sodium tetrachloroaurate(III) dehydrate NaAuCl₄·2H₂O in minimum amount of absolute ethanol at ambient temperature. In a separate beaker, solution of 114 mg (1.00 mmol) of the diaminocyclohexane in least amount of absolute ethanol was prepared, both solutions were mixed dropwise and stirred for around 30 min until a clear solution was obtained, which was filtered. In a separate beaker, a solution of 120 mg (1.0 mmol) of the 1,3-propylenediamine in least amount of absolute ethanol was prepared and added dropwise to the filtrated solution. Then, stirring was continued at RT for overnight resulting in a white precipitate. The product was separated, dissolved in 2ml of water and filtered through celite pad to remove NaCl.

Addition of 100 ml of cold methanol to the filtrate resulted in white solid precipitate which was filtered and washed with cold methanol. The produced solid was dried under reduced pressure with P₂O₅, yielding the corresponding gold complexes. The product yield was in the range of 75–80 %. Products were characterized by melting point (M.P.) and elemental analysis as given in Table 4.10 and their predicted chemical structures are shown in Figure 3.10.

Table 4.10 Melting point and elemental analysis of 1,2-diaminocyclohexane(propylenediamine)gold(III)chloride complexes

Complex	M. P. (°C)	Found(Calc.)%		
		H	C	N
[(<i>cis</i> -1,2-DACH)Au(III)(pn)]Cl ₃ (51)	161-163	6.57(6.88)	24.26(24.61)	12.61(12.75)
[(<i>trans</i> -(±)-1,2- DACH)Au(III)(pn)]Cl ₃ (52)	171-173	6.55(6.88)	24.37(24.61)	12.59(12.75)
[(1 <i>S</i> ,2 <i>S</i>)-(+)-DACH)Au(III)(pn)]Cl ₃ (53)	173-175	6.59(6.88)	24.41(24.61)	12.65(12.75)

4.11 Synthesis of Ammoniumdithiocarbamatodichloridogold(III) Chloride Complexes.

The syntheses of ammoniumdithiocarbamatodichloridogold(III) chloride complexes of (**54**)-(66) were performed following a modified literature procedure [152]. To a stirred suspension of the corresponding ammonium dithiocarbamate (0.5 mmol) in DMF (2 ml), cooled at 0°C in ice bath was added dropwise 199 mg (0.500 mmol) of sodium tetrachloroaurate(III) dehydrate NaAuCl₄·2H₂O dissolved in 2 ml of ether. After completion of the addition of two reactants, the reaction mixture was then warmed to RT

and stirred for 1 hour. The products were obtained as a yellow or orange solid by addition of 50 ml of ether. Then, the solvent was decanted and the solid was washed three times with 10 ml of ether. The produced solid was dried under flow of N₂ gas, yielding the corresponding gold complexes. The product yield was in the range of 75-80%. Products were characterized by elemental analysis, IR and ¹³C NMR as given, respectively, in Table 4.11, Table 4.12, Table 4.13 and Table 4.14. Their predicted chemical structures are shown in Figure 3.11.

Table 4.11 Elemental analysis of ammoniumdithiocarbamatodichloridogold(III) chloride complexes

Complex	Found (Calculated) %			
	%C	%H	%N	%S
[(en-DTC)Au(III)Cl ₂]Cl (54)	8.15(8.21)	1.86(1.83)	6.31(6.37)	14.61(14.59)
[(pn-DTC)Au(III)Cl ₂]Cl (55)	10.51(10.59)	2.26(2.22)	6.12(6.18)	14.22(14.14)
[(bn-DTC)Au(III)Cl ₂]Cl (56)	12.75(12.84)	2.62(2.59)	5.92(5.99)	13.76(13.71)
[(N-Me-en-DTC)Au(III)Cl ₂]Cl (57)	10.51(10.59)	2.25(2.22)	6.13(6.18)	14.21(14.14)
[(N-Et-en-DTC)Au(III)Cl ₂]Cl (58)	12.76(12.84)	2.52(2.59)	5.93(5.99)	13.67(13.71)
[(N- <i>i</i> -Pr-en-DTC)Au(III)Cl ₂]Cl (59)	14.89(14.96)	2.96(2.93)	5.77(5.82)	13.39(13.32)
[(N,N'-di-Me-en-DTC)Au(III)Cl ₂]Cl (60)	12.78(12.84)	3.03(2.59)	5.95(5.99)	13.66(13.71)
[(N,N'-di-Et-en-DTC)Au(III)Cl ₂]Cl (61)	16.87(16.96)	3.28(3.25)	5.61(5.65)	13.07(12.94)
[(N,N'-di- <i>n</i> -Pr-en-DTC)Au(III)Cl ₂]Cl (62)	20.56(20.64)	3.89(3.85)	5.31(5.35)	12.21(12.25)
[(N,N'-di- <i>i</i> -Pr-en-DTC)Au(III)Cl ₂]Cl (63)	20.56(20.64)	3.90(3.85)	5.31(5.35)	12.20(12.25)
[(N-Me-pn-DTC)Au(III)Cl ₂]Cl (64)	12.77(12.84)	2.64(2.59)	5.95(5.99)	13.65(13.71)
[(N-Et-pn-DTC)Au(III)Cl ₂]Cl (65)	14.87(14.96)	2.96(2.93)	5.78(5.82)	13.27(13.32)
[(N,N'-di-Et-pn-DTC)Au(III)Cl ₂]Cl (66)	18.76(18.85)	3.62(3.56)	5.46(5.50)	12.53(12.58)

Table 4.12 IR frequencies, ν (cm⁻¹) for ammoniumdithiocarbamatodichloridogold(III) chloride complexes

Compound	$\nu(\text{N-H})$	ν_{shift}	$\nu(\text{C-NSS})$	ν_{shift}	$\nu(\text{SC=S})$	$\nu(\text{SC-S})$	$\nu(\text{N}^+-\text{H}_2)$
(en-DTC) (1)	3310 m		1490 s		1051	980 s	2793, 2721
[(en-DTC)AuCl ₂]Cl (54)	3471 m	161	1590 s	100	-	978 s	2797
(pn-DTC) (2)	3311m		1495 s		1056	974 s	2795
[(pn-DTC)AuCl ₂]Cl (55)	3425 m	114	1554 s	59	-	965 s	2764
(bn-DTC) (3)	3201 m		1497 s		1029	929 s	
[(bn-DTC)AuCl ₂]Cl (56)	3412 m	211	1567 s	70	-	922 s	

Table 4. 13 Far-IR frequencies, ν (cm⁻¹) for ammoniumdithiocarbamatodichloridogold(III) chloride complexes

Compound	Au-S	Au-Cl
[(en-DTC)AuCl ₂]Cl (54)	423, 362	334, 329
[(pn-DTC)AuCl ₂]Cl (55)	431, 367	338, 326
[(bn-DTC)AuCl ₂]Cl (56)	451, 374	341, 331

Table 4.14 ¹³C NMR chemical shifts of free ligands and ammoniumdithiocarbamatodichloridogold(III) chloride complexes in D₂O

Compound	C=S	δ_{shift}	C1	δ_{shift}	C2	C3	C4
(en-DTC) (1)	215		44.1		39.6	-	-
[(en-DTC)AuCl ₂]Cl (54)	203	12	42.4	1.7	38.3		
(pn-DTC) (2)	213		44.7		37.6	27.2	-
[(pn-DTC)AuCl ₂]Cl (55)	198	15	40.6	4.1	35.7	24.3	
(bn-DTC) (3)	211		47.5		39.9	25.5	25.0
[(bn-DTC)AuCl ₂]Cl (56)	201	10	44.3	3.2	38.4	22.7	22.1

4.12 Synthesis of Dichlorido(2-cyclohexanaminiumdithiocarbamato)gold(III) Chloride Complexes

The synthesis of the dichlorido(2-cyclohexanaminiumdithiocarbamato)gold(III) chloride complexes (**67**)-(**69**) were performed following a modified literature procedure [152]. To a stirred suspension of 2-cyclohexanaminium dithiocarbamate (0.5 mmol) in DMF (2 ml) and cooled at 0 °C in ice bath was added dropwise 199 mg (0.500 mmol) sodium tetrachloroaurate(III) dihydrate NaAuCl₄·2H₂O dissolved in 2 ml of ether. After completion of the addition of two reactants, the reaction mixture was then warmed to RT and stirred for 1 hour. The products were obtained as a yellow or orange solid by addition of 50 ml of ether. Then, the solvent was decanted and the solid was washed three times with 10 ml of ether. The produced solid was dried under a flow of N₂ gas, yielding the corresponding gold complexes. The product yield was in the range of 84-88%. The elemental analysis data as given in Table 4.15 and their predicted chemical structures are shown in Figure 3.12.

Table 4.15 Melting point and elemental analysis of dichlorido(2-cyclohexanaminiumdithiocarbamato)gold(III) chloride complexes

Complex	Found (Calculated) %			
	%C	%H	%N	%S
[(<i>cis</i> -(1,2)-DACH-DTC)Au(III)Cl ₂]Cl (67)	8.15(8.21)	1.86(1.83)	6.31(6.37)	14.61(14.59)
[(<i>trans</i> -(±)-(1,2)-DACH-DTC)Au(III)Cl ₂]Cl (68)	10.51(10.59)	2.26(2.22)	6.12(6.18)	14.22(14.14)
[(1 <i>S</i> ,2 <i>S</i>)-(+)-DACH-DTC)Au(III)Cl ₂]Cl (69)	12.75(12.84)	2.62(2.59)	5.92(5.99)	13.76(13.71)

4.13 Synthesis of Mixed-Ligand Dithiocarbamatophosphanegold(I) Complexes.

There has been a great interest in the synthesis of derivatives containing the P–Au(I)–S unit because they are related to Aurofin, a drug used against the rheumatoid arthritis [101]. The synthesis of the dithiocarbamatotrialkylphosphanegold(I) complexes(70)-(93) were synthesized following a modified literature procedure [153]. To a stirred suspension of chloridotrialkylphosphanegold(I) (0.50 mmol) in methanol (20 ml), cooled at 0 °C in ice bath under atmospheric nitrogen gas flow, was added dropwise sodium dimethyldithiocarbamate (DMDT) or sodium diethyldithiocarbamate (DEDT) (0.50 mmol) solution dissolved in 5 ml of methanol. Rapidly, the solid was dissolved and the resulting yellow or orange solution was stirred for about 2 h. Then, the solution was filtered to remove insoluble materials. Evaporation of methanol at RT afforded a yellow or orange solid which was dissolved in diethyl ether (10 ml). To remove the byproduct sodium chloride, the organic layer was washed with water and extracted, dried with anhydrous Na₂SO₄ and filtered. Complete removal of the solvent afforded dithiocarbamatotrialkylphosphanegold(I) as a yellow or orange solid. It was dried under reduced pressure at RT overnight over P₂O₅, yielding the corresponding gold complexes with 81-86% yield. Products were characterized by elemental analysis, mid-IR, far-IR, ¹³C NMR and ³¹P NMR as given, respectively, in Table 4.16, Table 4.17, Table 4.18, Table 4.19 and Table 4.20. Their predicted chemical structures are shown in Figure 3.13.

Table 4.16 Elemental analysis of dithiocarbamatotrialkylphosphane-gold(I) complexes

Complex	Found (Calculated) %			
	%C	%H	%N	%S
(Me) ₃ PAu(I)(DMDT) (70)	18.26(18.32)	3.86(3.84)	3.48(3.56)	16.23(16.32)
(Me) ₃ PAu(I)(DEDT) (71)	22.65(22.81)	4.59(4.55)	3.30(3.32)	15.17(15.22)
(Et) ₃ PAu(I)(DMDT) (72)	24.75(24.83)	4.90(4.86)	3.18(3.22)	14.76(14.73)
(Et) ₃ PAu(I)(DEDT) (73)	28.43(28.51)	4.51(5.44)	2.98(3.02)	13.61(13.84)
(<i>i</i> -Pr) ₃ PAu(I)(DMDT) (74)	30.01(30.19)	5.74(5.70)	2.88(2.93)	13.32(13.43)
(<i>i</i> -Pr) ₃ PAu(I)(DEDT) (75)	33.18(33.27)	6.23(6.18)	2.69(2.77)	12.76(12.69)
(Ph) ₂ (Cy)PAu(I)(DMDT) (76)	42.93(43.08)	4.70(4.65)	2.31(2.39)	10.61(10.95)
(Ph) ₂ (Cy)PAu(I)(DEDT) (77)	44.84(45.02)	5.13(5.09)	2.25(2.28)	10.33(10.45)
(Ph) ₂ (Et)PAu(I)(DMDT) (78)	38.32(38.42)	3.99(3.98)	2.58(2.64)	12.14(12.07)
(Ph) ₂ (Et)PAu(I)(DEDT) (79)	40.56(40.79)	4.54(4.50)	2.86(2.90)	11.61(11.46)
(Ph)(NCCH ₂ CH ₂) ₂ PAu(I)(DMDT) (80)	33.53(33.78)	3.62(3.59)	7.79(7.88)	11.91(12.02)
(Ph)(NCCH ₂ CH ₂) ₂ PAu(I)(DEDT) (81)	36.28(36.37)	4.17(4.13)	7.41(7.48)	11.35(11.42)
(NCCH ₂ CH ₂) ₃ PAu(I)(DMDT) (82)	28.16(28.24)	3.62(3.55)	10.76(10.98)	12.60(12.57)
(NCCH ₂ CH ₂) ₃ PAu(I)(DEDT) (83)	31.14(31.23)	4.20(4.12)	10.34(10.41)	11.85(11.91)
(Ph) ₃ PAu(I)(DMDT) (84)	43.36(43.53)	3.68(3.65)	2.38(2.42)	11.16(11.07)
(Ph) ₃ PAu(I)(DEDT) (85)	45.31(45.47)	4.58(4.15)	2.27(2.31)	10.63(10.56)
(<i>p</i> -CH ₃ Ph) ₃ PAu(I)(DMDT) (86)	46.16(46.38)	4.43(4.38)	2.22(2.25)	10.21(10.32)
(<i>p</i> -CH ₃ Ph) ₃ PAu(I)(DEDT) (87)	47.75(48.07)	4.85(4.81)	4.12(4.16)	9.77(9.87)
(<i>m</i> -CH ₃ Ph) ₃ PAu(I)(DMDT) (88)	46.09(46.38)	4.43(4.38)	2.21(2.25)	10.22(10.32)
(<i>m</i> -CH ₃ Ph) ₃ PAu(I)(DEDT) (89)	47.75(48.07)	4.86(4.81)	4.09(4.16)	9.76(9.87)
(<i>o</i> -CH ₃ Ph) ₃ PAu(I)(DMDT) (90)	46.12(46.38)	4.41(4.38)	2.23(2.25)	10.19(10.32)
(<i>o</i> -CH ₃ Ph) ₃ PAu(I)(DEDT) (91)	46.79(48.07)	4.84(4.81)	4.08(4.16)	9.91(9.87)
(<i>p</i> -CH ₃ OPh) ₃ PAu(I)(DMDT) (92)	42.82(43.05)	4.09(4.06)	2.12(2.09)	14.49(9.58)
(<i>p</i> -CH ₃ OPh) ₃ PAu(I)(DEDT) (93)	44.52(44.76)	4.53(4.48)	2.03(2.01)	9.18(9.10)

Table 4.17 Mid-IR frequencies, $\nu(\text{cm}^{-1})$ for dithiocarbamatotrialkylphosphanegold(I) complexes

Compound	$\nu(\text{C-NSS})$	ν_{shift}	$\nu(\text{SC=S})$	ν_{shift}	$\nu(\text{SC-S})$	ν_{shift}
DMDT	1359 s	-	1043 s	-	963s	-
DEDT	1356 s	-	1064 s	-	986 s	-
$\text{Me}_3\text{PAu(I)DMDT}$ (70)	1369 s	10	974 s	-69	958 s	-5
$\text{Me}_3\text{PAu(I)DEDT}$ (71)	1374 s	18	986 s	-78	951 s	-35
$\text{Et}_3\text{PAu(I)DMDT}$ (72)	1367 s	8	996 s	-47	973 s	-10
$\text{Et}_3\text{PAu(I)DEDT}$ (73)	1371 s	15	1002	-62	984s	-2
<i>i</i> -Pr ₃ PAu(I)DMDT (74)	1368 s	9	994	-49	977s	-9

Table 4.18 Far-IR frequencies, $\nu(\text{cm}^{-1})$ for dithiocarbamatotrialkylphosphanegold(I) complexes

Compound	$\nu(\text{Au-S})$	$\nu(\text{Au-P})$
$\text{Me}_3\text{PAu(I)DMDT}$ (70)	392	332
$\text{Me}_3\text{PAu(I)DEDT}$ (71)	381	335
$\text{Et}_3\text{PAu(I)DMDT}$ (72)	375	331
$\text{Et}_3\text{PAu(I)DEDT}$ (73)	379	334
<i>i</i> -Pr ₃ PAu(I)DMDT (74)	380	328

Table 4.19 ^{13}C NMR chemical shifts of precursor complexes and dithiocarbamatotrialkylphosphanegold(I) complexes in CDCl_3

Compound	C=S	C1	C2	C3	C1'	C2'
$\text{Me}_3\text{PAu(I)Cl}$ (70)	-	16.3, 16.0	-	-	-	-
$\text{Me}_3\text{PAu(I)DMDT}$ (70)	207	16.6, 16.3	-	-	45.2	-
$\text{Me}_3\text{PAu(I)DEDT}$ (71)	206	16.4, 16.1	9.0	-	-	-
$\text{Et}_3\text{PAu(I)Cl}$ (72)	-	18.3, 18.0	-	-	-	-
$\text{Et}_3\text{PAu(I)DMDT}$ (72)	208	18.4, 18.2	8.8	-	45.0	-
$\text{Et}_3\text{PAu(I)DEDT}$ (73)	205	18.2, 17.9	9.3	35.7	49.0	12.6
$i\text{-Pr}_3\text{PAu(I)Cl}$ (74)	-	24.1, 23.3	20.3	20.3	-	-
$i\text{-Pr}_3\text{PAu(I)DMDT}$ (74)	208	23.9, 23.7	20.1	20.1	45.0	-

Table 4.20 ^{31}P NMR chemical shifts of precursor complexes and dithiocarbamatotrialkylphosphanegold(I) complexes in CDCl_3

Compound	P	δ_{shift}
$\text{Me}_3\text{PAu(I)Cl}$ (70)	-11	
$\text{Me}_3\text{PAu(I)DMDT}$ (70)	-8.7	2.3
$\text{Me}_3\text{PAu(I)DEDT}$ (71)	-8.8	2.2
$\text{Et}_3\text{PAu(I)Cl}$ (72)	29.4	
$\text{Et}_3\text{PAu(I)DMDT}$ (72)	31.9	2.5
$\text{Et}_3\text{PAu(I)DEDT}$ (73)	32.2	2.8
$i\text{-Pr}_3\text{PAu(I)Cl}$ (74)	-36.7	
$i\text{-Pr}_3\text{PAu(I)DMDT}$ (74)	-35.1	1.6

4.14 Synthesis of Mixed-Ligand 5-Methyl-2-mercaptobenzimidazolo(phosphane)gold(I) Complexes.

The synthesis of the 5-methyl-2-mercaptobenzimidazolo(phosphane)gold(I) complexes of **(94)**-**(99)** were performed following a literature procedure [153,154]. Suspension of substituted 5-methyl-2-mercaptobenzimidazole (1.0 mmol) in distilled water (20 ml) was treated with a solution of KOH 1.0 N (5.0ml, 5.0 mmol). The resulting clear solution was then added to 5 ml of a methanolic solution of 1.0 mmol chlorido phosphane gold(I) under stirring for 2 hours. The produced precipitate was then filtered off, washed with water and dried for 6 hours in oven at 40 °C. The product was in the range of 92–95% yield. Products were characterized by melting point (M.P.) and Elemental analysis as given in Table 4.21 and their predicted chemical structures are shown in Figure 3.14. Figure 4.1 shows the X-ray structure of (5-Me-2-MBI)Au(I)P(Ph)₃ (**96**).

Table 4.21 Melting point and elemental analysis of 5-methyl-2-mercaptobenzimidazolo(phosphane)gold(I) complexes

Complex	M. P. (°C)	Found (Calculated) %			
		%C	%H	%N	%S
(5-Me-2-MBI)Au(I)P(Me) ₃ (94)	241-243	30.01(30.28)	7.78(7.70)	6.38(6.42)	7.21(7.35)
(5-Me-2-MBI)Au(I)P(Et) ₃ (95)	183-185	34.94(35.15)	4.69(4.64)	5.72(5.86)	6.65(6.70)
(5-Me-2-MBI)Au(I)P(Ph) ₃ (96)	208-210	49.75(50.17)	3.62(3.56)	4.42(4.50)	5.01(5.15)
(5-Me-2-MBI)Au(I)P(Ph) ₂ (Et) (97)	154-156	45.89(46.00)	3.89(3.86)	4.65(4.88)	6.61(5.58)
(5-Me-2-MBI)Au(I)P(<i>t</i> -Bu) ₃ (98)	232-234	42.51(42.70)	6.14(6.09)	4.93(4.98)	5.62(5.70)
(5-Me-2-MBI)Au(I)P(<i>i</i> -Pr) ₃ (99)	179-181	39.12(39.23)	5.47(5.42)	5.23(5.38)	6.09(6.16)

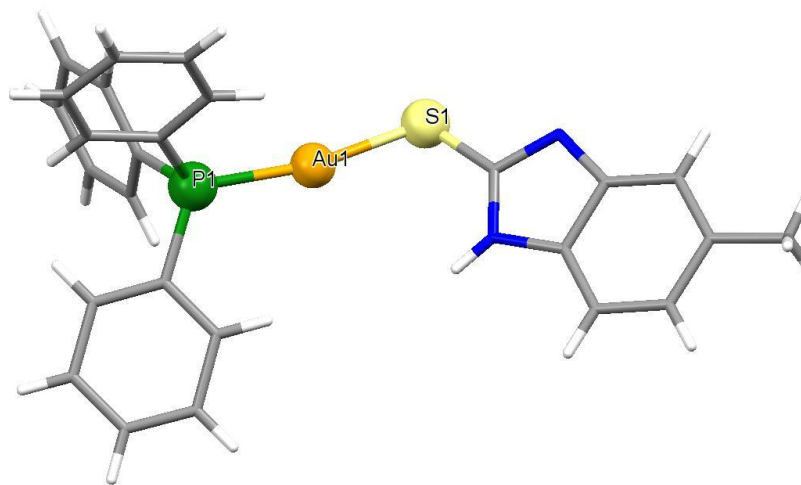


Figure 4.1 X-ray structure of $(\text{Ph})_3\text{PAu(I)}(5\text{-Me-2-MBI})$ (96)

4.15 Synthesis of Substituted 2-mercaptobenzimidazolo(trimethylphosphane)gold(I) Complexes.

The synthesis of the substituted 2-mercaptobenzimidazolotrimethylphosphane gold(I) complexes of **(100)**-**(105)** were performed following a literature procedure [153,154]. Suspension of the substituted 2-mercaptobenzimidazole (1.0 mmol) in distilled water (20 ml) was treated with a solution of KOH 1.0 N (5.0 ml, 5.0 mmol). The resulting clear solution was then added to it 5 ml of a methanolic solution of 308.5 mg (1.00 mmol) chloridotrialkylphosphane gold(I) under stirring for 2 hours. The produced precipitate was then filtered off, washed with water and dried for 6 hours in oven at 40 °C. The product was in the range of 93-96% yield. Products were characterized by melting point (M.P.) and elemental analysis as given in Table 4.22 and their predicted chemical structures are shown in Figure 3.15.

Table 4.22 Melting point and elemental analysis of substituted 2-mercaptobenzimidazolotrimethylphosphane gold(I) complexes

Complex	M. P. (°C)	Found (Calculated) %			
		%C	%H	%N	%S
(2-MBI)Au(I)P(Me) ₃ (100)	-	28.32(28.45)	3.40(3.34)	6.54(6.63)	7.83(7.95)
(5-F-2-MBI)Au(I)P(Me) ₃ (101)	225-227	27.04(27.28)	3.03(2.98)	6.28(6.36)	7.22(7.28)
(5-Cl-2-MBI)Au(I)P(Me) ₃ (102)	168-170	26.14(26.30)	2.92(2.87)	6.03(6.13)	6.89(7.02)
(5,6-di-Cl-2-MBI)Au(I)P(Me) ₃ (103)	238-240	24.15(24.46)	2.53(2.46)	5.65(5.70)	6.46(6.53)
(5-NO ₂ -2-MBI)Au(I)P(Me) ₃ (104)	170-172	25.63(25.71)	2.75(2.80)	8.92(8.99)	6.76(6.86)
(4-NO ₂ -2-MBI)Au(I)P(Me) ₃ (105)	180-182	25.59(25.71)	2.86(2.80)	8.94(8.99)	6.79(6.86)

4.16 Synthesis of Mixed-Ligand 4-Nitro-2-mercaptobenzimidazolo(phosphane)gold(I) Complexes.

The synthesis of the 4-nitro-2-mercaptobenzimidazolotrialkylphosphane gold(I) complexes of (**106**)-(111) were performed following the literature procedure [153,154]. Suspension of the substituted 4-nitro-2-mercaptobenzimidazole (1.0 mmol) in distilled water (20 ml) was treated with a solution of KOH 1.0 N (5.0ml, 5.0 mmol). The resulting clear solution was then added to 5 ml of a methanolic solution of 1.0 mmol chloridophosphine gold(I) under stirring for 3 hours. The produced precipitate was then filtered off, washed with water and dried for 6 hours in oven at 40 °C. The product was in the range of 95-96% yield. Products were characterized by melting point (M.P.) and elemental analysis as given in Table 4.23 and their predicted chemical structures are shown in Figure 3.16.

Table 4.23 Melting point and elemental analysis of 4-nitro-2-mercaptobenzimidazolotrialkylphosphanegold(I) complexes

Complex	M. P. (°C)	Found (Calculated) %			
		%C	%H	%N	%S
(4-NO ₂ -2-MBI)Au(I)P(Et) ₃ (106)	138-140	30.45(30.66)	3.86(3.76)	8.19(8.25)	6.25(6.30)
(4-NO ₂ -2-MBI)Au(I)P(Ph) ₂ (Et) (107)	117-119	41.23(41.66)	3.21(3.16)	6.91(6.94)	5.24(5.30)
(4-NO ₂ -2-MBI)Au(I)P(Ph)(Et)(Me) (108)	280-282	35.18(35.37)	3.16(3.15)	7.68(7.73)	5.84(5.90)
(4-NO ₂ -2-MBI)Au(I)P(Ph) ₃ (109)	238-240	45.48(45.95)	2.96(2.93)	6.32(6.43)	4.81(4.91)
(4-NO ₂ -2-MBI)Au(I)P(<i>t</i> -Bu) ₃ (110)	230-232	38.17(38.45)	5.35(5.26)	7.02(7.08)	5.49(5.40)
(4-NO ₂ -2-MBI)Au(I)P(<i>i</i> -Pr) ₃ (111)	120-122	34.54(34.85)	4.62(4.57)	7.56(7.62)	5.78(5.82)

4.17 Synthesis of Mixed-Ligand 5-Nitro-2-

Mercaptobenzimidazolophosphanegold(I) Complexes.

The synthesis of the 5-nitro-2-mercaptobenzimidazolotrialkylphosphanegold(I) complexes of (**112**)-(115) were performed following the literature procedure [153,154]. Suspension of the 5-nitro-2-mercaptobenzimidazole (1.0 mmol) in distilled water (20 ml) was treated with a solution of KOH 1 N (5ml, 5 mmol). The resulting clear solution was then added to 5 ml of a methanolic solution of 1.0 mmol chloridophosphanegold(I) under stirring for 3 hours. The produced precipitate was then filtered off, washed with water and dried for 6 hours in oven at 40 °C. The product was in the range of 91-94% yield. Products were characterized by melting point (M.P.) and elemental analysis as given in Table 4.24 and their predicted chemical structures are shown in Figure 3.17.

Table 4.24 Melting point and elemental analysis of 5-NO₂-2-mercaptobenzimidazolophosphane-gold(I) complexes

Complex	M. P. (°C)	Found (Calculated) %			
		%C	%H	%N	%S
(5-NO ₂ -2-MBI)Au(I)P(Et) ₃ (112)	183-185	30.48(30.66)	3.89(3.76)	8.15(8.25)	6.27(6.30)
(5-NO ₂ -2-MBI)Au(I)P(Ph) ₂ (Et) (113)	154-156	41.36(41.66)	3.23(3.16)	6.89(6.94)	5.23(5.30)
(5-NO ₂ -2-MBI)Au(I)P(Ph) ₃ (114)	208-210	45.67(45.95)	2.97(2.93)	6.36(6.43)	4.85(4.91)
(5-NO ₂ -2-MBI)Au(I)P(<i>t</i> -Bu) ₃ (115)	232-234	38.23(38.45)	5.29(5.26)	7.04(7.08)	5.36(5.40)

4.18 Synthesis of Substituted 2-Mercaptobenzimidazo{1,3-Bis(2,6-di-isopropylphenyl)imidazol-2-ylidene}gold(I) Complexes.

The synthesis of the substituted 2-Mercaptobenzimidazo(IPr)gold(I) (IPr = 1,3-bis(2,6-di-isopropylphenyl)imidazol-2-ylidene) complexes of (**116**)-(122) were performed following the similar literature procedure [153,154]. Suspension of substituted 2-mercaptobenzimidazole (0.50 mmol) in distilled water (10.0 ml) was treated with a solution of KOH 1.0 N (2.5ml, 2.5 mmol). The resulting clear colored solution was then added to it 5 ml of a methanolic solution of 311.0 mg (0.50 mmol) chlorido{1,3-Bis(2,6-di-isopropylphenyl)imidazol-2-ylidene}gold(I) under stirring for 3 hours. The produced precipitate was then filtered off, washed with water and dried for 6 hours in oven at 40 °C. The product was in the range of 87-93% yield. Products were characterized by Elemental analysis as given in Table 4.25 and their predicted chemical structures are shown in Figure 3.18.

Table 4.25 Melting point and elemental analysis of 2-mercaptobenzimidazolo(IPr)gold(I) complexes

Complex	Found (Calculated) %			
	%C	%H	%N	%S
(2-MBI)Au(I)P(IPr) (116)	55.15(55.50)	5.81(5.75)	6.51(7.61)	4.31(4.36)
(5-Me-2-MBI)Au(I)P(IPr) (117)	55.46(56.07)	5.94(5.91)	7.31(7.47)	4.21(4.28)
(5-F-2-MBI)Au(I)P(IPr) (118)	53.43(54.18)	5.57(5.48)	7.36(7.43)	4.21(4.25)
(5-Cl-2-MBI)Au(I)P(IPr) (119)	52.67(53.02)	5.43(5.37)	7.31(7.27)	4.04(4.16)
(5,6-di-Cl-2-MBI)Au(I)P(IPr) (120)	50.24(50.75)	5.09(5.01)	6.87(6.96)	3.94(3.99)
(5-NO ₂ -2-MBI)Au(I)P(IPr) (121)	51.86(52.30)	5.35(5.29)	8.78(8.97)	4.06(4.11)
(4-NO ₂ -2-MBI)Au(I)P(IPr) (122)	51.76(52.30)	5.34(5.29)	8.87(8.97)	4.03(4.11)

4.19 Synthesis of Dinuclear 2-MBI{1,3-bis(Diphenylphosphino)methane}gold(I) Complexes

The synthesis of dinuclear 2-MBI{1,3-bis(Diphenylphosphino)methane}gold(I) complexes of (**123**)-(129) were performed following similar literature procedure [153,154]. Suspension of a substituted 2-mercaptobenzimidazole (0.33 mmol) in distilled water (7 ml) was treated with a solution of KOH 1.0 N (1.7ml, 1.7 mmol). The resulting clear solution was then added to 2 ml of a methanolic solution of 283 mg (0.330 mmol) chlorido(DPPM)gold(I) [(DPPM = 1,3-bis(diphenylphosphino)methane)] under stirring for 3 hours. The produced precipitate was then filtered off, washed with water and dried overnight in a vacuum at 30 °C. The product was in the range of 93-96% yield. Products were characterized by melting point (M.P.) and elemental analysis as given in Table 4.26 and their predicted chemical structures are shown in Figure 3.19.

Table 4.26 Melting point and elemental analysis of Dinuclear 2-MBI{1,3-bis(Diphenylphosphino)methane}gold(I) complexes

Complex	Found (Calculated) %			
	%C	%H	%N	%S
{(2-MBI)Au(I)} ₂ (DPPM) (123)	43.26(43.50)	3.04(3.00)	5.14(5.20)	5.89(5.96)
{(5-Me-2-MBI)Au(I)} ₂ (DPPM) (124)	41.75(42.10)	2.76(2.72)	4.97(5.04)	5.61(5.76)
{(5-F-2-MBI)Au(I)} ₂ (DPPM) (125)	44.32(44.57)	3.32(3.28)	5.01(5.07)	5.76(5.81)
{(5-Cl-2-MBI)Au(I)} ₂ P(DPPM) (126)	40.61(40.89)	2.68(2.64)	4.78(4.89)	5.65(5.60)
{(5,6-di-Cl-2-MBI)Au(I)} ₂ (DPPM) (127)	38.27(38.57)	2.36(2.32)	4.56(4.61)	5.12(5.28)
{(5-NO ₂ -2-MBI)Au(I)} ₂ (DPPM) (128)	39.89(40.15)	2.66(2.59)	7.12(7.20)	5.43(5.50)
{(4-NO ₂ -2-MBI)Au(I)} ₂ (DPPM) (129)	39.85(40.15)	2.64(2.59)	7.15(7.20)	5.52(5.50)

4.20 Spectroscopic Characterization

4.20.1 Elemental Analysis

Elemental analysis and melting points were performed on Perkin Elmer Series 11 (CHNS/O), Analyzer 2400 and BÜCHI 510 melting point apparatus respectively. The CHN/CHNS results of metal complexes are given in Tables 4.1-4.26.

4.20.2 Mid-IR and Far-IR studies

The solid state Mid-IR spectra of the ligands and the compounds (**1**)-(129) were performed on a Perkin–Elmer FTIR 180 spectrophotometer or NICOLET 6700 FTIR using KBr pellets over the range 4000–400 cm⁻¹ and solid state Far-IR spectra were recorded for complexes at 4 cm⁻¹ resolution at room temperature using CsCl disks on a Nicolet 6700 FT-IR with Far-IR beam splitter.

4.20.3 UV-Vis Studies

Electronic spectra were obtained using Lambda 200, Perkin-Elmer UV-Vis spectrometer. UV-Vis spectroscopy was, also, used to determine the stability of the complexes in a physiological buffer (40 mM phosphate, 4 mM NaCl, pH 7.4). Electronic spectra were recorded on freshly prepared buffered solutions of each complex at room temperature. Then, their electronic spectra were monitored over certain time at 37 °C. All electronic spectral data obtained were given in tabulated form.

4.20.4 Solution NMR Measurements

The solution ^1H and ^{13}C NMR experiments were performed on Jeol 500 MHz NMR Spectrometer at 297 K using ca. 0.10 M solution of the complexes in the deuterated solvents (D_2O , DMSO, CDCl_3 and CD_3OD . etc.). The ^1H NMR spectra were obtained on a Jeol 500 MHz NMR spectrometer operating at a frequency of 500 MHz. ^{13}C NMR spectra were obtained at 125.65 MHz with ^1H broadband decoupling at 297K. The spectral conditions were: 32k data points, 0.967s acquisition time, 1.00s pulse delay and 45° pulse angle. ^1H and ^{13}C NMR Chemical shifts (δ) values were referenced to tetramethylsilane (TMS), 1,4-dioxane as, CD_3OD and dimethyl sulfoxide (DMSO).

^{31}P NMR spectra were obtained on Jeol 500 MHz Spectrometer operating at frequency 202.35 MHz with ^1H broadband decoupling at 297K. The spectral conditions were: 32k data points, 0.963 s acquisition time, 2.50 s pulse delay and 45° pulse angle. ^{31}P NMR chemical shifts (δ) values were external referenced to 0 ppm of 85% H_3PO_4 in D_2O solvent.

4.20.5 Solid State NMR Measurements

^{13}C solid-state NMR was recorded on a Bruker 400 MHz spectrometer at ambient temperature of 25°C. Samples were packed into 4 mm zirconium oxide rotors. Cross polarization and high power decoupling were employed. Pulse delay of 7.0 s and a contact time of 5.0 ms were used in the CPMAS experiments. The magic angle spinning rates were 4 and 8 kHz. Carbon chemical shifts were referenced to TMS by setting the high frequency isotropic peak of solid adamantane to 38.56 ppm

4.20.6 NMR Studies for Stability Determination

Selected complexes were tested for their stability in water, DMSO and mixed solvent of DMSO/water solution by ^{13}C and ^1H NMR. The hygroscopic nature of DMSO could unfortunately lead to stability issue [155]. To investigate the structural stability of the complexes, NMR spectra of the complexes dissolved in D_2O , DMSO and mixed DMSO- $d_6/\text{D}_2\text{O}$ (v/v: 3/1) solution were obtained on immediate dissolution and latter at certain time at RT in DMSO or mixed DMSO- $d_6/\text{D}_2\text{O}$ and at 37 °C in D_2O . A minimum of 30 mg/ml of representative gold complexes were subjected to ^1H and ^{13}C NMR spectra analysis following dissolution in D_2O and DMSO- $d_6/\text{D}_2\text{O}$ (v/v: 3/1, 1ml). Immediate dissolution and duplicate samples were then stored at RT and 37 °C, respectively, and analyzed again after 24 h and on day 3 or 7 to determine compounds' stability over this time period.

4.21 X-ray Structure Determination

The crystal structure determination was carried out on Bruker Single Crystal X-ray Diffractometer. For crystalline gold(III) complexes, X-ray quality single crystals were mounted in a thin-walled glass capillary on a Bruker-Axs Smart Apex diffractometer equipped with graphite monochromatized Mo K α radiation ($\lambda = 0.71073 \text{ \AA}$). The data were collected using SMART software[156]. The data integration was performed using SAINT[157]. An empirical absorption correction was carried out using SADABS[158]. The structure was solved with direct methods and refined by full matrix least square methods based on F^2 , using the structure determination package SHELXTL [159] based on SHELX 97 [160]. Graphics were generated using ORTEP-3 [161] and MERCURY [162].

Single crystal data collection was also performed at 173K (-100°C) on a Stoe Mark II-IPD System [163] equipped with a two-circle goniometer and using MoK α graphite monochromated radiation. Diffraction data was collected using ω rotation scans of 0° – 180° at $\phi = 0^\circ$ and of 0° – 180° at $\phi = 90^\circ$ with $\text{step}\Delta\omega = 1.0^\circ$, exposures of 1 minute per image, 2θ range = 2.29° – 59.53° and d_{min} – $d_{\text{max}} = 17.779$ – 0.716 \AA . The distance between the imaging plate and the sample was 100 mm. Structure was solved by direct methods using the program SHELXS-97 [160]. The refinement and all further calculations were carried out using SHELXL-97 [160]. The H-atoms were either located from Fourier difference maps and freely refined or included in calculated positions and treated as riding atoms using SHELXL default parameters. The non-H atoms were refined anisotropically, using weighted full-matrix least-squares on F^2 . Empirical or

multiscanabsorption corrections were applied using and MULSCANABS routines in PLATON [164.]

4.22 Computational Study

The structures of some complexes were built and optimized using GAUSSIAN09 Revision A.1 program package [165] and GAUSSIAN03, Revision B.04 program package [166] at DFT/B3LYP level with LANL2DZ (Los Alamos ECP plus double-zeta) basis set [167,168]. Geometry optimization for the built structures was also carried out using the same software program.

4.23 Electrochemistry

The electrochemical experiments were performed at room temperature using a potentiostat (SP-300, BioLogic Science Instruments) controlled by EC-Lab v10.34 software package. All the measurements were performed on solutions deaerated by bubbling ultrapure nitrogen for 15 min. The potential values here reported were measured with respect to the saturated calomel electrode (SCE) serves as a reference electrode. The cyclic voltammetry of the complexes (1), (2) and (3) were measured at scan rate of 50 mV/s on a reference buffer (40 mM phosphate, 4 mM NaCl, pH 7.4) using platinum as working electrode and graphite as a counter electrode with a concentration of 1.0 mM at RT. Ferrocene was used as pseudo reference to calibrate the working electrode. The couple $\text{Fe}^{\text{III/II}}$ formal potential of ferrocene occur at $E^{\circ'} = +0.44$ V (vs SCE) in 0.1M Bu_4NPF_6 acetonitrile solution which is similar to the report value under the same experimental condition [169]. Conversion to values vs ENH was obtained upon adding +0.24 V to the relevant SCE values.

4.24 Anticancer Properties

Human gastric cancer SGC7901 cells and prostate cancer cells PC3 were incubated. MTT assay were used to detect cell proliferation and assess the inhibitory effect on the proliferation of SGC7901 and PC3 cells. In one culture plate, human gastric cancer SGC7901 and PC3 cells were treated with the gold(III) complex and the control (water) and in the second plate, only the complex and SGC7901 cells were kept in these two sets for an entire day (24 h) and for 3 days (72 h). In other sets, complexes with fixed concentration were employed to determine the growth inhibitory effect for both PC3 and SGC7901 cells. After being treated with complexes, cell viability was examined by MTT assay.

4.24.1 Assessment of Cell Proliferation

MTT assay was used to obtain the number of living cells in the sample. SGC7901 and PC3 cells were seeded on 96-well plates at a predetermined optimal cell density to ensure exponential growth in the duration of the assay. After 24 h pre-incubation, growth medium was replaced with experimental medium containing the appropriate drug or control. Six duplicate wells were set up for each sample, and cells untreated with drug served as control. Treatment was conducted at 24 h and 72 h sequentially. After incubation, 10 μ L MTT (6 g/L, Sigma) was added to each well and the incubation was continued for 4 h at 37 °C. After removal of the medium, MTT stabilization solution (dimethylsulfoxide:ethanol = 1:1) was added to each well, and shaken for 10 min until all crystals were dissolved. Then, optical density was detected in a micro plate reader at 550

nm wavelength using an ELISA reader. Each assay was performed in triplicate. Cell number and viability were determined by trypan blue dye exclusion analysis.

4.24.2 *in vitro* Cytotoxic assay for Cisplatin Sensitive Prostate (PC3) and Cisplatin Resistance Gastric (SGC7901) Cells

MTT assay was used to obtain the number of living cells in the sample. SGC7901 and PC3 cells were seeded on 96-well plates at a predetermined optimal cell density to ensure exponential growth in the duration of the assay. After 24 h pre incubation, growth medium was replaced with experimental medium containing the appropriate drug or control. Six duplicate wells were set up for each sample, and cells untreated with drug served as control. Treatment was conducted at 24, and 72 h respectively. After incubation, 10 μ L MTT (6 g/L, Sigma) was added to each well and the incubation was continued for 4 h at 37 °C. After removal of the medium, MTT stabilization solution (dimethylsulfoxide:ethanol = 1:1) was added to each well, and shaken for 10 min until all crystals were dissolved. Then, optical density was detected in a micro plate reader at 550 nm wavelength using an ELISA reader. Each assay was performed in triplicate. Cell number and viability were determined by trypan blue dye exclusion analysis.

Prostate PC3 and Human gastric SGC7901 cells were used in this study. Cells were cultured in Dulbecco's Modified Eagle Medium (DMEM) supplemented with 10 % fetal calf serum (FCS), penicillin (100 kU L⁻¹) and streptomycin (0.1 g L⁻¹) at 37 °C in a 5 % CO₂-95 % air atmosphere. Human gastric SGC7901 cells, prostate PC3 were incubated with these compounds at fixed concentrations or with water as control to assess the inhibitory effect on cell proliferation. The standard MTT assay has been used to assess

inhibitory effect on cells growth. The cell survival versus drug concentration is plotted. Cytotoxicity was evaluated with reference to the IC₅₀ value. The half maximal inhibitory concentration (IC₅₀) is a measure of the effectiveness of a compound in inhibiting biological or biochemical function. According to the FDA, IC₅₀ represents the concentration of a drug or compound or complex that is required for 50 % inhibition *in vitro*. It is evaluated from the survival curves as the concentration needed for a 50 % reduction of survival. IC₅₀ values are expressed in μM [170]. IC₅₀ values were calculated from dose-response curves obtained in replicate experiments.

4.24.3 Assay For Inhibitory Effect Complexes (1-129) on Prostate (PC3) and Gastric (SGC7901) Cancer Cells

MTT assay was used to obtain the number of living cells in the sample. Human gastric cancer SGC7901 and prostate cancer PC3 cells were seeded on 96-well plates at a predetermined optimal cell density i.e.ca 6,000 cells/100 μL per well in 96-well plates to ensure exponential growth in the duration of the assay. After 24 h pre incubation, growth medium was replaced with experimental medium containing the appropriate drug using gold complex or control using water. Six duplicate wells were set up for each sample, and cells untreated with drug served as control. In one sets of culture plate, human gastric cancer SGC7901 and human prostate PC3 cells were treated with the complexes **(1-129)** as drug and the control (water) for 24, 48 and 72 h. In other sets, complexes with fixed concentration i.e. 10 μM were employed to determine the growth inhibitory effect for both PC3 and SGC7901 cells separately. After incubation, 10 μL MTT (6 g/L, Sigma) was added to each well and the incubation was continued for 4 h at 37 °C. After removal

of the medium, MTT stabilization solution [Dimethyl sulfoxide (DMSO): Ethanol = 1:1] was added to each well, and shaken for 10 min until all crystals were dissolved. Then, optical density was detected in a micro plate reader at 550 nm wavelength using an Enzyme-Linked Immuno-Sorbent Assay (ELISA) reader. After being treated with the complexes, cell viability was examined by MTT assay. Each assay was performed in triplicate. MTT assay for inhibitory effect has been used for all synthesized complexes **(1-129)** against PC3 and SGC7901 cells. These cells were treated with various concentrations of complexes (1-129) for 24-72 h.

CHAPTER 5

RESULTS AND DISCUSSION

5.1 Gold(III) 1,2-Diaminocyclohexane dichloridoComplexes

This work reports the synthesis of gold(III) complexes of the type [(DACH)AuCl₂]Cl derived from sodium tetrachloroaurate(III) dihydrate NaAuCl₄·2H₂O, where DACH is 1,2-diaminocyclohexane, have been synthesized.

5.1.1 MID-IR and Far-IR Spectroscopic Studies

Table 5.1 lists the significant IR bands of free DACH ligand and their gold(III) complexes. The N-H stretching band, which occurs around 3300 cm⁻¹ for the free ligands shifts towards higher frequency (blue shift) upon complexation by about 150 cm⁻¹. Another important vibrational band observed in IR spectra is the C-N stretching which also showed a slight shift to higher wave number indicating a shorter C-N bond in the complex than in the free ligand. The N-H band appears at much higher frequency in *trans*-DACH complexes and in the *cis*-DACH complex compare with free ligands. For example, the N-H frequency shift is about 137 and 364 cm⁻¹ in complexes (37) and (38) respectively, while this shift is about 93 cm⁻¹ in complex (36). The larger N-H wave number shifts designate the strong coordination of ligands in complexes (37) and (38) with the gold(III) centre. This may be due to the different in the stereochemistry of the *cis* and *trans*-1,2-DACH-gold(III).

Table 5.1 IR frequencies, $\nu(\text{cm}^{-1})$ for [(1,2-DACH)Au(III)Cl₂]Cl complexes

Complex	$\nu(\text{N-H})$	ν_{shift}	$\nu(\text{C-N})$	ν_{shift}
<i>cis</i> -(±)-1,2-(DACH)	3356 m, 3286 m		1092s	
(36)	3414 w	93	1183 s	91
<i>trans</i> -(±)-1,2-(DACH)	3348 m, 3271 m, 3183 m		1082 m	
(37)	3485 w, 3420 w, 3384 w	137, 149, 201	1175 m	93
(<i>S,S</i>)-(+)-1,2-(DACH)	3340 m, 3252 m, 3167 m		1082 m	
(38)	3604 m, 3340 m, 3306 m	364, 88, 139	1171 m	89

Table 5.2 lists the significant IR bands of NaAuCl₄precursor complex and gold(III) complexes (**36-38**). Far-IR showed absorption bands at 353 and 367cm⁻¹ for symmetric and asymmetric stretching of the Au-Cl, which is consistent with Au-Cl stretching mode *trans* to nitrogen [171,172]. Another group of bands at 395 and 437cm⁻¹ could be assigned for the symmetric and asymmetric stretching of the Au-N bond [173]. The red shift of the DACH complexes with respect to the auric acid shows the weakening of the Au-Cl bond.

Table 5.2 Far-IR frequencies, $\nu(\text{cm}^{-1})$ for [(1,2-DACH)Au(III)Cl₂]Cl complexes.

Species	$\nu(\text{Au-Cl})$	$\nu(\text{Au-N})$
NaAuCl ₄	369	
(36)	352, 367	437
(37)	353, 365	437
(38)	353, 366	395, 436

5.1.2 UV-Vis Studies

The λ_{max} values for the complexes studied are shown in Table 5.3. Au(III) complexes show absorption in the region 250–350nm (40000–28570cm⁻¹) which correspond to LMCT transitions signal at 300nm that could be assigned to Cl→Au charge transfer by

analogy to auric acid absorption spectra which give a band at 320nm [174], where this transition of high extinction coefficient cannot be assigned to the symmetry forbidden d-d transition. According to crystal field theory for d^8 complexes the LUMO orbital is $d_{x^2-y^2}$, so ligand to metal charge transfer could be due to $p_{\sigma} \rightarrow d_{x^2-y^2}$ transition [175]. The electronic spectra of these compounds remain unchanged which is consistent with the fact that the gold centre remains in the +3 oxidation state.

Table 5.3 UV–Vis spectra λ_{\max} for [(1,2-DACH)Au(III)Cl₂]Cl complexes

Complex	λ_{\max} (nm)
HAuCl ₄	320.0
NaAuCl ₄	292.5
(36)	302.5
(37)	301.6
(38)	301.5

5.1.3 Solution NMR Studies

The ^1H and ^{13}C NMR chemical shifts of compounds **(36)**-**(38)** along with their corresponding free ligand are listed in Table 5.4 and Table 5.5, respectively. Also, the ^1H and ^{13}C NMR spectra of complexes **(36)**-**(38)** are shown in Figures 5.1 and 5.2, respectively. Complexes **(36)**-**(38)** depicted one half of the total expected signals because the presence of the C_2 symmetry axis. 1,2-diaminocyclohexane ring is considered as a rigid conformer that allowed to distinguish equatorial H3 and H4 from axial H3 and H4 at room temperature. ^1H NMR downfield shift was observed for complexes with respect to the free diamine ligands. The significant downfield shift was observed at 3.59 ppm for **(36)** complex with respect to the free DACH ligand at 2.23 ppm. This can be attributed

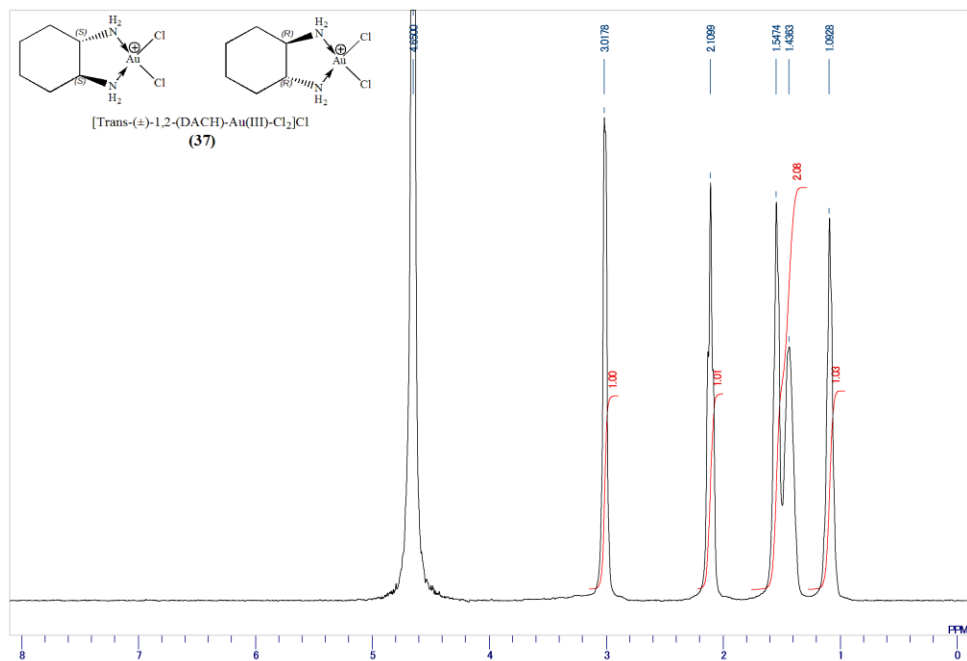
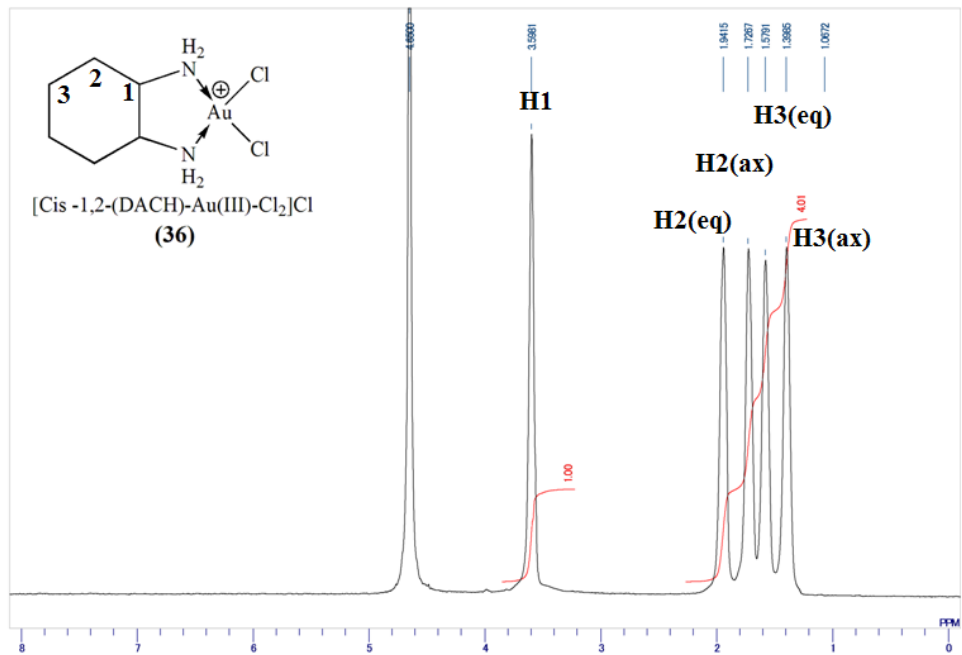
to the donation of nitrogen lone pairs to the gold that causes de-shielding of the proton(s) next to the bonding nitrogen. On the other hand, ^{13}C NMR downfield shift was observed only for the carbon next to the bonding nitrogen and the others carbons in the complex showed upfield shift. For instance, chemical shift of C3 and C4 for complex 1 observed at 26.78 and 21.43 ppm, respectively, whereas, for free diamine ligand it occurs at 35.26 and 26.36 ppm. It is also worth to mention that complexes **(36)**-**(38)**, even though they have same skeleton of DACH, their NMR chemical shifts aren't the same due to different in their stereochemistry upon complexation.

Table 5.4 ^1H NMR chemical shifts of free ligands and [(1,2-DACH)Au(III)Cl₂]Cl complexes in CD₃OD

Compound	^1H (δ in ppm)				
	H1,H2	H3,H6 (eq)	H3,H6 (ax)	H4,H5 (eq)	H4,H5 (ax)
(36')	2.23, <i>m</i>	1.85, <i>m</i>	1.69, <i>m</i>	1.28, <i>m</i>	1.12, <i>m</i>
(37')	2.25, <i>m</i>	1.85, <i>m</i>	1.68, <i>m</i>	1.28, <i>m</i>	1.11, <i>m</i>
(38')	2.24, <i>m</i>	1.85, <i>m</i>	1.69, <i>m</i>	1.28, <i>m</i>	1.11, <i>m</i>
(36)	3.60, <i>m</i>	1.95, <i>m</i>	1.73, <i>m</i>	1.58, <i>m</i>	1.40, <i>m</i>
(37)	3.04, <i>m</i>	2.18, <i>m</i>	1.69, <i>m</i>	1.54, <i>m</i>	1.22, <i>m</i>
(38)	3.09, <i>m</i>	2.20, <i>m</i>	1.67, <i>m</i>	1.55, <i>m</i>	1.22, <i>m</i>

Table 5.5 ^{13}C NMR chemical shifts of free ligands and [(1,2-DACH)Au(III)Cl₂]Cl complexes in CD₃OD.

Compound	^{13}C (δ in ppm)		
	C1,C2	C3,C6	C4,C5
(36')	58.20	35.26	26.36
(37')	58.46	35.55	26.63
(38')	58.27	35.32	26.43
(36)	63.33	26.78	21.43
(37)	65.87	33.58	24.85
(38)	65.94	33.47	24.65



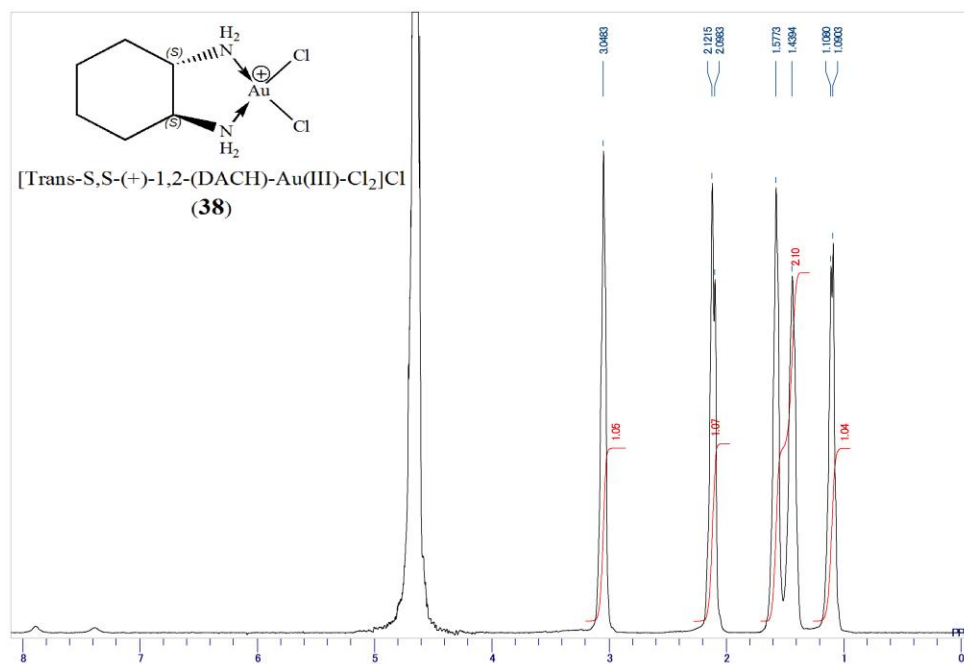
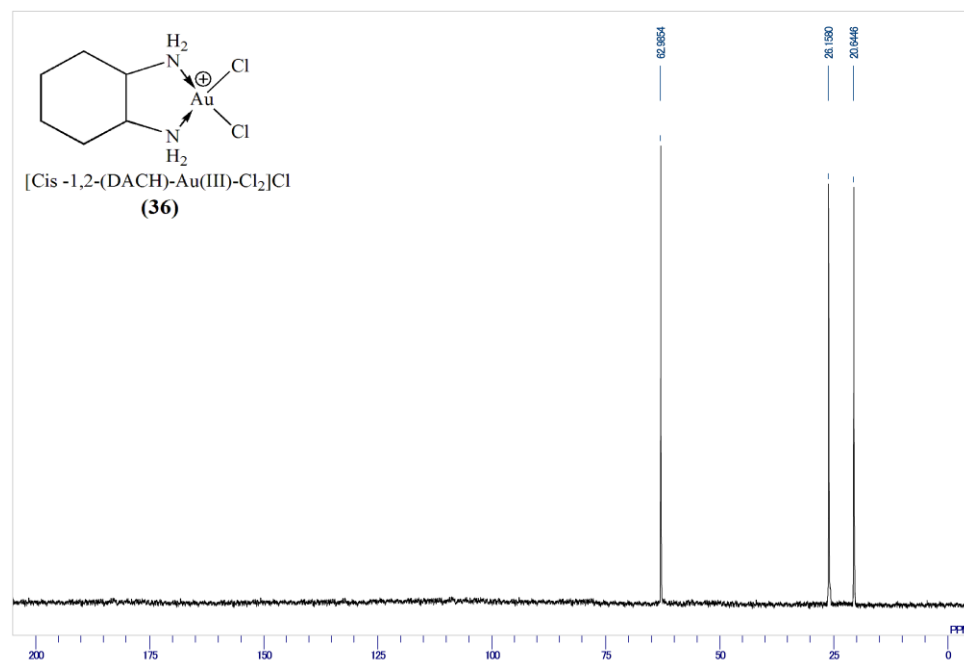


Figure 5.1 The 500-MHz ¹H solution NMR spectrum of [(1,2-DACH)Au(III)Cl₂]Cl complexes



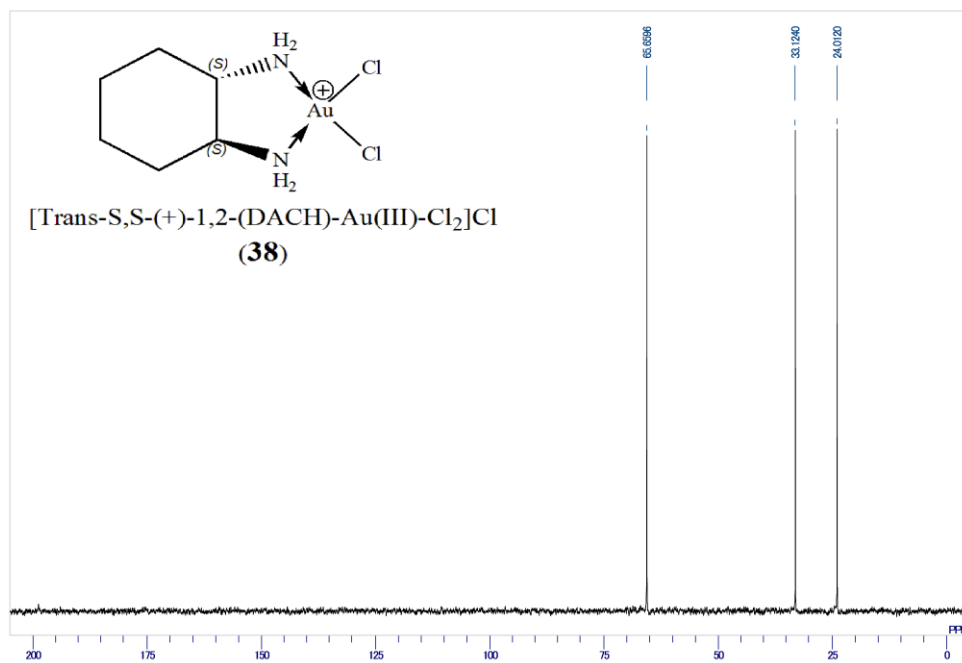
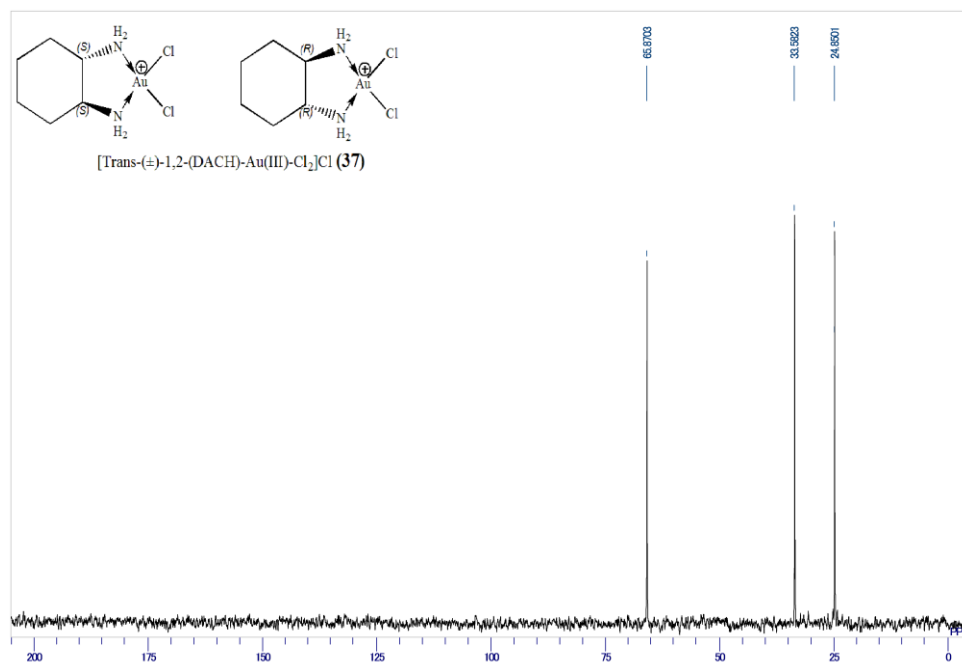


Figure 5.2 The 125.65-MHz $^{13}\text{C}\{^1\text{H}\}$ solution NMR spectrum of $[(1,2\text{-DACH})\text{Au}(\text{III})\text{Cl}_2]\text{Cl}$ complexes

5.1.4 Solid State NMR

The ^{13}C CPMAS NMR spectral data for complexes (**36-38**) are shown in Table 5.6. At the spinning rate of 8 kHz, only the isotropic signals were observed for the carbons, indicating small anisotropy due to the sp^3 hybridization of these atoms. Compared to solution chemical shifts, substantial de-shielding in solid state is observed with similarity in the chemical shift among all synthesized complexes (Table 5.6) which is a clear indication of the stability of the prepared complexes. Solid state NMR spectra of complexes (**36**) showed two sets of peaks with equal intensity which supports the idea of the inequivalency of all six carbon atoms of DACH. This indicates that complex (**36**) in the solid state lacks C_2 symmetry. However, complexes (**37**) and (**38**) showed C_2 symmetry in the solid state as shown in Figure 5.3 and Table 5.6.

Table 5.6 Solid ^{13}C NMR chemical shifts of [(1,2-DACH)Au(III)Cl₂]Cl complexes.

Compound	^{13}C (δ in ppm)		
	C1,C2	C3,C6	C4,C5
(36)	69.20, 65.35	30.98	27.02, 22.12
(37)	69.60	37.37	27.99
(38)	70.21	37.86	29.16

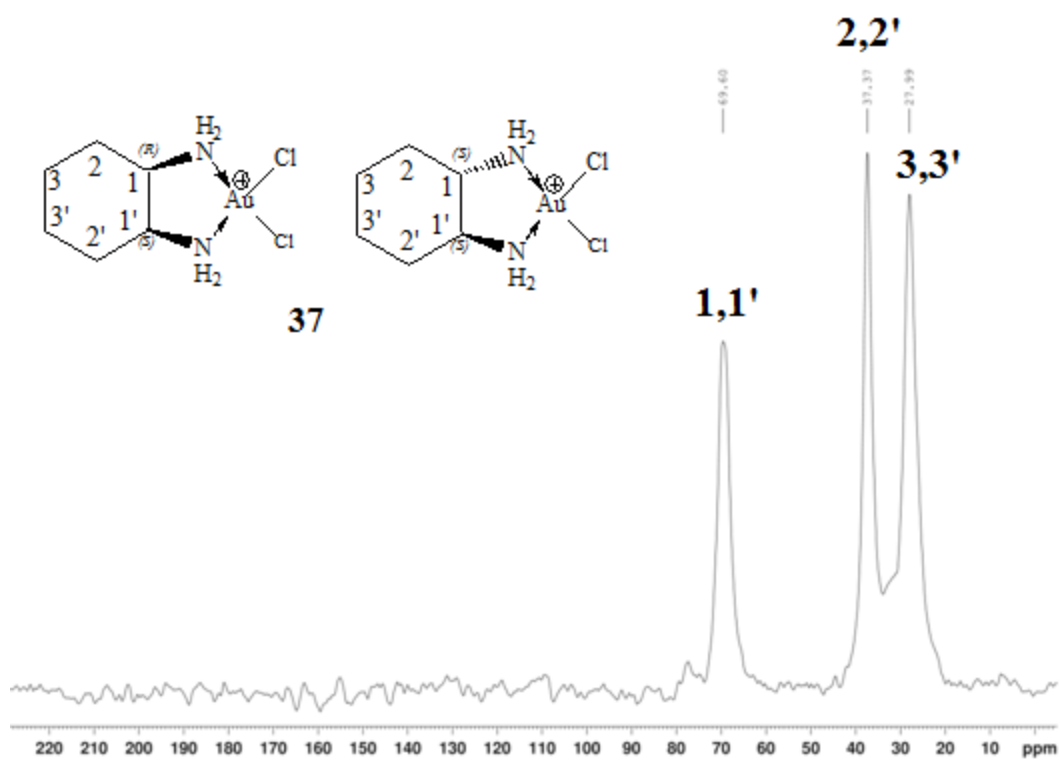
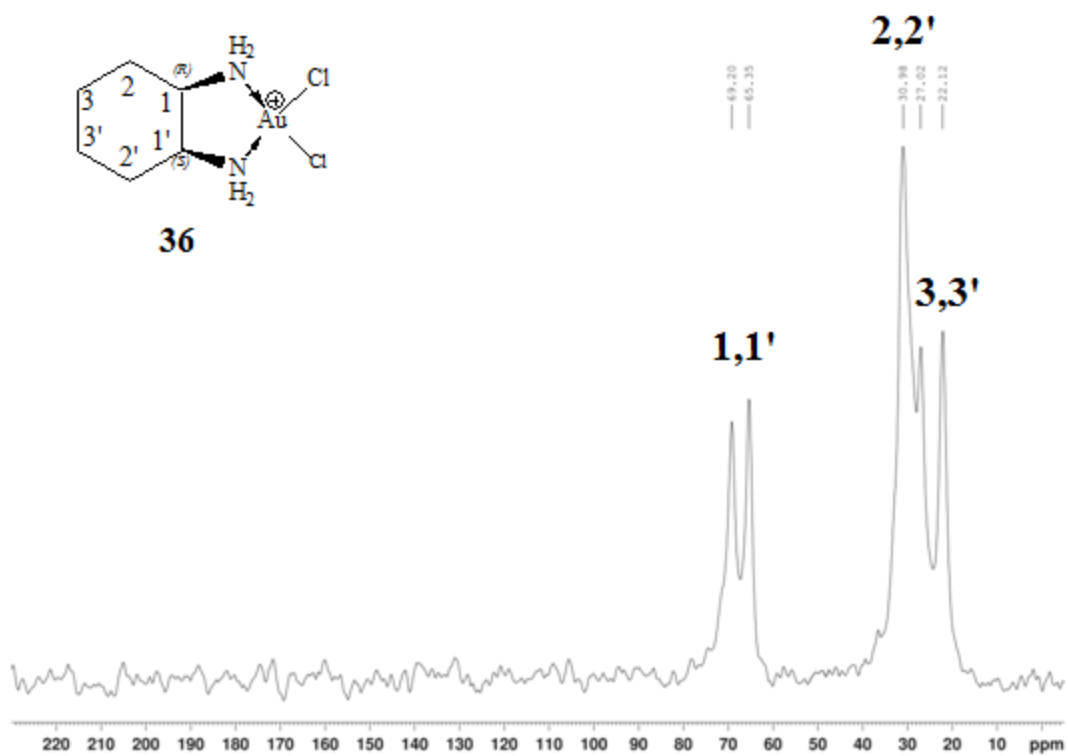


Figure 5.3 Solid state $^{13}\text{C}\{^1\text{H}\}$ NMR spectra of complexes 36 & 37

The chemical shifts of 69.2-70.21 ppm in solid state ^{13}C NMR, for complex (36-38) are slightly higher than that of the solution NMR chemical shifts 63.33-65.94 ppm (Table 5.5) which is a clear indication of the stability of the prepared complexes in solid state as well as the conservation of the bond topology in solution as in the solid form.

5.1.5 Crystal structure of complexes (36) and (37)

Figure 5.4 showed the crystal structure of complex (36). The gold(III) ion is bonded to two nitrogen atoms of the *cis*-cyclohexane-1,2-diamine ligand and two chloride ions in a distorted square planar geometry (Figure 5.4). The two Au-N bond distances are not significantly different (2.029(4) Å while Au-Cl bond distances are 2.261(1) Å and 2.268(1) Å respectively (Table 5.7 and Table 5.8). The Cl-Au-Cl and N-Au-N bond angles are 91.83(5) ° and 83.9(2) ° respectively. The later value reflects the chelation strain of the diamine ligand. These values are similar to those found in dichlorido-(ethylenediamine-N,N')-gold(III) chloride dehydrate [176] and dichlorido-(1,2-ethanediamine)-gold(III) nitrate [177]. The cyclohexyl ring adopts a chair conformation. The square planar geometry and the five-membered ring strain impose a torsion angle N1-C1-C2-N2 of 49.80°. All amine hydrogen atoms are engaged in hydrogen bonding with Cl⁻ counter ion. To the best of our knowledge this is the first X-ray structure of a gold complex based on cyclohexane-1,2-diamine [178]. A molecule of ethanol is present in the lattice. It presents an orientation disorder on a two-fold rotation axis. The metal complex molecules pack head to tail to generate molecular chains along the c axis, which in turn pack into layers, parallel to the ac plane (Figure 5.5). These are separated by sheets hosting columns of disordered ethanol molecules and Cl⁻ counter ions having hydrogen bonding interactions with the NH₂ groups of adjacent layers.

The crystal structure of complex **(37)** is depicted in Figure 5.6. In this case the asymmetric unit contains two cationic molecules of the gold complex, two chloride counter ions and one crystallization water molecule. Similarly to **(36)**, in both molecules the gold(III) ion is bonded to two nitrogen atoms of the trans-cyclohexane-1,2-diamine ligand and two chloride ions (Figure 5.6). The geometry is distorted square planar with Au-N and Au-Cl bond distances in the ranges (2.029(6)-2.054(7) Å) and (2.259(3)-2.276(2) Å) respectively, similar N-Au-N bond angles of 84.1(2) ° in addition to Cl-Au-Cl bond angles in the range (91.4(1)-93.81(8) °). The coordination sphere bond distances and bond angles are similar to those of compound **(36)**. The two cyclohexyl rings adopt a chair conformation with N1-C1-C6-N2 and N3-C7-C12-N4 torsion angle of 55.78° and 52.33° respectively. Hydrogen bonding interactions take place between the amino groups and the chloride counter ions.

Table 5.7 Crystal and structure refinement data for compounds **(36)** and **(37)**

Compound	(36)	(37)
CCDC deposit no.	831613	850216
Empirical formula	C ₁₄ H ₃₄ Au ₂ Cl ₆ N ₄ O	C ₁₂ H ₃₀ Au ₂ Cl ₆ N ₄ O
Formula weight	881.09	853.03
Temperature (K)	297(2)	295(2)
Wavelength (Å)	0.71073	0.71073
Crystal system	Orthorhombic	Monoclinic
Space group	Pbcn	P2 ₁
Unit cell dimensions		
<i>a</i> (Å)	19.792(1)	9.5898(7)
<i>b</i> (Å)	12.4662(7)	8.6106(6)
<i>c</i> (Å)	10.3212(6)	14.477(1)
β (°)		95.307(1)
Volume (Å ³)	2546.5(2)	1190.3(2)
Z	4	2
Calc. density (g.cm ⁻³)	2.298	2.38
Absorp. coefficient (mm ⁻¹)	12.152	12.994
F(000)	1656	796
Crystal size (mm)	0.40 x 0.37 x 0.26	0.52 x 0.49 x 0.16

θ range ($^{\circ}$)	1.93 - 28.29	1.41 - 28.28
Limiting indices	$-26 \leq h \leq 26$ $-16 \leq k \leq 16$ $-13 \leq l \leq 13$	$-12 \leq h \leq 12$ $-11 \leq k \leq 11$ $-19 \leq l \leq 19$
Max and min transmission	$T_{\min} = 0.0850$, $T_{\max} = 0.1443$	$T_{\min} = 0.0564$, $T_{\max} = 0.2244$
Data/restraints/parameters	3162 / 0 / 128	5835 / 2 / 230
Goodness-of-fit on F^2	1.051	1.017
Final R indices [$I > 2\sigma(I)$]	$R_1 = 0.0246$, $wR_2 = 0.0631$	$R_1 = 0.0308$, $wR_2 = 0.0739$
R indices (all data)	$R_1 = 0.0288$, $wR_2 = 0.0654$	$R_1 = 0.0329$, $wR_2 = 0.0747$
Largest diff. Peak and hole ($e \text{ \AA}^{-3}$)	1.766 and -1.544	0.796 and -1.555

Table 5.8 Selected bond lengths (\AA) and bond angles ($^{\circ}$) for compounds (36) and (37)

(36)	(37)	
Au1-N1 2.029(4)	Au1-N1 2.029(6)	Au2-N3 2.029(6)
Au1-N2 2.030(3)	Au1-N2 2.031(5)	Au2-N4 2.054(7)
Au1-Cl1 2.261(1)	Au1-Cl1 2.274(2)	Au2-Cl3 2.259(3)
Au1-Cl2 2.268(1)	Au1-Cl2 2.276(2)	Au2-Cl4 2.266(2)
N1-Au1-N2 83.9(2)	N1-Au1-N2 84.3(2)	N3-Au2-N4 84.1(2)
N1-Au1-Cl1 91.7(1)	N1-Au1-Cl1 92.0(2)	N3-Au2-Cl3 92.2(2)
N2-Au1-Cl1 175.4(1)	N2-Au1-Cl1 176.2(2)	N4-Au2-Cl3 176.2(2)
N1-Au1-Cl2 176.0(1)	N1-Au1-Cl2 174.2(2)	N3-Au2-Cl4 176.4(2)
N2-Au1-Cl2 92.6(1)	N2-Au1-Cl2 89.9(2)	N4-Au2-Cl4 92.3(2)
Cl1-Au1-Cl2 91.83(5)	Cl1-Au1-Cl2 93.81(8)	Cl3-Au2-Cl4 91.4(1)

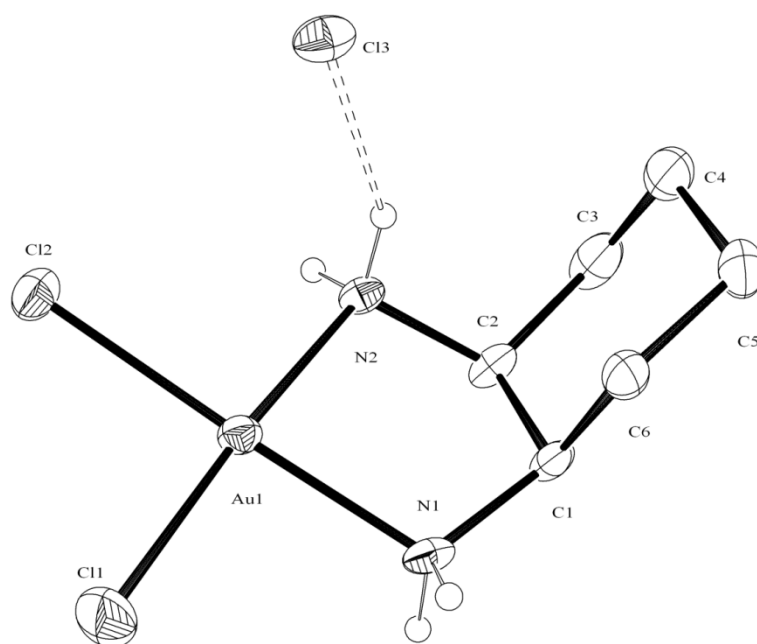


Figure 5.4 X-ray structure of $[cis-(1,2-DACH)Au(III)Cl_2]Cl$ (36)

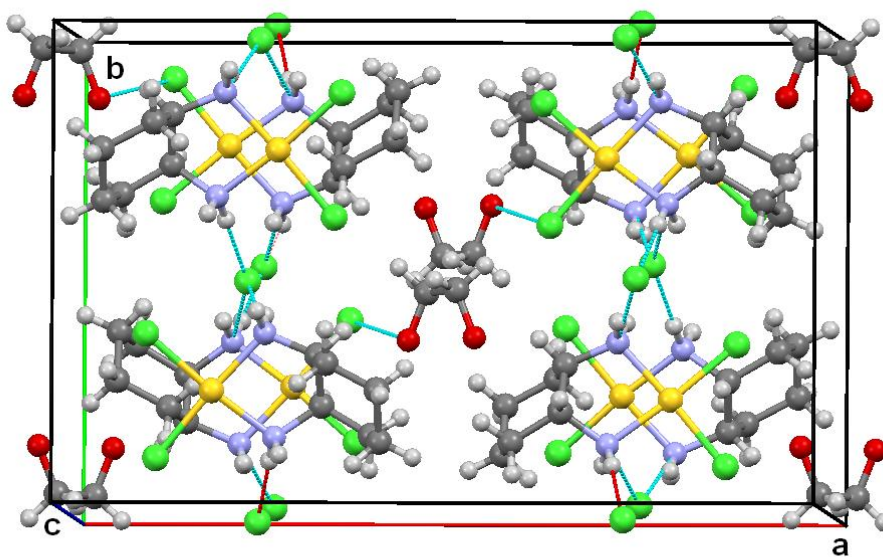


Figure 5.5 Molecular packing in $[cis-(1,2-DACH)Au(III)Cl_2]Cl$ (36)

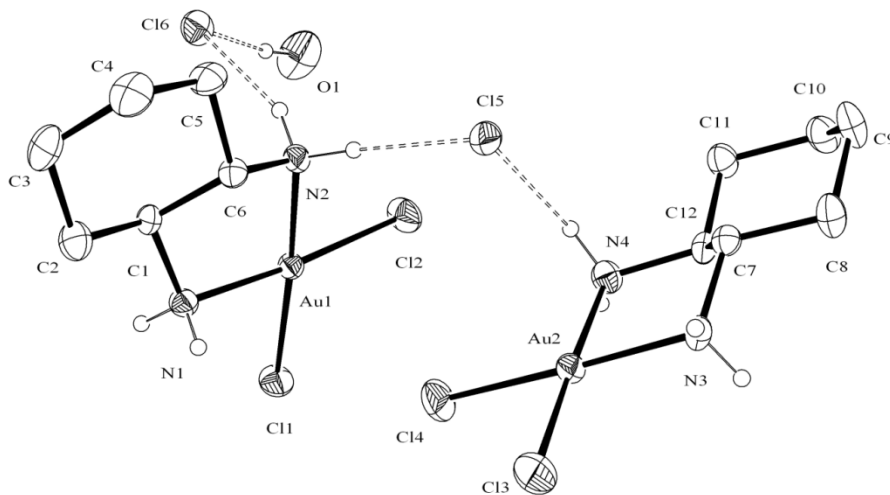


Figure 5.6 X-ray structure of compound [*trans*-(1,2-DACH)Au(III)Cl₂]Cl (**37**)

5.1.6 Effect of Complexes (**36**)-(**38**) on cell proliferation

The cytotoxicity assay was performed with compounds (**36-38**) on PC3 and SGC7901 cells. The bioassay tests were completed for compounds (**36-38**) under various experimental conditions. The cytotoxicity assay was performed with various concentrations of the synthesized gold(III) complexes on PC-3 and SGC-7901 cells. The experimental PC-3 and SGC-7901 cells were treated with various concentrations of (**36**), (**37**) and (**38**) for 24–72 h and the cell viability was determined as described above by MTT assay and the results are shown in Table 5.9 and Table 5.10 as well as in Figures 5.7–5.13. As depicted in Figures 5.7–5.9, *cis*-(±)-1,2-(DACH)-gold complex exhibited potentially high activity against gastric cancer cell SGC-7901 and human prostate cancer cells after 24 and 72 h of treatment with 10 μM. Whereas, *trans*-(±)-1,2-(DACH) and

purely chiral *trans*-(-)-1,2-(DACH) gold complexes showed moderate inhibition against SGC-7901 and PC-3 cell lines under the same assay experimental condition. From Figures 5.10-5.12, it is also quite clear that gold(III) complexes under study showed concentration dependent cytotoxic effect on cancerous cells PC-3 and SGC-7901. It can be concluded from Figures 5.8, 5.9, 5.11 and 5.12 that there isn't significant difference in the bioactivity between *trans*-(1*R*,2*R*)-(DACH) isomer and *trans*-(1*S*,2*S*)-(DACH) isomer. To the best of our knowledge these are the first bioassay tests reported for gold(III) complex based on cyclohexane-1,2-diamine.

In a time dependent activity studies, it is revealed that after 72 h of the experiment with compound **(36)** on PC-3 cell, the cell proliferation is bit higher than that of the SGC-7901 cells at fixed 10 μ M concentration (Figure 5.7). Furthermore, in Figure 5.13, the bioassay tests results demonstrate that the compound **(36)** at 10 μ M concentrations has higher anti-proliferation effect in comparison with the same concentrations of compounds **(37)** and **(38)**.

Table 5.9 Effect of compound **(36)** on PC3 cell line and SGC-7901 cell line (mean, SD) after incubation for 24h and 72h

Group	PC3 Cell line		SGC-7901 Cell line	
	Day 1 (24 h)	Day 3 (72 h)	Day 1 (24 h)	Day 3 (72 h)
Control	0.75 \pm 0.02	1.39 \pm 0.11	0.54 \pm 0.02	1.09 \pm 0.06
(36)	0.70 \pm 0.29	0.81 \pm 0.17	0.79 \pm 0.40	0.85 \pm 0.23

Table 5.10 Cytotoxicity of the compound [cis-(1,2-DACH)Au(III)Cl₂]Cl (36) toward different tumor cell lines. The data were collected after 72h exposure to compound

Compounds	SGC-7901	PC3
Cisplatin	1.1± 0.1	7.3± 0.5
[cis-(1,2-DACH)Au(III)Cl ₂]Cl(36)	8.5 ± 0.2	8.1 ± 0.2

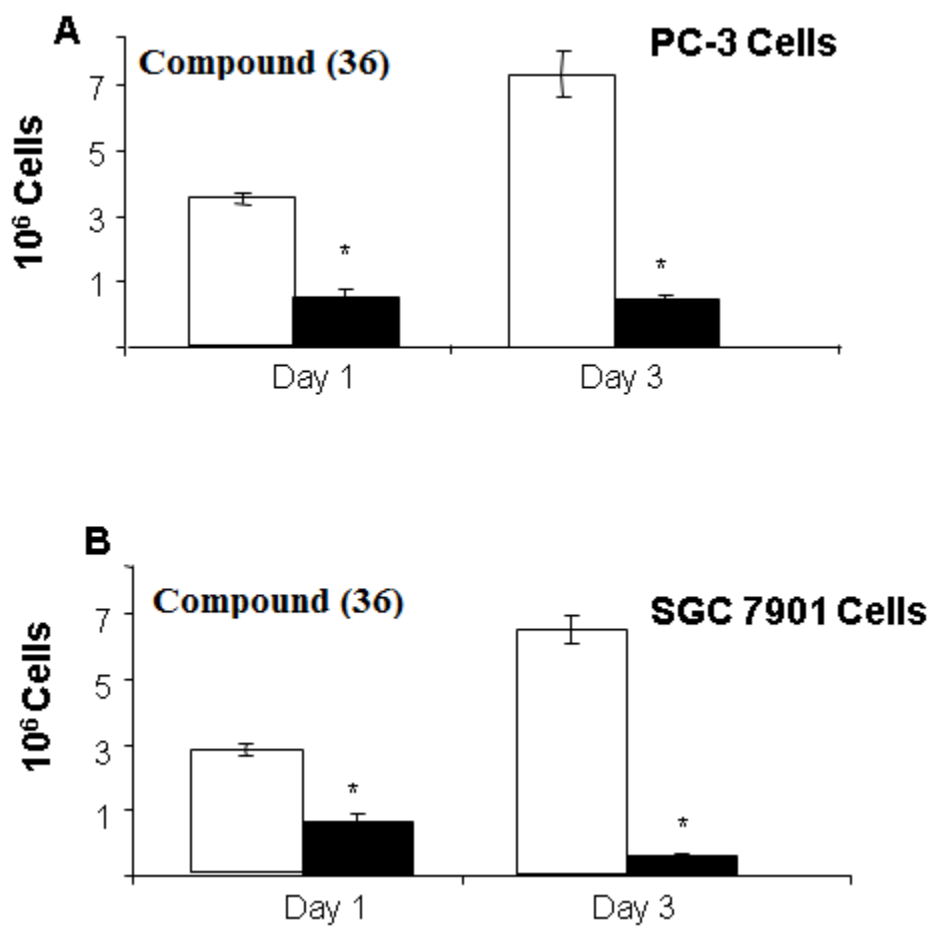


Figure 5.7 Effect of *cis*-(±)1,2-(DACH)-gold(III)complex on cell growth in (A) PC-3 and (B) SGC-7901 cells. The cells were treated with 10 μM for 1 day and 3 days. The anti-proliferative effect was measured by MTT assay. Results were expressed as the mean, SD. **P*<0.05

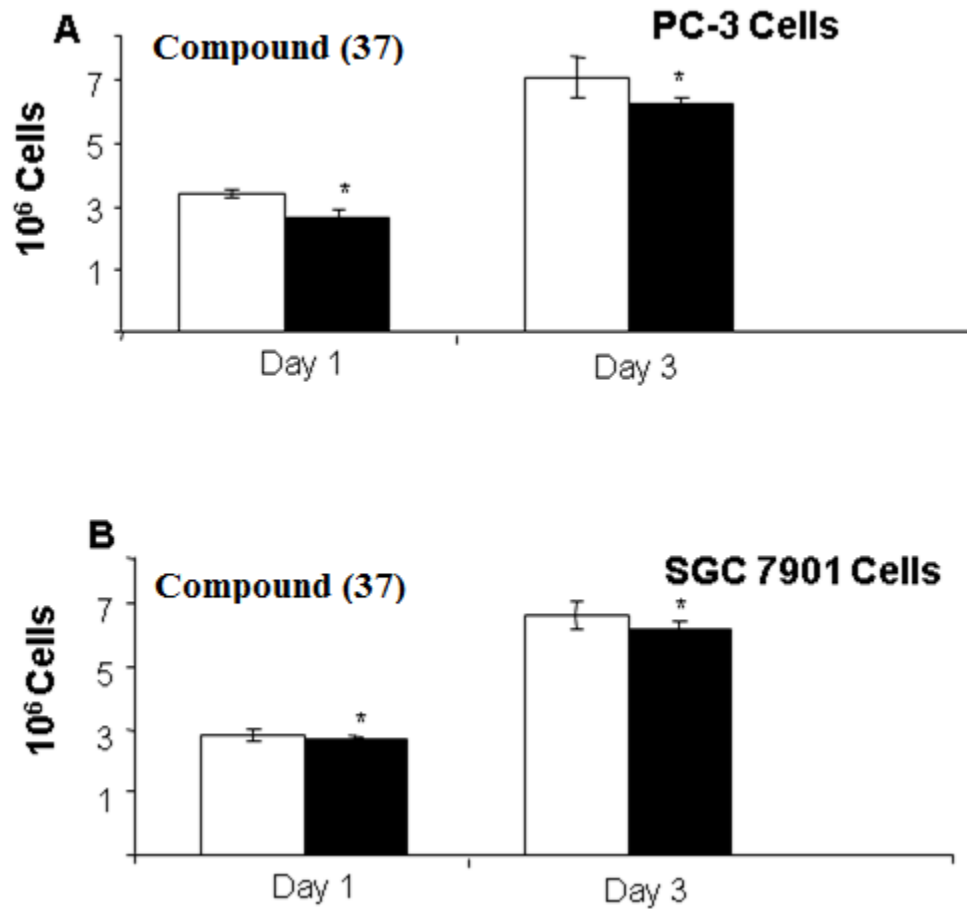


Figure 5. 8 Effect of *trans*-(±)1,2-(DACH)-gold(III) complex on cell growth in (A) PC-3 and (B) SGC-7901 cells. The cells were treated with 10 μ M for 1 day and 3 days. The anti-proliferative effect was measured by MTT assay. Results were expressed as the mean, SD. * P <0.05

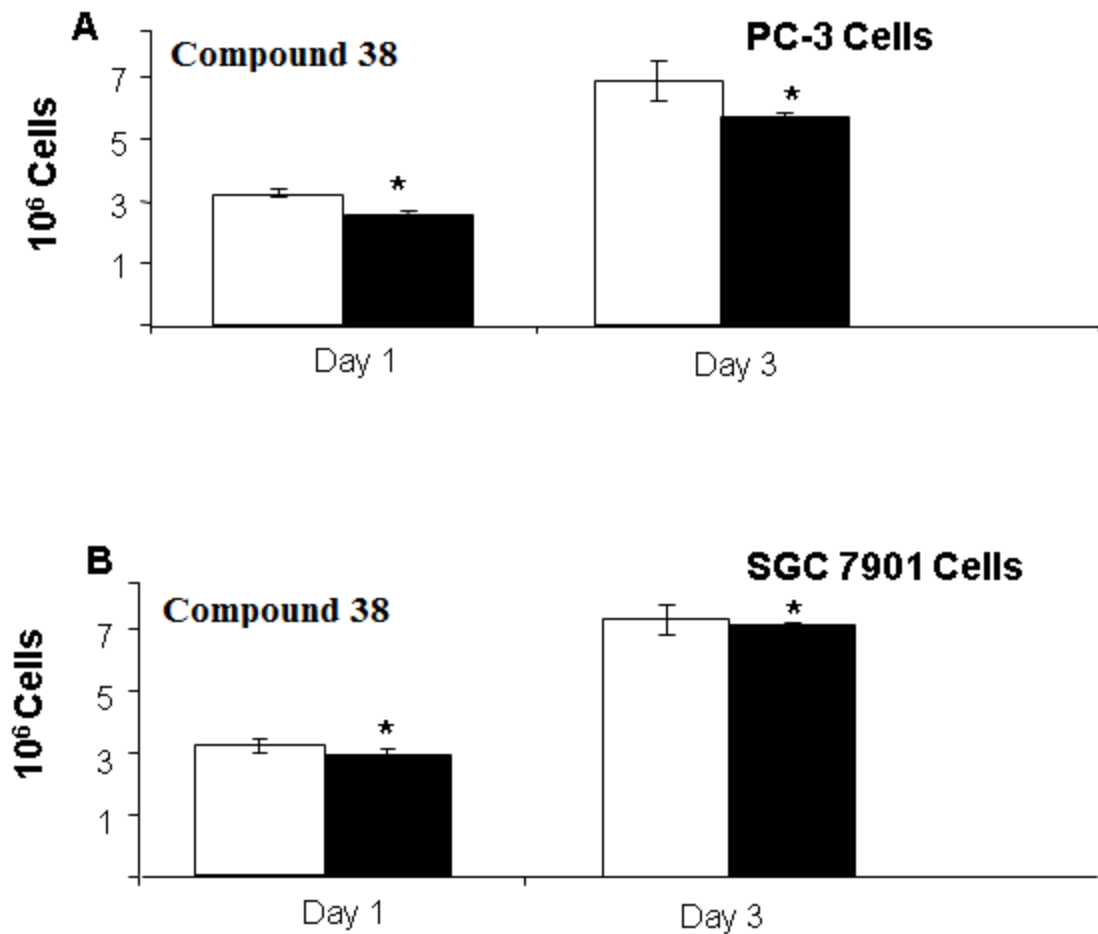


Figure 5.9 Effect of (*S,S*)-(+)-1,2-(DACH)-gold(III) complex on cell growth in (A) PC-3 and (B) SGC-7901 cells. The cells were treated with 10 μ M for 1 day and 3 days. The anti-proliferative effect was measured by MTT assay. Results were expressed as the mean, SD. * P <0.05

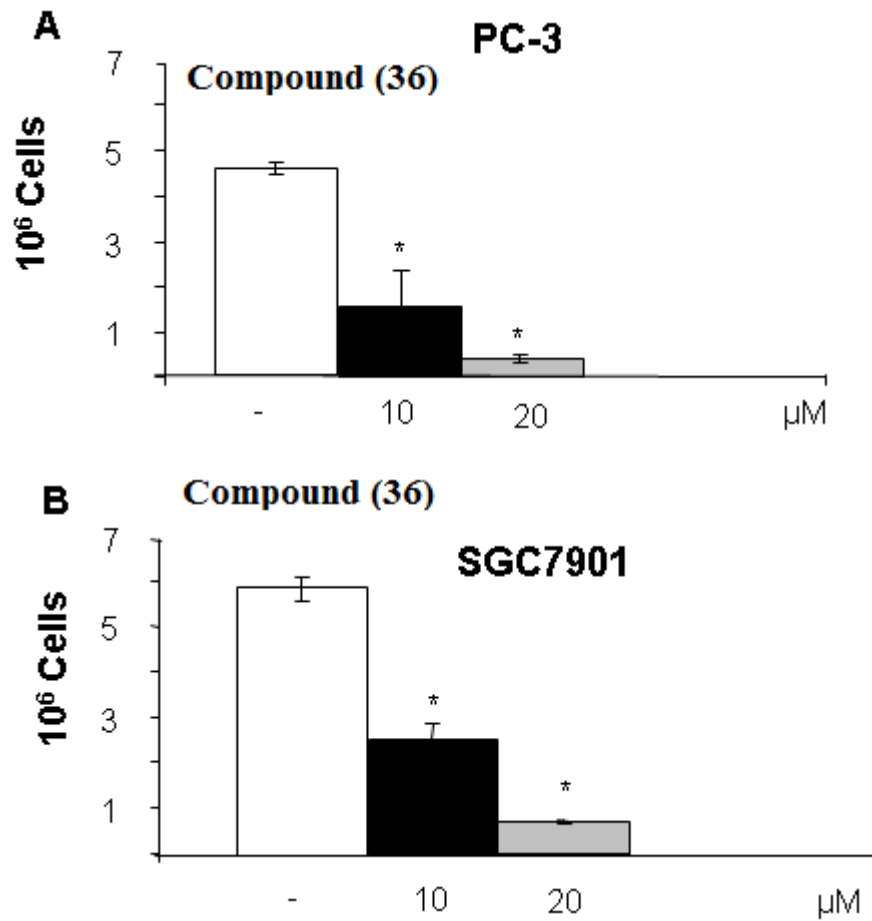


Figure 5.10 Effect of *cis*-(±)-1,2-(DACH)-gold complex on cell growth in (A) PC-3 and (B) SGC-7901 cells. The cells were treated with various concentrations for 24 h. The anti-proliferative effect was measured by MTT assay. Results were expressed as the mean, SD. * $P < 0.05$

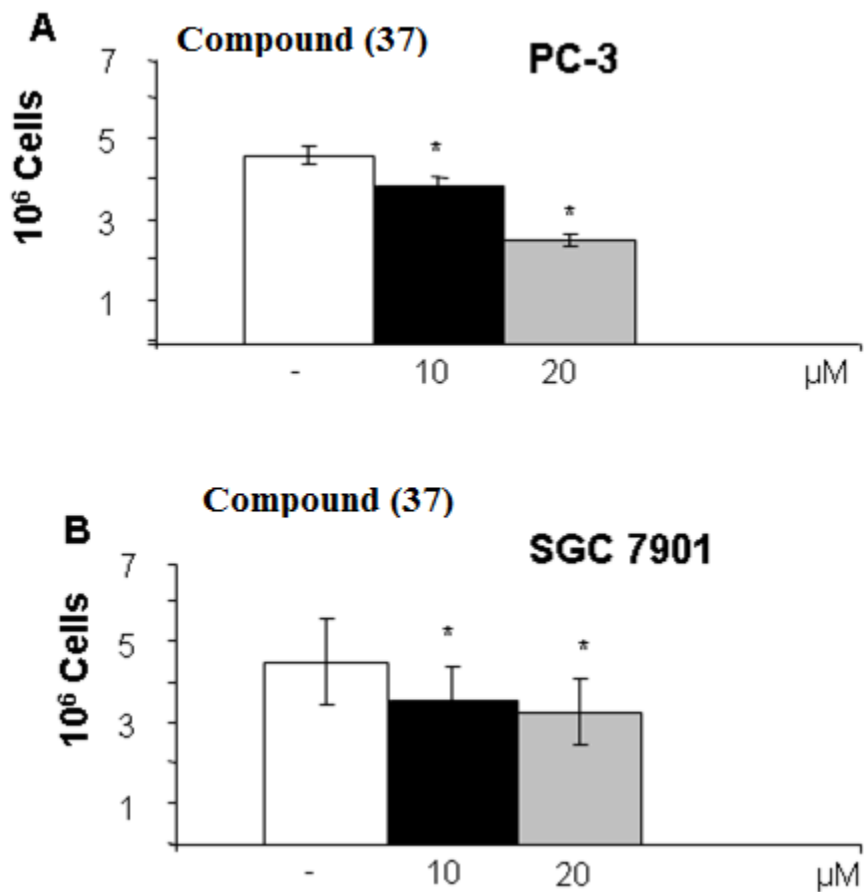


Figure 5.11 Effect of *trans*-(±)-1,2-(DACH)-gold complex on cell growth in (A) PC-3 and (B) SGC-7901 cells. The cells were treated with various concentrations for 24 h. The anti-proliferative effect was measured by MTT assay. Results were expressed as the mean, SD. * $P < 0.05$

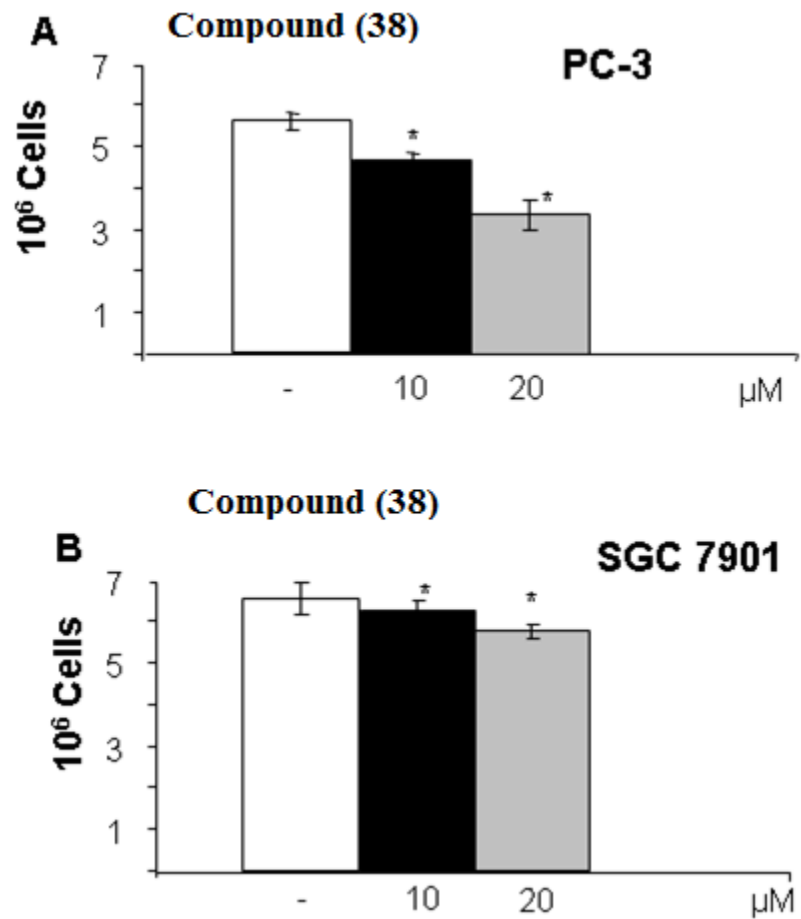


Figure 5.12 Effect of (*S,S*)-(+)-1,2-(DACH)-gold(III) complex on cell growth in (A) PC-3 and (B) SGC-7901 cells. The cells were treated with various concentrations for 24 h. The anti-proliferative effect was measured by MTT assay. Results were expressed as the mean, SD. **P*<0.05

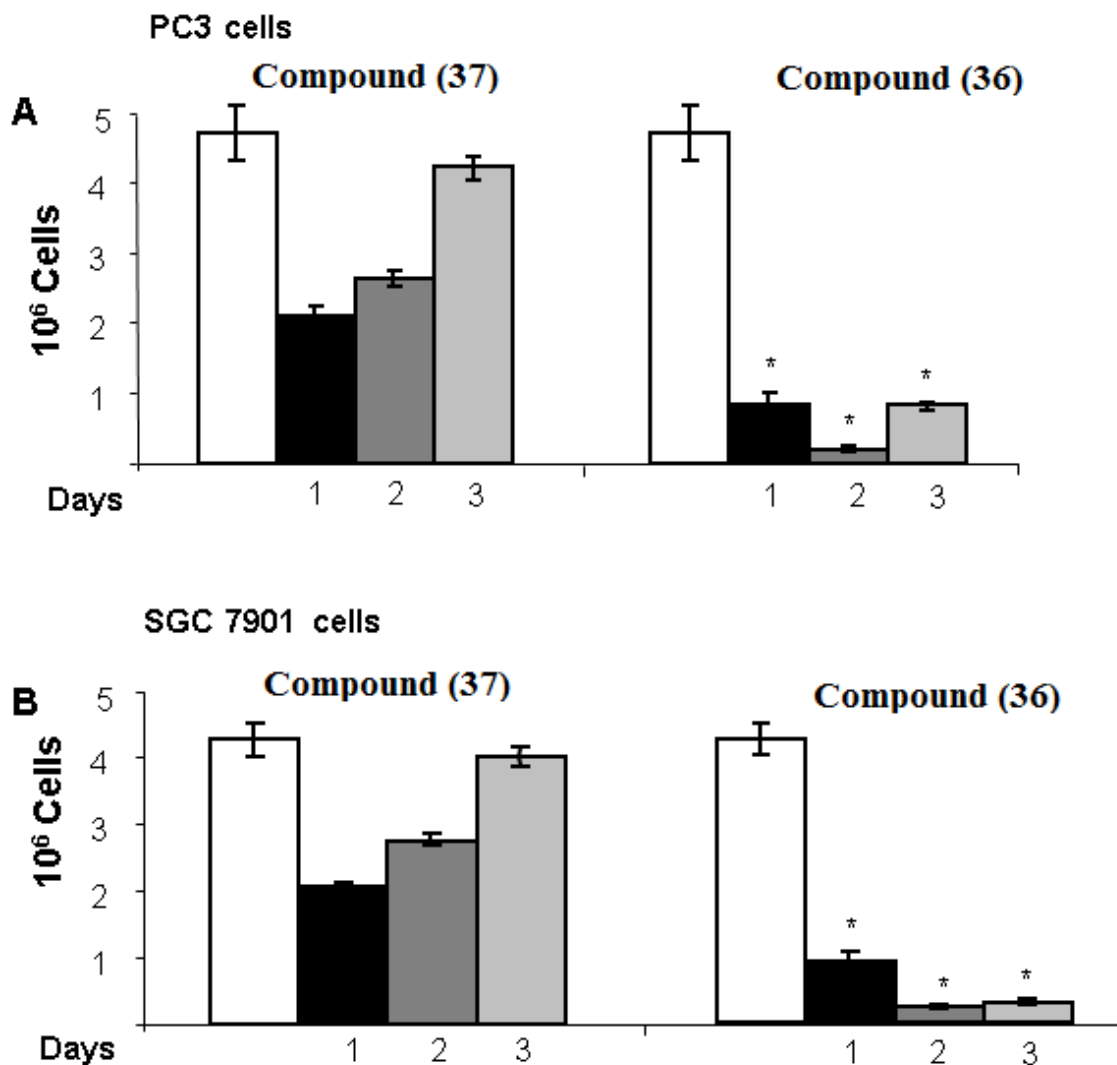


Figure 5.13 Effect of compounds 37 and 36 on cell growth in (A) PC-3 and (B) SGC-7901 cells. The cells were treated with 10 μ M for day 1, day2 and day 3. The anti-proliferative effect was measured by MTT assay. Results were expressed as the mean, SD. * P <0.05

5.1.7 Conclusion

Gold along with its therapeutic and beneficial effect on human health is among the most ancient of all metals used in medicine. The use of gold complexes in modern medicine has allowed information regarding toxicological and clinical administration to become available along with valuable studies concerning its metabolism and molecular targets. Therefore, gold has become one of the most promising metals for drug development in

medicine. Three mono gold(III) complexes based on DACH with different configurations were prepared. These gold(III) complexes were characterized using elemental analysis, solution and solid NMR, UV, Mid-IR, Far-IR spectroscopy and X-ray crystallography. The analytical data showed strong support for the formation of the type [(DACH)AuCl₂]Cl complex. Also, the X-ray crystallography demonstrates that gold coordination sphere of this complex adopts distorted square planar geometry. According to our biological assays, complex (36) with *cis* configuration is a more promising candidate as an anti-cancer agent than the *trans* isomers (37) and (38). The exact mechanisms are not clearly known, but the inhibitory effect of [(*cis*-DACH)AuCl₂]Cl on the proliferation of rapidly dividing cells may be attributed to the induction of cell cycle blockage, interruption of the cell mitotic cycle, programmed cell death (apoptosis) or premature cell death (necrosis). Therefore, [(*cis*-DACH)AuCl₂]Cl might be a promising chemo preventative and chemotherapeutic agent against human gastric carcinogenesis. As cytotoxic activity of [(*cis*-DACH)AuCl₂]Cl complex is high towards some cancer cell lines; further biological evaluation for this class of complexes is worthy of efforts especially in order to evaluate activities *in vivo*.

5.2 Gold(III) Complexes of Bis(1,2-Diaminocyclohexane) Ligands

This work reports the synthesis of bis-diaminocyclohexane containing gold(III) complexes of the type [Au(1,2-DACH)₂]Cl₃, where, 1,2-DACH = 1,2-Diaminocyclohexane using trihydrate tetrachloroauric acid HAuCl₄.3H₂O as gold(III) precursor and different isomers of 1,2-Diaminocyclohexane (1,2-DACH) i.e. *cis*-1,2-DACH, *trans*-(±)-1,2-DACH and (*S,S*)-(+)-(1,2-DACH) as ligands.

5.2.1 Mid and Far-IR Spectroscopic Studies

The most significant bands recorded in the IR spectra of free ligands, mono- and bis-DACH complexes have been reported in Table 5.11 and Table 5.12. It is noted that N-H stretching vibrations of complexes (45-47) exhibit, in the range 3333-3438 cm^{-1} , blue shifting compared with the amino ($-\text{NH}_2$) group of the corresponding free ligands. This is most likely due to stronger H-bonding interactions in the free ligands as compared to the coordinated- NH_2 corresponding complexes (45-47). The amino coordination with Au(III) ions and Au-N bond formation can be supported by the presence of $\nu(\text{Au-N})$ at 419-428 cm^{-1} as indicated by Far-IR data [174]. The C-N stretching bands also showed a significant shift to higher wave number indicating a shorter C-N bond in the complex than in the free ligand. Furthermore, there was no signal observed at 352 and 367 cm^{-1} corresponding to the symmetric and asymmetric stretching of the Au-Cl, indicating the absence of the gold mono-DACH complex. The bis-DACH complexes show N-H stretching frequencies generally lower in comparison with mono-DACH complexes (Table 10), most probably due to stronger hydrogen bonding interactions with the chloride anions in the bis-DACH complexes. Furthermore the Au-N stretching frequencies are consistent with weaker Au-N bond strength in complexes (45-47) compared to the mono-DACH complexes.

Table 5.11 Mid-IR frequencies, $\nu(\text{cm}^{-1})$ for [(1,2-DACH)₂Au(III)]Cl₃ complexes

Complex	$\nu(\text{N-H})$	ν_{shift}	$\nu(\text{C-N})$	ν_{shift}
(36')	3356 m, 3286 m		1092s	
(36)	3414 w	93	1183 s	91
(45)	3409m, 3338 m	53, 52	1185 s	93
(37')	3348 m, 3271 m, 3183 m		1082 m	
(37)	3485 w, 3420 w, 3384 w	137, 149, 201	1175 m	93
(46)	3416m, 3364m, 3333m	68, 93, 150	1176 m	94
(38')	3340 m, 3252 m, 3167 m		1082 m	
(38)	3604 m, 3340 m, 3306 m	364, 88, 139	1171 m	89
(47)	3438 m, 3410m, 3368 m	98, 158, 201	1181 m	99

Table 5.12 Far-IR frequencies, $\nu(\text{cm}^{-1})$ for [(1,2-DACH)₂Au(III)]Cl₃ complexes

Species	Au-Cl	Au-N
HAuCl ₄	369	-
(36)	352, 367	437
(45)	-	428
(37)	353, 365	437
(46)	-	419
(38)	353, 366	395, 436
(47)	-	427

5.2.2 Solution NMR Characterization

The ¹H and ¹³C NMR chemical shifts of free ligands along with their corresponding complexes (45-47) are listed in Table 5.13 and Table 5.14, respectively. Figures 5.14 and 5.15 show the ¹H and ¹³C NMR spectra, respectively. The spectra of complexes (46) and (47), show one quarter of the total expected signals observed because of the *D*_{2d} symmetry. Whereas, ¹³C NMR spectra of complexes (45) indicated the presence of *C*₂

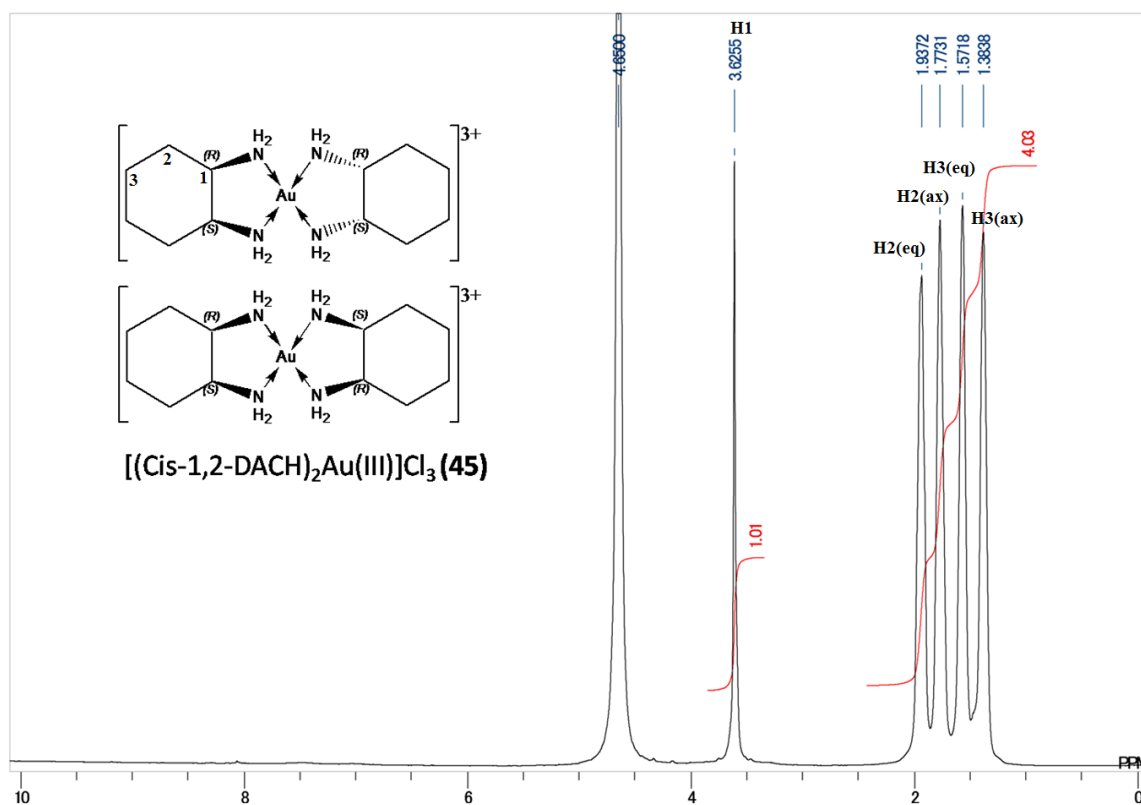
symmetry axis as one half of the total expected carbon peaks were noticed. The 1,2-diaminocyclohexane (DACH) ring is considered as a rigid conformer that allowed to distinguish equatorial H3 and H4 from axial H3 and H4 at room temperature. The signals of C-H protons connected through carbon to the amino (-NH₂) groups occur at 2.96-3.62 ppm as a multiplet, shifting downfield compared with the corresponding signals (2.23-2.25 ppm) in the free diamine ligands. The significant downfield shift was observed at 3.62 ppm for complex **(45)** with respect to the free DACH ligand at 2.23 ppm. This can be attributed to the donation of nitrogen lone pairs to the gold(III) center that causes deshielding of the proton(s) next to the bonding nitrogen. ¹³C NMR downfield shift was observed only for the carbon next to the bonding nitrogen. Conversely, the others carbons of the coordinated ligand (DACH) in the complex showed upfield shift. For instance, chemical shift of C3 and C4 for complex **(45)** observed at 26.46 and 20.80 ppm, respectively, whereas, for free 1,2-diaminocyclohexane(1,2-DACH) ligand it occurs at 35.26 and 26.36 ppm. It is also worth-mentioning that complexes **(45-47)**, even though they have the same skeleton of DACH, their carbon chemical shifts were not the same due to a different stereochemistry upon complexation.

Table 5.13 ¹H NMR chemical shifts of free ligands and corresponding [(1,2-DACH)₂Au(III)]Cl₃ complexes in D₂O

Compound	H1,H2,H1',H2'	H3,H6,H3',H6'	H3,H6,H3',H6'	H4,H5,H4',H5'	H4,H5,H4',H5'
		Equatorial	Axial	equatorial	axial
(36')	2.23, <i>m</i>	1.85, <i>m</i>	1.69, <i>m</i>	1.28, <i>m</i>	1.12, <i>m</i>
(45)	3.62, <i>m</i>	1.94, <i>m</i>	1.77, <i>m</i>	1.57, <i>m</i>	1.38, <i>m</i>
(37')	2.25, <i>m</i>	1.85, <i>m</i>	1.68, <i>m</i>	1.28, <i>m</i>	1.11, <i>m</i>
(46)	2.97, <i>m</i>	2.05, <i>m</i>	1.48, <i>m</i>	1.39, <i>m</i>	1.03, <i>m</i>
(38')	2.24, <i>m</i>	1.85, <i>m</i>	1.69, <i>m</i>	1.28, <i>m</i>	1.11, <i>m</i>
(47)	2.96, <i>m</i>	2.03, <i>m</i>	1.47, <i>m</i>	1.47, <i>m</i>	1.03, <i>m</i>

Table 5.14 Solution ^{13}C NMR chemical shifts of free ligands and corresponding $[(1,2\text{-DACH})_2\text{Au(III)}]\text{Cl}_3$ complexes in D_2O

Compound	^{13}C (δ in ppm)		
	C1,C2, C1',C2'	C3,C6, C3',C6'	C4,C5, C4',C5'
(36')	58.2	35.26	26.36
(45)	61.87, 61.80	26.46, 26.24	20.8
(37')	58.46	35.55	26.63
(46)	64.56	32.93	24.15
(38')	58.27	35.32	26.43
(47)	64.49	32.93	24.1



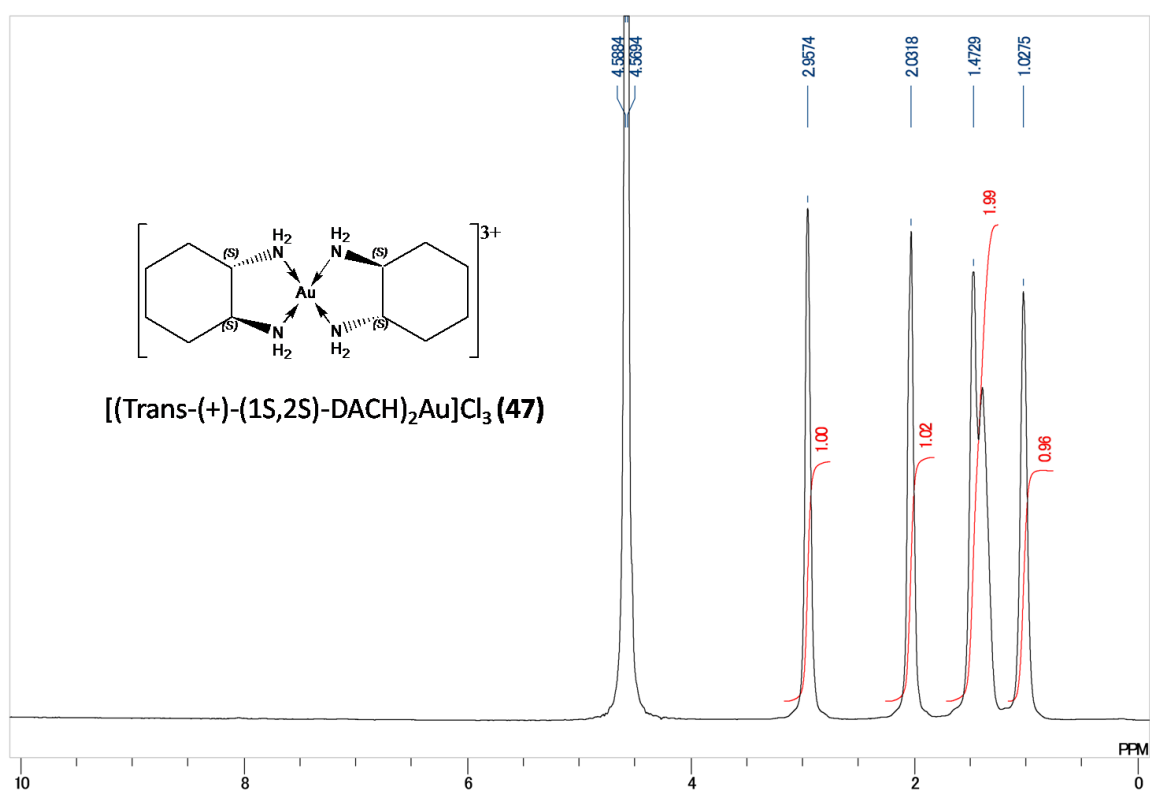
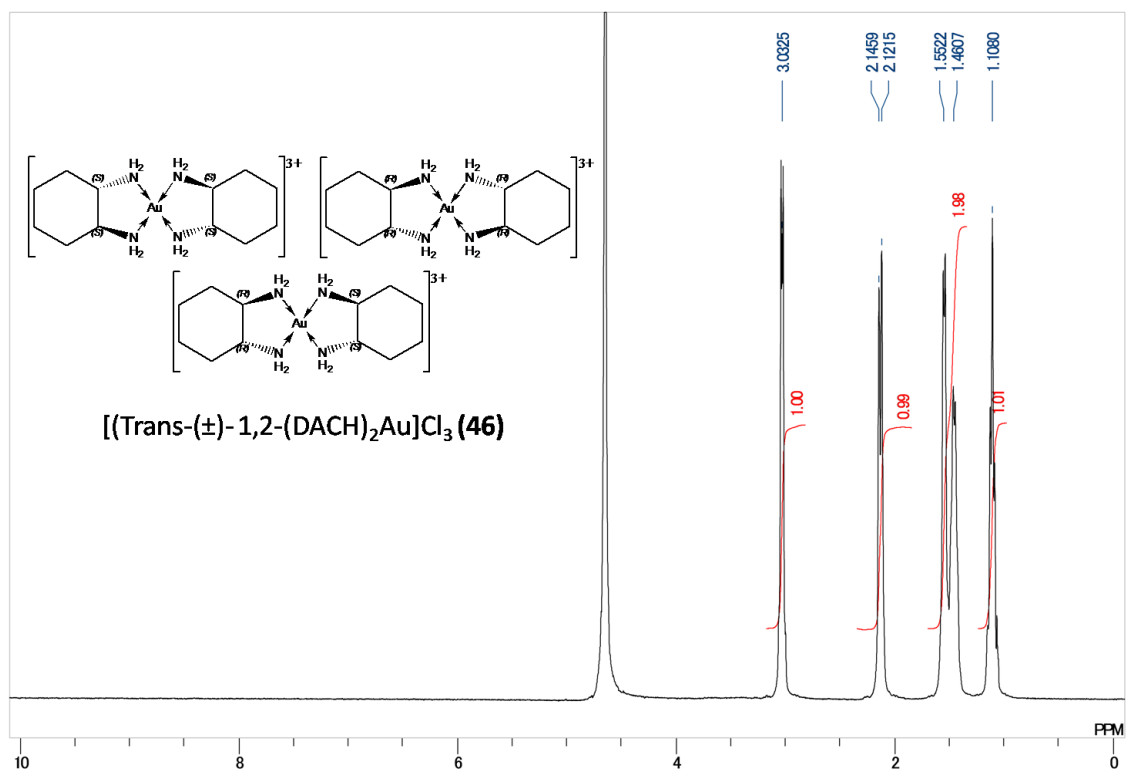
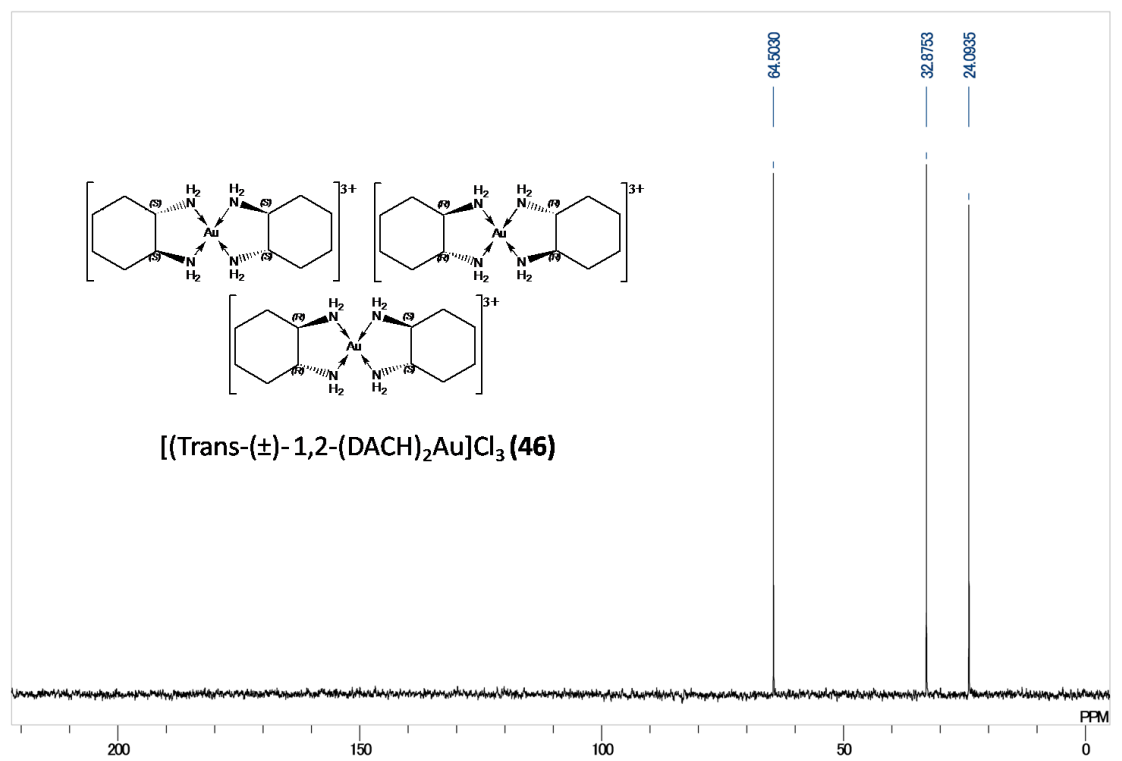
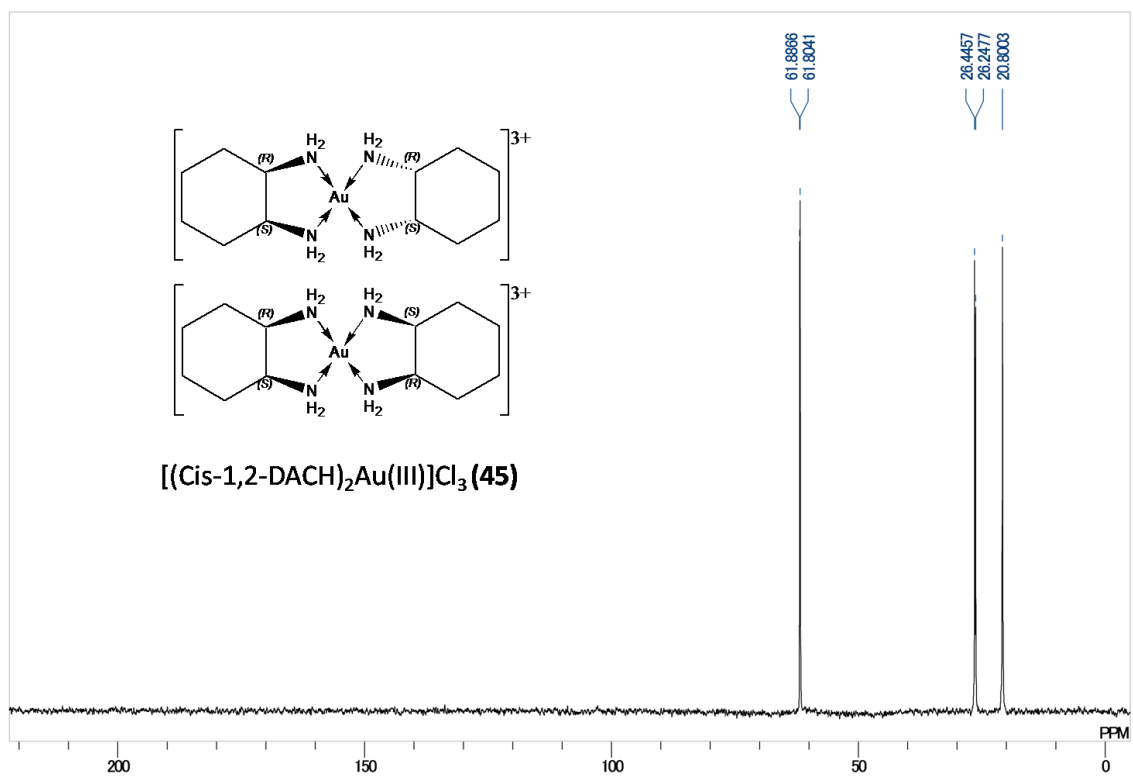


Figure 5.14 The 500-MHz ^1H solution NMR spectra of $[(1,2\text{-DACH})_2\text{Au(III)}]\text{Cl}_3$ (**45-47**) complexes



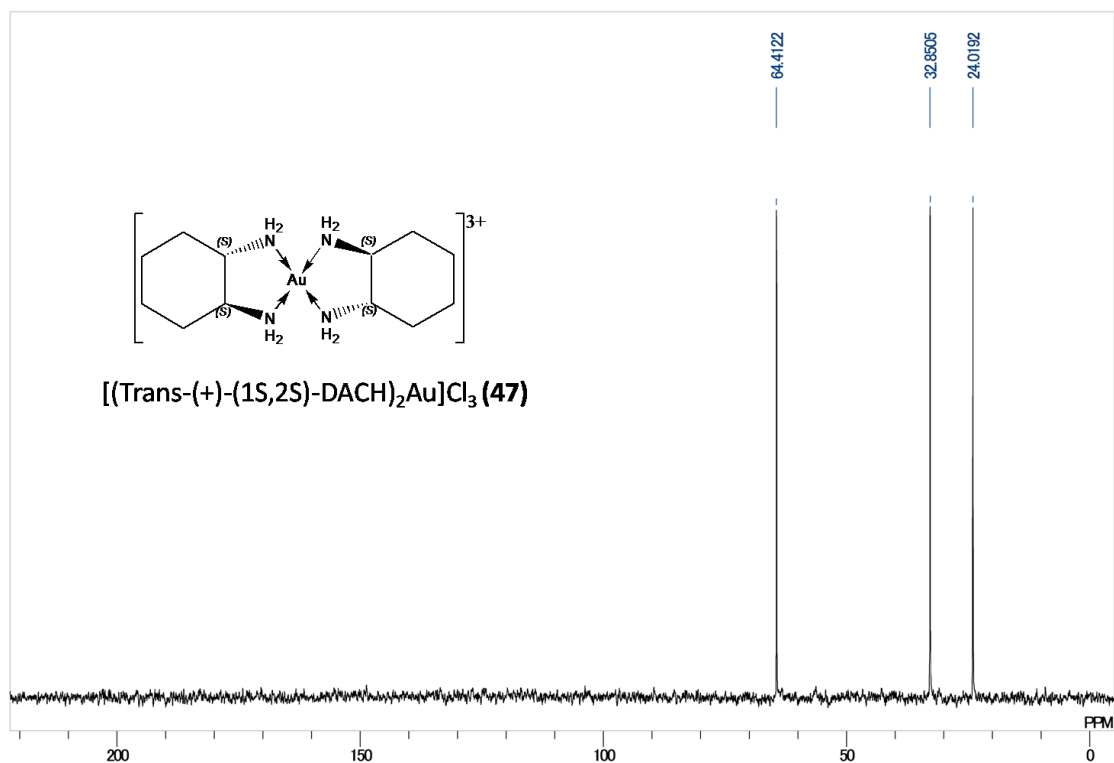


Figure 5.15 The 500-MHz ^1H solution NMR spectra of [(1,2-DACH) $_2\text{Au(III)}$] Cl_3 (45-47) complexes

5.2.3 Solid State NMR Characterization

At the spinning rate of 4 kHz, only the isotropic signals were observed for the carbons, indicating small anisotropy due to the sp^3 hybridization of these atoms, except for compound (45) where a minor anisotropy was observed as shown in Figure 5.16. It, also, illustrates the four different peaks for the carbons connected to the amino ($-\text{NH}_2$) group with equal intensity which supports the idea of the inequivalency of the four carbon atoms, indicating that gold coordination sphere adopts a distorted square planer geometry. Compared to solution chemical shifts, significant de-shielding in solid state is observed with similarity in chemical shift trend among all compounds (45-47) as given in Table 5.15 which is a clear indication of stability of the compounds (45-47) in solid state.

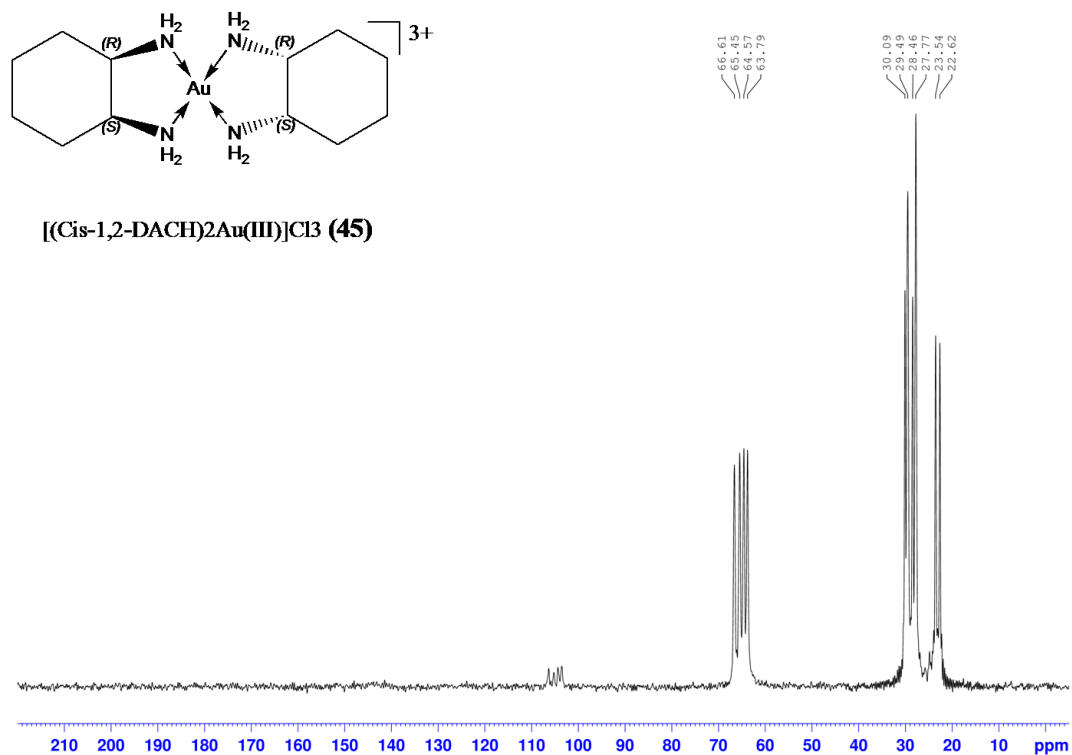


Figure 5.16 Solid state $^{13}\text{C}\{^1\text{H}\}$ NMR spectrum of complex $[(\text{cis-1,2-DACH})_2\text{Au(III)}]\text{Cl}_3$ (45)

Table 5.15 Solid state ^{13}C NMR chemical shifts of free ligands and corresponding $[(1,2\text{-DACH})_2\text{Au(III)}]\text{Cl}_3$ (45-47) complexes

Compound	^{13}C (δ in ppm)		
	C1,C2, C1',C2'	C3,C6, C3',C6'	C4,C5, C4',C5'
(36)	69.20, 65.35	30.98	27.02, 22.12
(45)	66.61, 65.45, 64.57, 63.79	30.09, 29.49, 28.46, 27.77	23.54, 22.62
(37)	69.6	37.37	27.99
(46)	69.14	36.89	28.42
(38)	70.21	37.86	29.16
(47)	68.39, 66.74, 66.61	36.41	28.66, 26.32

5.2.4 X-ray Crystal Structure of Complexes (45) and (46)

For compound (46), all attempts to grow single crystals using different solvents and techniques always led to the formation of co-crystals of mono- and bis(*trans*-(±)-1,2-DACH)gold(III) complexes as shown in Figure 15.19. The optimized crystal growth was observed in water over two weeks. However, complex(46) was stable as dissolved in water as it is observed by solution ^1H and ^{13}C NMR in D_2O . For instance, Figure 15.17 shows the ^{13}C NMR spectrum of complex(46) (a), the co-crystals of mono- and bis{*trans*-(±)-1,2-DACH}Au(III) (b) along with its mono-{*trans*-(±)-1,2-DACH}Au(III) (c). As shown in Figure 15.17(b), compound (46) and its mono-1,2-DACH gold compound exhibit different chemical shift for C2 and C3. The chemical shift of C2 and C3 for complex(46) observed at 64.46 and 32.82 ppm, respectively, whereas, for its corresponding mono-1,2-DACH compound it occurs at 65.68 and 33.15 ppm. Comparison of ^{13}C NMR spectrum of the co-crystal with both the mono-1,2-DACH and bis-1,2-DACH compounds confirms the identity of complex(46) as bis-1,2-DACH compound.

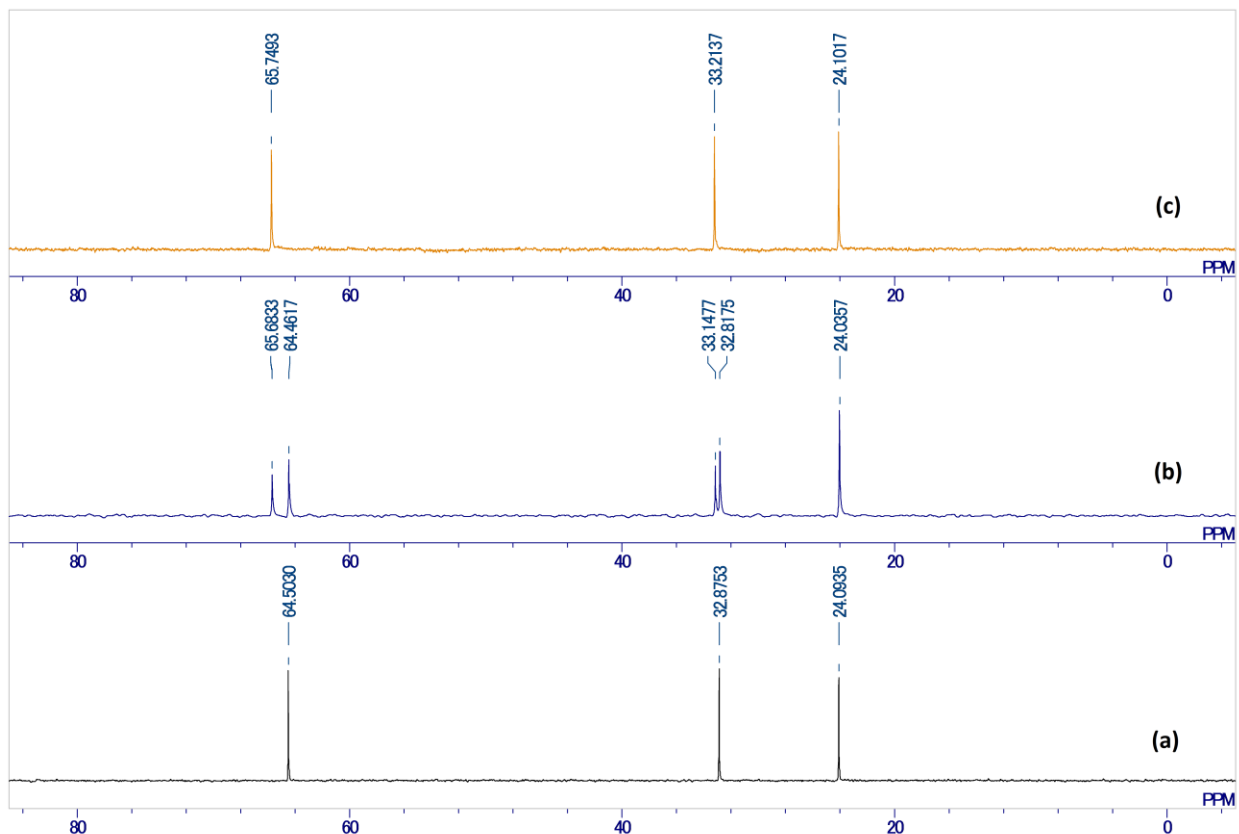


Figure 5.17 Solution $^{13}\text{C}\{^1\text{H}\}$ NMR spectra of compound (46) (a), co-crystal of mono- and bis(*trans*-DACH)gold(III) (b) and mono-*trans*-(DACH)gold(III) (c)

The X-ray molecular structure of compound $[\text{Au}\{\textit{cis}\text{-}1,2\text{-DACH}\}]_2\text{Cl}_3$ (**45**) is shown in Figure 5.18. It crystallizes as crystal of the bis(1,2-DACH)-chelate $[\{(R,S)\text{-DACH}\}_2\text{Au}]\text{Cl}_3$. The asymmetric unit contains two Au(1,2-DACH) moieties with the gold(III) ions each located on an inversion center. In both molecules, the metal ion is bonded to four nitrogen atoms of two *cis*-cyclohexane-1,2-diamine ligands in a distorted square planar geometry. The Au-N bond distances are in the range 2.031(2) - 2.038(2) Å and the N-Au-N chelate bond angles are 83.77(7)° and 83.22(7)° respectively for molecules (**45**) and (**46**) (Table 5.16). These values are similar to those reported for bis(ethylene-1,2-diamine)gold(III)tris(perhenate) [179]. The cyclohexyl rings adopt a

chair conformation. The square planar geometry and the five-membered ring strain impose torsion angles N1-C1-C2-N2 of 51.31° and N3-C7-C12-N4 of 47.91° respectively for molecules **(45)** and **(46)**. Amine hydrogen atoms are engaged in hydrogen bonding interactions with Cl⁻ counter ions and the hydration water molecules generating a three-dimensional hydrogen bonding network (Figure 5.20).

Compound **(46)** crystallizes as a (1:1) co-crystal of the bis-chelate [$\{(S,S)\text{-}(1,2\text{-DACH})\}_2\text{Au}\text{Cl}_3$] and the monochelate [$\{(S,S)\text{-}(1,2\text{-DACH})\}\text{AuCl}_2\text{Cl}$] (Figure 5.19). The structure of the first component of the co-crystal, namely [$\{(S,S)\text{-}(1,2\text{-DACH})\}_2\text{Au}\text{Cl}_3$], is distorted square planar with the Au-N bond distances in the range 2.013(6) - 2.049(6) Å and the two N-Au-N chelate bond angles being 83.3(2) and 83.7(2)° respectively. These geometrical values are similar to those found for **(45)** and other bis(diamino)gold(III) compounds [179]. Similarly to compound **(45)**, the cyclohexyl rings adopt a chair conformation and the NH₂ groups have hydrogen bonding interactions with the chlorides and water molecules. The structure of the second component of the co-crystal: [$\text{Au}\{(S,S)\text{-}(+)\text{-DACH}\}_2\text{Cl}_2\text{Cl}$], has been reported previously by our group [180]. H atoms of DACH were placed at calculated positions using a riding model for both compounds **(45)** and **(46)**. Both compounds crystallize as hydrates in the water solvent, while the water H atoms in **(45)** were located on the Fourier difference map and refined isotropically, those of compound **(46)** could not be located and therefore could not be placed at adequate positions. Crystal and structure refinement data are given in Table 5.16. Selected bond lengths and bond angles are given in Table 5.17.

Table 5.16 Crystal and structure refinement data for compounds (45) and (46)

Compound	(45)	(46)
CCDC deposit no.	889510	925974
Empirical formula	C ₁₂ H ₃₄ AuCl ₃ N ₄ O ₃	C ₁₈ H ₄₆ Au ₂ Cl ₆ N ₆ O ₂
Formula weight	585.75	985.24
Crystal size/mm	0.42 × 0.35 × 0.25	0.29 × 0.26 × 0.20
Wavelength/Å	0.71073	0.71073
Temperature/K	297 (2)	296 (2)
Crystal symmetry	Triclinic	Monoclinic
Space group	P -1	P 2 ₁
Unit cell dimensions		
a/Å	7.5342 (3)	7.3996 (13)
b/Å	11.7086 (5)	20.650 (4)
c/Å	12.0149 (5)	10.5543 (19)
α/°	103.096 (1)	90
β/°	91.041 (1)	93.558 (3)
γ/°	104.119 (1)	90
Volume (Å ³)	998.11 (7)	1609.6 (5)
Z	2	2
Calc. density (g.cm ⁻³)	1.949	2.033
μ(Mo-Kα)/mm ⁻¹	7.79	9.63
F(000)	576	944
θ Limits/°	1.8–28.3	1.9–28.3
Collected reflections	13644	21865
Unique reflections(R _{int})	4175(0.021)	7311(0.043)
Observed reflections [I > 2σ (I)]	4932	7964
Goodness-of-fit on F ²	1.05	1.01
R ₁ (F), [I > 2σ (I)]	0.016	0.029
wR ₂ (F ²), [I > 2σ(I)]	0.042	0.072
Largest diff. Peak and hole (e Å ⁻³)	0.99, -1.10	2.01, -0.89

Table 5.17 Selected bond lengths (Å) and bond angles (°) for compounds (45) and (46)

Bond Angles (°)		Bond Lengths (Å)	
Compound (45)			
N2—Au1—N2 ⁱ	180.00 (13)	Au1—N2	2.0314 (17)
N2—Au1—N1	83.77 (7)	Au1—N2 ⁱ	2.0314 (17)
N2 ⁱ —Au1—N1	96.23 (7)	Au1—N1	2.0375 (18)
N2—Au1—N1 ⁱ	96.23 (7)	Au1—N1 ⁱ	2.0375 (18)
N2 ⁱ —Au1—N1 ⁱ	83.77 (7)	Au2—N4	2.0309 (18)
N1—Au1—N1 ⁱ	180.00 (13)	Au2—N4 ⁱⁱ	2.0309 (18)
N4—Au2—N4 ⁱⁱ	180.00 (14)	Au2—N3 ⁱⁱ	2.0346 (18)
N4—Au2—N3 ⁱⁱ	96.78 (7)	Au2—N3	2.0346 (18)
N4 ⁱⁱ —Au2—N3 ⁱⁱ	83.22 (7)	N1—C1	1.505 (3)
N4—Au2—N3	83.22 (7)		
N4 ⁱⁱ —Au2—N3	96.78 (7)		
N3 ⁱⁱ —Au2—N3	180.00 (9)		
C1—N1—Au1	109.95 (13)		
Compound (46)			
N1—Au1—N2	84.80 (19)	Au1—N1	2.038 (4)
N1—Au1—Cl2	90.78 (14)	Au1—N2	2.040 (5)
N2—Au1—Cl2	175.57 (15)	Au1—Cl2	2.272 (2)
N1—Au1—Cl1	175.01 (14)	Au1—Cl1	2.2727 (17)
N2—Au1—Cl1	90.21 (15)	Au2—N5	2.013 (6)
Cl2—Au1—Cl1	94.21 (9)	Au2—N6	2.029 (5)

N5—Au2—N6	83.7 (2)	Au2—N4	2.034 (6)
N5—Au2—N4	95.5 (2)	Au2—N3	2.049 (6)
N6—Au2—N4	179.2 (3)	N1—C1	1.488 (7)
N5—Au2—N3	178.8 (2)		
N6—Au2—N3	97.5 (2)		
N4—Au2—N3	83.3 (2)		
C1—N1—Au1	107.9 (3)		

Symmetry codes: (i) $-x+1, -y+2, -z+1$; (ii) $-x, -y, -z$

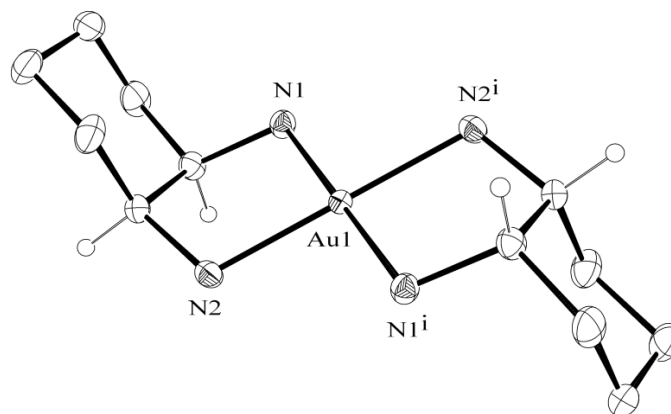


Figure 5.18 X-ray molecular structure of compound $[(cis-1,2-DACH)_2Au(III)]Cl_3$ (45)

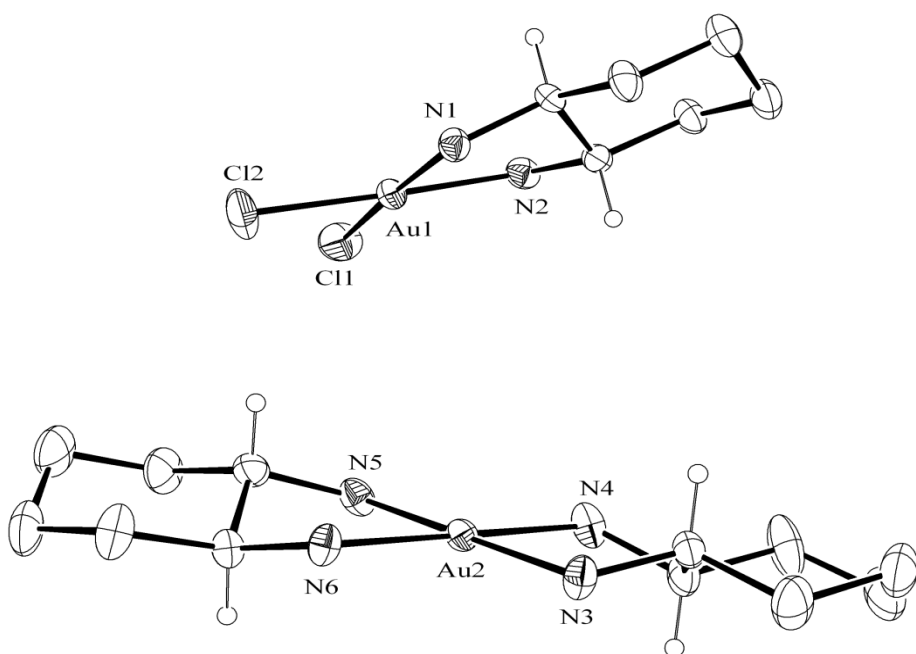


Figure 5.19 X-ray molecular structures of the two components of co-crystal $[(trans-1,2-DACH)_2Au(III)]Cl_3$ (46)

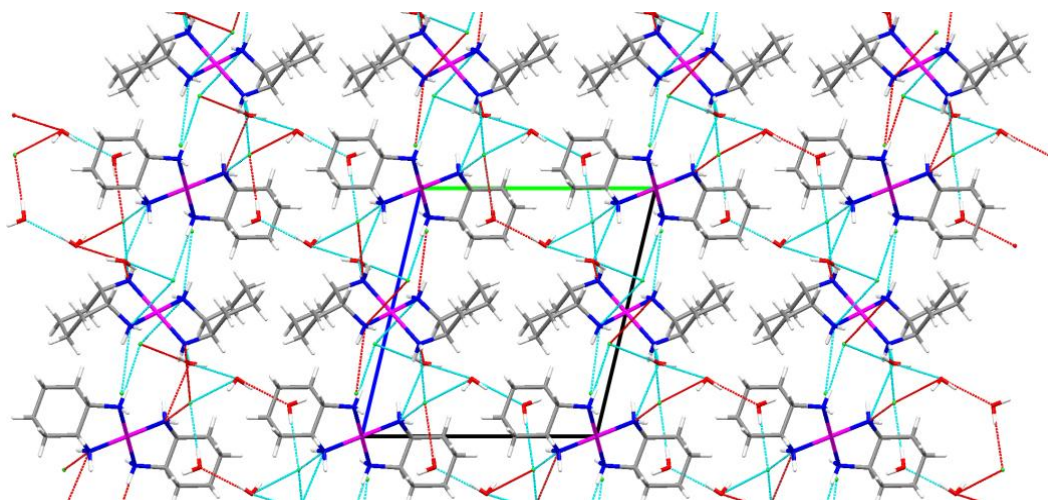


Figure 5.20 Hydrogen bonding network in compound $[(cis-1,2-DACH)_2Au(III)]Cl_3$ (45)

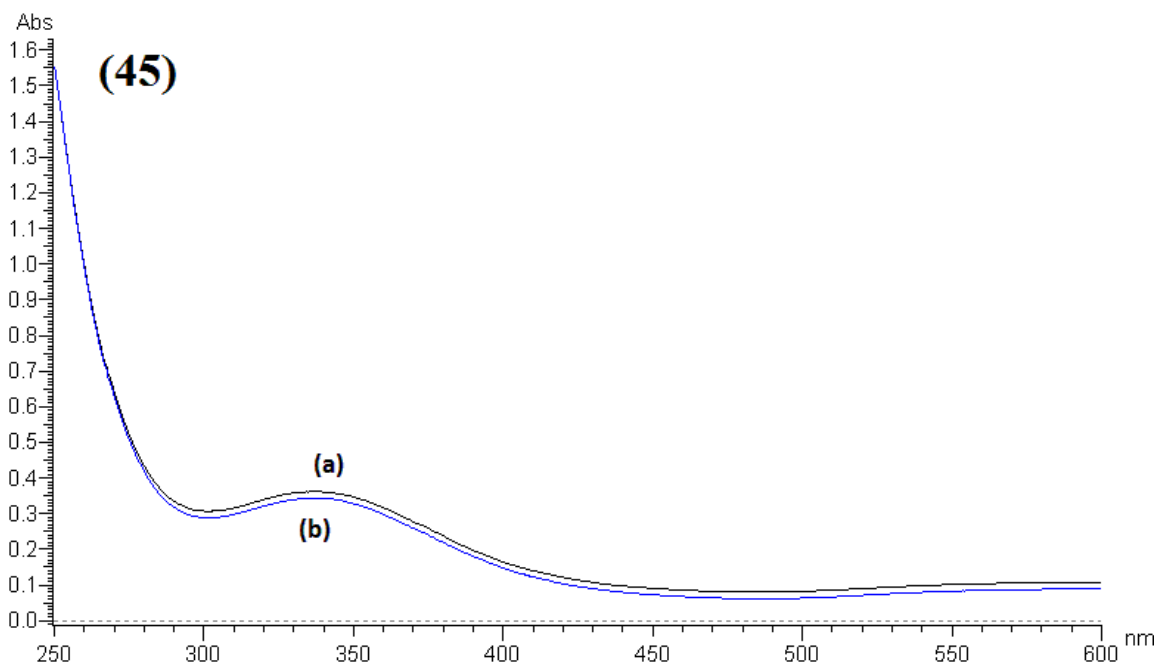
5.2.5 UV-Vis Spectra

The λ_{\max} values for the compounds studied along with their corresponding mono-DACH compounds are shown in Table 5.18. The gold(III) compounds **(45)**, **(46)** and **(47)** exhibit, in a reference buffered phosphate solution, intense transitions in the range 335-339 nm, which are assigned as ligand-to-metal charge-transfer transitions characteristically associated to the gold(III) center [181]. In related compounds, these absorption bands were assigned as NH⁻ to a gold(III) charge-transfer bands [181]. It is worth to notice that these spectral features appear only at relatively high pH values (pH > 6-7) at which ligand deprotonation has fully occurred. According to crystal field theory for d^8 compounds the LUMO orbital is $d_{x^2-y^2}$, so ligand to metal charge transfer could be due to $p_{\sigma} \rightarrow d_{x^2-y^2}$ transition [174]. It is worth to notice that mono-1,2-DACH [180] compare with their corresponding bis-1,2-DACH gold(III) compounds exhibit different λ_{\max} values.

Table 5.18 λ_{\max} values for [(1,2-DACH)₂Au(III)]Cl₃ (45-47) complexes obtained from UV-Vis spectra

Compound	λ_{\max} (nm)
HAuCl ₄ ·3H ₂ O	320.0
[Au{ <i>cis</i> -(1,2-DACH)}Cl ₂]Cl (36)	302.5
[Au{ <i>cis</i> -(1,2-DACH)} ₂]Cl ₃ (45)	338.0
[Au{ <i>trans</i> -(±)-(1,2-DACH)}Cl ₂]Cl (37)	301.6
[Au{ <i>trans</i> -(±)-(1,2-DACH)} ₂]Cl ₃ (46)	339.5
[Au{(S,S)-(+)-(1,2-DACH)}Cl ₂]Cl ₃ (38)	301.5
[Au{(S,S)-(+)-(1,2-DACH)} ₂]Cl ₃ (47)	339.0

The electronic spectra of the compounds (45), (46) and (47) in the buffer solution, were monitored at 37 °C over 3 days after mixing; electronic spectra for all compounds at mixing and after 3 days are depicted in Figure 5.21. It is apparent that the observed transitions remain substantially unmodified over 3 days observation, implying a substantial stability of these compounds under the present solution conditions. Nevertheless, a slight decrease in intensity, of the characteristic bands, was noticed with time without significant shape modifications. Also, this observation indicates that the gold center in these compounds remains in the +3 oxidation state [174,181]. In general, however, loss of spectral intensity is lower than 5% of the original intensity within the observation period of 3 days which indicates high stability of these compounds in the buffer. This is a possible suggestion that in the physiological milieu, the compounds would be able to undergo the necessary reactions required for bioactivity.



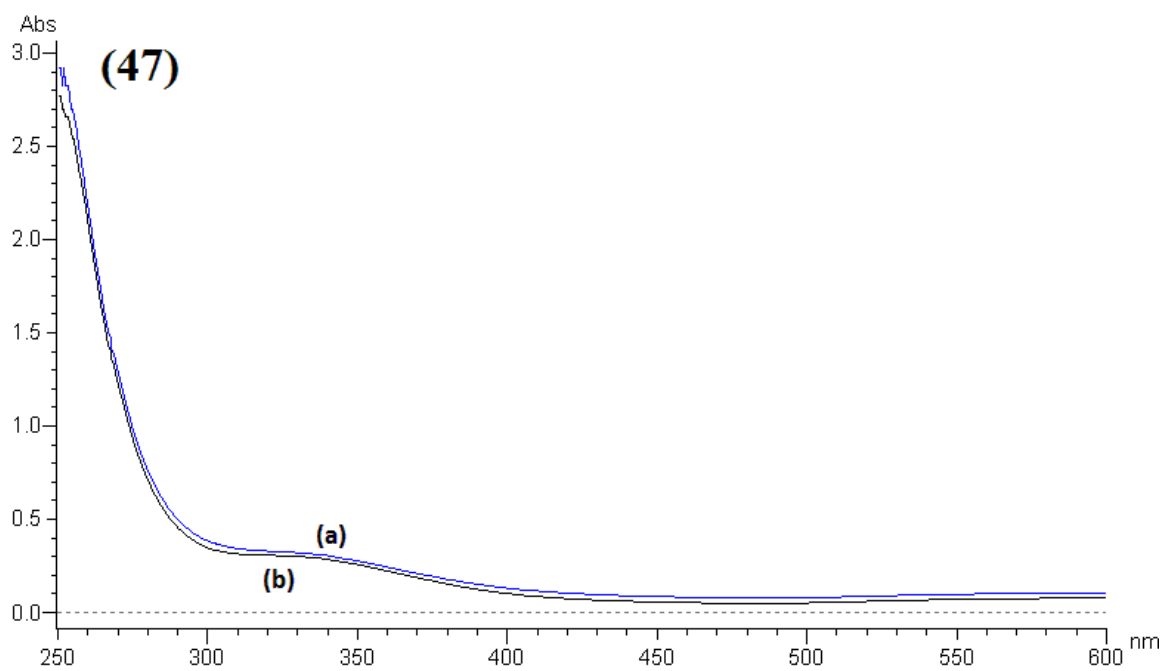
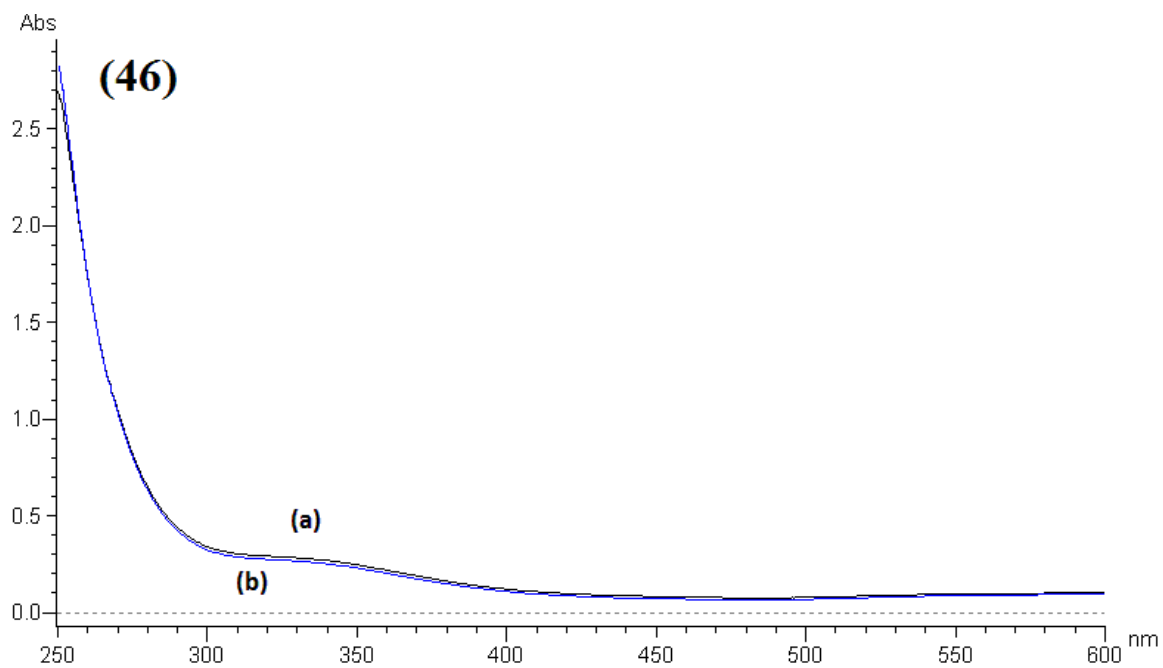


Figure 5.21 UV-Vis spectra of [(1,2-DACH)₂Au(III)]Cl₃ (45-47) complexes, followed by dissolution in the buffer solution (a) just after mixing and (b) after 3 days at 37 °C.

5.2.6 Stability Studies of Gold(III) Compounds (45)-(47)

NMR spectra of the compounds dissolved in D₂O and mixed DMSO-*d*₆/D₂O (v/v: 3:1) solution were obtained on immediate dissolution to serve as reference spectra and latter at 24 h and after 3 days at 37 °C in D₂O and at room temperature in mixed DMSO-*d*₆/D₂O to determine their stability. In general, all compounds showed high stability in D₂O as well as in the mixed DMSO-*d*₆/D₂O and their NMR profiles remained unchanged over 3 days. For example, Figures 5.22-5.23 illustrated, respectively, ¹H and ¹³C NMR profiles of the compound (46) at mixing and after 3 days in D₂O. Furthermore, these compounds in mixed DMSO-*d*₆/D₂O were also observed stable and their NMR profiles remained unchanged at the experimental conditions. Figures 5.24-5.25 show, respectively, ¹H and ¹³C NMR profiles of compound (46) in DMSO-*d*₆/D₂O at mixing and after 3 days.

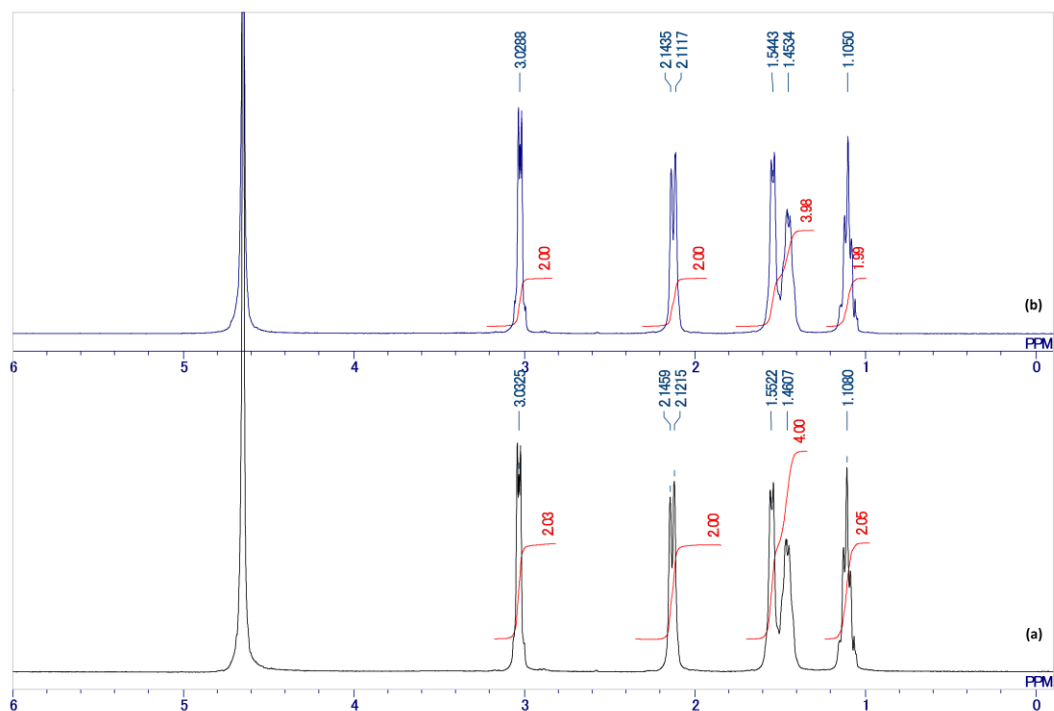


Figure 5.22 ¹H NMR spectra of compound (46) in D₂O (a) just after mixing and (b) after 3 days.

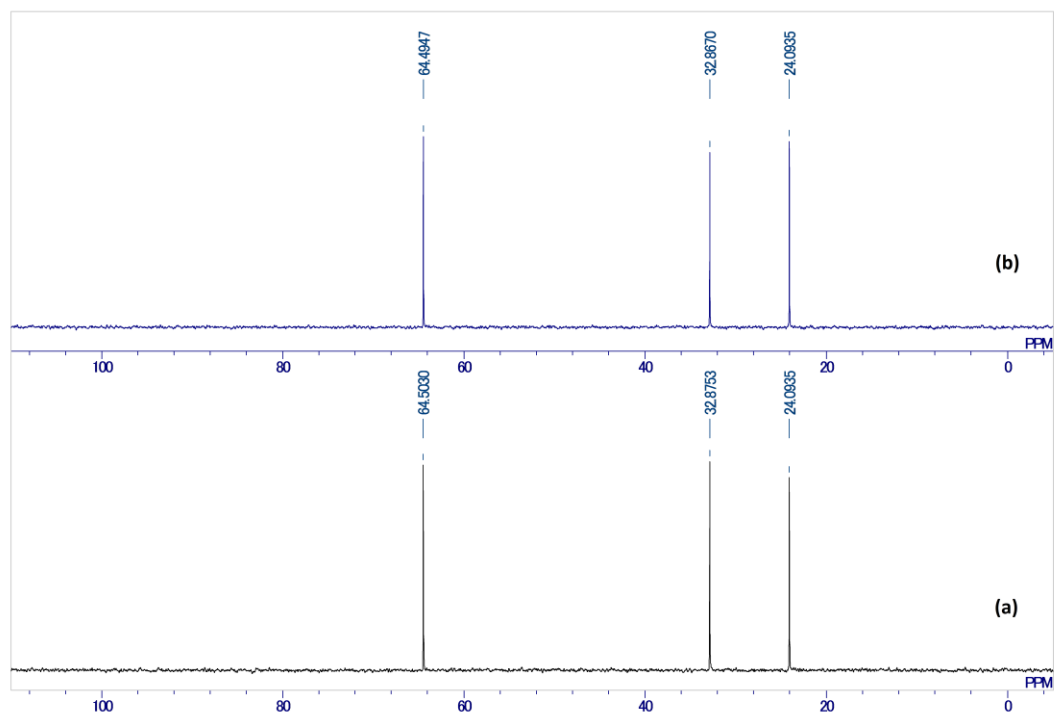


Figure 5.23 Solution $^{13}\text{C}\{^1\text{H}\}$ NMR spectra of $[(\text{trans-1,2-DACH})_2\text{Au(III)}]\text{Cl}_3$ (46) in D_2O (a) after mixing and (b) after 3 days.

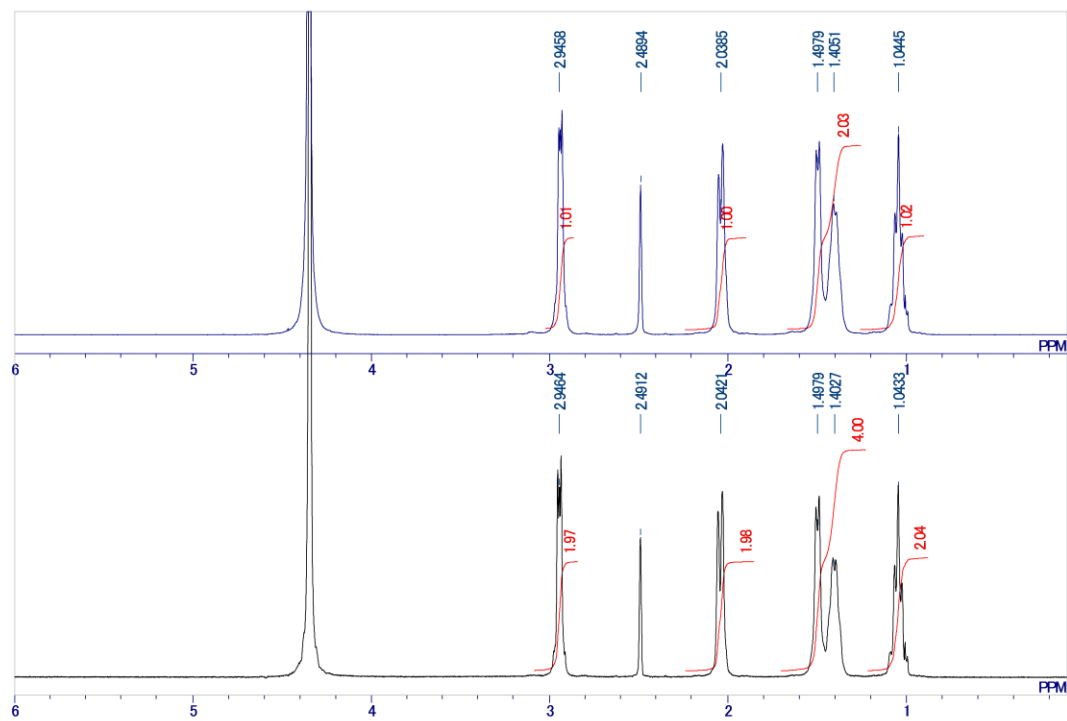


Figure 5.24 ^1H NMR spectra of $[(\text{trans-1,2-DACH})_2\text{Au(III)}]\text{Cl}_3$ (46) in $(\text{DMSO}/\text{D}_2\text{O}, 3:1)$ (a) just after mixing and (b) after 3 days.

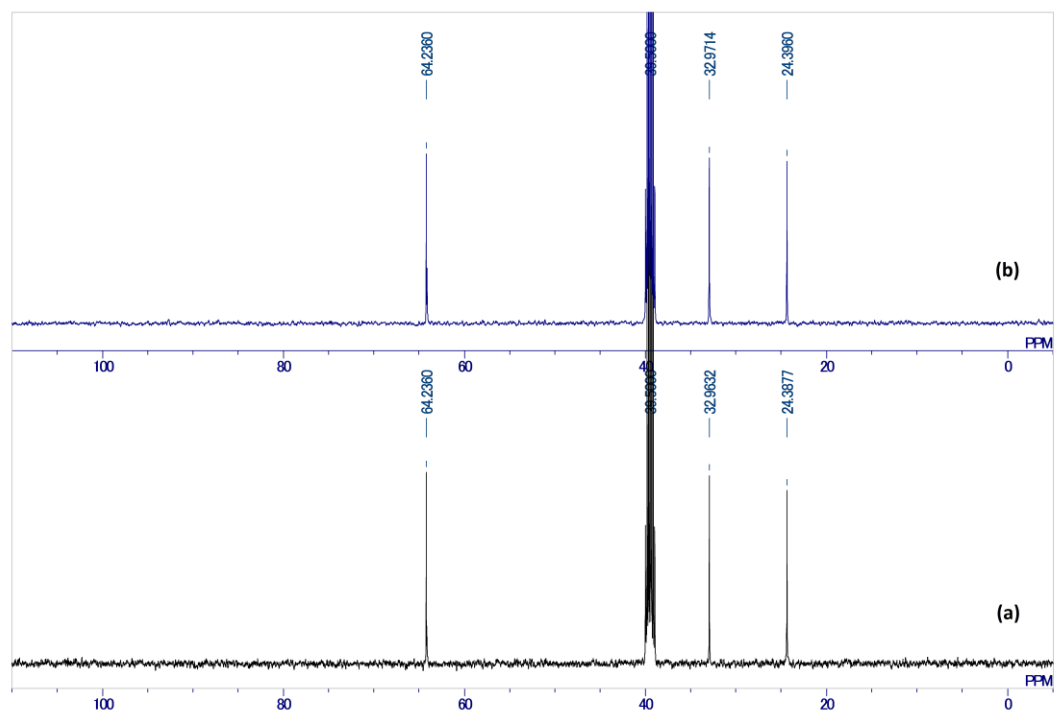


Figure 5.25 Solution $^{13}\text{C}\{^1\text{H}\}$ NMR spectra of $[(\text{trans-1,2-DACH})_2\text{Au(III)}]\text{Cl}_3$ (**46**) in (DMSO/ D_2O , 3:1) (a) after mixing and (b) after 3 days.

5.2.7 Electrochemistry of Gold(III) Compounds (**36-38**) and (**45-47**)

The electrochemical behavior of compounds (**45**), (**46**) and (**47**) along with their corresponding mono-DACH gold(III) compounds (**36**), (**37**) and (**38**) was investigated in a physiological environment through cyclic voltammetry to study the effect of the bidentate amino coordination at gold(III) on the stability of the compounds. The cyclic voltammetric curves of the compounds (**45**), (**46**) and (**47**) and their corresponding mono-DACH gold(III) compounds (**36**), (**37**) and (**38**) are shown in Figure 5.26 and Table 5.19 summarizes the cyclic voltammetric data of all the studied compounds. The potential values vs. NHE for the reduction processes exhibited by the compounds (**45**), (**46**) and (**47**), in a reference buffered phosphate, are in the range (+465)-(+498) mV against the

range of (+490)-(+525) mV for their corresponding mono-1,2-DACH gold(III) compounds(**36**), (**37**) and (**38**). In general, bis-1,2-DACH gold(III) compounds showed lower peak potential values compare with their corresponding mono-1,2-DACH gold(III) compounds as listed in Table 5.19. This is attributed to the fact that amino bidentate ligand stabilized the compounds. In addition to that, cyclicvoltammetric data indicated that *cis*-1,2-DACH configuration is slightly more stable than the *trans*-(±)-1,2-DACH configuration of the compounds which is also indicated by UV-Visible analysis. All studied gold(III) compounds show one irreversible reduction process which, in controlled potential coulometry, involves three electrons per mole. The occurrence of Au(III)/Au(0) reduction is confirmed by the appearance of the thin gold layer deposited on the platinum electrode surface after exhaustive electrolysis (E_w , -0.7 V). In general, cyclicvoltammetric results suggested that these compounds are quite stable under the physiological conditions.

Table 5.19 Peak potential values (vs ENH) for reduction of compounds [Au(1,2-DACH)Cl₂]Cl and [Au(1,2-DACH)₂]Cl₃

Compound	E_p(mV)
[Au{ <i>cis</i> -(1,2-DACH)}Cl ₂]Cl (36)	490
[Au{ <i>cis</i> -(1,2-DACH)} ₂]Cl ₃ (45)	465
[Au{ <i>trans</i> -(±)-(1,2-DACH)}Cl ₂]Cl (37)	525
[Au{ <i>trans</i> -(±)-(1,2-DACH)} ₂]Cl ₃ (46)	495
[Au{(S,S)-(+)-(1,2-DACH)}Cl ₂]Cl ₃ (38)	522
[Au{(S,S)-(+)-(1,2-DACH)} ₂]Cl ₃ (47)	498

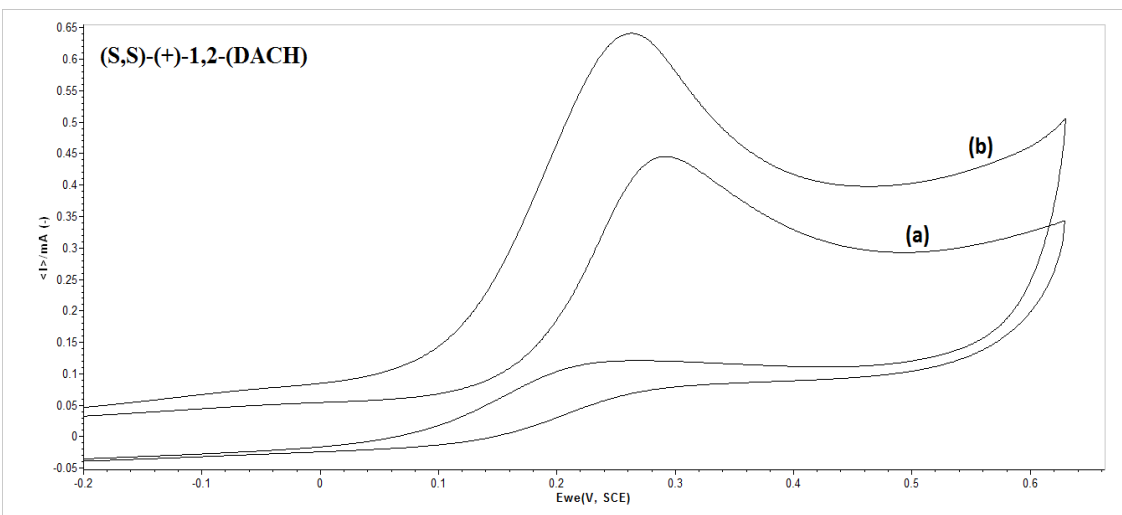
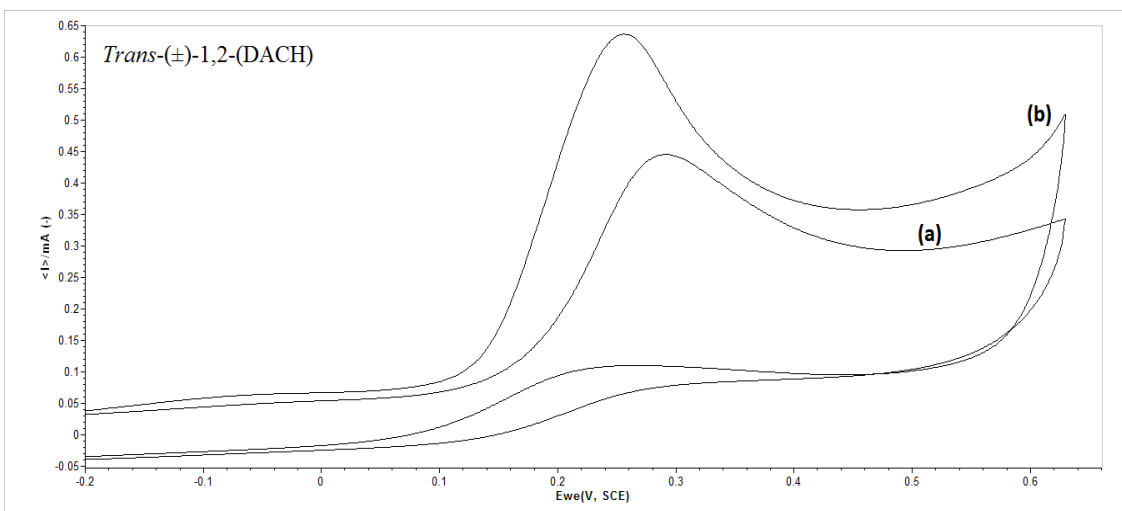
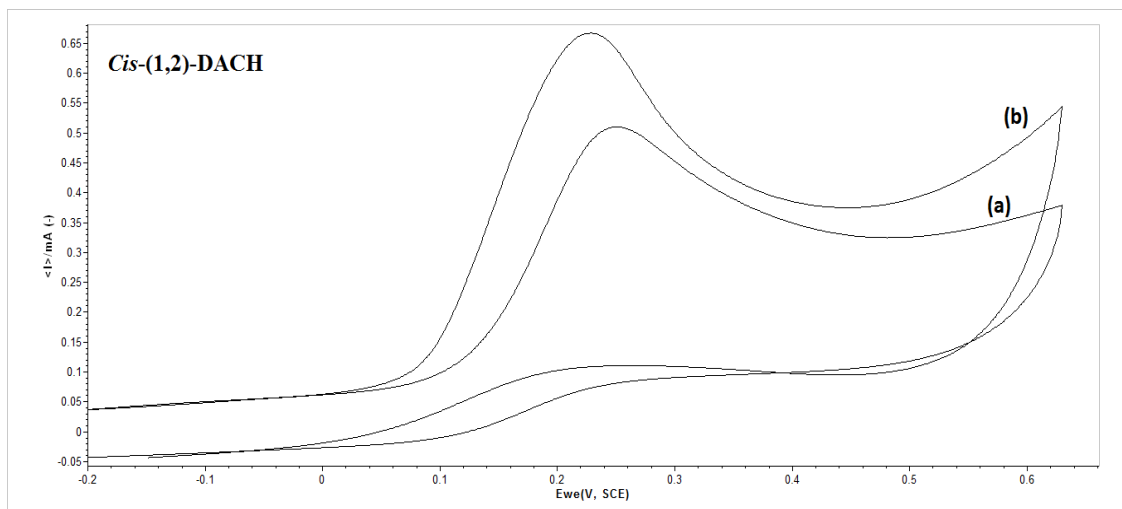


Figure 5.26 Cyclic voltammetric curves of the compounds (45-47) and their corresponding mono-DACH gold(III) compounds (36-38). Curve labeled with (a) is corresponding to the bis-DACH, while, (b) corresponding to mono-DACH

5.2.8 Anticancer Activity of [(1,2-DACH)₂Au(III)]Cl₃(45-47) on PC3 and SGC7901 Cancer Cell Lines

The MTT assay for time dependent inhibitory effect was performed with fixed concentration of the synthesized gold(III) compounds (45), (46) and (47) on PC3 and SGC7901 cells for 24 h (1day) and 72 h (3 day). As illustrated in Figures 5.27-5.29, compound (46) and purely optical active isomer compound (47) exhibited potentially high anticancer activity against gastric cancer cells SGC7901 and prostate cancer cells PC3 after 24 and 72 h of treatment with 10 μ M. Whereas, compound (45) showed substantial inhibition against PC3 and SGC7901 cell lines under the same assay experimental condition.

From Figures 5.30-5.32, it is also quite clear that gold(III) compounds (45-47) under study showed concentration dependence *in vitro* on the growth of cancerous cells PC3 and SGC7901 after 24 h. In addition to that, Figure 5.33 illustrates the anticancer activity of compound 1-3 against the two cell lines for a purpose of comparison illustrates that compound [({*trans*-(\pm)-1,2-(DACH)₂Au}]Cl₃ shows the highest bioactivity.

The *in vitro* cytotoxicity of the compounds (45-47) was evaluated in terms of their IC₅₀ values against prostate cancer cell lines (PC3) and gastric carcinoma cell lines (SGC7901). The IC₅₀ data is shown in Table 5.20. The IC₅₀ data for the Au(III) complexes (45), (46) and (47) showed reasonable cytotoxicity in the 6–10 μ M range for SGC7901 cells, as given in Table 5.20. For SGC7901 cells, complex (46) was recognized as being as effective cytotoxic agent as cisplatin, while compound (45) and (47)

demonstrated about 1.3 to 1.4-fold lower potency. For PC3 cells line, compounds 1-3 showed almost 6–13-fold lower cytotoxicity as compared to cisplatin.

An independent assessment of compounds (**45-47**) revealed an interesting feature that SGC7901 gastric cancer cells exhibit 7 to 8-fold intrinsic resistance relative to the PC3 cancer cells with respect to cisplatin [182]. However, almost 1-fold resistance to compounds (**45-47**) was observed for PC3, as shown in Table 5.20. This suggests that the intrinsic factors regulating cellular sensitivity to cisplatin are different for PC3 and SGC7901 cells. The factors affecting the sensitivity of PC3 and SGC7901 cells are analogous in compounds (**45-47**). There is no doubt that the present study is helpful for further exploiting and defining the potential role of gold(III) complexes in the combat against prostate and gastric cancers.

The cytotoxicity result for the compounds (45-47) reveals that gold(III) complex (**46**) with *trans*-(±)-(1,2-DACH)₂ configuration demonstrated higher cytotoxic effect in comparison with the complexes (**45**) and (**47**). It is worth to notice that complex (**46**) is a racemic mixture, consisting of (1*S*,2*S*)-bis-(DACH) complex (**47**) and *trans*-(1*R*,2*R*)-bis-(DACH) complex. Comparison of the cytotoxicity values of compounds (**46**) and (**47**) enable us to conclude that *trans*-(1*R*,2*R*)-bis-(DACH) gold(III) complex poses higher cytotoxicity activity than (1*S*,2*S*)-bis-(DACH) complex (**47**).

Table 5.20 *in vitro* cytotoxicity data of compounds [(1,2-DACH)₂Au(III)]Cl₃ (45-47) for 72 h exposure on PC3 and SGC7901 cancer cell lines

Compound	IC ₅₀ (μM)		Fold resistance SGC7901/PC3	Ref.
	PC3	SGC7901		
Cisplatin	1.1 ± 0.10	7.3 ± 0.50.	6.64	[182]
45	13.1 ± 0.13	10.4 ± 0.21	0.79	a
46	6.5 ± 0.07	5.8 ± 0.11	0.89	a
47	9.9 ± 0.21	9.5 ± 0.05	0.96	a

^athis work

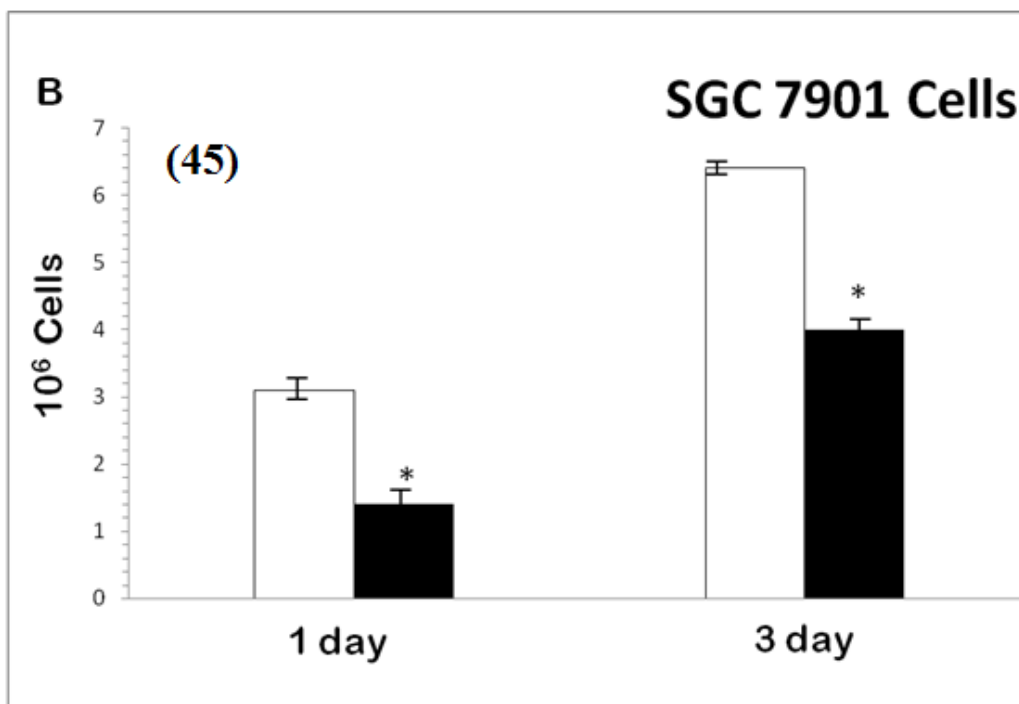
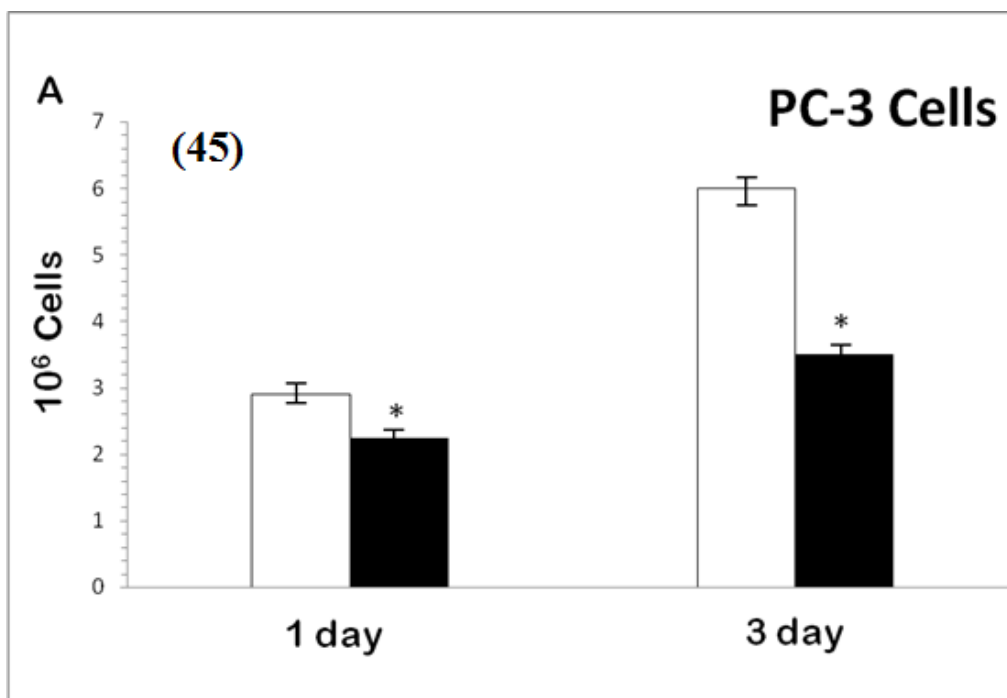


Figure 5.27 Time dependent inhibitory effect of 10 μ M [*cis*-1,2-(DACH)₂Au]Cl₃ on growth of (A) PC3 and (B) SGC7901 cells for 1 day and 3 days using MTT assay. Results were expressed as the mean, SD. **P*<0.05

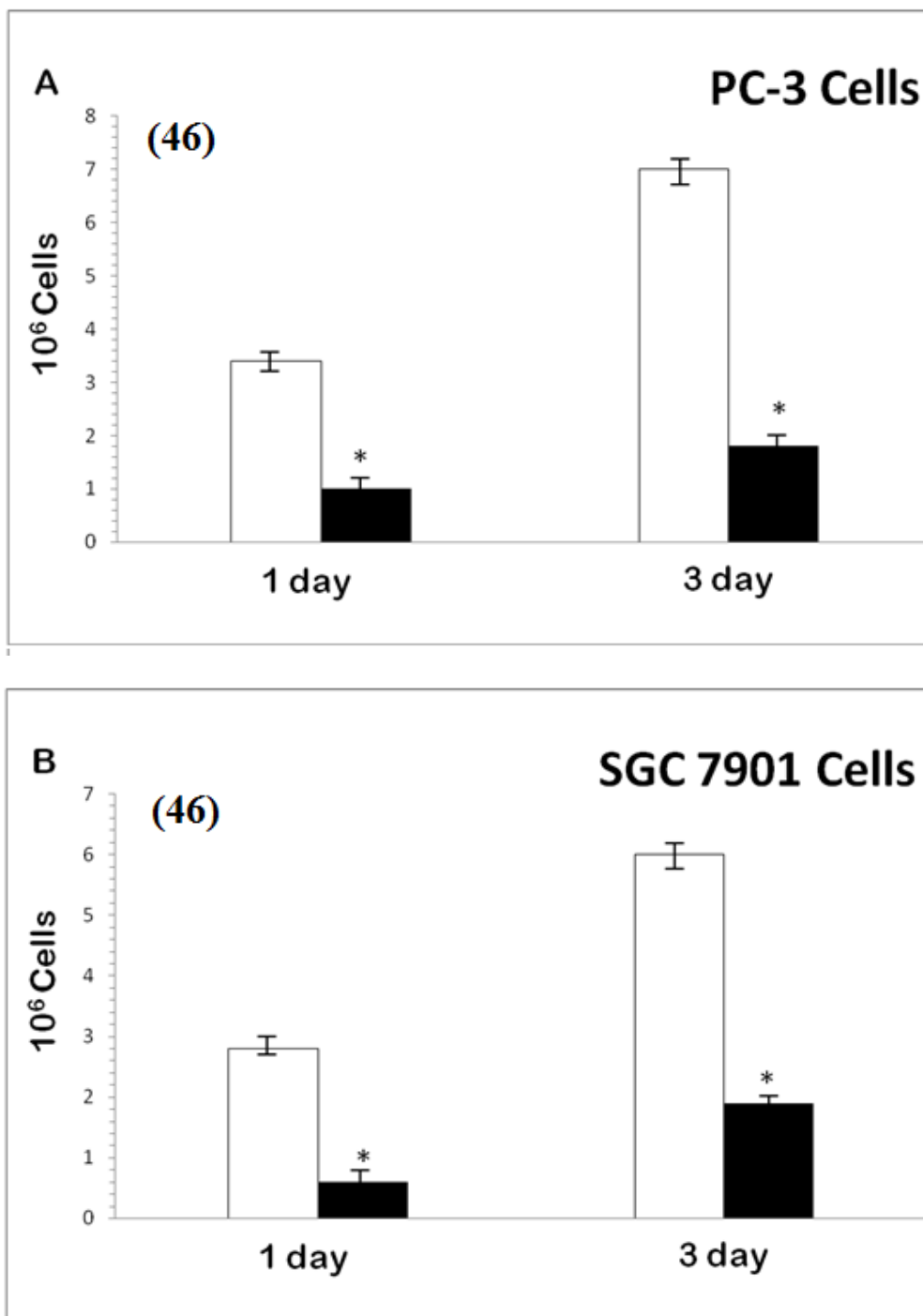


Figure 5.28 Time dependent inhibitory effect of 10 μM [*trans*-(\pm)-1,2-(DACH)₂Au]Cl₃ on growth of (A) PC3 and (B) SGC7901 cells for 1 day and 3 days using MTT assay. Results were expressed as the mean, SD. * $P < 0.05$

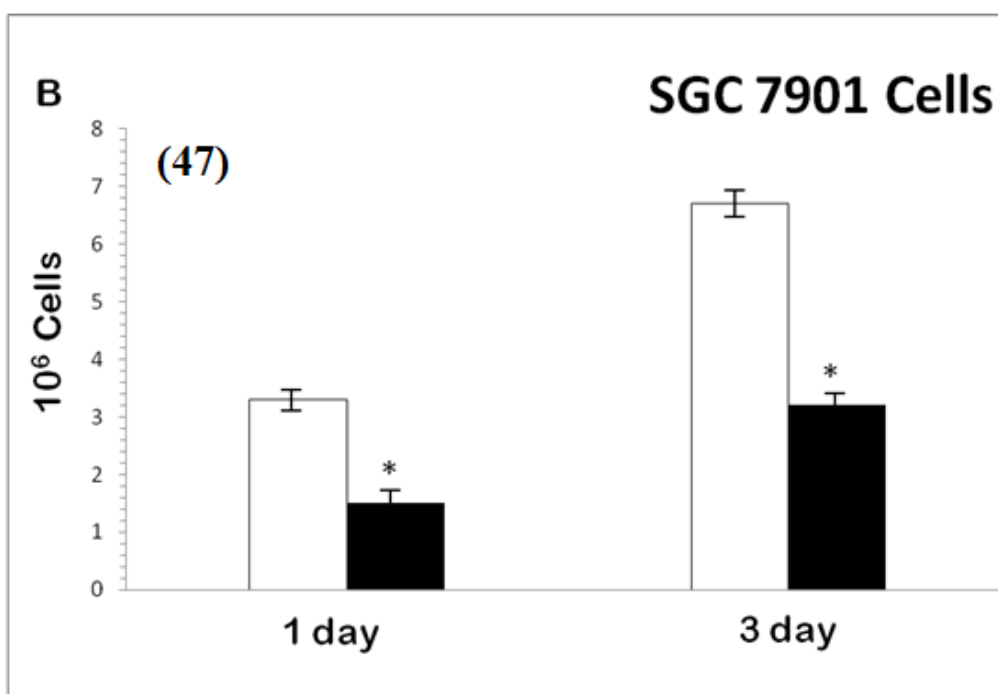
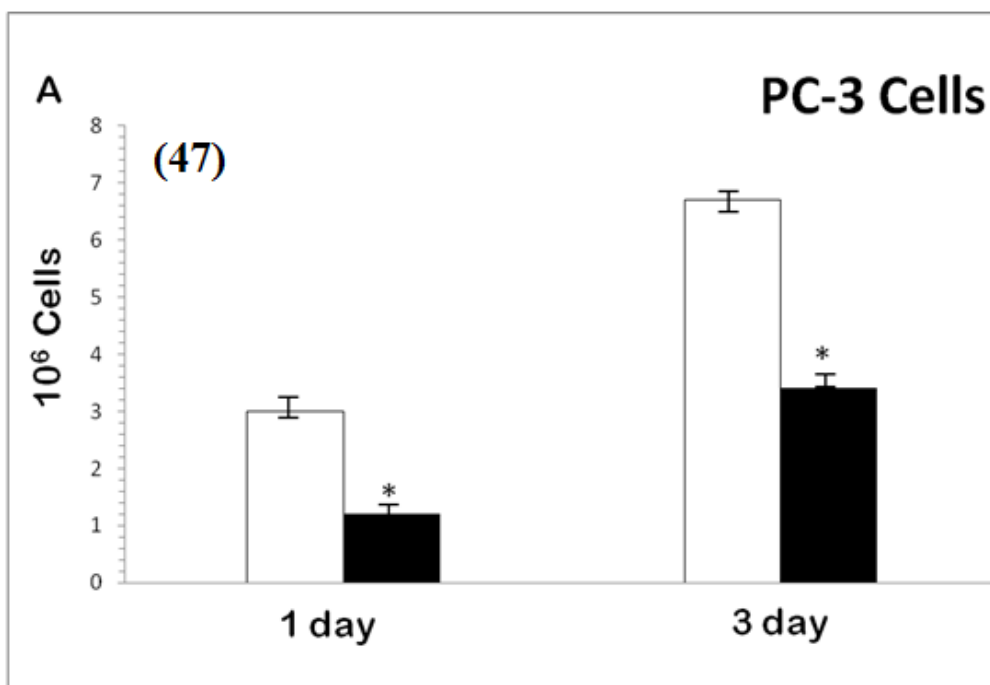


Figure 5.29 Time dependent inhibitory effect of 10 μM $[(1S,2S)\text{-}(+)\text{-(DACH)}_2\text{Au}]\text{Cl}_3$ on growth of (A) PC3 and (B) SGC7901 cells for 1 day and 3 days using MTT assay. Results were expressed as the mean, SD. $P < 0.05$

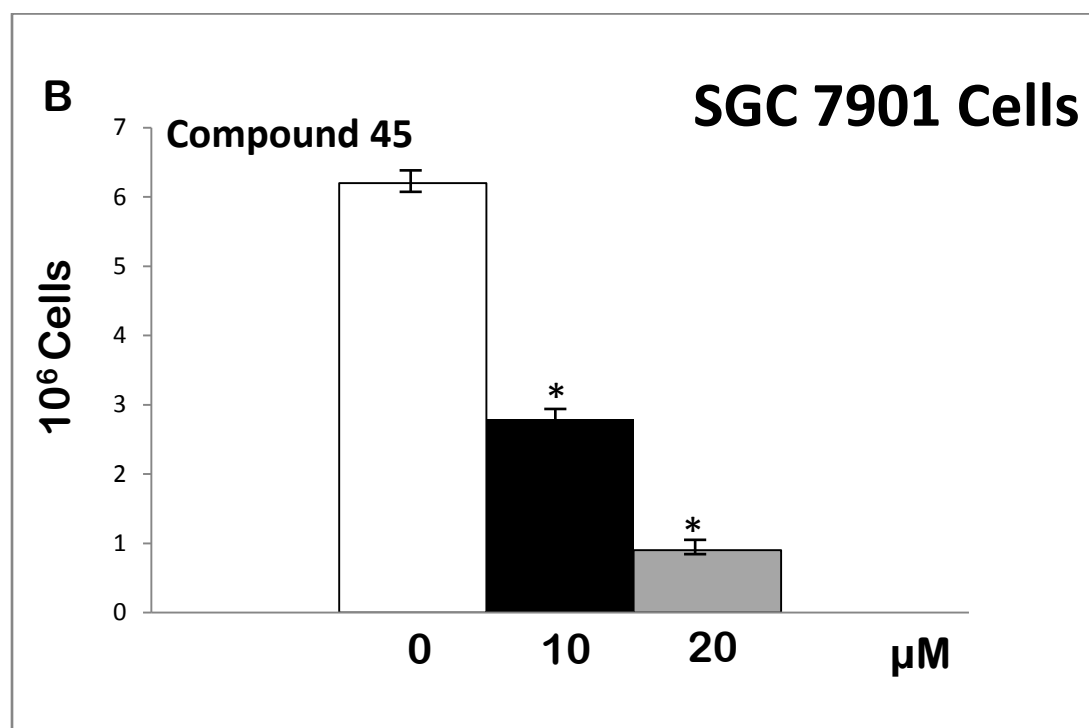
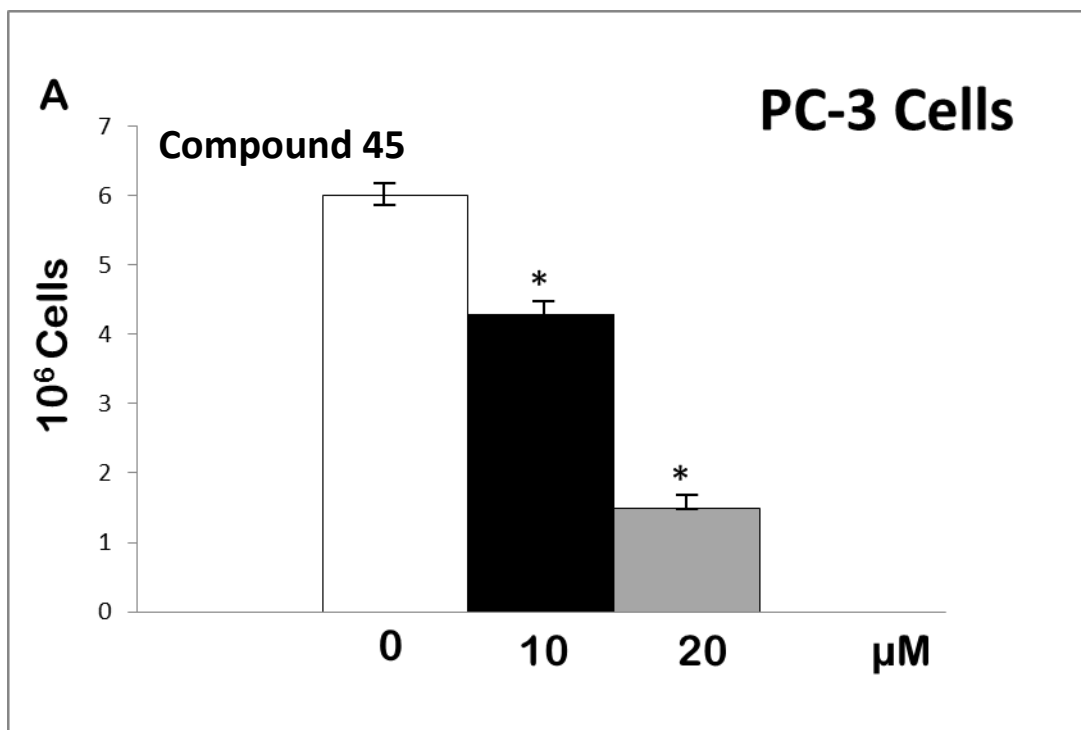


Figure 5.30 Effect of $[[cis-1,2-(DACH)_2Au]Cl_3]$ complex on cell growth in (A) PC-3 and (B) SGC-7901 cells. The cells were treated with various concentrations for 24 h. The anti-proliferative effect was measured by MTT assay. Results were expressed as the mean, SD. $P < 0.05$

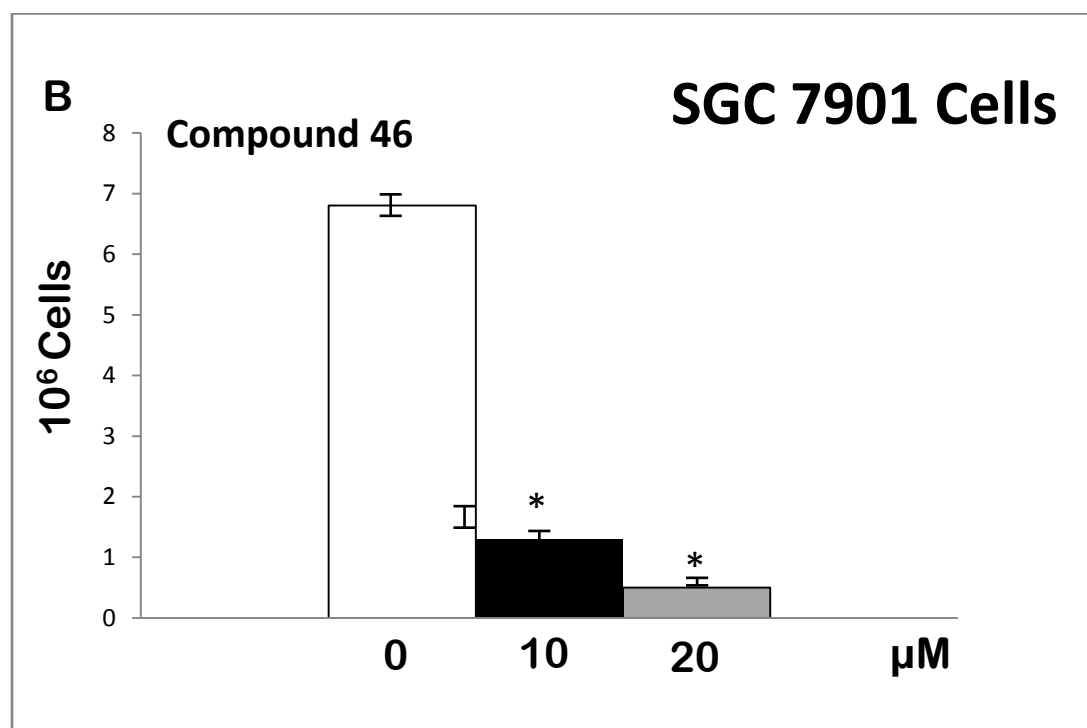
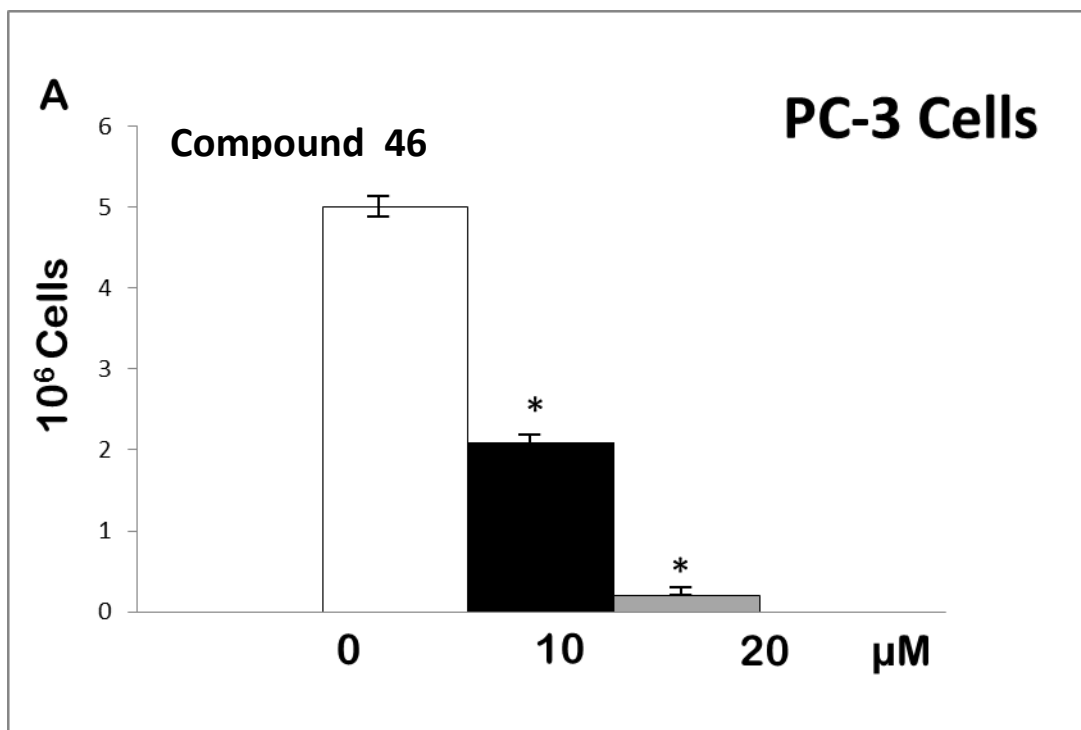


Figure 5.31 Effect of [*trans*-(±)-1,2-(DACH)₂Au]Cl₃ complex on cell growth in (A) PC-3 and (B) SGC-7901 cells. The cells were treated with various concentrations for 24 h. The anti-proliferative effect was measured by MTT assay. Results were expressed as the mean, SD. **P*<0.05

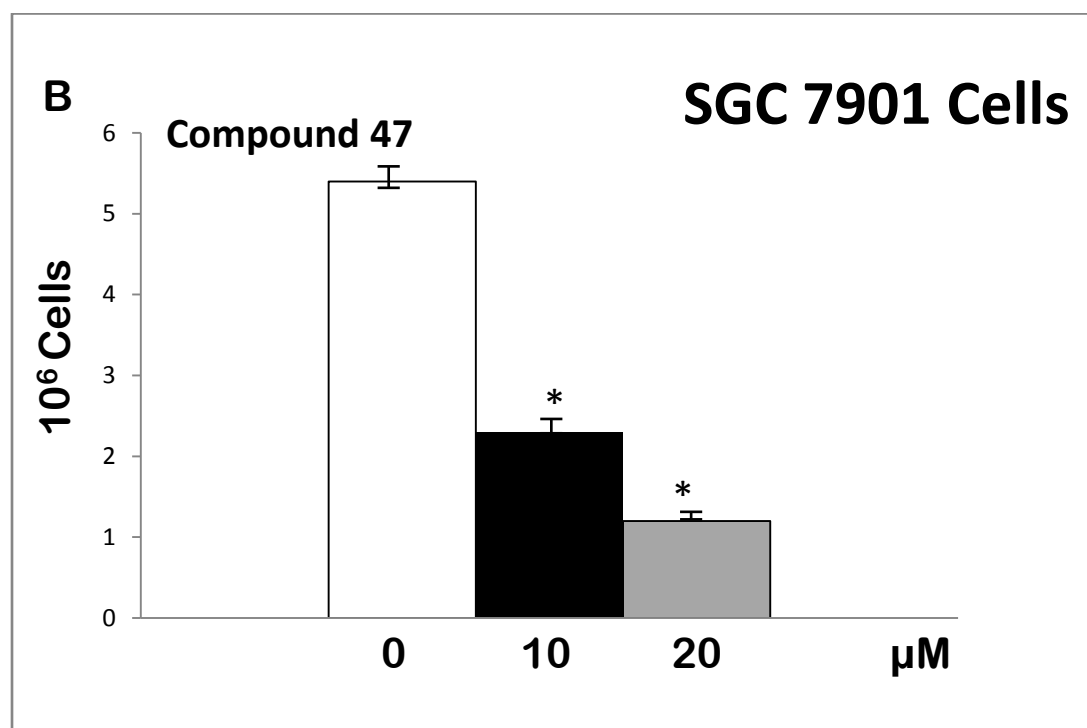
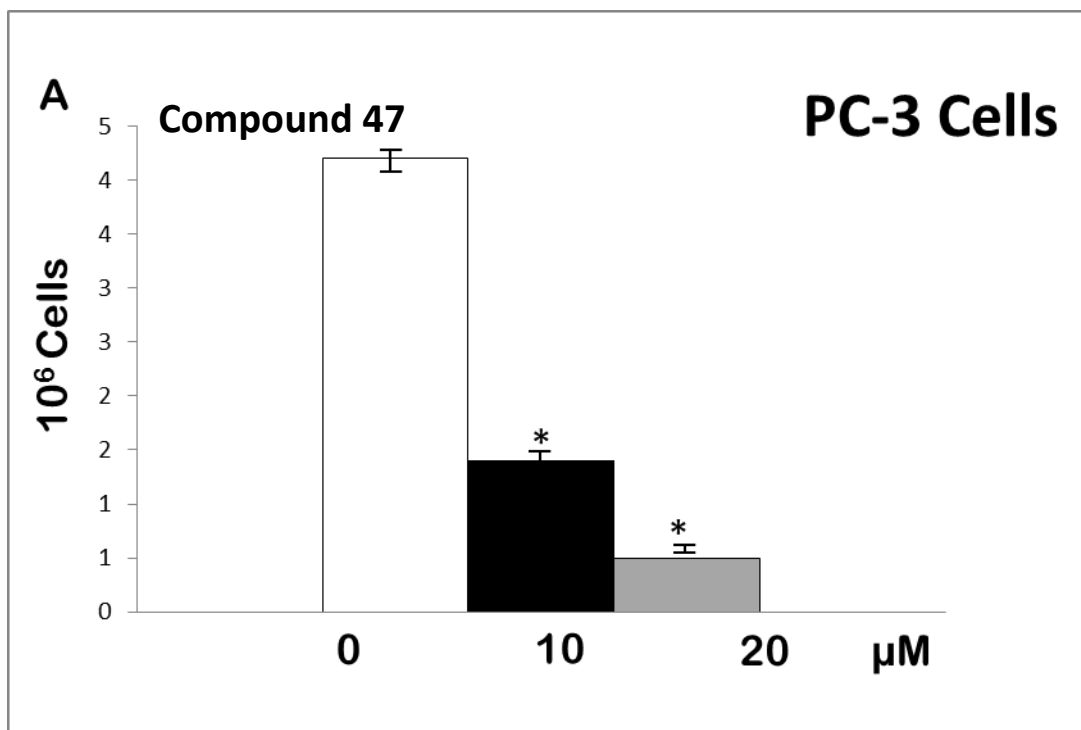


Figure 5.32 Effect of $[(1S,2S)\text{-}(+)\text{-(DACH)}_2\text{Au}]\text{Cl}_3$ complex on cell growth in (A) PC-3 and (B) SGC-7901 cells. The cells were treated with various concentrations for 24 h. The anti-proliferative effect was measured by MTT assay. Results were expressed as the mean, SD. * $P < 0.05$

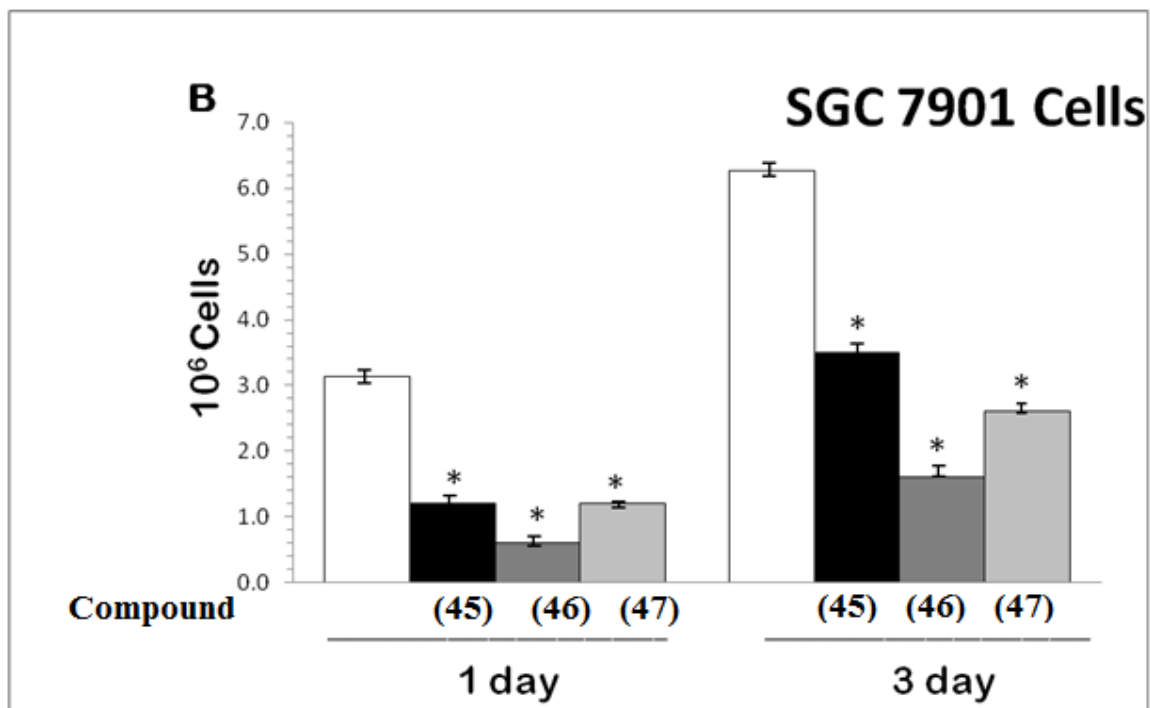
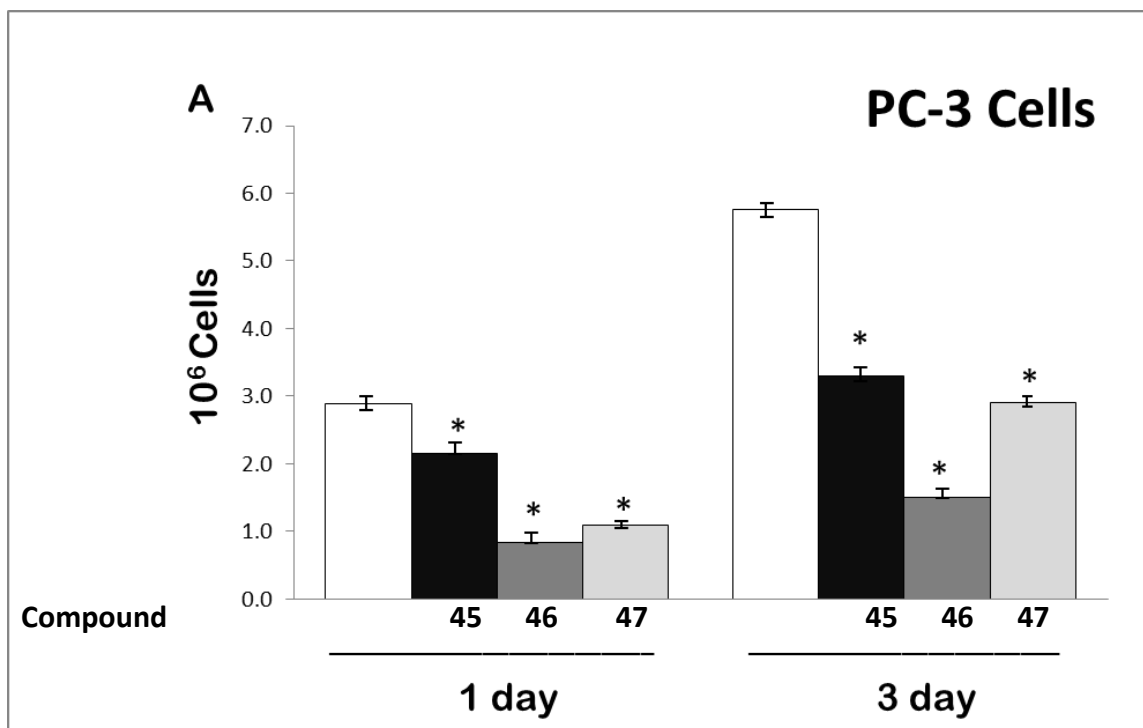


Figure 5.33 Comparative time dependent inhibitory effects for 10 μ M of compounds (45-47) on growth of (A) PC3 and (B) SGC7901 cells for day 1, day 2 and day 3 using MTT. Results were expressed as the mean, SD. * $P < 0.05$

5.2.9 Conclusion

Three new gold(III) compounds (**45**), (**46**) and (**47**) with general chemical formula of $[\text{Au}(\text{1,2-DACH})_2]\text{Cl}_3$ have successfully been synthesized. These gold(III) compounds were characterized using CHN analysis, UV-Vis, mid-FTIR, Far-FTIR spectroscopy; solution and solid-state NMR measurements; and X-ray crystallography. The CHN analysis data showed strong support for the formation of the type $[(\text{1,2-DACH})_2\text{Au}]\text{Cl}_3$ compound. Also, the X-ray crystallography demonstrates that gold coordination sphere of this compound adopts a distorted square planar geometry. According to our biological assays, compound (**46**) with *trans* configuration is a more promising candidate as an anti-cancer agent than the *trans* isomers (**45**) and (**47**) compounds. $[(\text{trans-DACH})_2\text{Au}]\text{Cl}_3$, in particular (1*S*,2*S*)-bis-(1,2-DACH) isomer, might be a promising chemo preventative and chemotherapeutic agent against human gastric carcinogenesis. As cytotoxic activity of $[(\text{trans-DACH})_2\text{Au}]\text{Cl}_3$ compound is high towards some cancer cell lines; further biological evaluation for this class of compounds is worthy of efforts especially in order to evaluate their activities *in vivo*.

5.3 Mixed-Ligand 1,2-Diaminocyclohexane(ethylenediamine)gold(III) Chloride Complexes

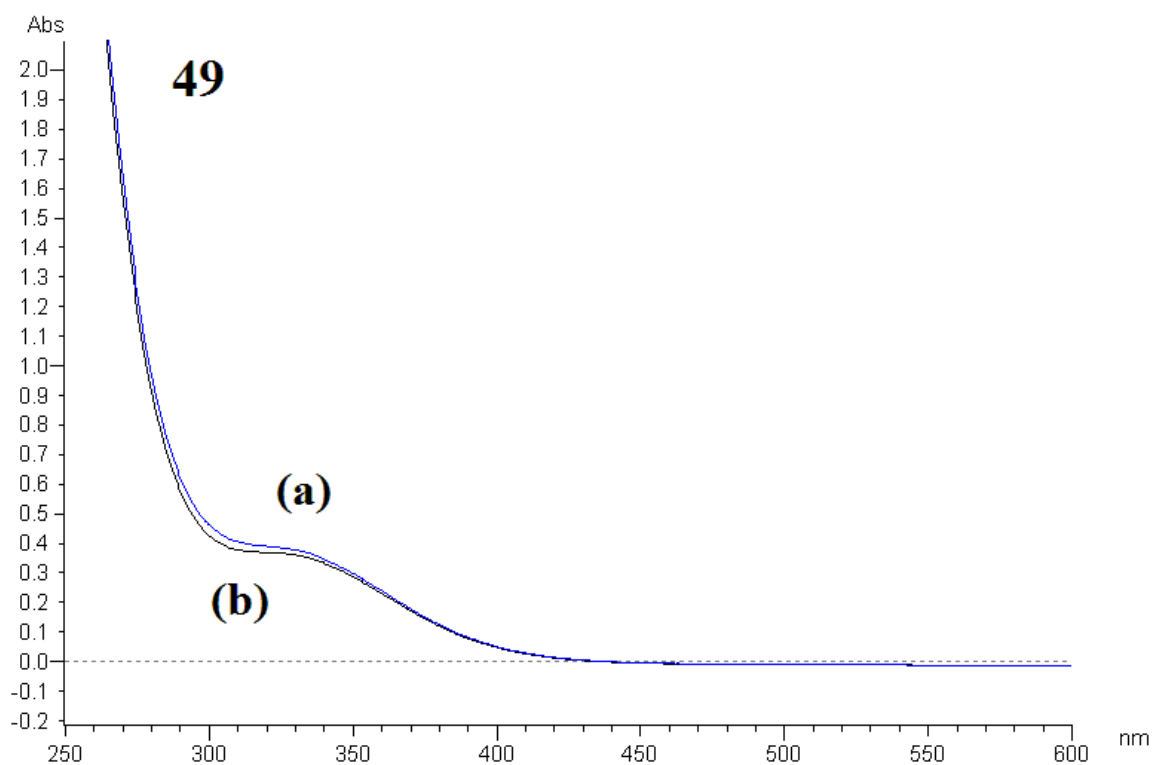
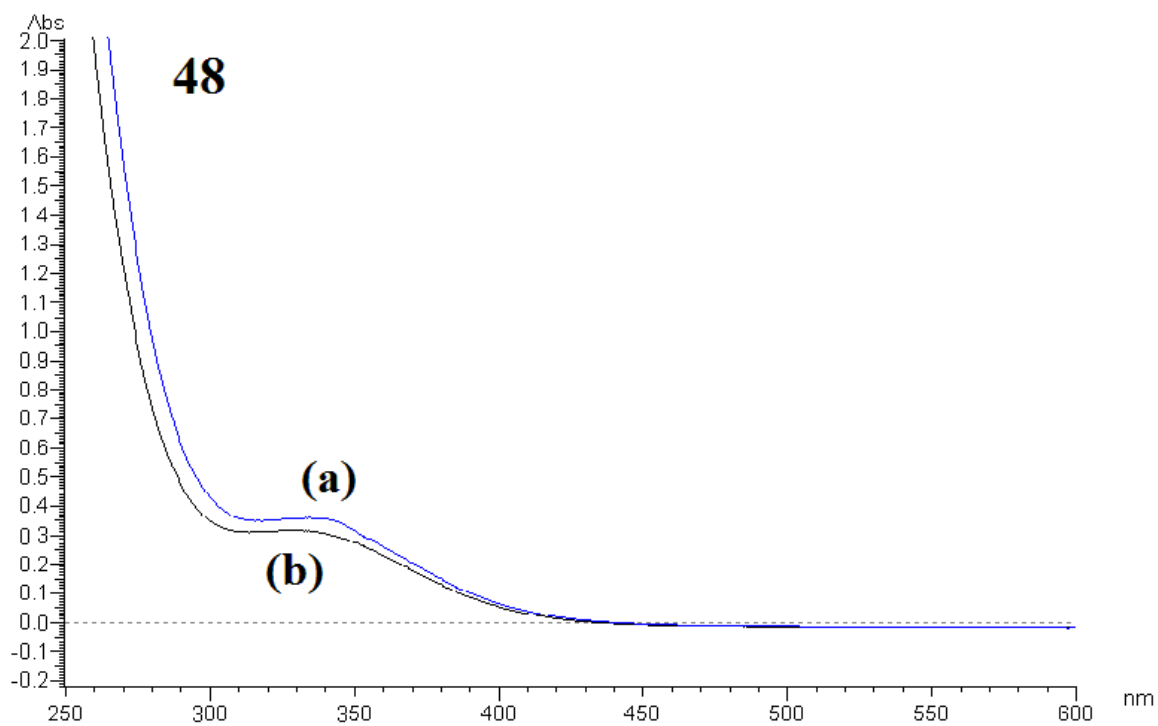
This work reports the synthesis and characterization of 1,2-diaminocyclohexane(ethylenediamine)gold(III) chloride complexes of the type $[(\text{DACH})\text{Au}(\text{en})]\text{Cl}_3$, (where DACH = *cis* and *trans*-1,2-diaminocyclohexane, *en* = ethylenediamine).

5.3.1 Electronic spectra

The λ_{\max} values for the complexes studied are shown in Table 5.21. The gold(III) complexes **(48)**, **(49)** and **(50)** exhibit, in a reference buffered phosphate solution, intense transitions in the range 335-339 nm, which are assigned as ligand-to-metal charge-transfer transitions characteristically associated to the gold(III) center [181]. In related compounds, absorption bands were assigned as -NH⁺ to a gold(III) charge-transfer bands [181]. These spectral features appear only at relatively high pH values (pH > 6-7) at which ligand deprotonation has fully occurred. According to crystal field theory for d^8 complexes the LUMO orbital is $d_{x^2-y^2}$, so ligand to metal charge transfer could be due to $p_{\sigma} \rightarrow d_{x^2-y^2}$ transition [175].

The electronic spectra of the complexes **(48)**, **(49)** and **(50)** in the buffer solution, were monitored at 37 °C over 7 days after mixing. The spectra for all compounds at mixing and after 7 days are depicted in Figure 5.34. It is apparent that the observed transitions remain substantially unmodified over 7 days observation, implying a substantial stability of these complexes under the present solution conditions. Nevertheless, a slight decrease in intensity, of the characteristic bands, was noticed with time without significant shape modifications. Also, this observation indicates that the gold center in these complexes remains in the +3 oxidation state [175-181]. The minor spectral changes that are generally observed within the first hours may be ascribed either to dissociation of the amine ligands from the gold(III) complex or to partial reduction of gold(III) to metallic gold. In general, however, loss of spectral intensity is lower than 10% of the original intensity within the observation period of 7 days which indicates high stability of these

compounds in the buffer. This is a possible suggestion that in the physiological milieu, the compounds would be able to undergo the necessary reactions required for bioactivity.



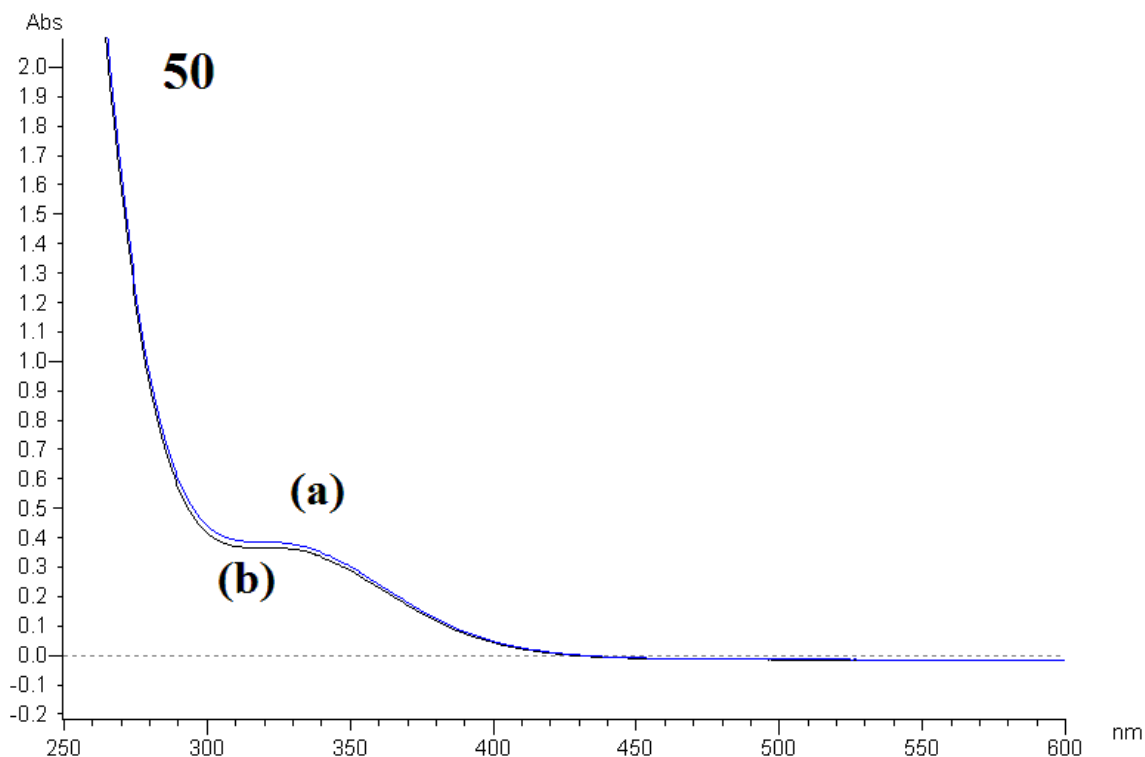


Figure 5.34 Time effect on electronic spectra of complexes (48)-(50) following dissolution in the buffer solution at mixing (a) and after 7 days (b) at 37 °C

Table 5.21 UV-Vis spectra λ_{\max} for complexes (48)-(50) dissolved in the reference physiological buffer solution.

Complex	λ_{\max} (nm)
NaAuCl ₄	293
[(en)Au{ <i>cis</i> -(1,2-DACH)}]Cl ₃ (48)	335
[(en)Au{ <i>trans</i> -(±)-(1,2-DACH)}]Cl ₃ (49)	338
[(en)Au{ <i>trans</i> -(+)-(1 <i>S</i> ,2 <i>S</i> -DACH)}]Cl ₃ (50)	339

5.3.2 Mid and Far-IR Spectroscopic Studies

The most significant bands recorded in the FT-IR spectra of the free ligands and [(1,2-DACH)(en)Au(III)]Cl₃ complexes have been reported in Table 5.22 and Table 5.23. It is noted that N-H stretching vibrations of complexes (48-50) exhibit, in the range 3386-3432 cm⁻¹, blue shifting compared with the amino group of the corresponding free

ligands. This is most likely due to stronger hydrogen bonding interactions in the free ligands. The amino coordination with Au(III) ions and Au-N bond formation can be supported by the presence of $\nu(\text{Au-N})$ at 417-442 cm^{-1} as indicated by Far-IR data [173]. The C-N stretching bands also showed a significant shift to higher wave number indicating a shorter C-N bond in the complex than in the free ligand. Furthermore, there was no signal observed at 352 and 367 cm^{-1} corresponding to the symmetric and asymmetric stretching of the Au-Cl indicating the absence of the gold mono-DACH complex [180]. The [(1,2-DACH)(en)Au(III)]Cl₃ complexes (**48-50**) show N-H stretching frequencies generally lower in comparison with mono-DACH complexes(**36-38**) (Table 5.21), most probably due to stronger hydrogen bonding interactions with the chloride anions in the [(1,2-DACH)(en)Au(III)]Cl₃ complexes. Furthermore the Au-N stretching frequencies are consistent with weaker Au-N bond strength in complexes (**48-50**) compared to the mono-DACH complexes.

Table 5.22 Mid-IR frequencies, $\nu(\text{cm}^{-1})$ for 1,2-cyclohexanediamine(ethylenediamine)Au(III) chloride complexes.

Species	$\nu(\text{N-H})$	ν_{shift}	$\nu(\text{C-N})$	ν_{shift}
(en)	3393 w		1033 m	
[(en)AuCl ₂]Cl	3422 br	29	1045 m	12
<i>Cis</i> -1,2-(DACH) (36')	3356 m, 3286 m		1092 s	
[<i>Cis</i> -1,2-(DACH)AuCl ₃]Cl (36)	3414 w	93	1183 s	91
[(en)Au{ <i>Cis</i> -1,2-(DACH)}]Cl ₃ (48)	3395 br	74 ^a , 2 ^b	1182 w	90 ^a , 149 ^b
<i>Trans</i> -(±)-1,2-(DACH) (37')	3348 m, 3271 m, 3183 m		1082 m	
[{ <i>Trans</i> -(±)-1,2-(DACH)}AuCl ₂]Cl (37)	3485 w, 3420 w, 3384 w	137, 149, 201	1175 m	93
[(en)Au{ <i>Trans</i> -(±)-1,2-(DACH)}]Cl ₃ (49)	3432 br	168 ^a , 39 ^b	1180 m	93 ^a , 147 ^b
(1 <i>S</i> ,2 <i>S</i>)-(+)-1,2-(DACH) (38')	3340 m, 3252 m, 3167 m		1082 m	
[(1 <i>S</i> ,2 <i>S</i>)-(+)-1,2-(DACH)AuCl ₂]Cl (38)	3604 m, 3340 m, 3306 m, 3168 m	132, 27	1171 m	89
[(en)Au(1 <i>S</i> ,2 <i>S</i>)-(+)-1,2-(DACH)]Cl ₃ (50)	3386 br	132 ^a , -7 ^b	1180 m	98 ^a , 147 ^b

^a with respect with (DACH), ^b with respect to (en)

Table 5.23 Far-IR frequencies, $\nu(\text{cm}^{-1})$ for 1,2-cyclohexanediamine(ethylenediamine)Au(III) chloride complexes.

Species	Au-Cl	Au-N	Refs.
NaAuCl ₄	365	-	a
[(en)AuCl ₂]Cl	-	391,474	[183]
[<i>Cis</i> -1,2-(DACH)AuCl ₃]Cl (36)	352, 367	437	[180]
[(en)Au{ <i>Cis</i> -1,2-(DACH)}]Cl ₃ (48)	-	326, 417	a
[{ <i>Trans</i> -(±)-1,2-(DACH)}AuCl ₂]Cl (37)	353, 365	437	[180]
[(en)Au{ <i>Trans</i> -(±)-1,2-(DACH)}]Cl ₃ (49)	-	391, 442	a
[(1 <i>S</i> ,2 <i>S</i>)-(+)-1,2-(DACH)AuCl ₂]Cl (38)	353, 366	395, 436	[180]
[(en)Au(1 <i>S</i> ,2 <i>S</i>)-(+)-1,2-(DACH)]Cl ₃ (50)	-	376, 440	a

^a this work

5.3.3 Solution NMR Characterization

The ¹H and ¹³C NMR chemical shifts are given in Table 5.24 and Table 5.25, respectively. All ¹H NMR supported the structures of the synthesized complexes as indicated by the integration of the signals of C-H protons connected to the amino groups of the (DACH) and (en). For example, the ratio of the protons attached to amino group in both (DACH) and (en) for complex (**50**) is 1:2 as depicted in Figure 5.35. Its ¹³C NMR spectrum is also confirmed the complex's structure as shown in Figure 5.36. The ¹H and ¹³C NMR chemical shifts of compounds (**48-50**) along with their corresponding free ligands are listed in Tables 5.24 and 5.25, respectively. In the ¹H and ¹³C NMR spectra of complexes (**48**), (**49**) and (**50**), one half of the total expected signals were noticed because of the C₂ symmetry axis. 1,2-diaminocyclohexane ring is considered as a rigid conformer that allowed, for instance, to distinguish equatorial H3 and H6 from axial H3 and H6 at room temperature. The signals of C-H protons connected to the amino groups for both

(DACH) and (*en*) occur in the spectra at 3.05 to 3.61 ppm, shifting downfield compared with the corresponding signals (2.23-2.65 ppm) in the free diamine ligands. The significant downfield shift was observed at 3.62 ppm for **(48)** complex with respect to the free DACH ligand at 2.23 ppm. This can be attributed to the donation of nitrogen lone pairs to the gold that causes de-shielding of the proton(s) next to the bonding nitrogen. On the other hand, ^{13}C NMR downfield shift was observed only for the carbon next to the bonding nitrogen and the others carbons in the complex for (DACH) showed upfield shift. For instance, chemical shift of C3 and C4 for complex **(48)** observed at 26.13 and 20.64 ppm, respectively, whereas, for free diamine ligand it occurs at 35.26 and 26.36 ppm. It is also worth to mention that complexes **(48-50)**, even though they have the same skeleton of (DACH) and (*en*), their NMR chemical shifts specifically for (DACH) aren't the same due to a different stereochemistry upon complexation.

Table 5.24 ^1H NMR chemical shifts of free ligands and 1,2-cyclohexanediamine(ethylenediamine)Au(III) chloride complexes in D_2O

Compound	$^1\text{H}(\delta$ in ppm)					
	H1,H2,	H3,H6 (eq)	H3,H6 (ax)	H4,H5 (eq)	H4,H5 (ax)	H1',H2'
(en)	-	-	-	-	-	3.2, <i>s</i>
(36')	2.23, <i>m</i>	1.85, <i>m</i>	1.69, <i>m</i>	1.28, <i>m</i>	1.12, <i>m</i>	-
(37')	2.25, <i>m</i>	1.85, <i>m</i>	1.68, <i>m</i>	1.28, <i>m</i>	1.11, <i>m</i>	-
(38')	2.24, <i>m</i>	1.85, <i>m</i>	1.69, <i>m</i>	1.28, <i>m</i>	1.11, <i>m</i>	-
(48)	3.61, <i>m</i>	1.96, <i>m</i>	1.77, <i>m</i>	1.59, <i>m</i>	1.41, <i>m</i>	3.16, <i>s</i>
(49)	3.05, <i>m</i>	2.11, <i>m</i>	1.54, <i>m</i>	1.48, <i>m</i>	1.10, <i>m</i>	3.14, <i>s</i>
(50)	3.08, <i>m</i>	2.19, <i>m</i>	1.63, <i>m</i>	1.54, <i>m</i>	1.19, <i>m</i>	3.17, <i>s</i>

Table 5.25 ^{13}C NMR chemical shifts of free ligands and 1,2-cyclohexanediamine(ethylenediamine)Au(III) chloride complexes in D_2O .

Compound	^{13}C (δ in ppm)			
	C1,C2	C3,C6	C4,C5	C1', C2'
(en)	-	-	-	37.67
(36')	58.20	35.26	26.36	-
(37')	58.46	35.55	26.63	-
(38')	58.27	35.32	26.43	-
(48)	61.74	26.13	20.64	50.39
(49)	64.59	32.95	24.12	50.63
(50)	64.44	32.84	24.02	50.48

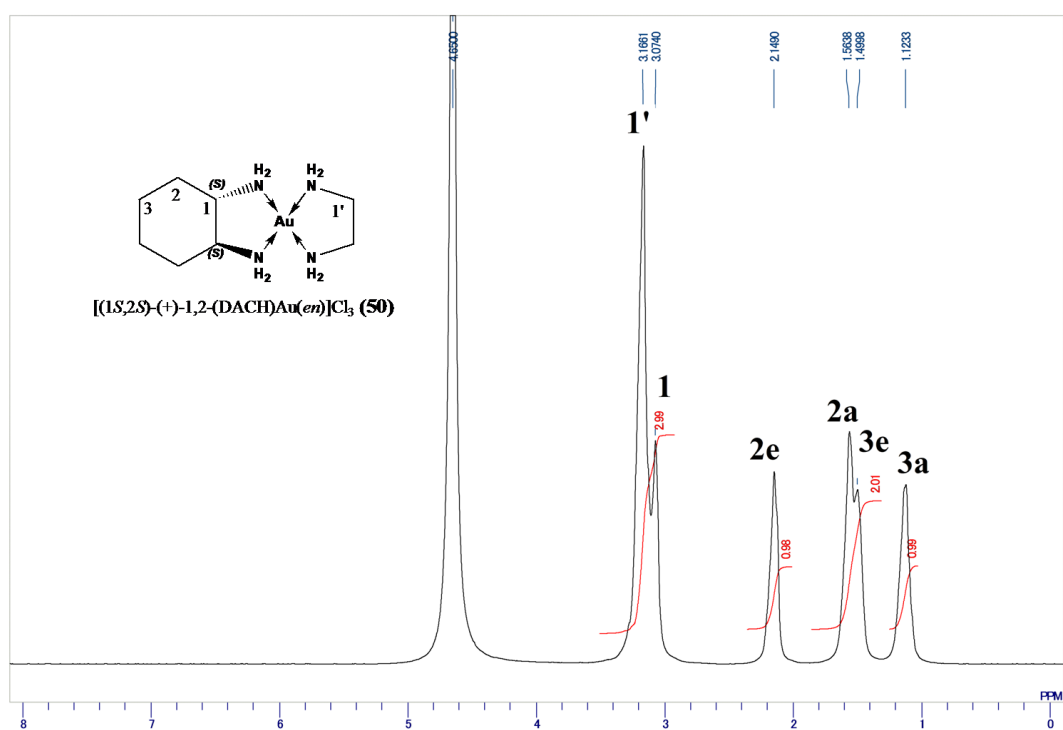


Figure 5.35 The 500-MHz ^1H solution NMR spectrum of $[(1S,2S)\text{-}(+)\text{-}(\text{DACH})\text{Au}(\text{en})]\text{Cl}_3$ complex.

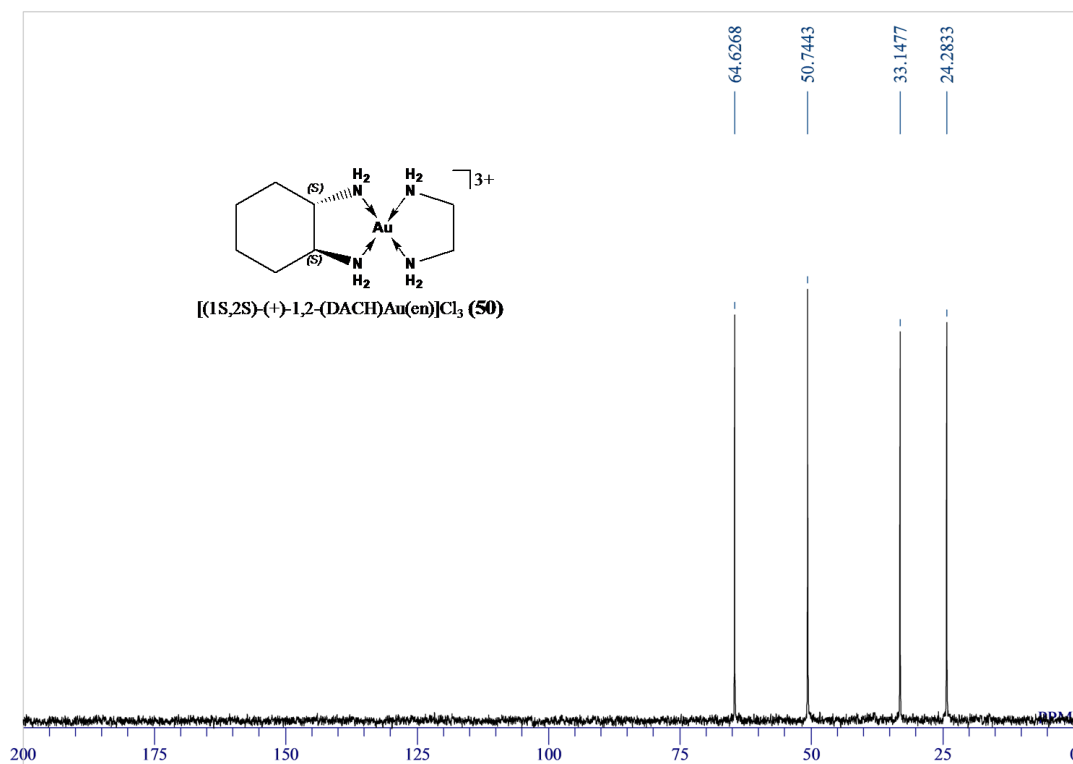


Figure 5.36 The 125.65-MHz $^{13}\text{C}\{^1\text{H}\}$ solution NMR spectrum of [(1S,2S)-(+)-1,2-(DACH)Au(en)]Cl₃ complex.

5.3.4 Solid-State NMR

As listed in Table 5.26, solid state NMR spectrum of complex (**50**) showed equivalency in the chemical shifts of carbon atoms (C1,C2), (C3,C6), (C4,C6) and (C1',C2') where two sets of peaks were observed, whereas, a similar behavior was not observed for carbon atoms of (DACH) in complexes (**48**)&(**49**). This indicates that these complexes (**48**)&(**49**) in the solid state lack C_2 symmetry. In contrast, all synthesized complexes (**48**), (**49**)&(**49**) showed C_2 symmetry in the solution state as indicated earlier by solution ^1H and ^{13}C NMR.

Compared to solution chemical shifts, significant de-shielding in solid state is observed with similarity in the chemical shift among all synthesized complexes (Table 5.28) which is a clear indication of stability of the prepared complexes in solid state.

Table 5.26 Solid ^{13}C NMR chemical shifts of free ligands and 1,2-cyclohexanediamine(ethylenediamine)Au(III) chloride complexes.

Compound	^{13}C (δ in ppm)				Refs.
	C1,C2	C3,C6,	C4,C5	C1', C2'	
<i>Cis</i> -1,2-(DACH)AuCl ₃ (48)	66.20, 65.35 64.32	30.98 28.85	27.02, 22.12 28.85, 22.94	- 54.30	[180] ^a
<i>Trans</i> -(\pm)-1,2-(DACH)AuCl ₃ (49)	69.60 69.60, 65.45	37.37 36.63	27.99 27.53	- 54.08	[180] ^a
(<i>S,S</i>)-(+)-1,2-(DACH)AuCl ₃ (50)	70.21 67.1	37.86 36.19	29.16 27.65	- 54.18	[180] ^a

^a this work

5.3.5 Computational Study

The optimized structures of the [(DACH)Au(en)]³⁺ complexes as obtained from the B3LYP/LANL2DZ level of calculations are shown in Figure 5.37. Selected quantitative structural parameters are also listed in Table 5.27. The complexes show a distorted square planar geometry structure around the gold atom. The N – Au – N angles in most of the conformations are within less than a degree from the perfect square planar geometry. The Au – N bond distance was predicted to be in the range of 2.12 to 2.15 Å for both (DACH) and (en) bidentating ligands. The C – N bond length shows a significant increase (by approximately 0.1 Å) when compared with the same type of bonds in normal amines [184]. The four nitrogen atoms are predicted to adopt *sp*³ type of hybridization as can be viewed from the calculated bond angles (Table 5.27). From the computed energetics of the four structures of the complex (Table 5.28), the *trans* conformations are more preferable compared to the *cis* conformations with more than 3.5 kcal/mol difference.

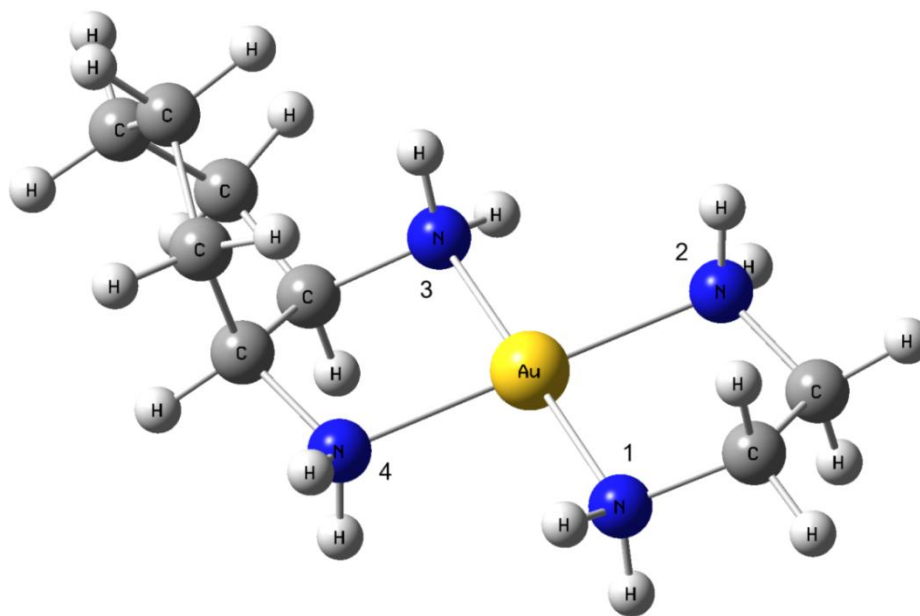
The most possible explanation of this energy variation is the ring configuration of the DACH ligand, where in the *cis* form the CH₂ units experience more steric repulsion compared to the *trans* form.

Table 5.27 Calculated bond lengths and bond angles of the [(1,2-DACH)(en)Au(III)]³⁺ complex in its four possible conformations

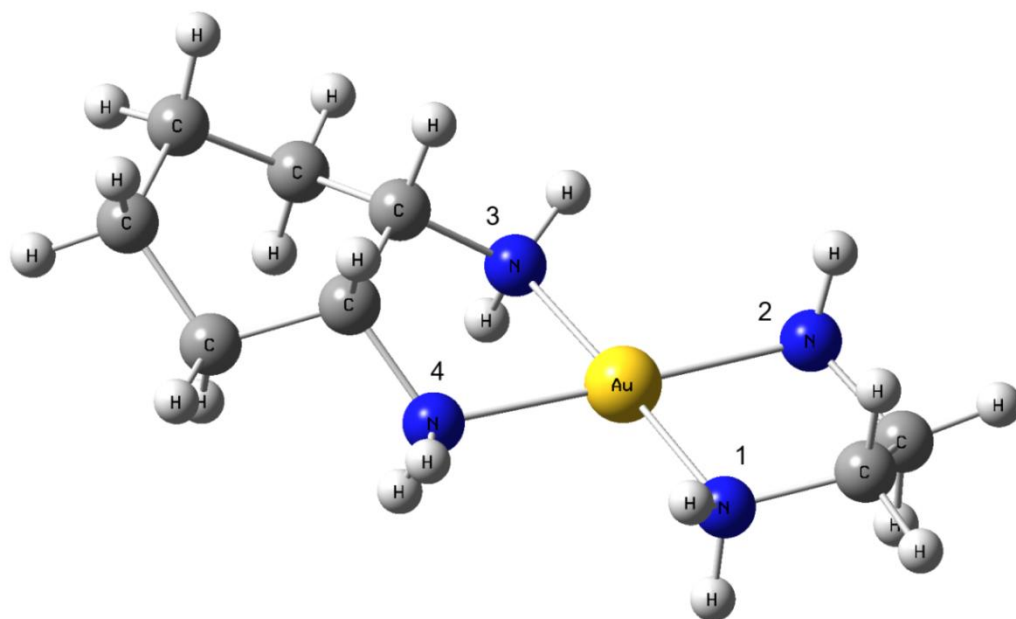
	48(a)	48(b)	49(a)	49(b)
Bond lengths (Å)				
Au – N ₁	2.147	2.140	2.145	2.146
Au – N ₂	2.147	2.132	2.145	2.146
Au – N ₃	2.131	2.118	2.134	2.135
Au – N ₄	2.132	2.127	2.134	2.135
N ₁ – C	1.538	1.540	1.539	1.539
N ₂ – C	1.538	1.541	1.539	1.539
N ₃ – C	1.544	1.559	1.545	1.544
N ₄ – C	1.545	1.552	1.545	1.544
Bond angles (deg.)				
N ₁ – Au – N ₃	177.7	179.5	179.4	179.5
N ₂ – Au – N ₄	177.6	179.4	179.4	179.5
N ₁ – Au – N ₂	81.8	82.1	82.0	81.9
N ₂ – Au – N ₃	100.5	98.3	98.6	98.6
N ₃ – Au – N ₄	77.2	81.7	80.9	80.9
N ₄ – Au – N ₁	100.6	97.9	98.5	98.6
Au – N ₁ – C	109.3	109.1	109.0	109.0
Au – N ₂ – C	109.1	109.1	109.0	109.0
Au – N ₃ – C	111.4	109.5	110.7	110.8
Au – N ₄ – C	111.8	109.4	110.7	110.8

Table 5.28 Relative energies (kcal/mol) of the four possible conformations of [(1,2-DACH)(en)Au(III)]³⁺ complexes.

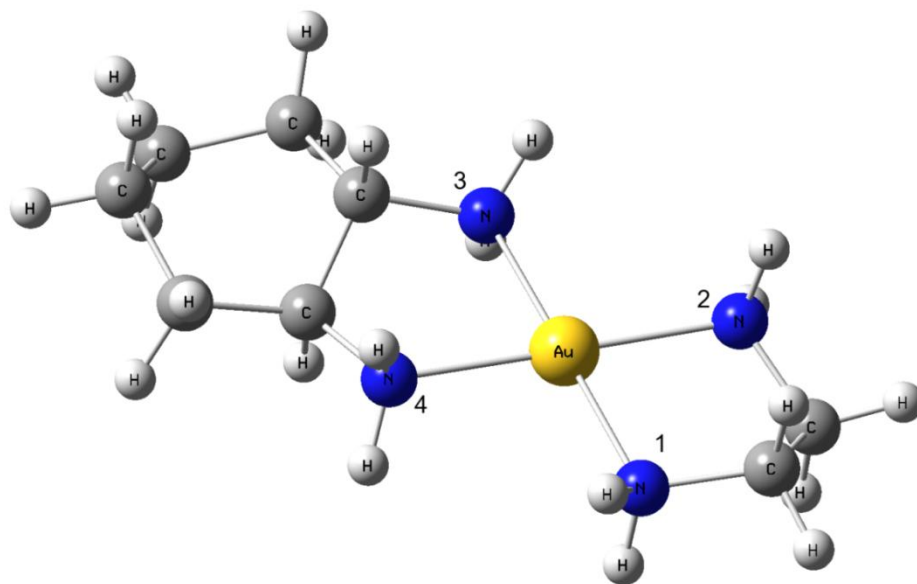
Conformation	Relative Energy (kcal/mol)
<i>48(a)</i>	3.61
<i>48(b)</i>	3.10
<i>49(a)</i>	0.00
<i>49(b)</i>	0.11



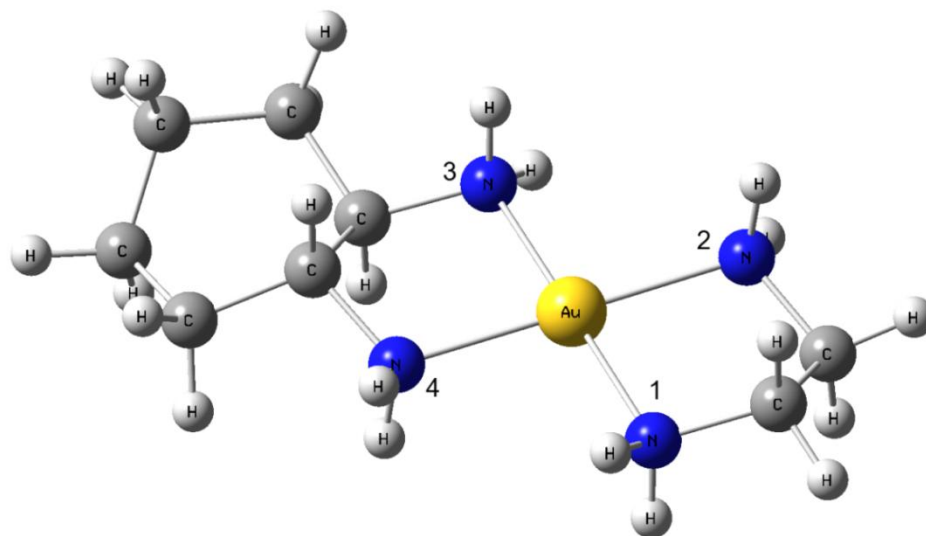
48(a)



48(b)



49(a)



49(b)

Figure 5.37 Optimized geometries of $[(1,2\text{-DACH})\text{Au}(\text{III})(\text{en})]^{+3}$, obtained at the B3LYP/LanL2DZ level of theory using GAUSSIAN09 W

5.3.6 NMR Profiles Stability Study.

NMR spectra of the complexes dissolved in D_2O and mixed $\text{DMSO-}d_6/\text{D}_2\text{O}$ (v/v: 2/1) solution were obtained on immediate dissolution to serve as reference spectra and latter at 24 h and after 7 days at 37 °C in D_2O and at RT in mixed $\text{DMSO-}d_6/\text{D}_2\text{O}$ to determine their stability. In general, all complexes showed high stability in D_2O and their NMR profiles remained unchanged over 7 days. For example, Figures 5.38-5.39 illustrated, respectively, the ^1H and ^{13}C NMR profiles of the compound (**48**) at mixing and after 7 days. Whereas, these compounds in mixed $\text{DMSO-}d_6/\text{D}_2\text{O}$ were slightly less stable at the experimental conditions, in which, minor dissociation of (en) out off the gold complexes

was observed from day one. On the other hand, no dissociation was observed for (DACH). Among all synthesized complexes, the maximum dissociation for (en) after 7 days was experienced for compound (**50**) with 25%. Figures 5.40-5.41 showed, respectively, ^1H and ^{13}C NMR profiles of compound (**50**) in $\text{DMSO-}d_6/\text{D}_2\text{O}$ at mixing and after 7 days. ^1H and ^{13}C NMR of compound (**50**) spectra after 7 days in $\text{DMSO-}d_6/\text{D}_2\text{O}$ showed extra peak at 3.07 and 37.24 ppm as shown in Figures 5.40 (b)-5.41 (b), respectively, corresponding to the free (en) atoms. It is clear that the bond between gold(III) and (DACH) is stronger than the bond between gold(III) and (en) in these complexes suggesting that (en) could be a better leaving group.

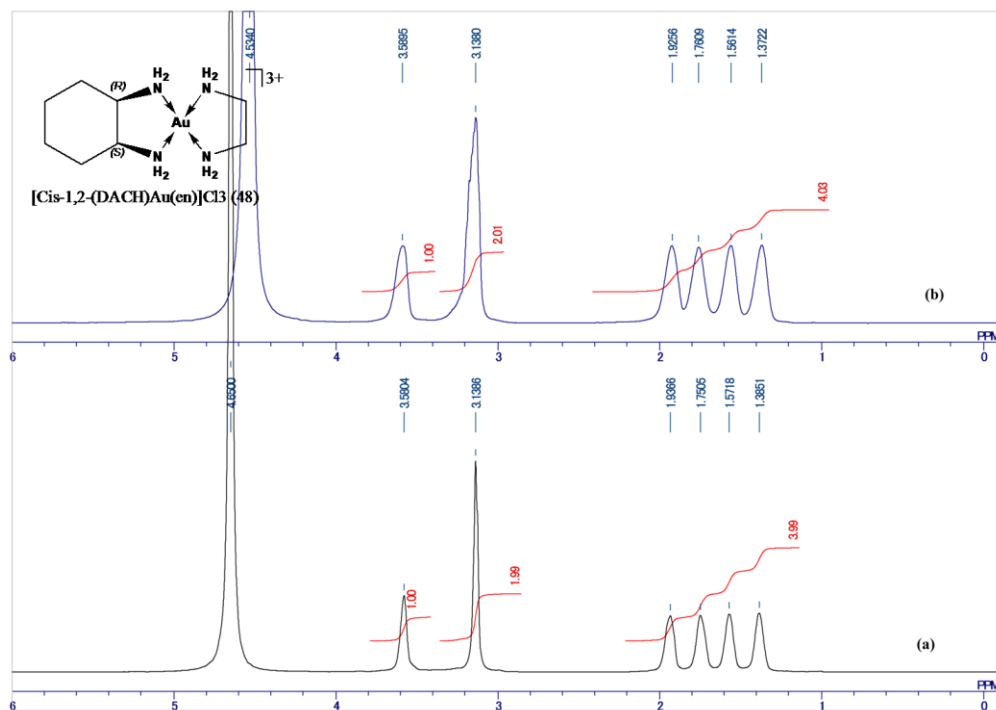


Figure 5.38 The 500-MHz ^1H solution NMR spectra of [cis-1,2-(DACH)Au(en)]Cl₃ complex in D_2O at mixing (a) and after 7 days (b)

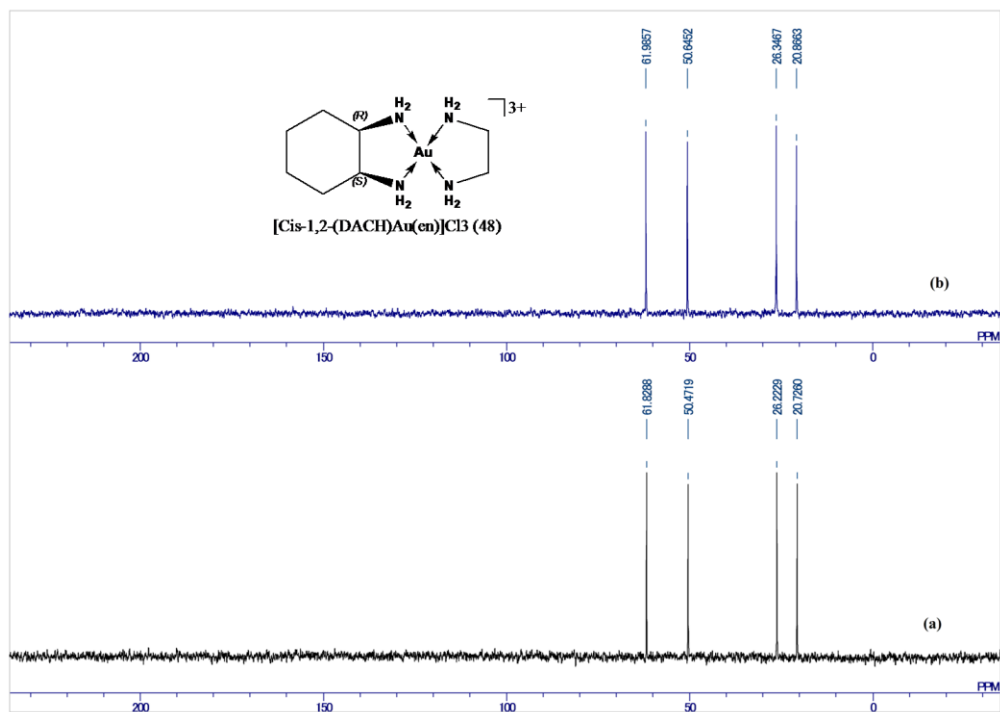


Figure 5.39 The 125.65-MHz $^{13}\text{C}\{^1\text{H}\}$ solution NMR spectra of $[\text{Cis-1,2-(DACH)Au(en)}]\text{Cl}_3$ complex in D_2O at mixing (a) and after 7 days (b).

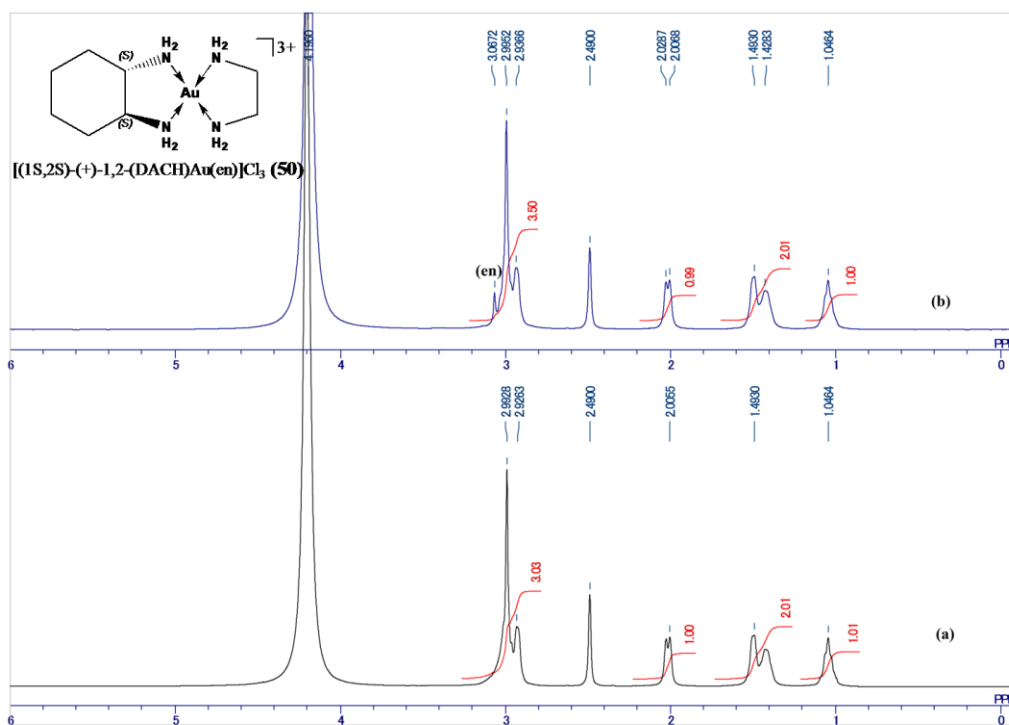


Figure 5.40 The 500-MHz ^1H solution NMR spectra of $[(1\text{S},2\text{S})-(+)\text{-}(\text{DACH)Au(en)}]\text{Cl}_3$ complex in $\text{D}_2\text{O}/\text{DMSO}$ at mixing (a) and after 7 days (b)

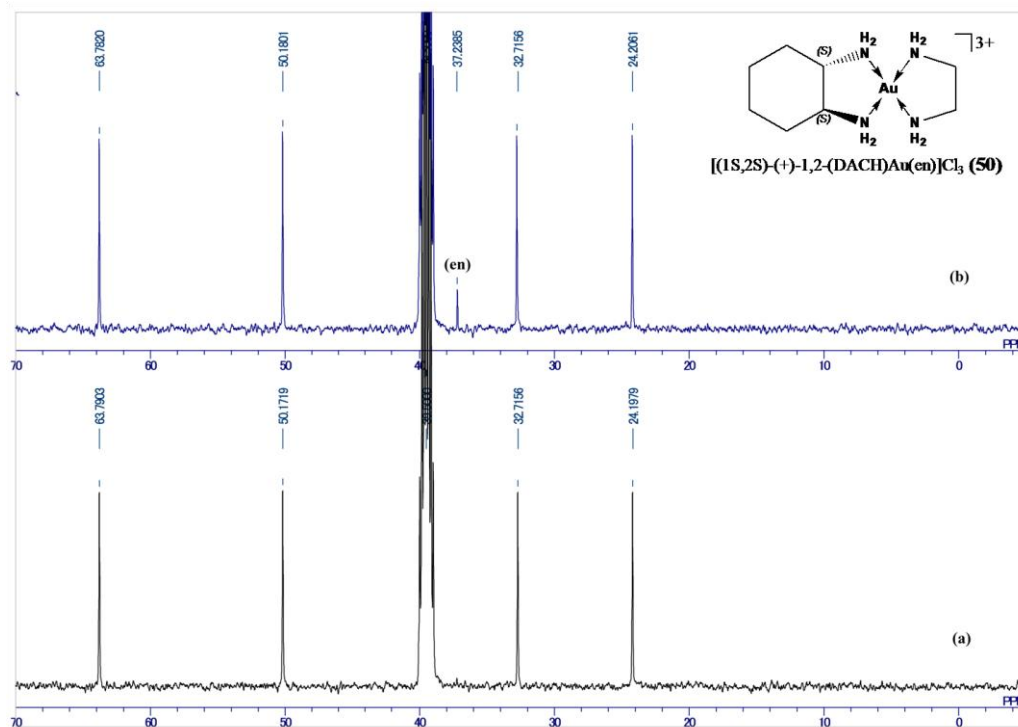


Figure 5.41 The 125.65-MHz $^{13}\text{C}\{^1\text{H}\}$ solution NMR spectra of $[(1\text{S},2\text{S})-(+)\text{-}1,2\text{-}(\text{DACH})\text{Au}(\text{en})\text{Cl}_3$ complex in (DMSO/D $_2$ O, 1:2) at mixing (a) and after 7 days (b)

5.3.7 Electrochemical Studies of Compounds 48-50.

The electrochemical behavior of compounds (48), (49) and (50) was investigated in a physiological environment through cyclic voltammetry. The voltammetric curves of the complexes (48), (49) and (50) are shown in Figure 5.42, and Table 5.29 summarizes the voltammetric data of all the study compounds. The potential values vs. NHE for the reduction processes exhibited by the complexes (48), (49) and (50), in a reference buffered phosphate, in the range (+0.46)-(+0.51) V. Voltammetric data indicated that *trans*-DACH conformer isomer is slightly more stable than the *cis*-DACH conformer of the complexes which is consistent with UV-Visible analysis. Gold(III) complexes (48), (49) and (50) show one irreversible reduction process which in controlled potential coulometry involves three electrons per mole. The occurrence of Au(III)/Au(0) reduction

is confirmed by the appearance of the thin gold layer deposited on the platinum electrode surface after exhaustive electrolysis (E_w , -0.7 V). In general, voltammetric results suggested that these compounds are quite stable under the physiological conditions.

We also checked the stability of the gold(III) compounds in the reference buffer following addition of stoichiometric amounts of the biologically important reducing agent sodium ascorbate. It was observed that all complexes were quickly and completely reduced and the process was nearly complete after 60 min.

Table 5.29 Peak potential values (vs ENH) for reduction of the gold(III) complexes (48-50) in the buffered aqueous solution processes at the platinum electrode.

Complex	E_p(V)
$[(en)Au\{Cis-1,2-(DACH)\}]Cl_3$ (48)	+0.49
$[(en)Au\{Trans-(\pm)-1,2-(DACH)\}]Cl_3$ (49)	+0.46
$[(en)Au(1S,2S)-(+)-(DACH)]Cl_3$ (50)	+0.51

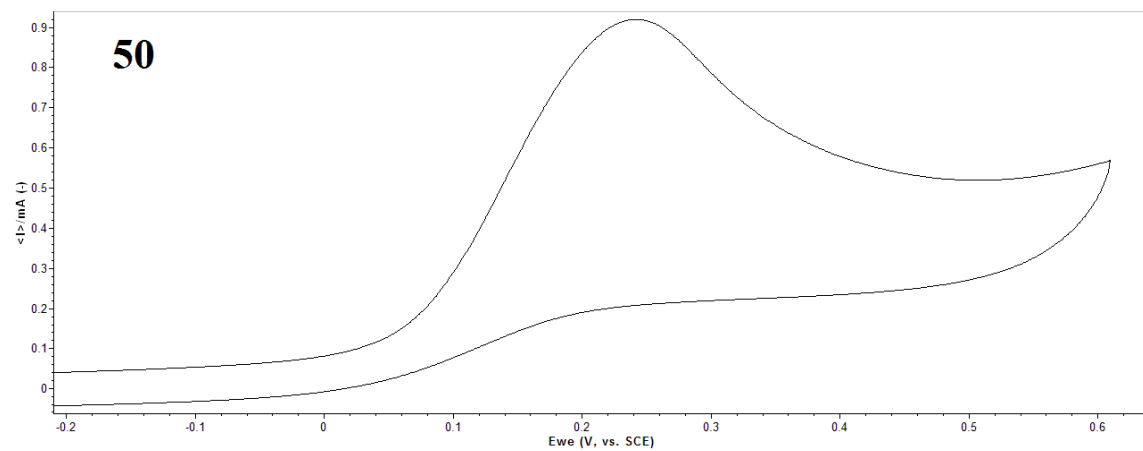
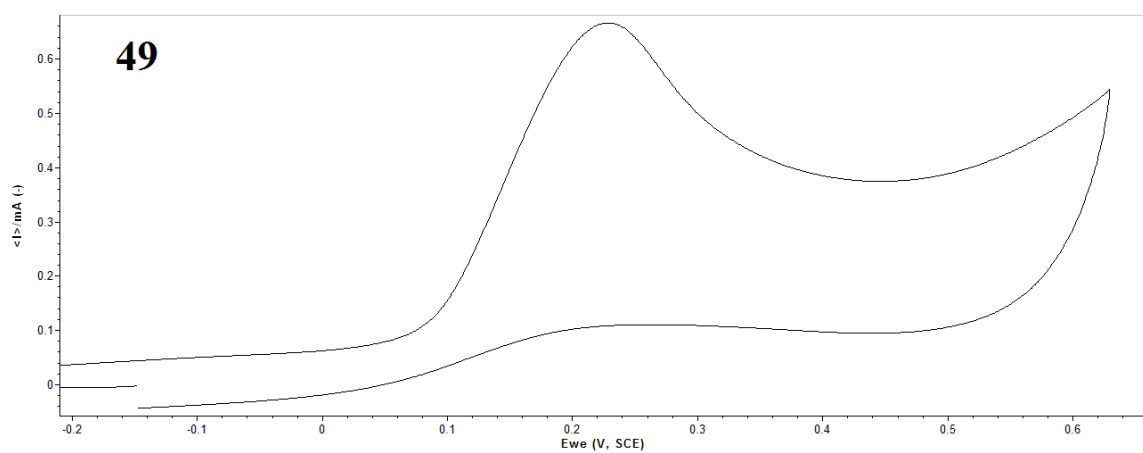
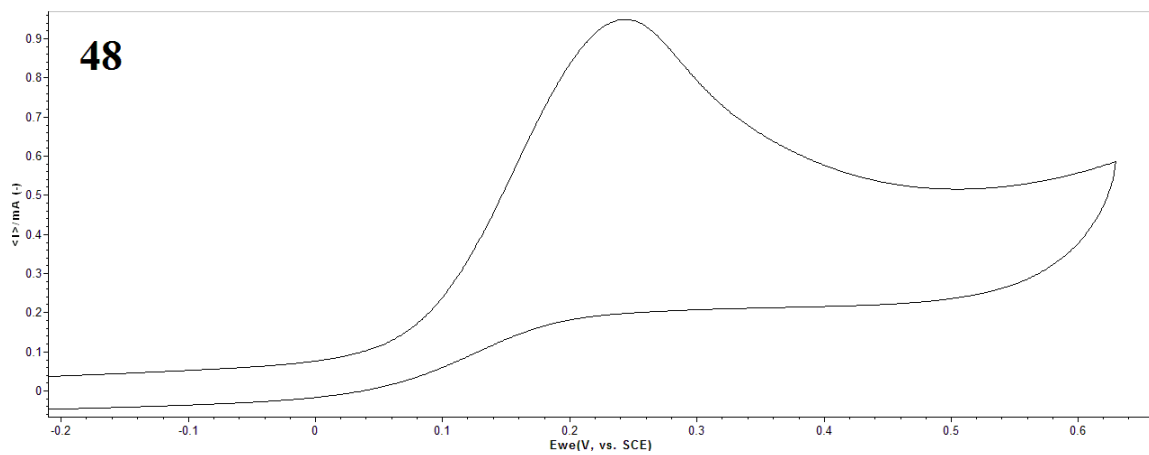


Figure 5. 42 Cyclic voltammograms of compound 48, 49 and 50 in the phosphate buffer at platinum electrode.

5.3.8 Effect of Compounds (48), (49) and (50) on Cell Proliferation

The bioassay tests were completed for compounds (48)-(50) under various experimental conditions. The cytotoxicity assay was performed with various concentrations of the synthesized gold(III) complexes on PC-3 and SGC-7901 cells. The PC-3 and SGC-7901 cell lines were treated with various concentrations of (48), (49) and (50) for 24-72 h and the cell viability was determined as described above by MTT assay and the results are shown in Tables 5.32 and 5.33 as well as in Figures 5.43-5.49. Complexes [*cis*-1,2-(DACH)Au(III)(en)]Cl₃ (48), [*trans*-(±)-1,2-(DACH)Au(III)(en)]Cl₃ (49) and purely chiral [*trans*-(+)-1,2-(DACH)Au(III)(en)]Cl₃ (50) exhibit potentially high activity against gastric cancer cell SGC-7901 as well as human prostate cancer cells after 24 and 72 h of treatment with 10 μM (see Table 5.30) under the same assay experimental conditions. In addition to that and as illustrated in Figures 5.46-5.48, The gold(III) complexes under study showed concentration dependent cytotoxic effect on cancerous cells PC-3 as well as SGC-7901. Also, it can be concluded from Figures 5.43-5.48 that [*cis*-1,2-(DACH)Au(III)(en)]Cl₃ (48) complex demonstrates higher anti-proliferation activity compared with both *trans* isomers [*trans*-(±)-1,2-(DACH)Au(III)(en)]Cl₃ (49) and [*trans*-(+)-1,2-(DACH)Au(III)(en)]Cl₃ (50). In addition to that and as shown in Figures 5.44, 5.45, 5.47 and 5.48 that illustrated the cells anti-proliferation assay of *trans* complexes (49) and (50), there is a significant difference in the bioactivity between [*trans*-(±)-1,2-(DACH)Au(III)(en)]Cl₃ (49) and [*trans*-(+)-1,2-(DACH)Au(III)(en)]Cl₃ (50). The former possesses higher cytotoxicity activity as well as its cells anti-proliferation activity is similar to the *cis*-DACH compound (48). To the best of our knowledge this is the first bioassay tests has been reported for gold(III) complexes based on cyclohexane-1,2-

diamine and ethylenediamine. Figure 5.49 illustrates the anticancer activity of compound (48)-(50) against the two cell lines for a comparison purpose.

In a time dependent activity studies, it is revealed that after 72 h of the experiment with the *cis* isomer (48) on SGC-7901 cells, the cells anti-proliferation is bit higher than that of the PC-3 cells at fixed 10 μ M concentration (Figures 5.43-5.48). While, with *trans* complexes (49) and (50) it is reversed where the PC-3 cells anti-proliferation is bit higher than that of the SGC-7901 cells at the same concentration.

Table 5.30 Effect of compounds 48, 49 and 50 on cell/proliferation and cell cycle of PC3 cell line and SGC-7901 cell line (Mean, SD) after incubation for 24 h and 72 h.

Group	PC3 Cell line		SGC-7901 Cell line	
	Day 1 (24 h)	Day 3 (72 h)	Day 1 (24 h)	Day 3 (72 h)
Control	1.48 \pm 0.03	2.86 \pm 0.04	1.56 \pm 0.02	2.64 \pm 0.04
(48)	0.49 \pm 0.34	0.49 \pm 0.19	0.83 \pm 0.21	0.68 \pm 0.19
(49)	0.35 \pm 0.11	0.37 \pm 0.14	0.64 \pm 0.20	0.44 \pm 0.19
(50)	0.25 \pm 0.09	0.22 \pm 0.07	0.64 \pm 0.21	0.45 \pm 0.16

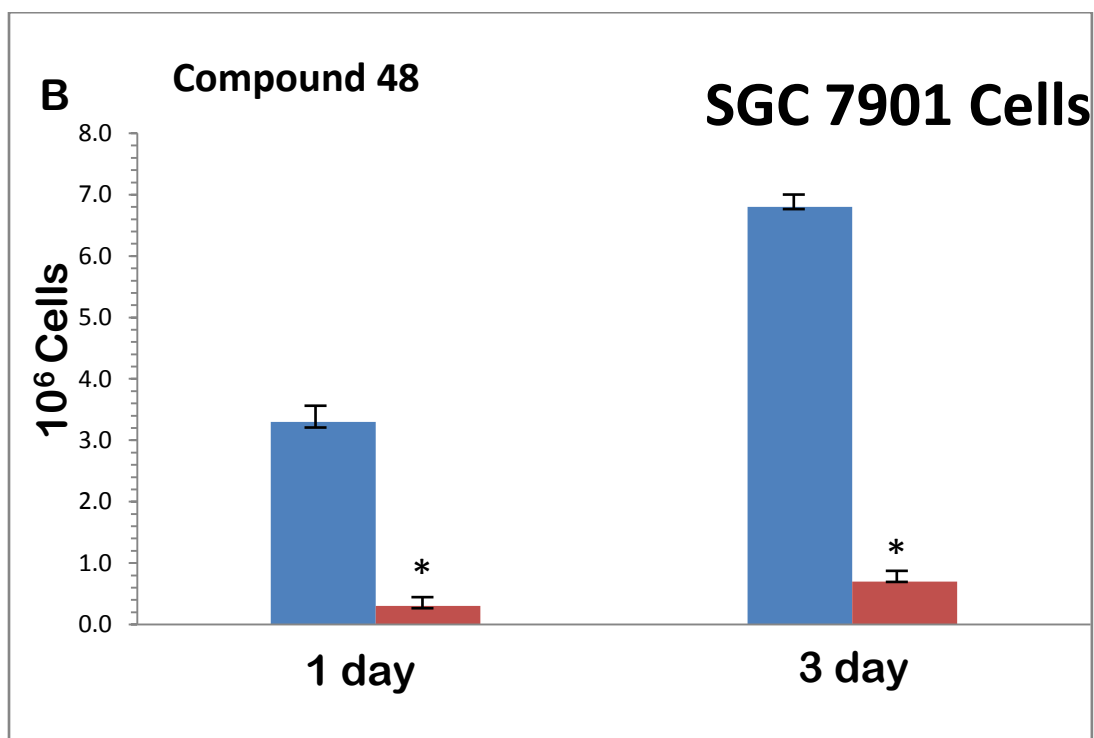
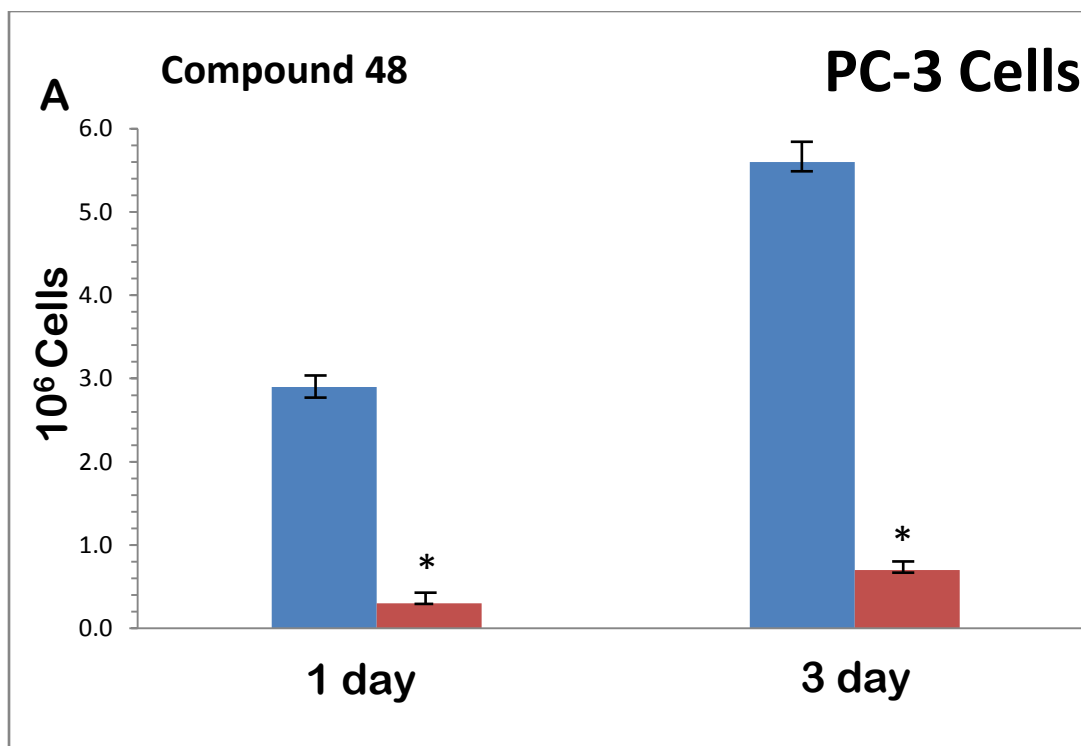


Figure 5.43 Effect of $[cis-1,2-(DACH)gold(III)(en)]Cl_3$ complex on cell growth in (A) PC3 and (B) SGC7901 cells. The cells were treated with 10 μ M for 1 day and 3 days. The anti-proliferative effect was measured by MTT assay. Results were expressed as the mean, SD. * $P < 0.05$

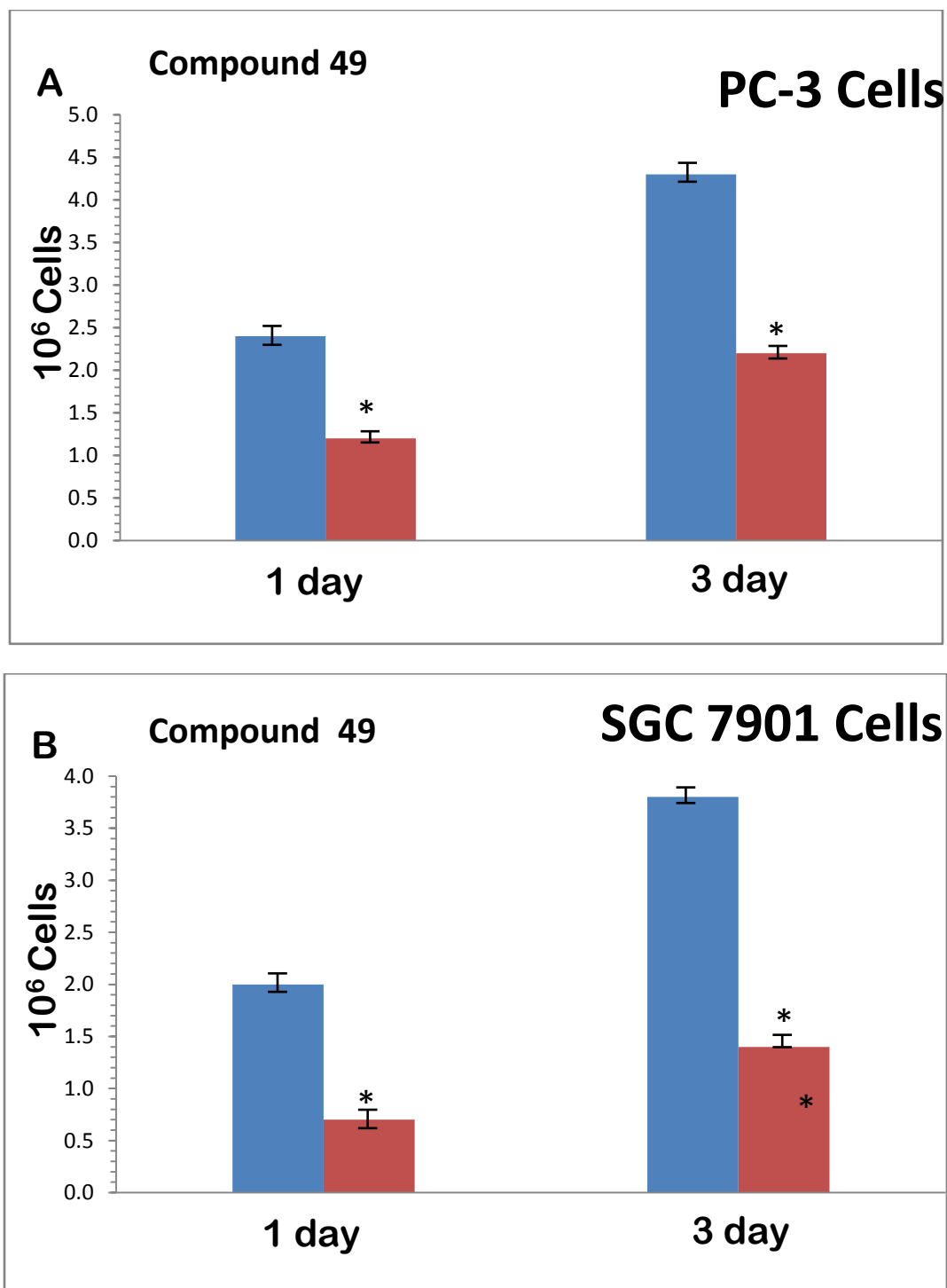


Figure 5.44 Effect of $[trans-(\pm)\text{-}1,2\text{-}(\text{DACH})\text{gold(III)(en)}]\text{Cl}_3$ complex on cell growth in (A) PC-3 and (B) SGC-7901 cells. The cells were treated with $10\ \mu\text{M}$ for 1 day and 3 days. The anti-proliferative effect was measured by MTT assay. Results were expressed as the mean, SD. $*P < 0.05$

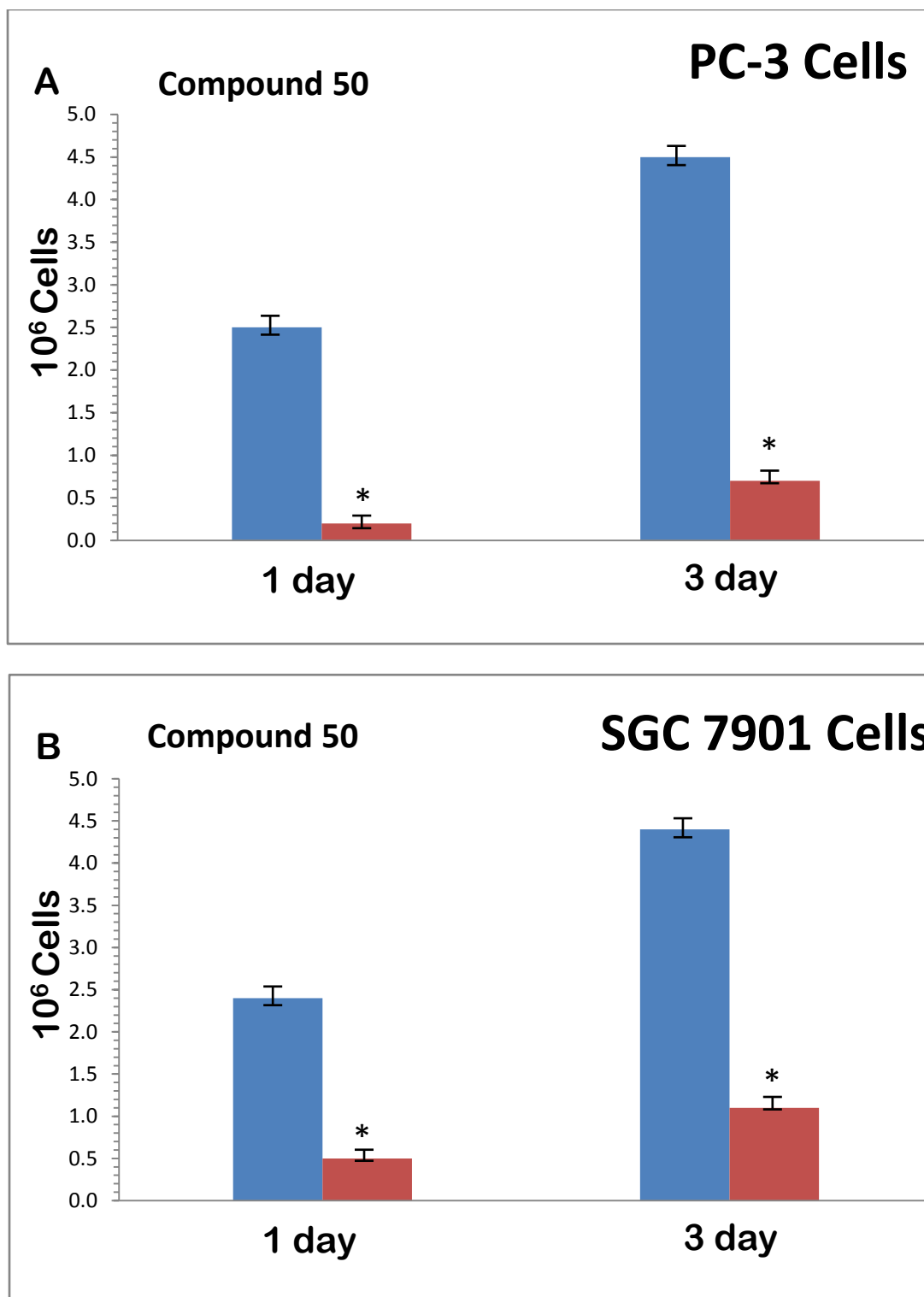


Figure 5.45 Effect of [(S,S)-(+)-1,2-(DACH)gold(III)(en)]Cl₃ complex on cell growth in (A) PC-3 and (B) SGC-7901 cells. The cells were treated with 10 μ M for 1 day and 3 days. The anti-proliferative effect was measured by MTT assay. Results were expressed as the mean, SD. * $P < 0.05$

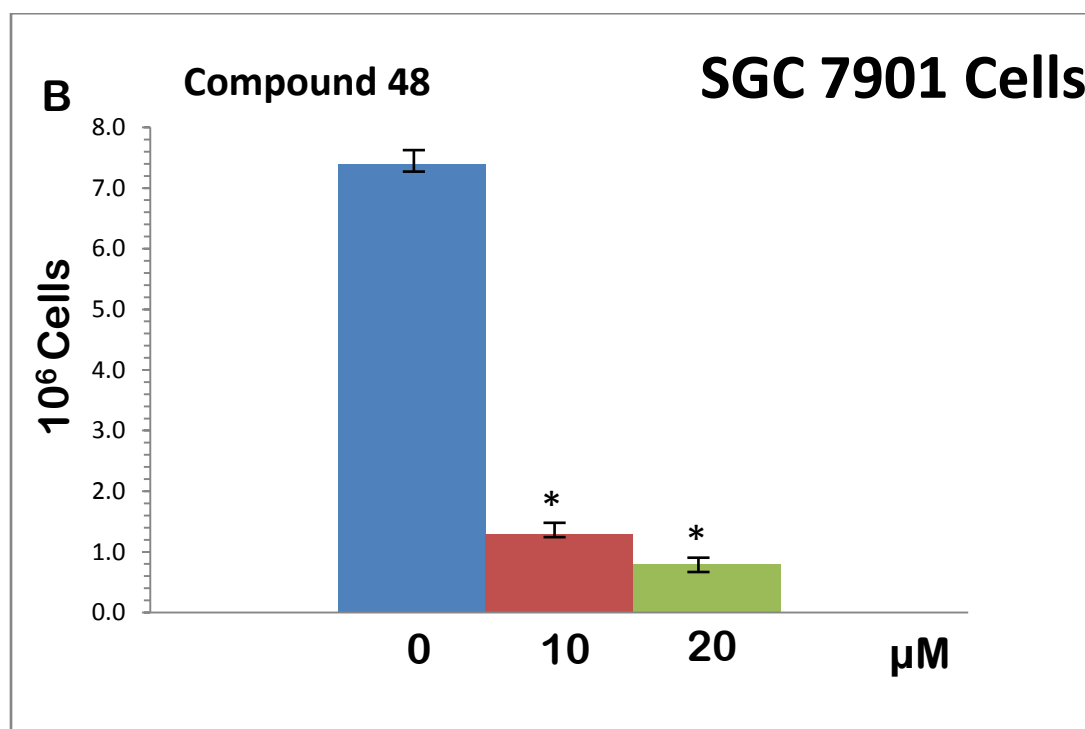
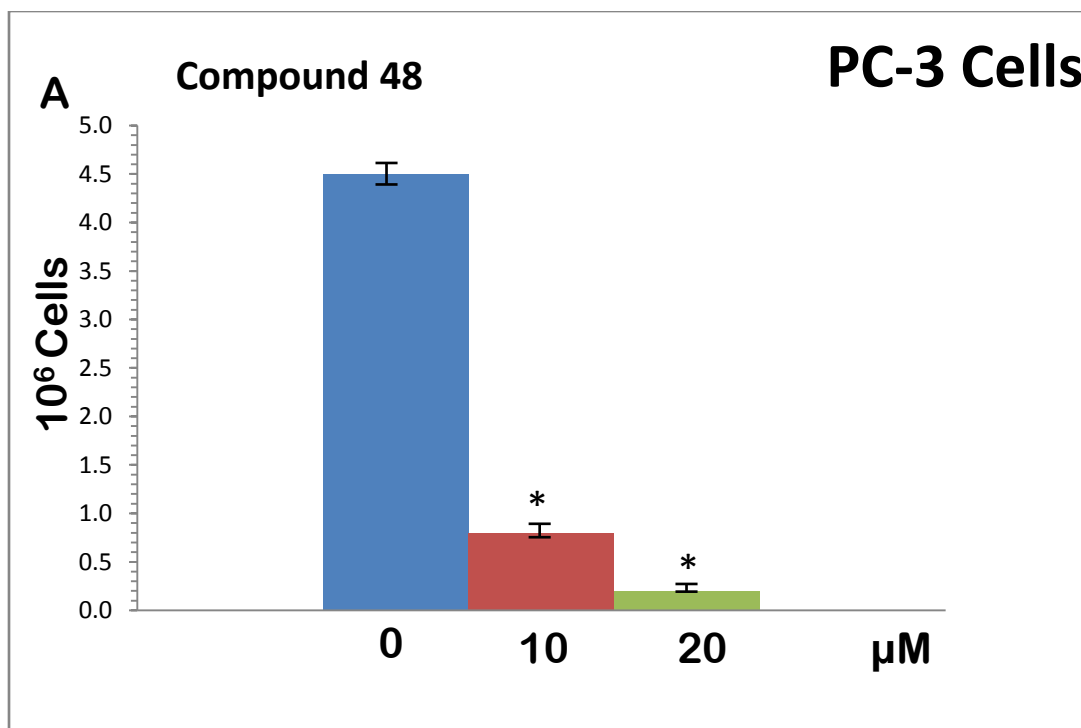


Figure 5.46 Effect of $[cis-1,2-(DACH)gold(III)(en)]Cl_3$ complex on cell growth in (A) PC-3 and (B) SGC-7901 cells. The cells were treated with various concentrations for 24 h. The anti-proliferative effect was measured by MTT assay. Results were expressed as the mean, SD. * $P < 0.05$

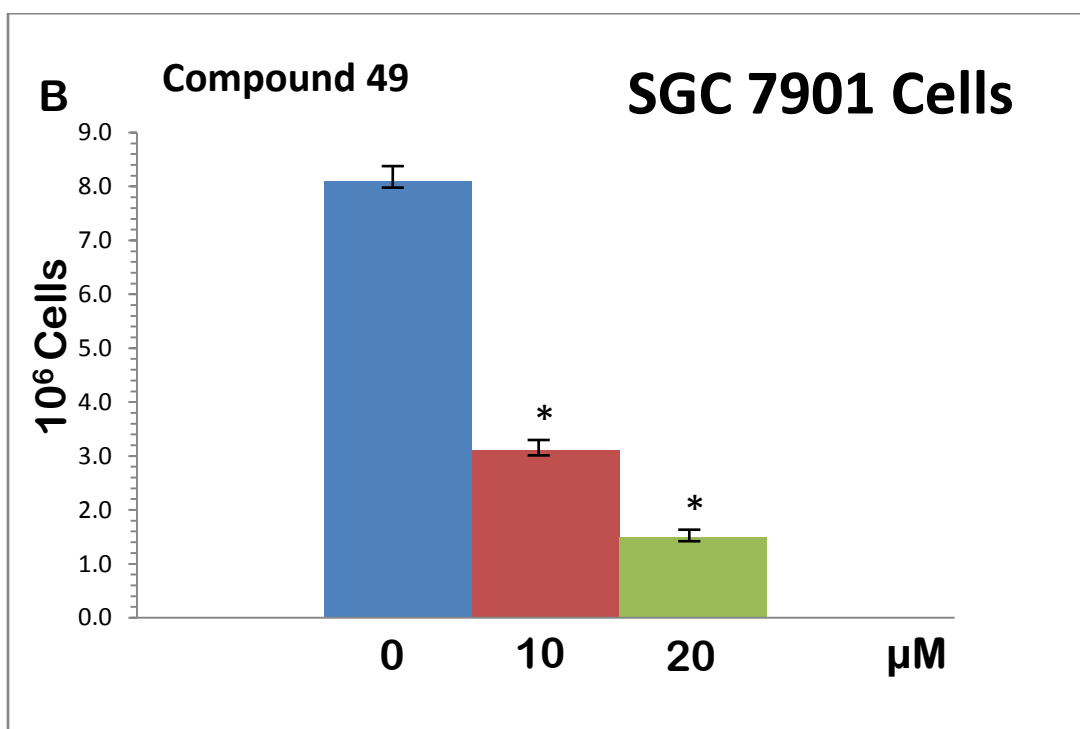
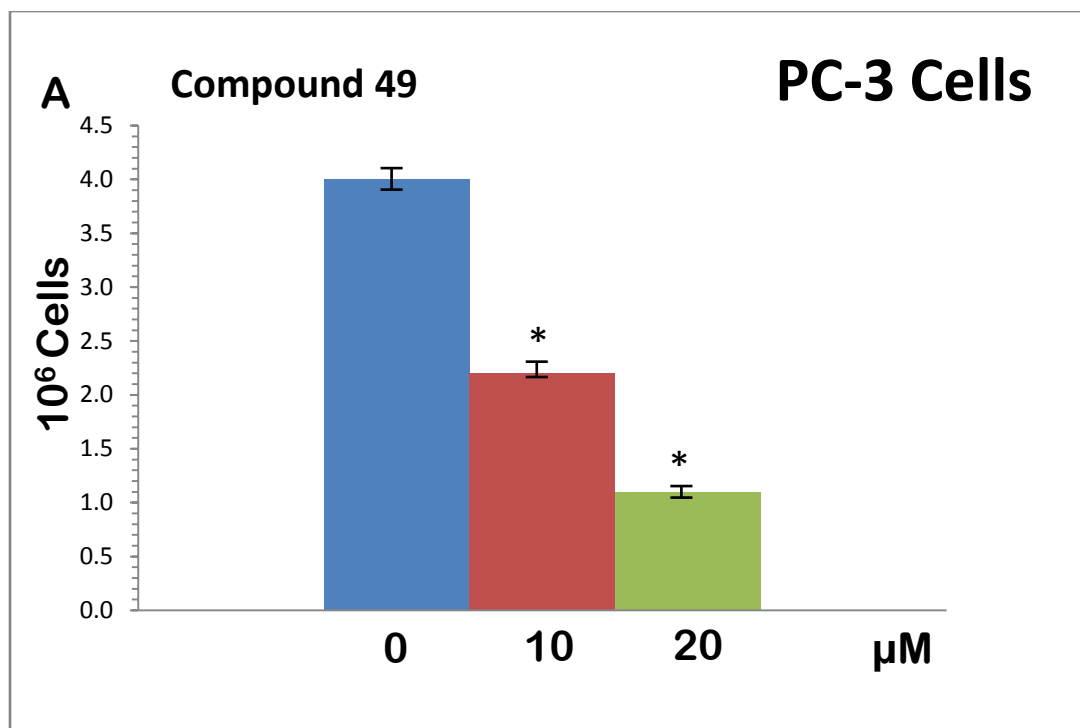


Figure 5. 47 Effect of [*trans*-(±)-1,2-(DACH)gold(III)(en)]Cl₃ complex on cell growth in (A) PC-3 and (B) SGC-7901 cells. The cells were treated with various concentrations for 24 h. The anti-proliferative effect was measured by MTT assay. Results were expressed as the mean, SD. **P* < 0.05

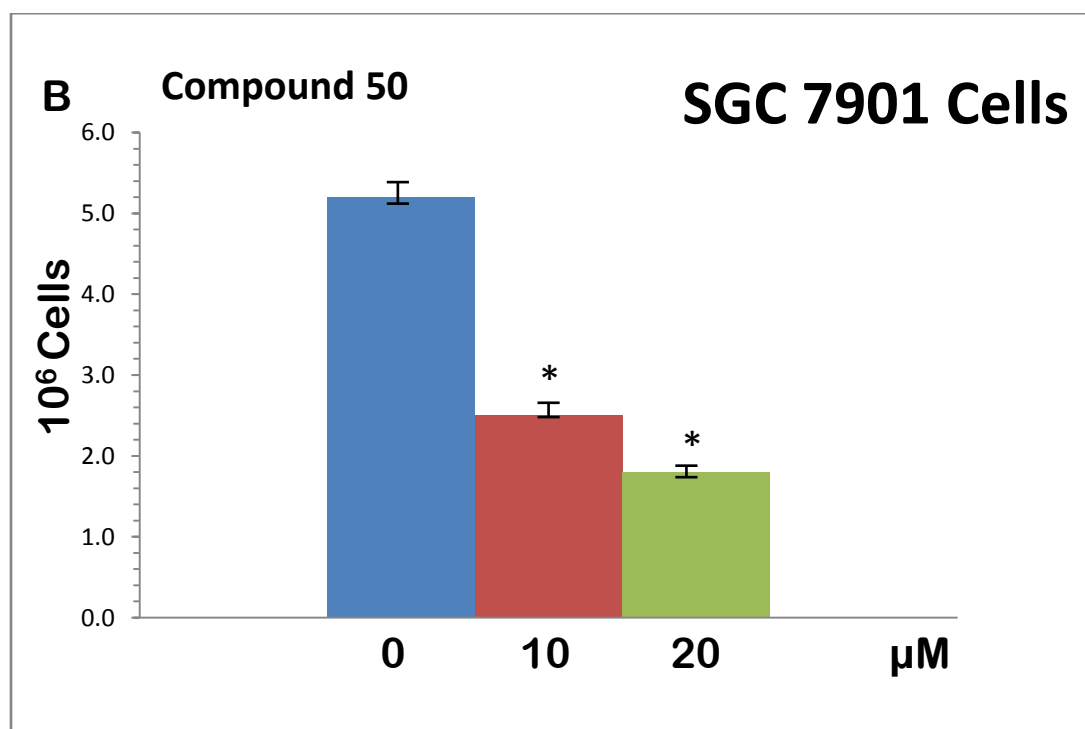
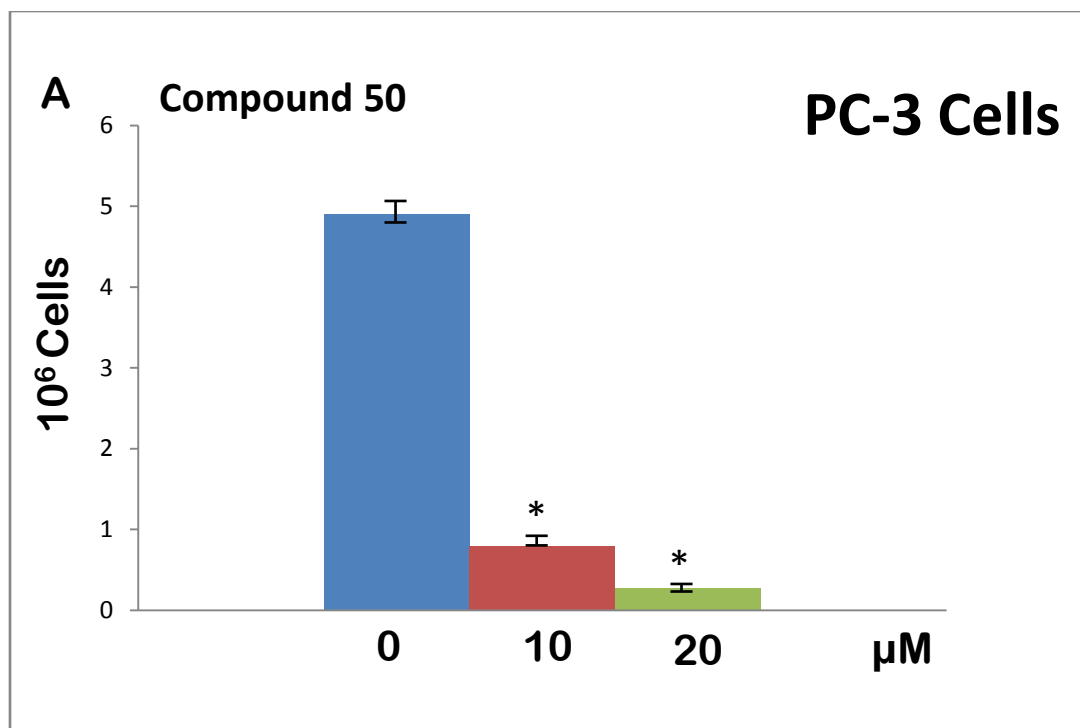


Figure 5.48 Effect of [(S,S)-(+)-1,2-(DACH)gold(III)(en)]Cl₃ complex on cell growth in (A) PC-3 and (B) SGC-7901 cells. The cells were treated with various concentrations for 24 h. The anti-proliferative effect was measured by MTT assay. Results were expressed as the mean, SD. **P* < 0.05

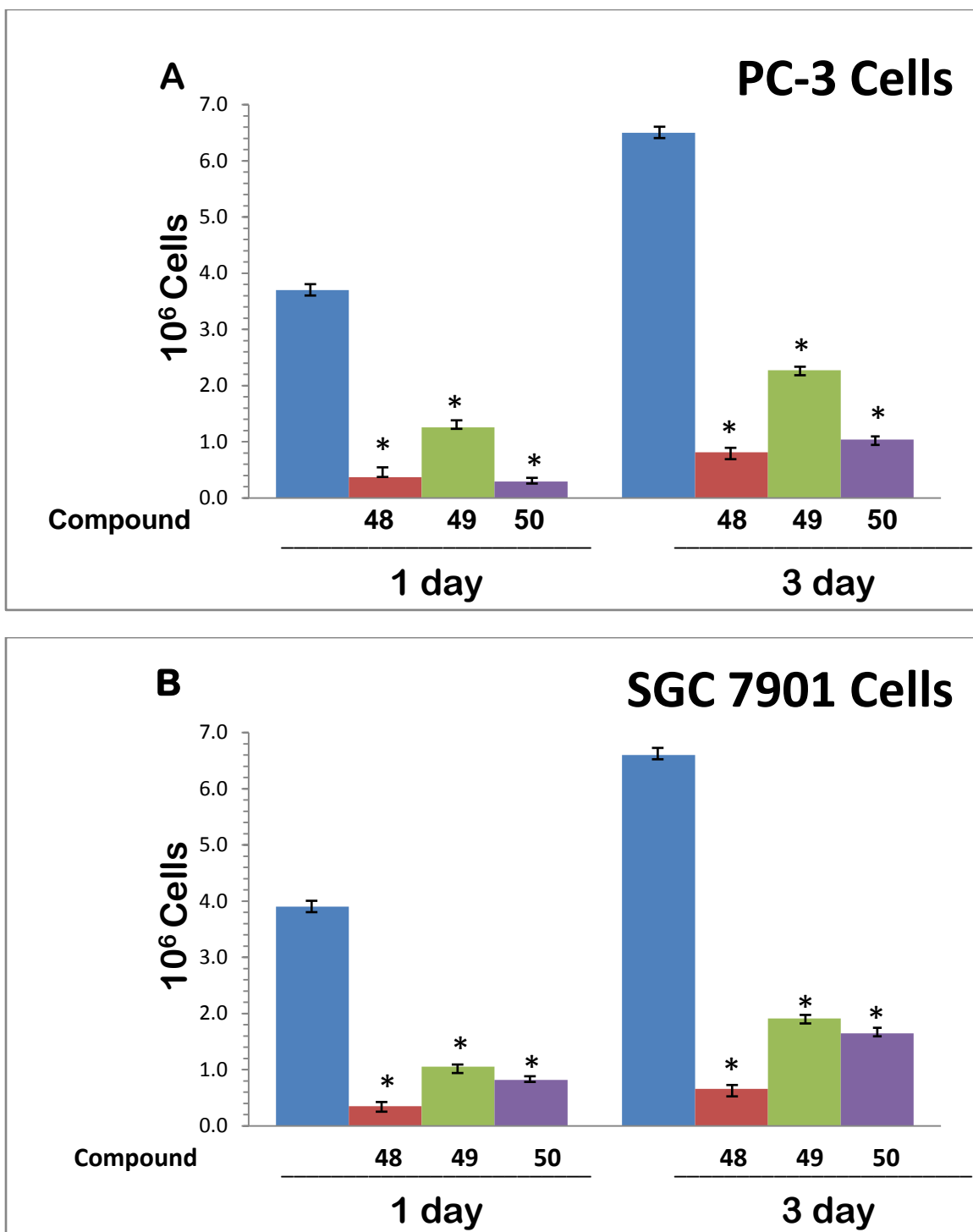


Figure 5. 49 Effect of compounds (48-50) on cell growth in (A) PC-3 and (B) SGC-7901 cells. The cells were treated with 10 μ M for day 1 and day 3. The anti-proliferative effect was measured by MTT assay. Results were expressed as the mean, SD. * $P < 0.05$

The *in vitro* cytotoxicity of the compounds (48-50) was evaluated in terms of their IC_{50} values against prostate cancer cell lines (PC3) and gastric carcinoma cell lines

(SGC7901). The IC₅₀ data is shown in Table 5.31. The IC₅₀ data for the Au(III) complexes (**48-50**) showed reasonable cytotoxicity in the 5–9 μM range for SGC7901 cells, as given in Table 5.31. For SGC7901 cells, complexes (**48**) and (**50**) were recognized as being as effective cytotoxic agent as *cis*-platin, while compound (**49**) demonstrated about 1.1-fold lower potency. For PC3 cells line, compounds (**48-50**) showed almost 4–8-fold lower cytotoxicity as compared to cisplatin.

An independent assessment of compounds (**48-50**) revealed an interesting feature that SGC7901 gastric cancer cells exhibit 7 to 8-fold intrinsic resistance relative to the PC3 cancer cells with respect to *cis*-platin [182]. However, almost 1-fold resistance to compounds (**48-50**) was observed for PC3, as shown in Table 5.31. This suggests that the intrinsic factors regulating cellular sensitivity to *cis*-platin are different for PC3 and SGC7901 cells. The factors affecting the sensitivity of PC3 and SGC7901 cells are analogous in compounds (**48-50**). There is no doubt that the present study is helpful for further exploiting and defining the potential role of gold(III) complexes in the combat against prostate and gastric cancers.

Table 5.31 IC₅₀ Cytotoxicity values of the complexes towards different tumor cell lines. The data were collected after 72 h exposure to compound (**48-50**)

Compounds	IC ₅₀ (μM)		Fold resistance SGC7901/PC3	Ref.
	PC3	SGC-7901		
<i>Cis</i>-platin	1.1 ± 0.1	7.3 ± 0.5	6.64	[182]
(48)	4.8 ± 0.1	5.5 ± 0.2	1.15	b
(49)	8.9 ± 0.1	7.9 ± 0.2	0.89	b
(50)	6.1 ± 0.1	5.8 ± 0.2	0.95	b

5.3.9 Conclusion

These gold(III) complexes were characterized using elemental analyzer, solution and solid NMR, UV, IR, Far-IR spectroscopy and cyclic voltammetry. The analytical data showed strong support for the formation of the [(1,2-DACH)Au(en)]Cl₃ complexes, exhibiting fair stability in the reference buffer. The computational study demonstrates that [*trans*-(1,2-DACH)Au(en)]Cl₃ isomer is more stable than the [*cis*-(1,2-DACH)Au(en)]Cl₃ isomer and gold coordination sphere of these complexes adopt distorted square planar geometry. According to the biological assays, complexes (**48**) and (**50**), with *cis* and *trans* configurations of (DACH), respectively, are more promising candidates as anti-cancer agents than the (1*S*,2*S*) isomers of (**49**). The exact mechanisms are not clearly known, but the inhibitory effect of [(*cis*-1,2-DACH)Au(en)]Cl₃ on the proliferation of rapidly dividing cells would be attributed to the induction of cell cycle blockage, interruption of the cell mitotic cycle, programmed cell death (apoptosis) or premature cell death (necrosis). Therefore, [(*cis*-1,2-DACH)Au(en)]Cl₃ isomer, might be a promising chemo preventative and chemotherapeutic agent against human gastric carcinogenesis. As cytotoxic activity of [(*cis*-1,2-DACH)Au(en)]Cl₃ complex is high towards some cancer cell lines; further biological evaluation for this class of complexes is worthy of efforts especially in order to evaluate activities *in vivo*.

5.4 Mixed-Ligand Diaminocyclohexane(propylenediamine)gold(III) Chloride Complexes

This work reports the synthesis and characterization of 1,2-diaminocyclohexane(propylenediamine)gold(III) chloride complexes of the type [(1,2-DACH)Au(pn)]Cl₃, where DACH and pn are 1,2-diaminocyclohexane and 1,3-propylenediamine, respectively.

5.4.1 Electronic Spectra

The λ_{\max} values for the complexes studied are shown in Table 5.32. The gold(III) complexes **(51)**, **(52)** and **(53)** exhibit, in a reference buffered phosphate solution, intense transitions in the range 330-340 nm, which are assigned as ligand-to-metal charge-transfer transitions characteristically associated to the gold(III) center [181]. These absorption bands were previously assigned as NH⁻ to a gold(III) charge-transfer bands [181]. It is worth to notice that these spectral features appear only at relatively high pH values (pH > 6-7) at which ligand deprotonation has fully occurred. According to crystal field theory for d^8 complexes the LUMO orbital is $d_{x^2-y^2}$, so ligand to metal charge transfer could be due to $p_{\sigma} \rightarrow d_{x^2-y^2}$ transition [175].

The electronic spectra of the complexes **(51)**, **(52)** and **(53)** in the buffer solution, were monitored at 37 °C over 7 days after mixing. The electronic spectra for all compounds at mixing and after 7 days are depicted in Figure 5.50. It is apparent that the observed transitions remain substantially unmodified over 7 days observation, implying a

substantial stability of these complexes under the present solution conditions. Nevertheless, a slight decrease in intensity, of the characteristic bands, was noticed with time without significant shape modifications. Also, this observation indicates that the gold center in these complexes remains in the +3 oxidation state [175-181]. The minor spectral changes that are generally observed within the first hours may be ascribed either to dissociation of the amine ligands from the gold(III) complex or to partial reduction of gold(III) to metallic gold. In general, however, loss of spectral intensity is lower than 15% of the original intensity within the observation period of 7 days which indicates high stability of these compounds in the buffer. This is a possible suggestion that in the physiological milieu, the compounds would be able to undergo the necessary reactions required for bioactivity.

Table 5.32 UV-Vis spectra λ_{\max} for complexes of [(diaminocyclohexane)(ethylenediamine)Au(III)]chloride dissolved in the reference physiological buffer solution.

Complex	λ_{\max} (nm)
NaAuCl ₄	293
[(pn)Au{ <i>cis</i> -(1,2-DACH)}]Cl ₃ (51)	332
[(pn)Au{ <i>trans</i> -(±)-(1,2-DACH)}]Cl ₃ (52)	339
[(pn)Au{ <i>trans</i> -(+)-(1 <i>S</i> ,2 <i>S</i> -DACH)}]Cl ₃ (53)	341

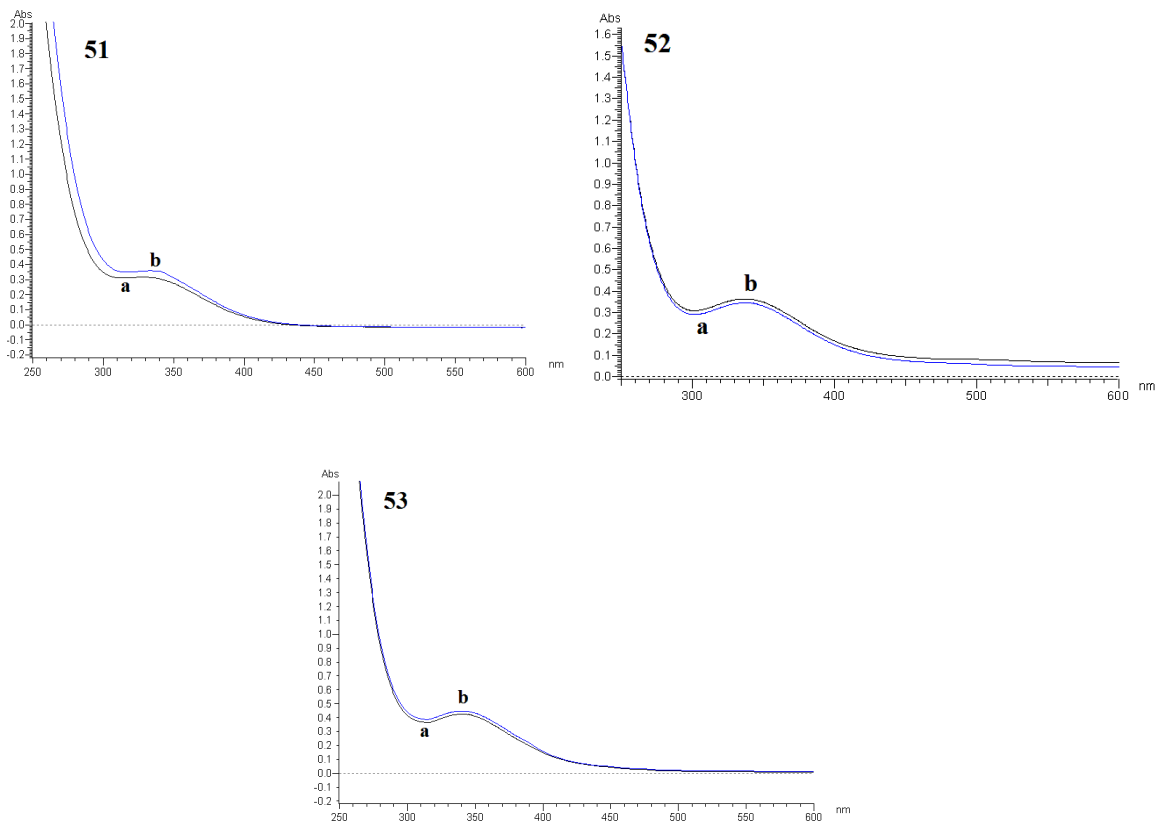


Figure 5.50 Electronic spectra with time of 1,2-diaminocyclohexane(propylenediamine)gold(III) chloride complexes following dissolution in the buffer solution at mixing (a) and after 7 days (b) at 37 °C.

5.4.2 Mid and Far-IR spectroscopic studies

The most significant bands recorded in the FT-IR spectra of the ligand, [(1,2-DACH)Au(III)(pn)]Cl₃ complexes have been reported in Table 5.33 and Table 5.34. It is noted that N-H stretching vibrations of complexes (**51-53**) exhibit, in the range 3444-3452cm⁻¹, blue shifting compared with the amino group of the corresponding free ligands. This is most likely due to stronger hydrogen bonding interactions in the free ligands. The amino coordination with Au(III) ions and Au-N bond formation can be supported by the presence of $\nu(\text{Au-N})$ at 420-447 cm⁻¹ as indicated by Far-IR data [173]. The C-N stretching bands also showed a significant shift to higher wave number

indicating a shorter C-N bond in the complex than in the free ligand. Furthermore, there was no signal observed at 325 and 388 cm⁻¹ corresponding to the symmetric and asymmetric stretching of the Au-Cl indicating the absence of the gold mono-DACH complex [180]. The [(1,2-DACH)Au(III)(pn)]Cl₃ complexes (**51-53**) show N-H stretching frequencies generally lower in comparison with mono-DACH complexes (**36-38**) (Table 5.33), most probably due to stronger hydrogen bonding interactions with the chloride anions in the [(1,2-DACH)Au(III)(pn)]Cl₃ complexes. Furthermore the Au-N stretching frequencies are consistent with weaker Au-N bond strength in complexes (**51-53**) compared to the mono-DACH complexes.

Table 5.33 Mid IR frequencies, $\nu(\text{cm}^{-1})$ for 1,2-cyclohexanediamine(1,3-Propylenediamine)Au(III) chloride complexes.

Complex	$\nu(\text{N-H})$	ν_{shift}	$\nu(\text{C-N})$	ν_{shift}
(pn)	3357 m, 3282 m		1093 w	
(pn)AuCl ₃	3447 br	127	1178 s	85
<i>Cis</i> -1,2-(DACH)	3356 m, 3286 m		1092 s	
<i>Cis</i> -1,2-(DACH)AuCl ₃	3414 w	93	1183 s	91
(51)	3427 br	106 ^a , 108 ^b	1139 w	47 ^a , 46 ^b
<i>Trans</i> -(±)-1,2-(DACH)	3348 m, 3271 m, 3183 m		1082 m	
<i>Trans</i> -(±)-1,2-(DACH)AuCl ₃	3485 w, 3420 w, 3384 w	137, 149, 201	1175 m	93
(52)	3409 br	141 ^a , 90 ^b	1179 m	97 ^a , 86 ^b
(<i>S,S</i>)-(+)-1,2-(DACH)	3340 m, 3252 m, 3167 m		1082 m	
(<i>S,S</i>)-(+)-1,2-(DACH)AuCl ₃	3604 m, 3340 m, 3306 m, 3168 m	132, 27	1171 m	89
(53)	3433 br	179 ^a , 113 ^b	1184 m	102 ^a , 91 ^b

^a with respect with (DACH), ^b with respect to (pn), ^c this work.

Table 5.34 Far-IR frequencies, $\nu(\text{cm}^{-1})$ for 1,2-cyclohexanediamine(1,3-Propylenediamine)Au(III) chloride complexes.

Species	$\nu(\text{Au-Cl})$	$\nu(\text{Au-N})$
NaAuCl ₄	365	-
[(pn)AuCl ₂]Cl	-	391,474
[<i>Cis</i> -1,2-(DACH)AuCl ₃]Cl (36)	352, 367	437
[(pn)Au{ <i>Cis</i> -1,2-(DACH)}]Cl ₃ (51)	-	331, 425
[{ <i>Trans</i> -(±)-1,2-(DACH)}AuCl ₂]Cl (37)	353, 365	437
[(pn)Au{ <i>Trans</i> -(±)-1,2-(DACH)}]Cl ₃ (52)	-	392, 448
[(1 <i>S</i> ,2 <i>S</i>)-(+)-(DACH)AuCl ₂]Cl (38)	353, 366	395, 436
[(pn)Au(1 <i>S</i> ,2 <i>S</i>)-(+)-(DACH)]Cl ₃ (53)	-	383, 451

5.4.3 Solution NMR characterization

. All ¹H NMR supported the structures of the synthesized complexes as indicated by the integration of the signals of C-H protons connected to the amino groups of the (DACH) and (pn). For example, the ratio of the protons attached to amino group in both (DACH) and (pn) for a complex (**53**) and (**51**) is 1:2 as depicted in Figures 5.51 and 5.52. Their ¹³C NMR spectrum is also confirmed the complexes' structure as shown in Figures 5.53 and 5.54. The ¹H and ¹³C NMR chemical shifts of compounds (**51-53**) along with their corresponding free ligands are listed in Table 5.35 and Table 5.36, respectively. In the ¹H and ¹³C NMR spectra of complexes (**51**), (**52**) and (**53**), one half of the total expected signals was noticed because of the presence of the C₂ symmetry axis. 1,2-diaminocyclohexane ring is considered as a rigid conformer that allowed, for instance, to distinguish equatorial H2 and H3 from axial H2 and H3 at room temperature. The signals of C-H protons connected to the amino groups for (DACH) occurs in the spectra at 3.07 to 3.65 ppm, shifting downfield compared with the corresponding signals (2.23-2.25ppm)

in the free DACH ligands. The significant downfield shift was observed at 3.65 ppm for (**51**) complex with respect to the free DACH ligand at 2.23 ppm. This can be attributed to the donation of nitrogen lone pairs to the gold that causes de-shielding of the proton(s) next to the bonding nitrogen. With respect to (pn), no significant change was observed for its protons chemical shift upon the complexation. On the other hand, ¹³C NMR downfield shift was observed only for the carbon next to the bonding nitrogen and the others carbons in the complex for (DACH) showed upfield shift. For instance, chemical shift of C2 and C3 for complex (**51**) observed at 26.25 and 20.73 ppm, respectively, whereas, for free diamine ligand it occurs at 35.26 and 26.36 ppm. It is also worth to mention that complexes (**51-53**), even though they have the same skeleton of (DACH) and (pn), their NMR chemical shifts specifically for (DACH) aren't the same due to a different stereochemistry upon complexation.

Table 5.35 ¹H NMR chemical shifts of free ligands and cyclohexanediamine propylenediamine Au(III) complexes in D₂O.

Compound	¹ H(δ in ppm)						H1',H1'	H2'	Refs.
	H1,H1	H2,H2 (eq)	H2,H2 (ax)	H3,H3 (eq)	H3,H3 (ax)				
(pn)	-	-	-	-	-	-	2.98 <i>t</i>	1.94, <i>p</i>	a
<i>Cis</i> -1,2-(DACH)	2.23, <i>m</i>	1.85, <i>m</i>	1.69, <i>m</i>	1.28, <i>m</i>	1.12, <i>m</i>	-	-	-	[180]
<i>Trans</i> -(±)-(DACH)	2.25, <i>m</i>	1.85, <i>m</i>	1.68, <i>m</i>	1.28, <i>m</i>	1.11, <i>m</i>	-	-	-	[180]
(1 <i>S</i> ,2 <i>S</i>)-(+)-(DACH)	2.24, <i>m</i>	1.85, <i>m</i>	1.69, <i>m</i>	1.28, <i>m</i>	1.11, <i>m</i>	-	-	-	[180]
(51)	3.65, <i>m</i>	1.96, <i>m</i>	1.79, <i>m</i>	1.60, <i>m</i>	1.41, <i>m</i>	2.94, <i>m</i>	1.96, <i>m</i>	-	a
(52)	3.07, <i>m</i>	2.11, <i>m</i>	1.56, <i>m</i>	1.47, <i>m</i>	1.10, <i>m</i>	2.91, <i>m</i>	2.12, <i>m</i>	-	a
(53)	3.08, <i>m</i>	2.11, <i>m</i>	1.56, <i>m</i>	1.47, <i>m</i>	1.11, <i>m</i>	2.91, <i>m</i>	2.13, <i>m</i>	-	a

^a this work

Table 5.36 ^{13}C NMR chemical shifts of free ligands and cyclohexanediaminepropylenediamine Au(III) complexes in D_2O .

Compound	^{13}C (δ in ppm)				
	C1,C1	C2,C2	C3,C3	C1', C1'	C2'
(pn)	-	-	-	37.47	25.69
<i>Cis</i> -1,2-(DACH)	58.20	35.26	26.36	-	-
<i>Trans</i> -(\pm)-1,2-(DACH)	58.46	35.55	26.63	-	-
(1 <i>S</i> ,2 <i>S</i>)-(+)-(DACH)	58.27	35.32	26.43	-	-
(51)	61.98	26.92	20.73	40.95	26.92
(52)	64.47	32.88	23.91	40.90	26.90
(53)	64.50	32.90	23.94	40.92	26.92

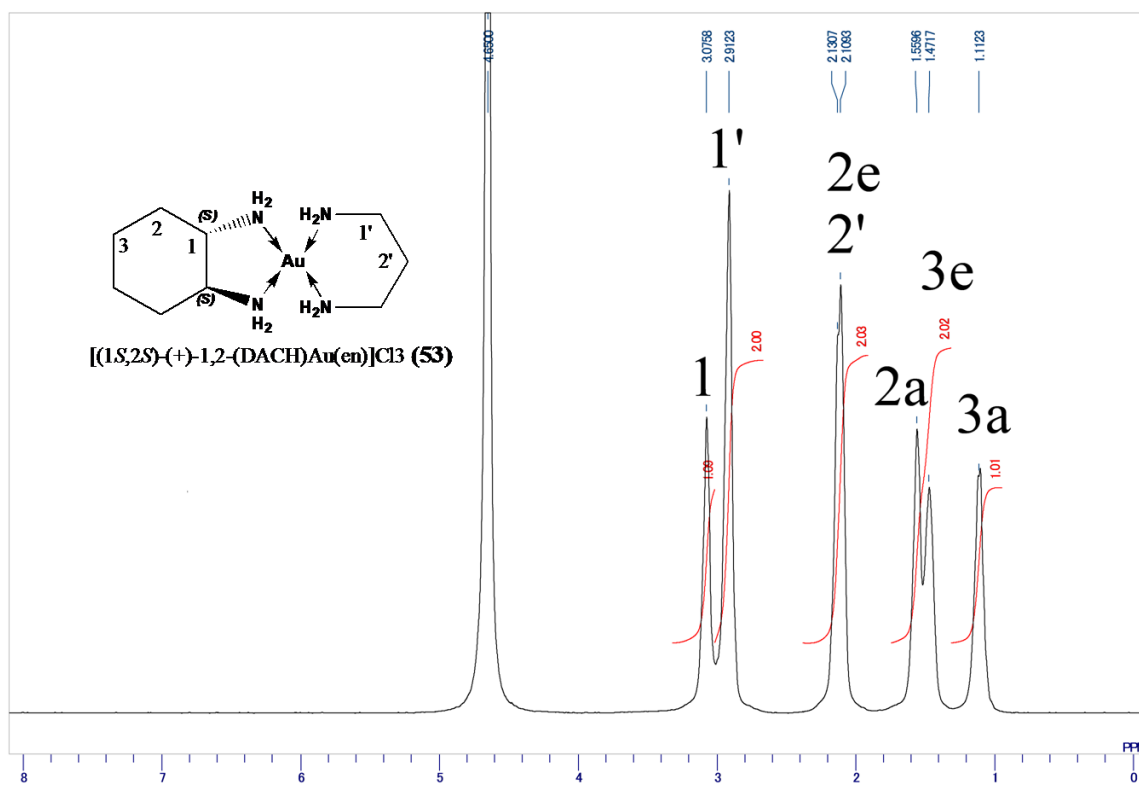


Figure 5.51 The 500-MHz ^1H solution state NMR spectrum of $[(1*S*,2*S*)-(+)-(DACH)Au(pn)]\text{Cl}_3$ complex.

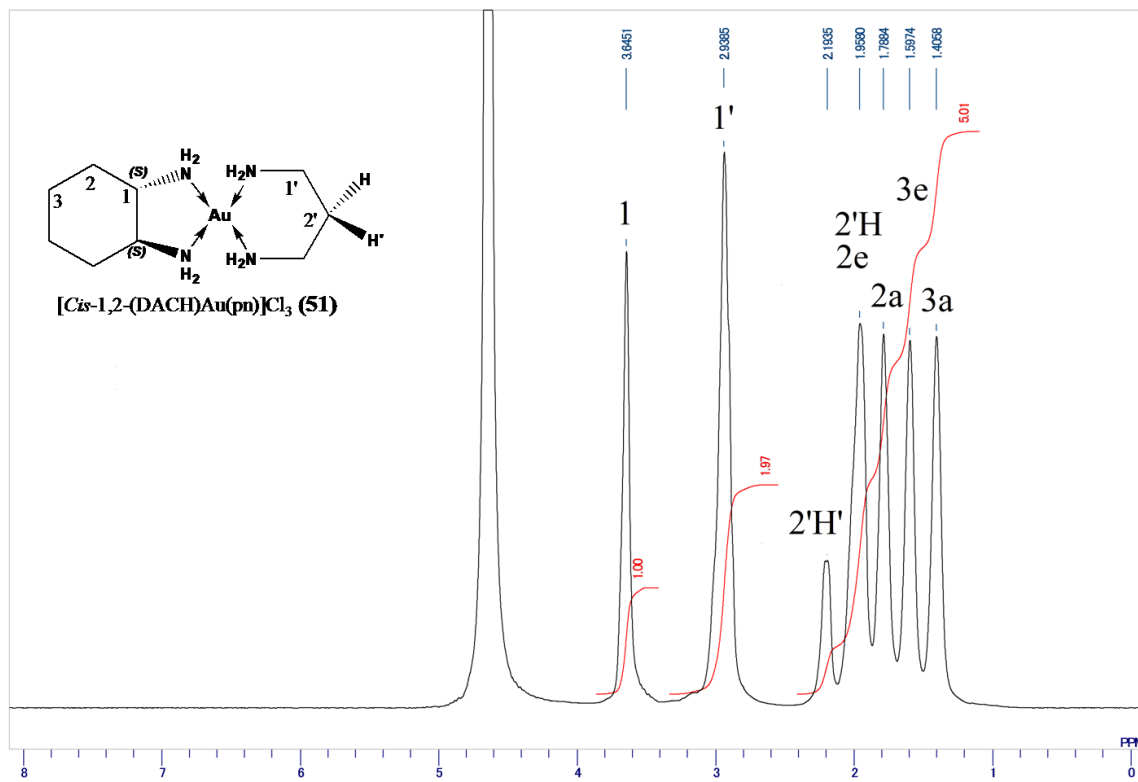


Figure 5.52 The 500-MHz 1H solution state NMR spectrum of $[cis-1,2-(DACH)Au(pn)]Cl_3$ complex.

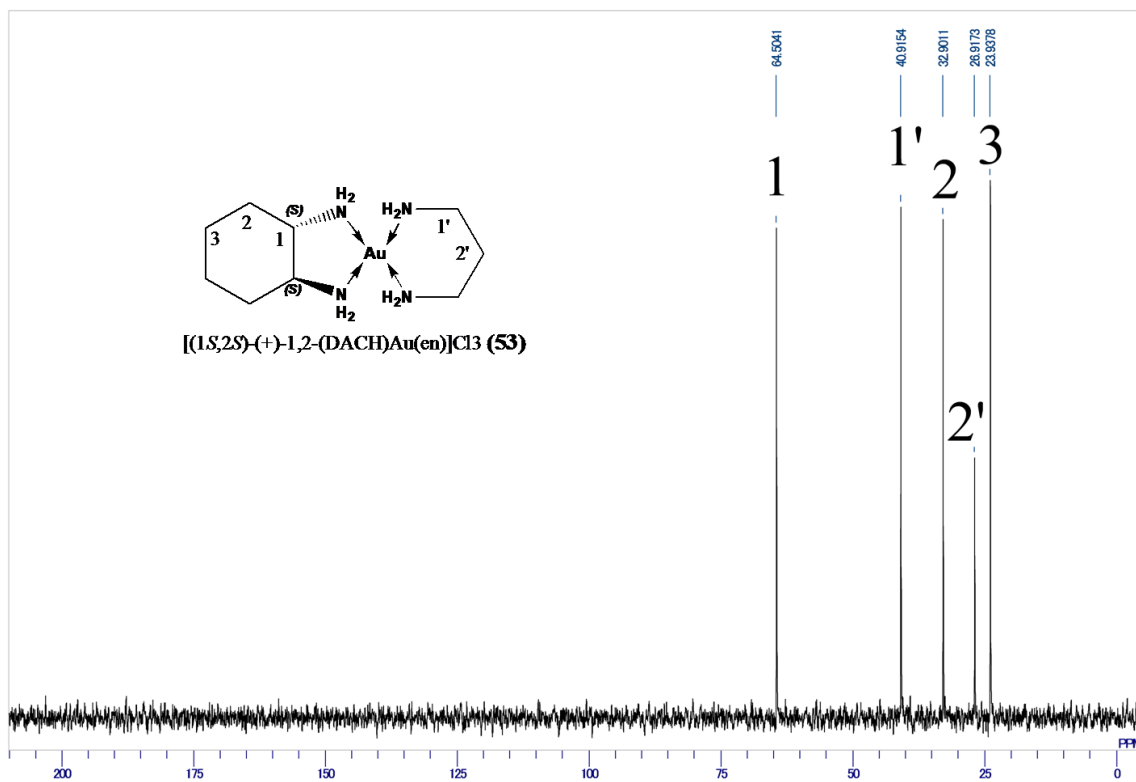


Figure 5.53 The 125.65-MHz $^{13}\text{C}\{^1\text{H}\}$ solution state NMR spectrum of $[(1S,2S)\text{-}(+)\text{-}1,2\text{-}(\text{DACH})\text{Au}(\text{en})]\text{Cl}_3$ complex.

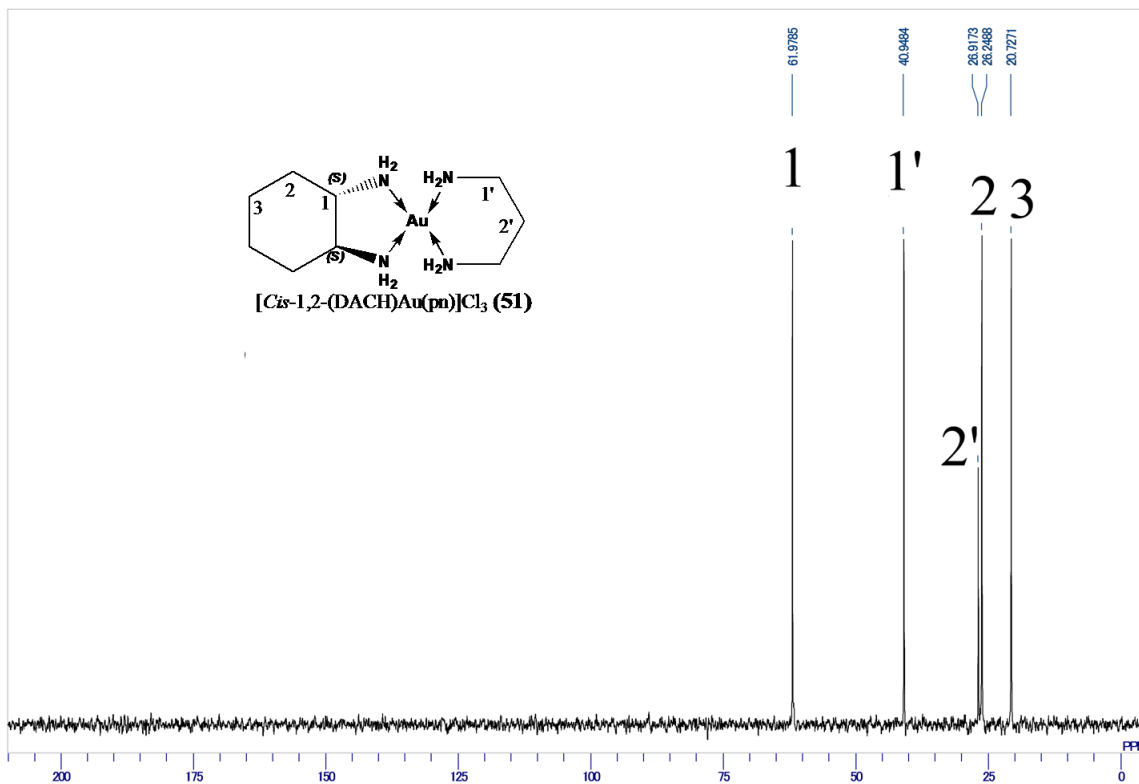


Figure 5.54 The 125.65-MHz $^{13}\text{C}\{^1\text{H}\}$ solution state NMR spectrum of $[\text{cis-1,2-(DACH)Au(pn)}]\text{Cl}_3$ complex.

5.4.4 Solid-state NMR

At the spinning rate of 4 kHz, the isotropic signals for all complexes weren't observed for the carbons, indicating the absence of the anisotropy that could take place due to the sp^3 hybridization of these atoms. Solid state NMR spectrum of complex (53) showed no equivalency in the chemical shifts of carbon atoms (C1,C1) and (C2,C2) two sets of peaks with the same intensity where observed. Whereas, similar observation didn't notice for carbon atoms of (DACH) in complexes (51) & (52) as listed in Table 5.37. This indicates that complex (53) in the solid state lacks C_2 symmetry. In contrast, all

synthesized complexes **(51)**, **(52)** & **(53)** showed C_2 symmetry in the solution state as indicated earlier by solution ^1H and ^{13}C NMR.

Table 5.37 Solid ^{13}C NMR chemical shifts of free ligands and (1,2-DACH)Au(III)(pn) complexes.

Compound	^{13}C (δ in ppm)					Refs.
	C1,C1	C2,C2,	C3,C3	C1', C1'	C2'	
[<i>cis</i> -1,2-(DACH)AuCl ₂]Cl	66.20, 65.35	30.98	27.02, 22.12	-		[7]
(51)	64.03	29.31	21.74	44.57	28.01	^a
[<i>trans</i> -(\pm)-1,2-(DACH)AuCl ₂]Cl	69.60	37.37	27.99	-		[7]
(52)	66.80	37.35	28.09	45.76	28.09	^a
[(1 <i>S</i> ,2 <i>S</i>)-(+)-(DACH)AuCl ₂]Cl	70.21	37.86	29.16	-		[7]
(53)	67.31, 64.41	36.05, 34.10	27.92	45.65	27.92	^a

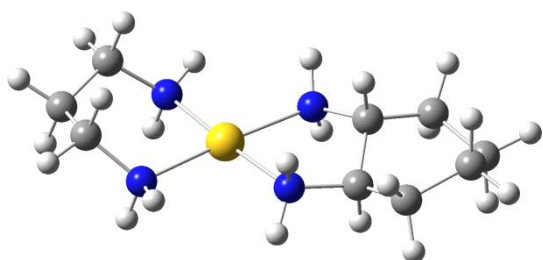
^a this work

Compared to solution chemical shifts, significant de-shielding in solid state is observed with similarity in the chemical shift among all synthesized complexes (Table 5.37) which is a clear indication of stability of the prepared complexes in solid state.

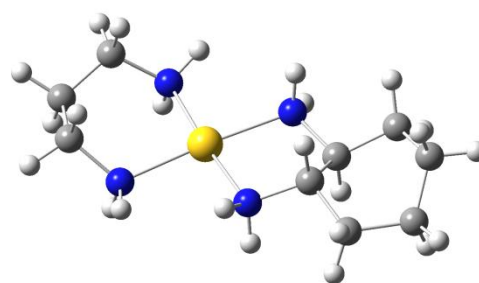
5.4.5 Computational Study

The optimized structures of the [(DACH)Au(pn)]³⁺ complexes as obtained from the B3LYP/LANL2DZ level of calculations are shown in Figure 5.55. Selected quantitative structural parameters are also listed in Table 5.40. The two *trans* configurations are mirror images. The complexes show a distorted square planar geometry structure around the gold atom. The N – Au – N angles in most of the conformations are within less than a degree from the perfect square planar geometry. The Au – N was predicted to be in the range of 2.14 to 2.15 Å for both (DACH) and (pn) bidentating ligands. The C – N bond length shows a significant increase (by approximately 0.1 Å) when compared with the same type of bonds in normal amines [76]. The four nitrogen atoms are predicted to adopt sp^3 type of hybridization as can be viewed from the calculated bond angles (Table 5.40).

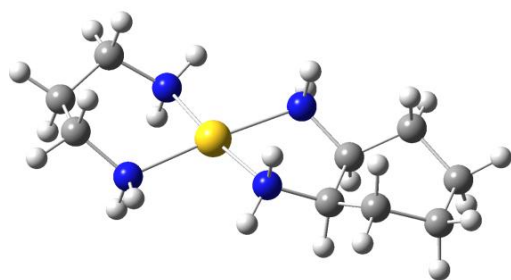
From the computed energetics of the four structures of the complex (Table 5.38), the *trans* conformations are more preferable compared to the *cis* conformations with more than 3.6 kcal/mol difference. The most possible explanation of this energy variation is the ring configuration of the DACH ligand, where in the *cis* form the CH₂ units experience more steric repulsion compared to the *trans* form.



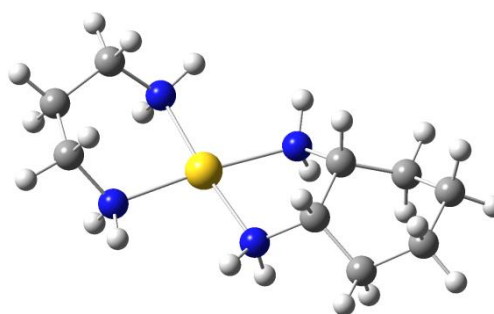
[(trans-1R,2R-DACH)Au(pn)]Cl₃



[(trans-1S,2S-DACH)Au(pn)]Cl₃



[(cis-1S,2R-DACH)Au(pn)]Cl₃



[(cis-1R,2S-DACH)Au(pn)]Cl₃

Figure 5.55 Optimized geometries of ***[(1,2-DACH)Au(III)(pn)]Cl₃***, obtained at the B3LYP/LanL2DZ level of theory using GAUSSIAN09 W

Table 5.38 Relative energies (kcal/mol) of the four possible conformations of the [(DACH)Au(pn)]³⁺ complex.

Conformation	Relative Energy (kcal/mol)
[(<i>trans</i> -1,2-DACH)Au(pn)]Cl ₃	0.00
[(<i>cis</i> -1 <i>S</i> ,2 <i>R</i> -DACH)Au(pn)]Cl ₃	3.31
[(<i>cis</i> -1 <i>R</i> ,2 <i>S</i> -DACH)Au(pn)]Cl ₃	3.59

5.4.6 Crystal Structure of [(*cis*-1*S*,2*R*-DACH)Au(pn)]Cl₃.

The molecular structure of complex [(*cis*-1*S*,2*R*-DACH)Au(pn)]Cl₃(**51**) is shown in Figure 5.56. It is a mononuclear complex containing one *cis*-1,2-cyclohexanediamine (DACH) and 1,3-propanediamine(pn)ligand molecules. There are three chloride ions in the outer sphere of the complex. The coordination geometry around the gold(III) ion is pseudo-square planar as confirmed by crystallographic data and supported by density functional calculations, and central gold(III) atom is coordinated with four NH₂ donor groups of the *cis*-1,2-cyclohexanediamine and 1,3-propanediamine mixed ligand molecules. Table 5.40 presents a good agreement between the experimental and calculated structural parameters for almost all bond distances and angles, which provides more support to the crystallographic findings. The mononuclear cation contains one five-membered chelate cycle AuN₂C₂ and one six-membered chelate cycle AuN₂C₃.

Au1–N1 and Au1–N2 bond distances are 2.03 (3) & 2.01 (3) Å, respectively, in a good agreement with the calculated DFT values (2.145 & 2.144). The N1–Au1–N1ⁱ & N2–Au1–N2ⁱ bond angles are 87 (2)°. The bond angles around gold(III) atom in mononuclear complex are unexpectedly the same (Table 5.40). These observations provide an additional evidence for the presence of centro-symmetric geometry in [(*cis*-1*S*,2*R*-

DACH)Au(pn)]Cl₃ (**51**). A summary of crystal data and refinement details for [(*cis*-1*S*,2*R*-DACH)Au(pn)]Cl₃ (**51**) are given in Table 5.39.

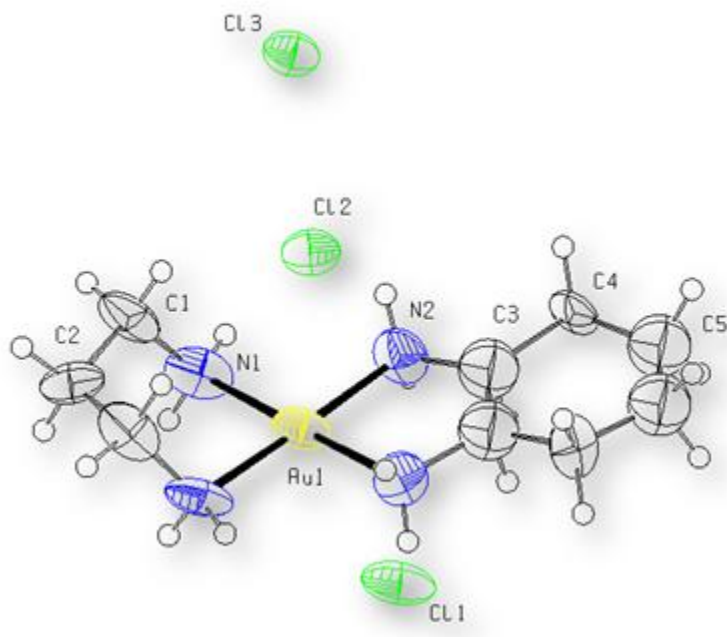


Figure 5.56 X-ray structure of [(*cis*-1*S*,2*R*-DACH)Au(pn)]Cl₃ (**51**)

Table 5.39 Crystallographic data for [(*cis*-1*S*,2*R*-DACH)Au(pn)]Cl₃ (**51**)

Empirical formula	C ₉ H ₂₄ AuCl ₃ N ₄
Formula weight	491.64
Crystal size/mm	<u>0.15 × 0.3 × 0.09</u>
Wavelength/Å	<u>0.71073</u>
Temperature/K	<u>173 (2)</u>
Crystal symmetry	Monoclinic
Space group	<u>P2₁/m</u>

$a/\text{\AA}$	10.139 (2)
$b/\text{\AA}$	7.2586 (11)
$c/\text{\AA}$	11.458 (4)
$\alpha/^\circ$	<u>90</u>
$\beta/^\circ$	115.55 (2)
$\gamma/^\circ$	<u>90</u>
$V/\text{\AA}^3$	760.8 (3)
Z	4
$D_c/\text{Mg m}^{-3}$	2.146
$\mu(\text{Mo-K}\alpha)/\text{mm}^{-1}$	<u>6.92</u>
$F(000)$	<u>472</u>
θ Limits/ $^\circ$	<u>2.0–25.7</u>
Collected reflections	5312è
Unique reflections(R_{int})	985 (0.269)
Observed efections[$F_o > 2\sigma(F_o)$]	1565
Goodness of fit on F^2	<u>1.05</u>
$R_1(F)$, ^a [$I > 2\sigma(I)$]	0.158
$wR_2(F^2)$, ^b [$I > 2\sigma(I)$]	0.407
Largest diff.peak, hole/e \AA^{-3}	7.02, -2.72

Table 5.40 Selected bond distances and bond angles for [(*cis*-1*S*,2*R*-DACH)Au(pn)]Cl₃(51)

Bond Length (Å)			Bond Angles (°)		
		Calculated			Calculated
Au1—N1	2.03 (3)	2.147	N1—Au1—N1 ⁱ	87 (2)	88.9
Au1—N1 ⁱ	2.03 (3)	2.147	N1—Au1—N2 ⁱ	177.8 (15)	174.2
Au1—N2 ⁱ	2.01 (3)	2.138	N1 ⁱ —Au1—N2 ⁱ	93.2 (15)	96.9
Au1—N2	2.01 (3)	2.137	N1—Au1—N2	93.2 (15)	96.9
N1—C1	1.54 (6)	1.537	N1 ⁱ —Au1—N2	177.8 (15)	174.2
N2—C3	1.48 (6)	1.545	N2 ⁱ —Au1—N2	77 (2)	76.3
			C1—N1—Au1	113 (2)	115.9
			C3—N2—Au1	109 (3)	111.3

The Au-N bond distances vary from 2.041(12)–2.0375(2) Å and correspond to those found in the 1,3-diaminopropane and 1,2-cyclohexanediamine gold(III) complexes [182,186]. Similarly, the N–Au–N bond angles vary from 83.9(2)–94.5 (5)° are much different from those found in gold(III) complex [182,186].

The presence of Cl[−] counter ions, lattice water molecule and –NH₂ groups of the 1,2-cyclohexanediamine ligand molecules results in hydrogen bond formation in the crystal structure of compound (**51**), which leads to the formation of a low-dimensional hydrogen bonded network as shown in Figure 5.57.

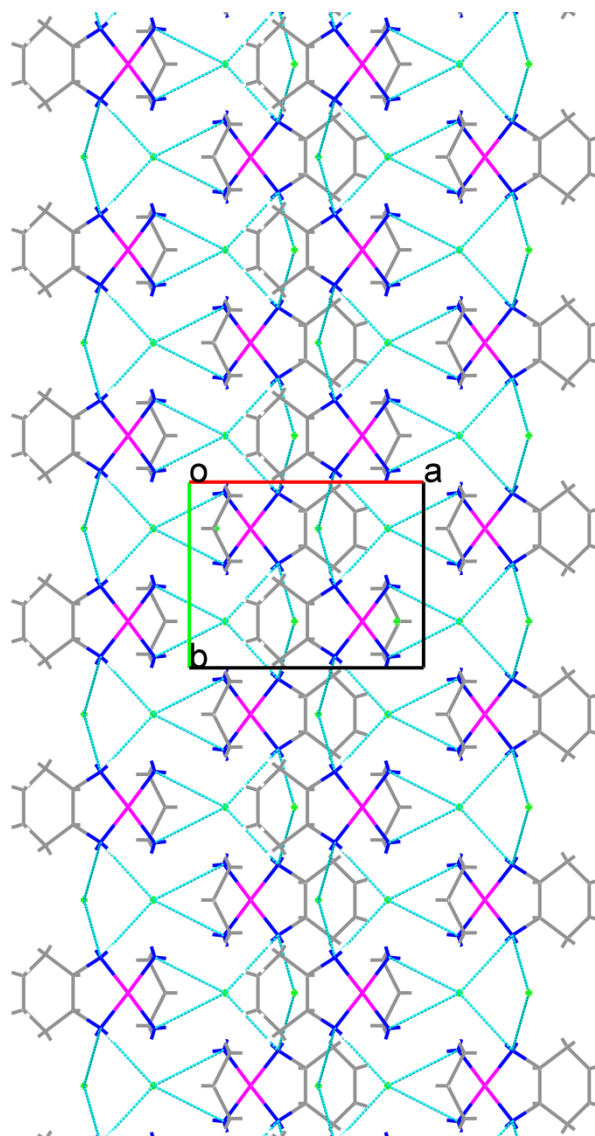


Figure 5.57 View of the hydrogen bonded network of $[(cis-1S,2R-DACH)Au(pn)]Cl_3$ (51) along plane c -axis of the unit cell. Blue dotted lines show hydrogen bonds between different functional groups of molecules

5.4.7 NMR Profiles Stability Study.

NMR spectra of the complexes dissolved in D_2O and mixed $DMSO-d_6/D_2O$ (v/v: 2/1) solution were obtained on immediate dissolution to serve as reference spectra and latter at 24 h and after 7 days at 37 °C in D_2O and at RT in mixed $DMSO-d_6/D_2O$ to determine

their stability. In general, all complexes showed high stability in D₂O and their NMR profiles remained unchanged over 7 days. For example, Figures 5.58-5.59 illustrated, respectively, the ¹H and ¹³C NMR profiles of the compound (**53**) at mixing and after 7 days. Whereas, these compounds in mixed DMSO-*d*₆/D₂O were not stable at the experimental conditions, in which, major dissociation of (pn) out off the gold complexes was observed from day one. On the other hand, no dissociation was observed for (DACH). Among all synthesized complexes, the maximum dissociation for (en) after 7 days was experienced for compound (**51**) with 80%. Figures 5.60-5.61 showed, respectively, ¹H and ¹³C NMR profiles of compound (**53**) in DMSO-*d*₆/D₂O at mixing and after 7 days. ¹H and ¹³C NMR of compound (**53**) spectra after 7 days in DMSO-*d*₆/D₂O showed extra peak at 2.86 & 1.85 and 37.3 & 25.8 ppm as shown in Figures 5.60 (b)-5.61 (b), respectively, corresponding to the free (pn) atoms. It is clear that the bond between gold(III) and (DACH) is stronger than the bond between gold(III) and (pn) in these complexes suggesting that (pn) could be a better leaving group.

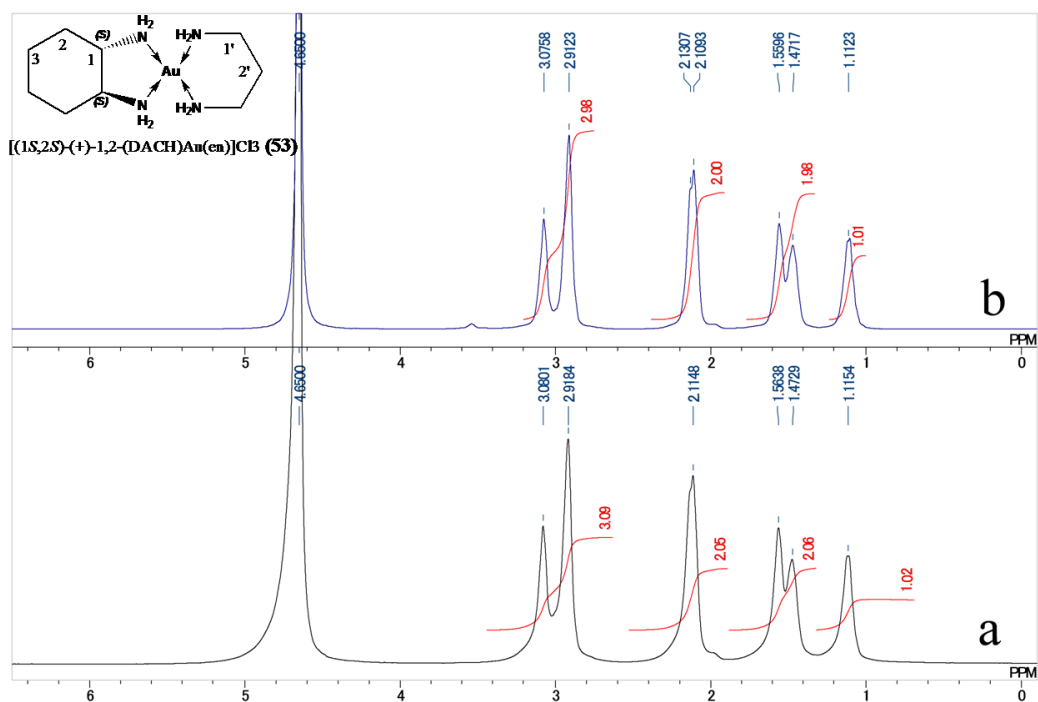


Figure 5.58 The 500-MHz ^1H solution state NMR spectrum of $[(1S,2S)\text{-}(+)\text{-}1,2\text{-}(\text{DACH})\text{Au}(\text{en})]\text{Cl}_3$ complex in D_2O at mixing (a) and after 7 days (b)

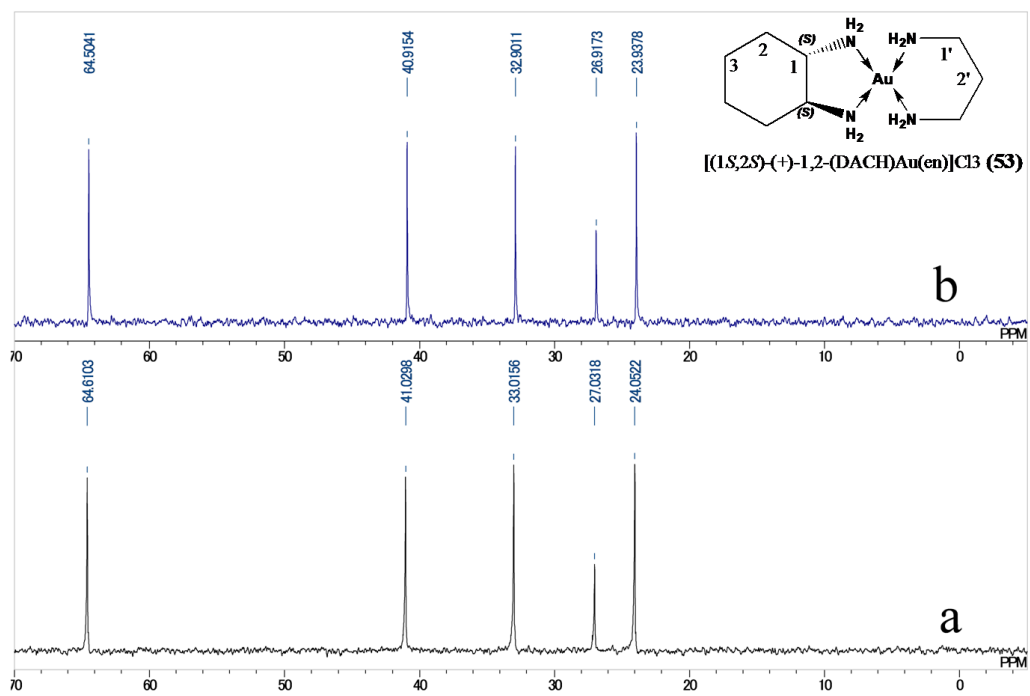


Figure 5.59 The 125.65-MHz $^{13}\text{C}\{^1\text{H}\}$ solution state NMR spectrum of $[(1S,2S)\text{-}(+)\text{-}1,2\text{-}(\text{DACH})\text{Au}(\text{en})]\text{Cl}_3$ complex in D_2O at mixing (a) and after 7 days (b).

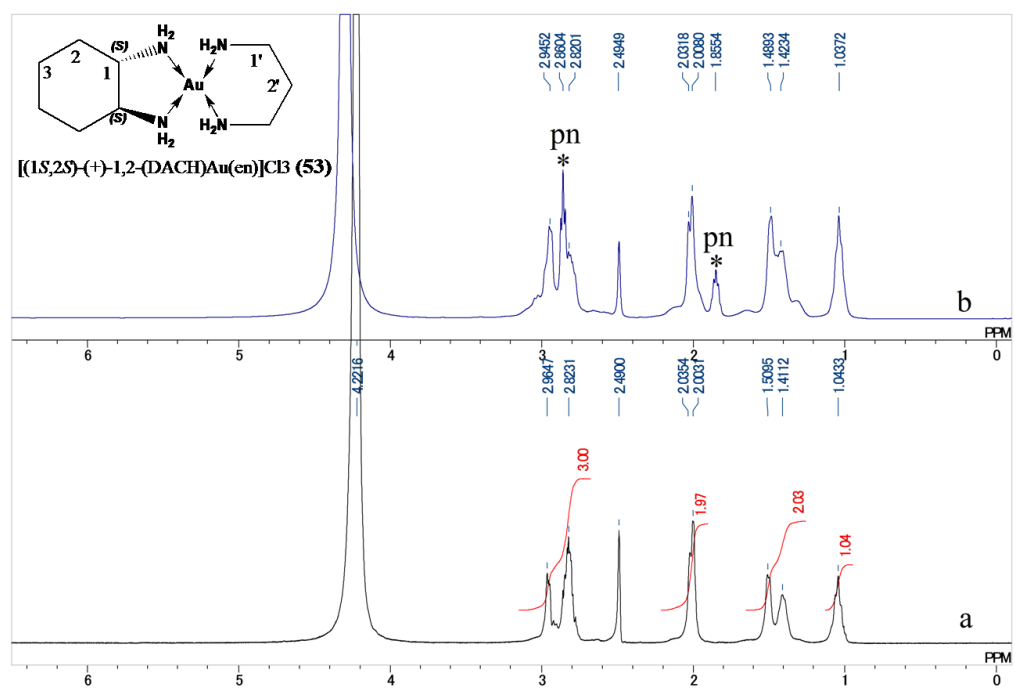


Figure 5.60 The 500-MHz ^1H solution state NMR spectrum of $[(1S,2S)\text{-}(+)\text{-}1,2\text{-}(\text{DACH})\text{Au}(\text{pn})]\text{Cl}_3$ complex in $\text{D}_2\text{O}/\text{DMSO}$ at mixing (a) and after 7 days (b)

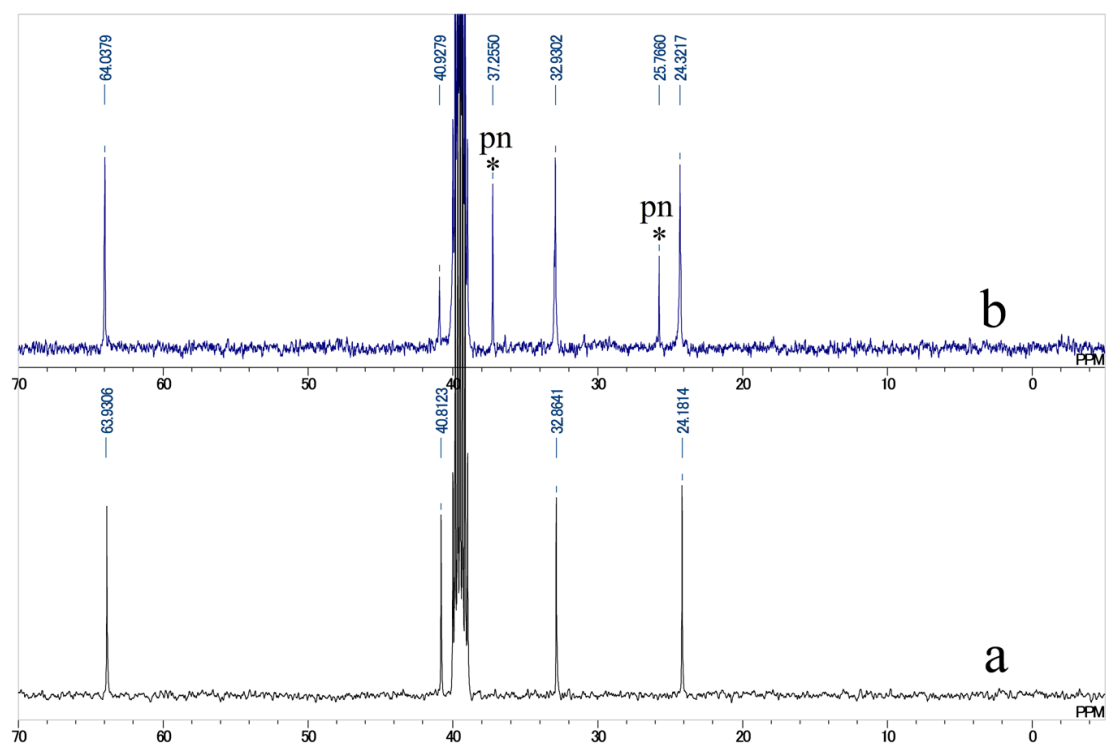


Figure 5.61 The 125.65-MHz $^{13}\text{C}\{^1\text{H}\}$ solution state NMR spectrum of $[(1S,2S)\text{-}(+)\text{-}1,2\text{-}(\text{DACH})\text{Au}(\text{pn})]\text{Cl}_3$ complex in $\text{DMSO}/\text{D}_2\text{O}$ (1:2) at mixing (a) and after 7 days (b)

5.4.8 Electrochemical Studies of Compounds 51-53.

The electrochemical behavior of compounds (51), (52) and (53) was investigated in a physiological environment through cyclic voltammetry. The voltammetric curves of the complexes (51), (52) and (53) are shown in Figure 5.62, and Table 5.41 summarize the voltammetric data of all the study compounds. The potential values vs. NHE for the reduction processes exhibited by the complexes (51), (52) and (53), in a reference buffered phosphate, in the range (+0.48)-(+0.58) V. Voltammetric data indicated that trans-DACH conformer is more stable than the cis-DACH conformer of the complexes which is also indicated by UV-Visible analysis. Gold(III) complexes (51), (52) and (53) show one irreversible reduction process which in controlled potential coulometry involves three electrons per mole. The occurrence of Au(III)/Au(0) reduction is confirmed by the appearance of thin gold layer deposited on the platinum electrode surface after exhaustive electrolysis (E_w , -0.7 V). In general, voltammetric results suggested that these compounds are fairly stable under the physiological conditions.

We also checked the stability of the gold(III) compounds in the reference buffer following addition of stoichiometric amounts of the biologically important reducing agent sodium ascorbate. It was observed that all complexes were quickly and completely reduced and the process was nearly complete after 60 min.

Table 5.41 Peak Potential values (vs ENH) for reduction of the present gold(III) complexes in the buffered aqueous solution processes at the platinum electrode

Complex	E_p (V)
[(en)Au{ <i>Cis</i> -1,2-(DACH)}]Cl ₃ (48)	+0.58
[(en)Au{ <i>Trans</i> -(±)-1,2-(DACH)}]Cl ₃ (49)	+0.49
[(en)Au(1 <i>S</i> ,2 <i>S</i>)-(+)-1,2-(DACH)]Cl ₃ (50)	+0.48

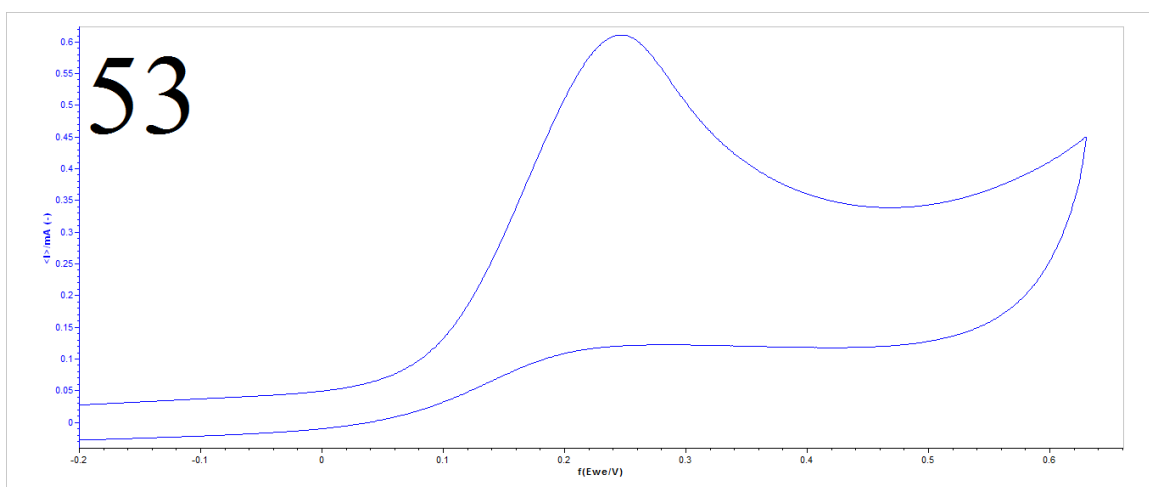
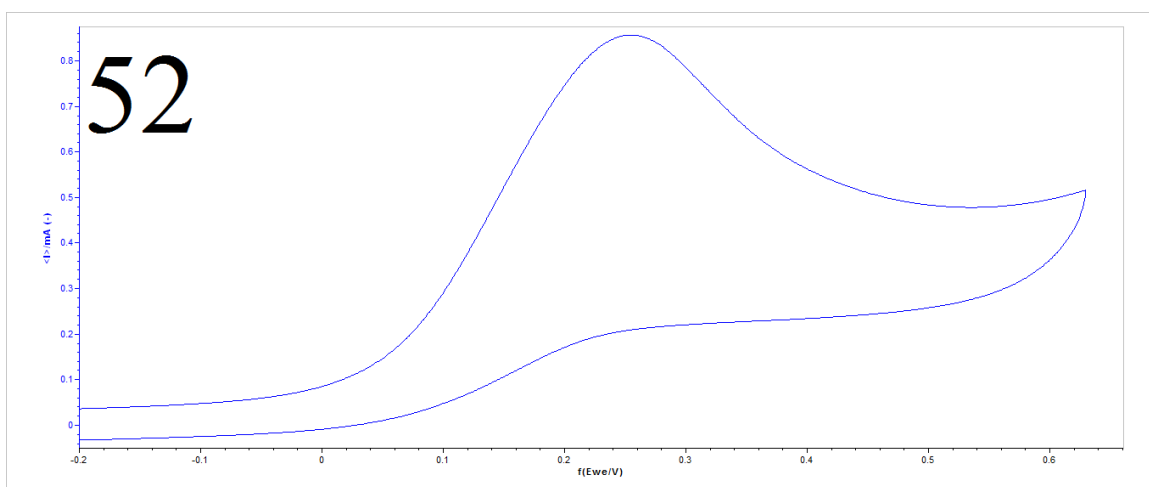
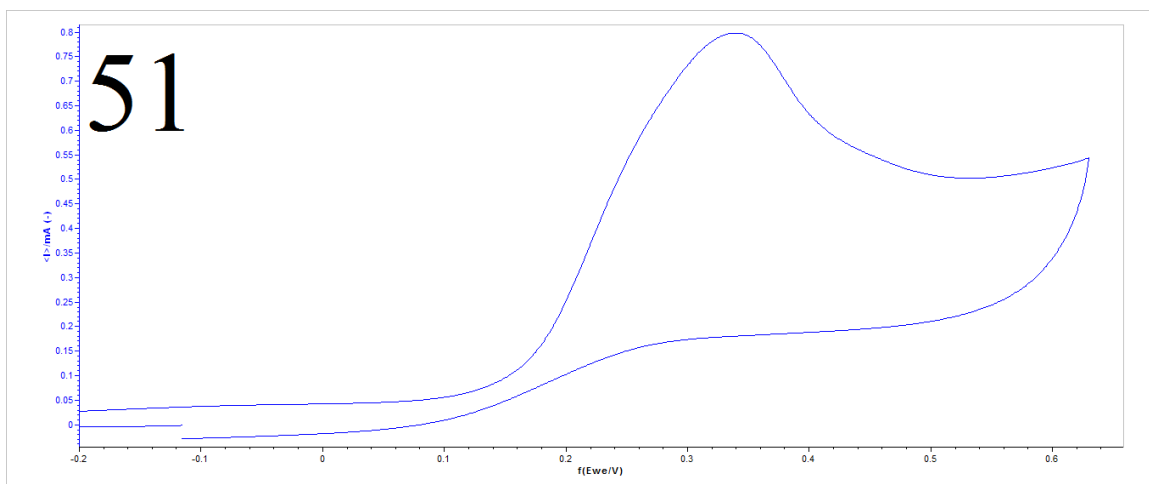


Figure 5.62 Cyclic voltammograms of compound 48, 49 and 50 in the phosphate buffer at platinum electrode.

5.4.9 Effect of Compounds (51), (52) and (53) on Cell Proliferation

The bioassay tests were completed for compounds (51)-(53) under various experimental conditions. The experimental PC-3 and SGC-7901 cells were treated with various concentrations of (51), (52) and (53) for 24-72 h and the cell viability was determined as described above by MTT assay and the results are shown in Tables 10 and 11 as well as in Figures 5.63-5.69. As depicted in Figures 5.63-5.65, complexes (51), (52) and (53) exhibited potentially high activity against gastric cancer cell SGC-7901 as well as human prostate cancer cells after 24 and 72 h of treatment with 10 μ M (see Table 11) under the same assay experimental condition. From Figs. 5.66-5.68, it is also quite clear that gold(III) complexes under study showed concentration dependent cytotoxic effect on cancerous cells PC-3 and SGC-7901. All synthesized complexes show similar bioactivity under the same experimental conditions as indicated by their cytotoxicity results (Table 5.42). To the best of our knowledge this is the first bioassay tests has been reported for gold(III) complexes based on cyclohexane-1,2-diamine and 1,3-propylenediamine.

Table 5.42 IC₅₀ Cytotoxicity values of the complexes towards different tumor cell lines. The data were collected after 72 h exposure to compound (51), (52) and (53)

Compounds	IC ₅₀ (μ M)	
	SGC-7901	PC3
(1)	10.8 \pm 0.22	9.5 \pm 0.22
(2)	10.9 \pm 0.12	11.2 \pm 0.12
(3)	11.0 \pm 0.14	9.1 \pm 0.14

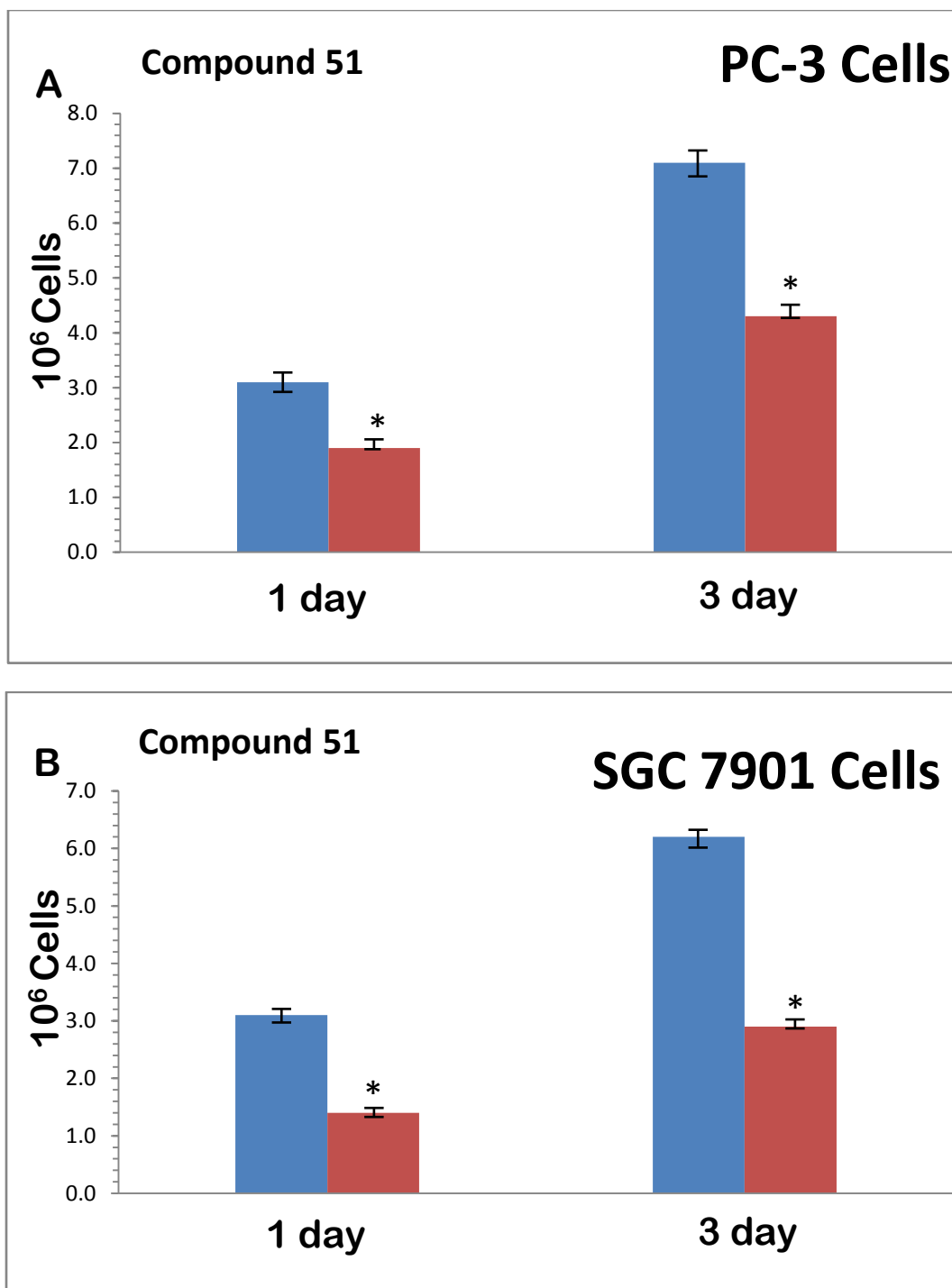


Figure 5.63 Effect of *cis*-1,2-(DACH)gold(III)(pn)complex (51) on cell growth in (A) PC-3 and (B) SGC-7901 cells. The cells were treated with 10 μ M for 1 day and 3 days. The anti-proliferative effect was measured by MTT assay. Results were expressed as the mean, SD. * $P < 0.05$

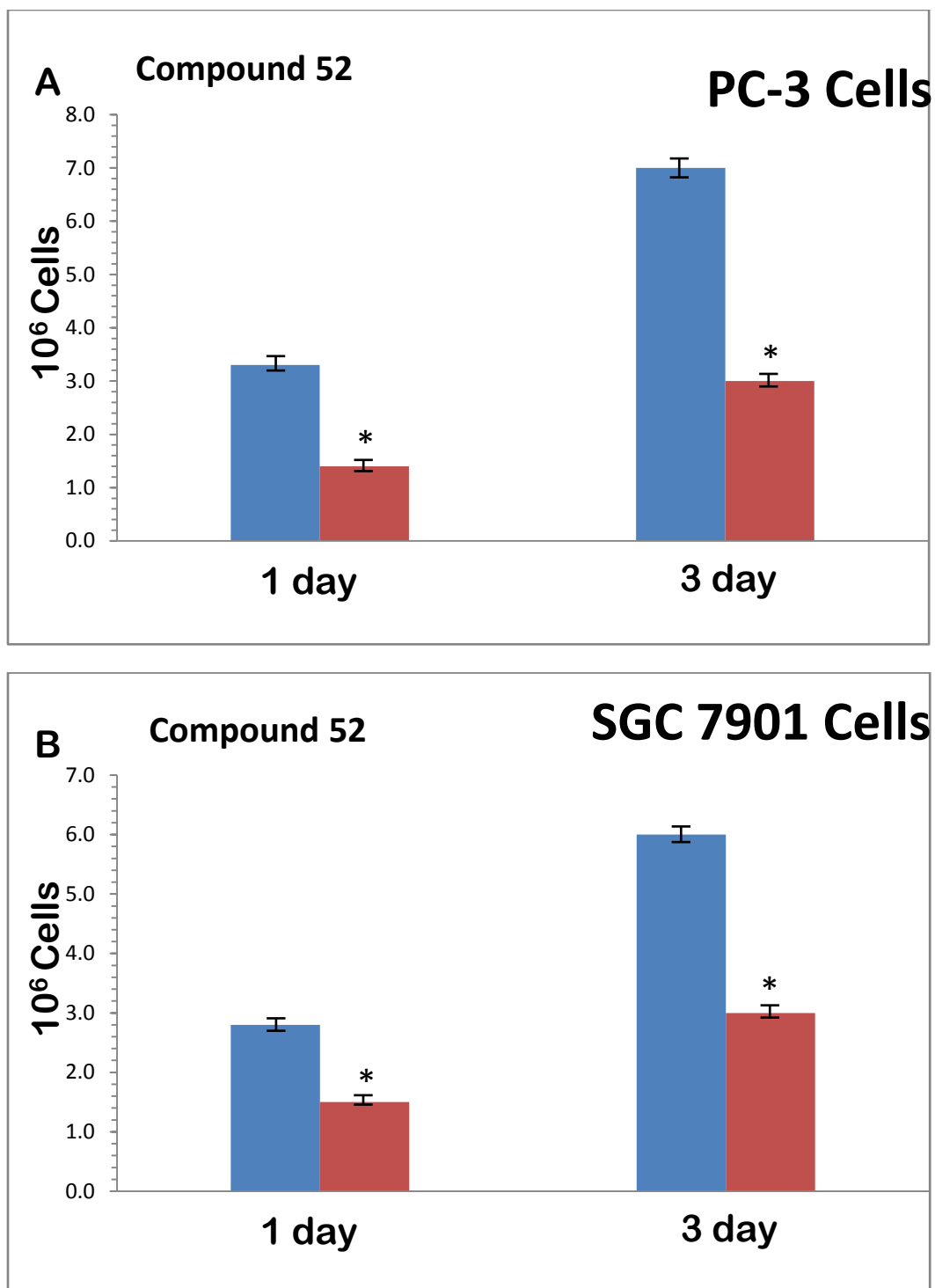


Figure 5.64 Effect of *trans*-(±)-1,2-(DACH)gold(III)(pn)complex (52) on cell growth in (A) PC-3 and (B) SGC-7901 cells. The cells were treated with 10 μ M for 1 day and 3 days. The anti-proliferative effect was measured by MTT assay. Results were expressed as the mean, SD. * $P < 0.05$

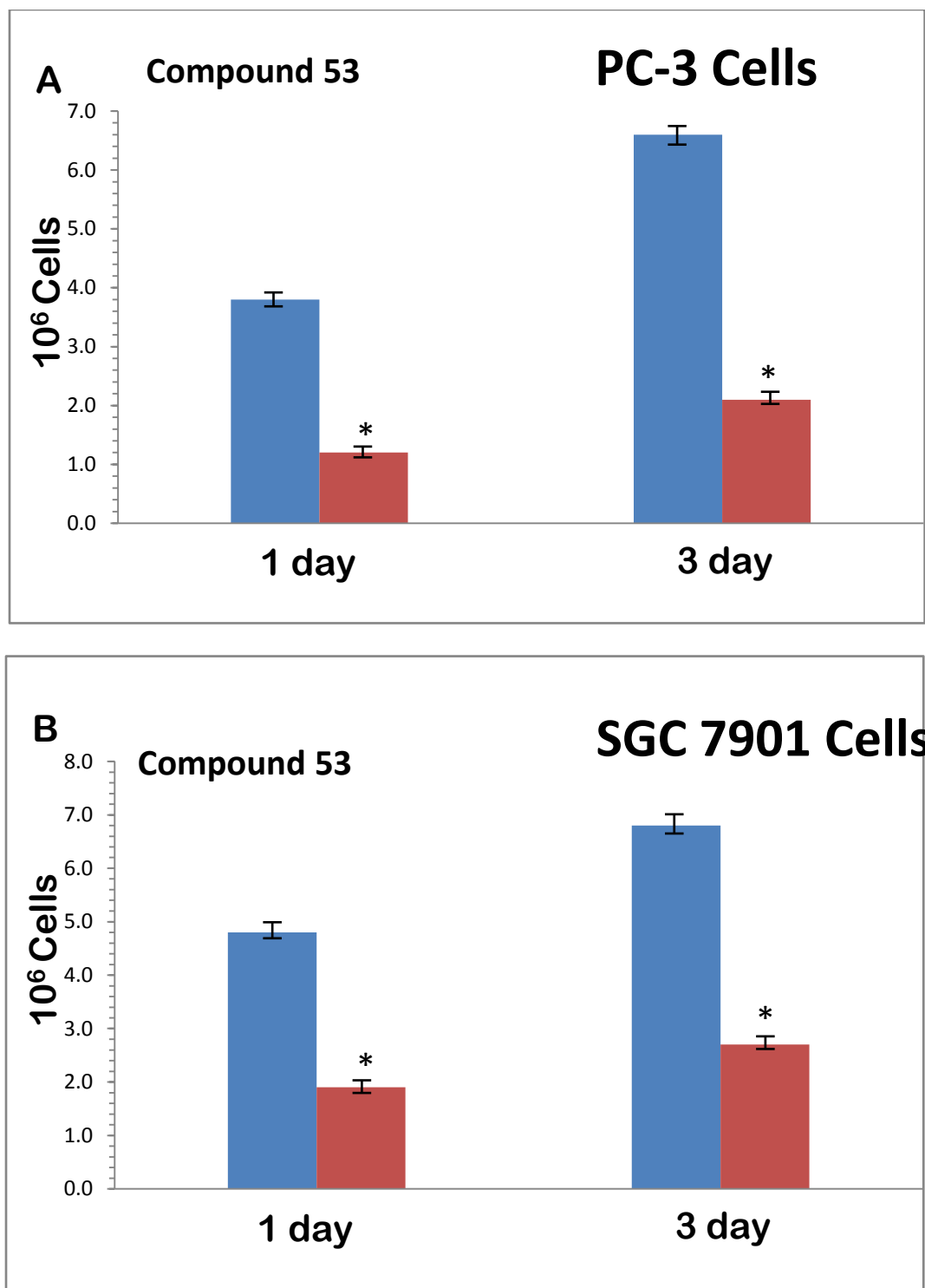


Figure 5.65 Effect of (*S,S*)-(+)-1,2-(DACH)gold(III)(pn) complex (53) on cell growth in (A) PC-3 and (B) SGC-7901 cells. The cells were treated with 10 μ M for 1 day and 3 days. The anti-proliferative effect was measured by MTT assay. Results were expressed as the mean, SD. * $P < 0.05$

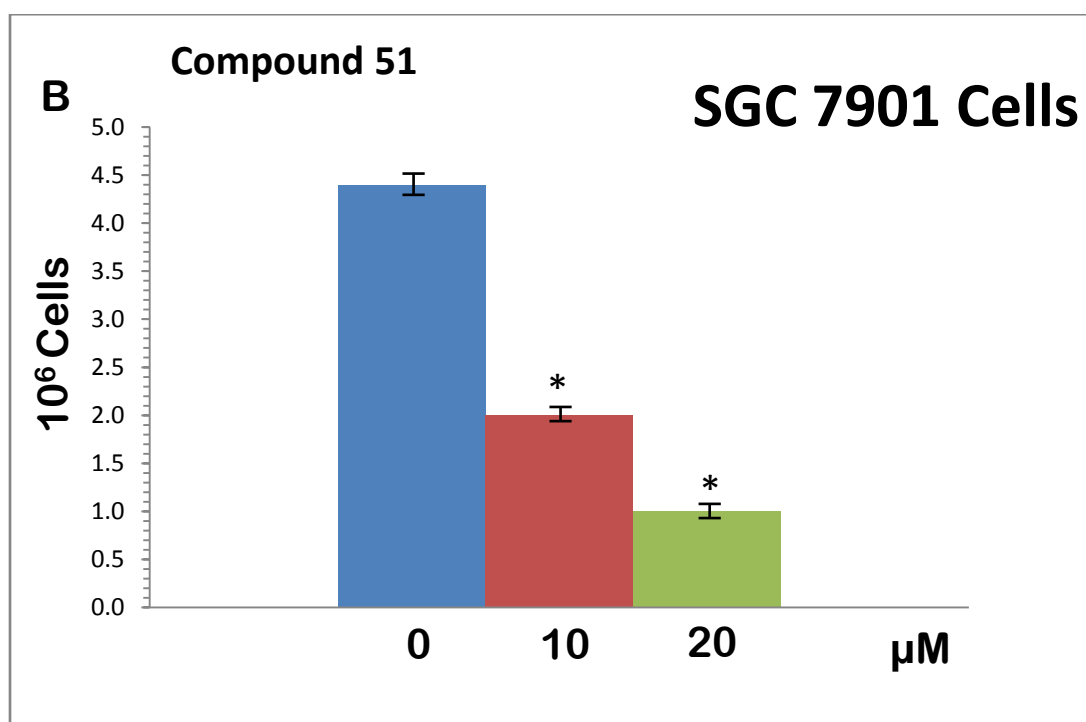
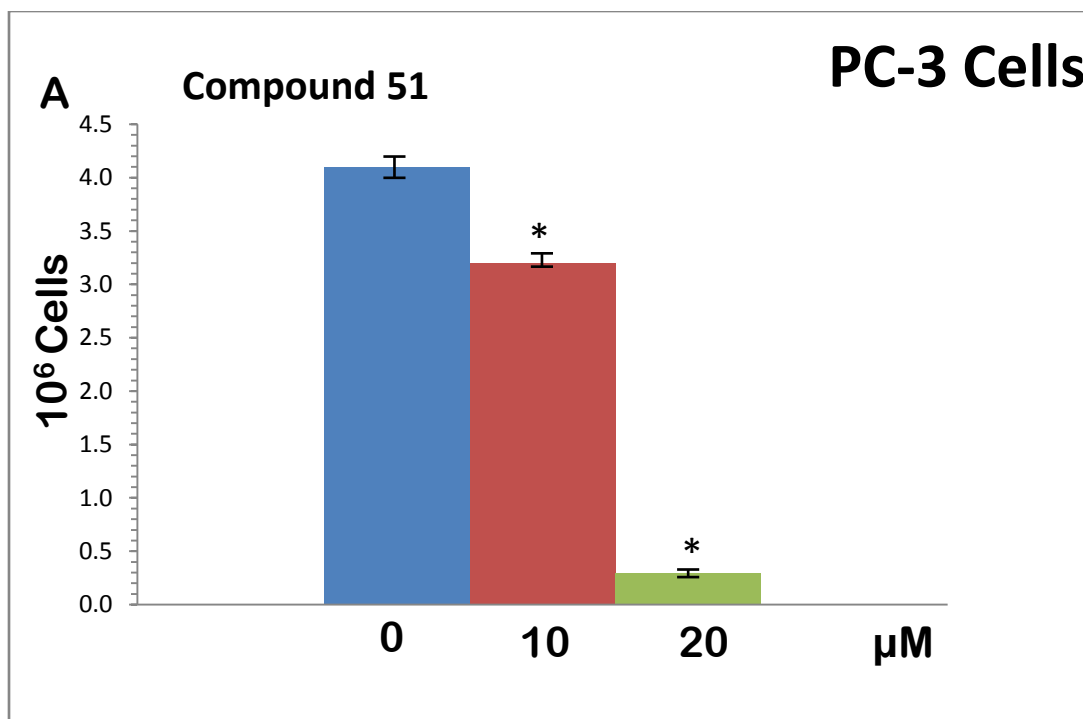


Figure 5.66 Effect of *cis*-1,2-(DACH)gold(pn) complex (51) on cell growth in (A) PC-3 and (B) SGC-7901 cells. The cells were treated with various concentrations for 24 h. The anti-proliferative effect was measured by MTT assay. Results were expressed as the mean, SD. * $P < 0.05$

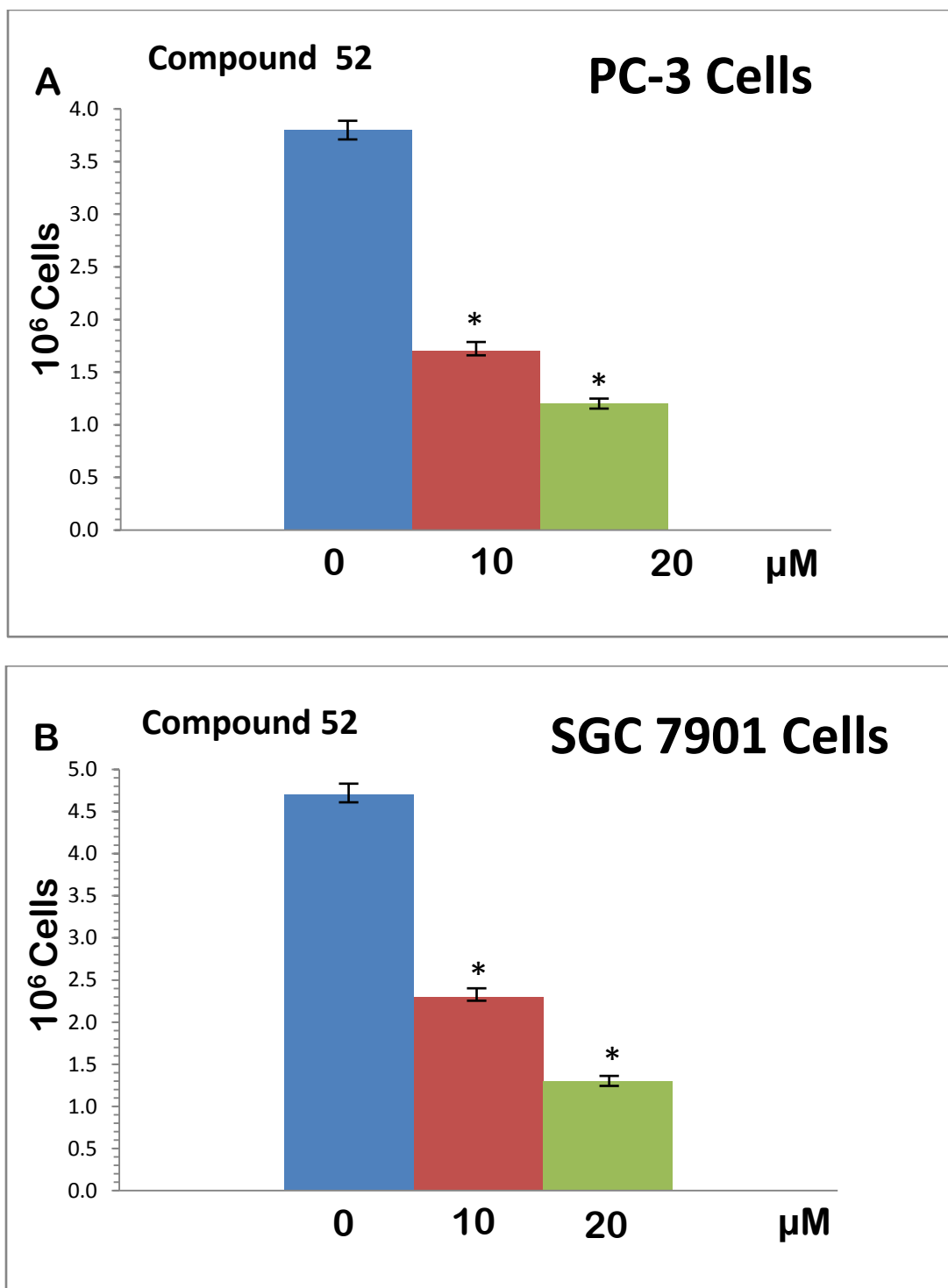


Figure 5.67 Effect of *trans*-(±)-1,2-(DACH)gold(pn) complex (52) on cell growth in (A) PC-3 and (B) SGC-7901 cells. The cells were treated with various concentrations for 24 h. The anti-proliferative effect was measured by MTT assay. Results were expressed as the mean, SD. * $P < 0.05$

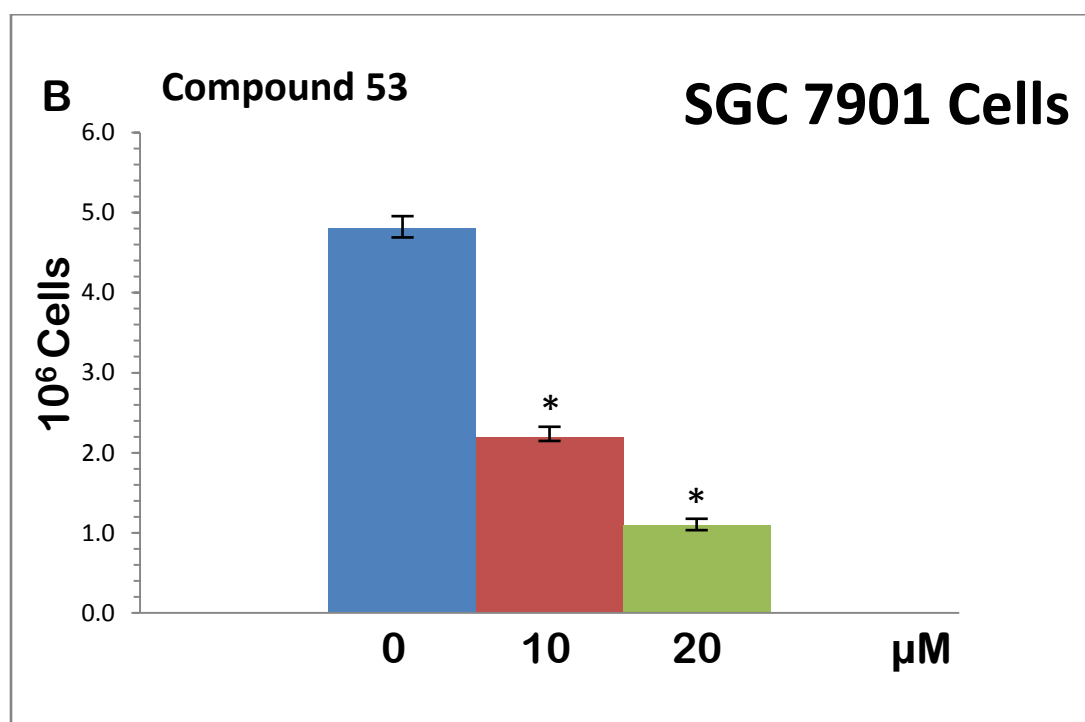
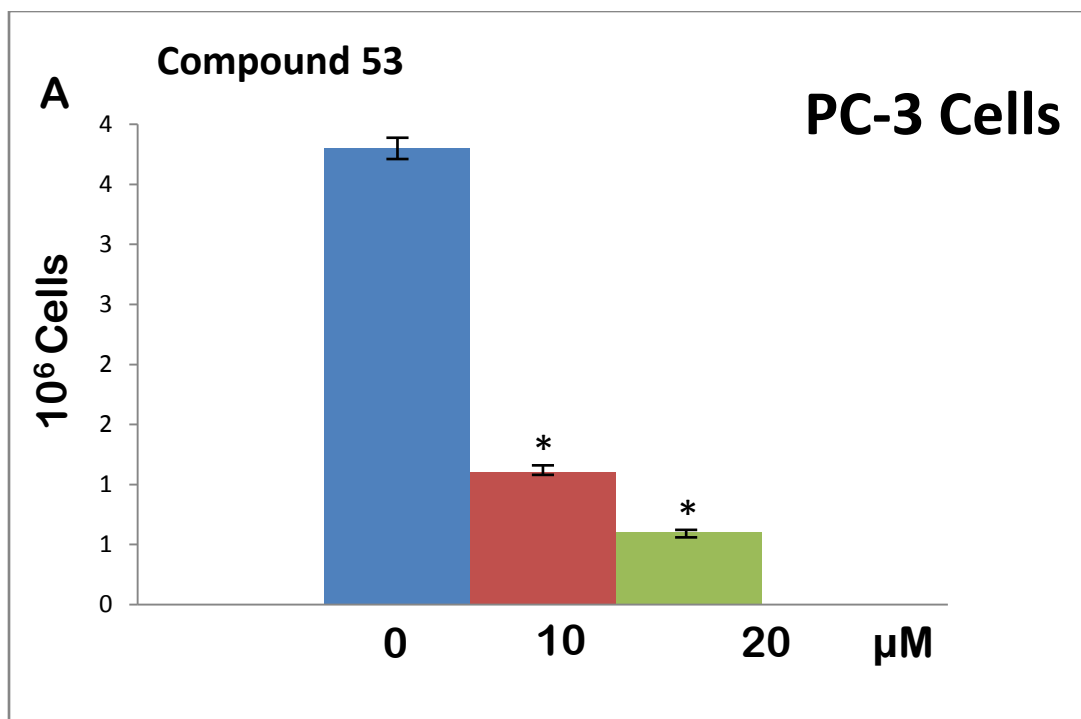


Figure 5.68 Effect of (*S,S*)-(+)-1,2-(DACH)gold(III)(pn) complex (53) on cell growth in (A) PC-3 and (B) SGC-7901 cells. The cells were treated with various concentrations for 24 h. The anti-proliferative effect was measured by MTT assay. Results were expressed as the mean, SD. * $P < 0.05$

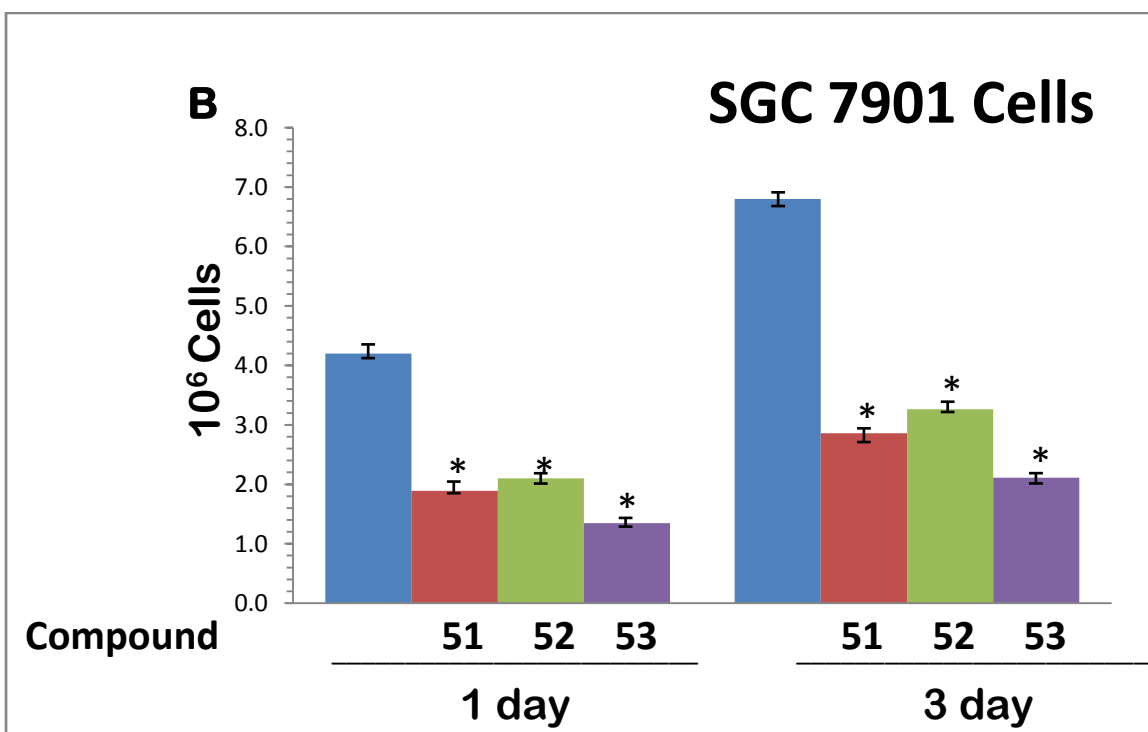
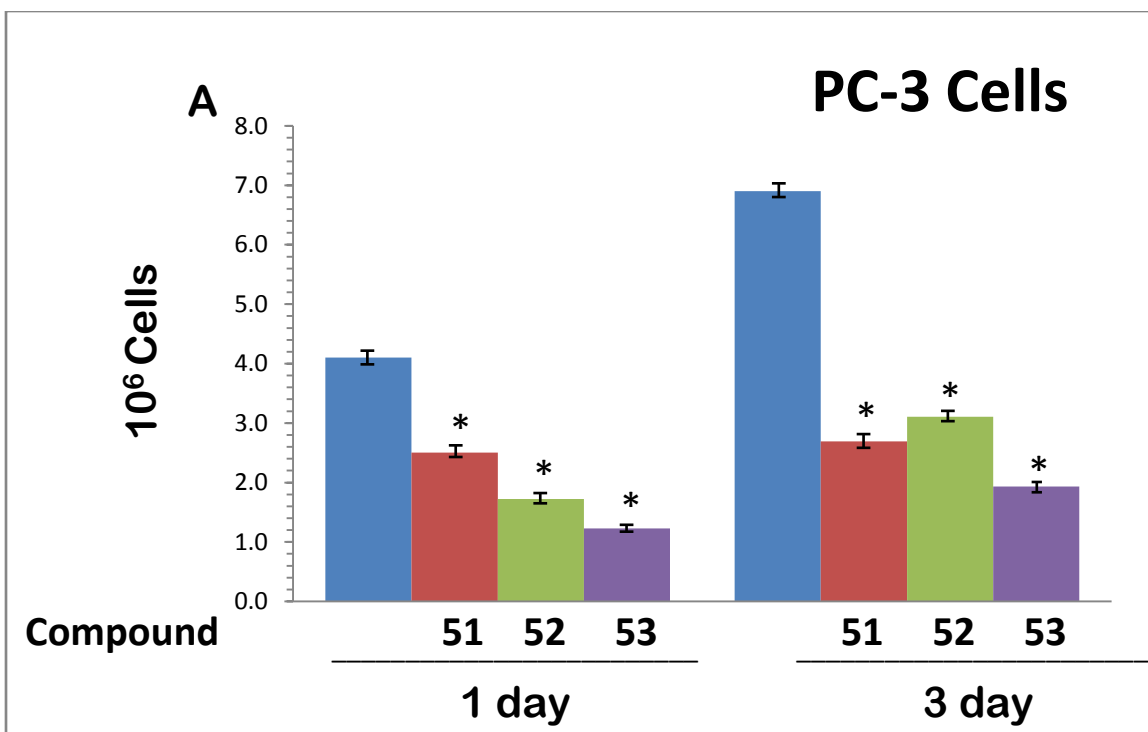


Figure 5.69 Effect of compounds (51-53) and on cell growth in (A) PC-3 and (B) SGC-7901 cells. The cells were treated with 10 μ M for day 1, day2 and day 3. The anti-proliferative effect was measured by MTT assay. Results were expressed as the mean, SD. * $P < 0.05$

5.4.10 Conclusion

These [(1,2-DACH)gold(III)(pn)]Cl₃ complexes were characterized using elemental analyzer, solution and solid NMR, UV, IR, Far-IR spectroscopy and X-ray crystallography. The analytical data showed strongly support for the formation of the type [(1,2-DACH)gold(III)(pn)]Cl₃ complex. Also, computational study demonstrates that *trans*-(1,2-DACH)-gold-(pn) isomer is more stable than the *cis*-(1,2-DACH)gold(pn) isomer and gold coordination sphere of these complexes adopts distorted square planar geometry. According to our biological assays, complexes (51) and (53), respectively, with *cis* and (1*S*,2*S*)-(DACH)structures are more promising candidate as an anti-cancer agent than the *trans*-(±)-(1,2-DACH) isomers of (52). The exact mechanisms are not clearly known, but the inhibitory effect of [(1*S*,2*S*-DACH)Au(pn)]Cl₃ on the proliferation of rapidly dividing cells would be attributed to the induction of cell cycle blockage, interruption of the cell mitotic cycle, programmed cell death (apoptosis) or premature cell death (necrosis). Therefore, [(1*S*,2*S*-DACH)Au(pn)]Cl₃ isomer, might be a promising chemo preventative and chemotherapeutic agent against human gastric carcinogenesis. As cytotoxic activity of [(1*S*,2*S*-DACH)Au(pn)]Cl₃ complex is high towards some cancer cell lines; further biological evaluation for this class of complexes is worthy of efforts especially in order to evaluate activities *in vivo*.

5.5 Crystal Structure of Compound [Me₃PAu(DMDT)] (70)

Molecular structure of [Me₃PAu(S₂CNMe₂)] (70) is shown in Figure 5.70A view of the molecular structure of complex (70), with partial atom labelling scheme and displacement ellipsoids are drawn at 50% probability level.. In this structure gold(I) is coordinated with

one P donor atom of trimethylphosphine and S donor atom of dimethyldithiocarbamate ligand molecules. A summary of crystal data and refinement details for compound (70) are given in Table 5.43.

The Au–S and Au–P bond distances are 2.326 (3) and 2.249 (3) Å, respectively. The Au–P and Au–S bond distances are comparable with [Et₃PAu(S₂CNEt₂)] complex [187]. The geometry around Au(I) metal atom is linear and similar to other Au(I) complexes [188–191]. In [Me₃PAu(S₂CNMe₂)] (70) structure S–Au–P bond angle is 176.88 (13). The S–Au–P bond angle value shows considerable deviation from ideal linear angle of 180° (Table 5.44 Selected bond lengths and bond angles in compound and confirms the presence of distorted linear geometry in this molecule. The short contacts interactions between different functional groups of the molecules result three-dimensional network as shown in Figure 5.71 View of the crystal packing diagram of compound (70) along *plane* *c*-axis of the unit cell. Blue and red dotted lines show short contacts between different functional groups of molecules.

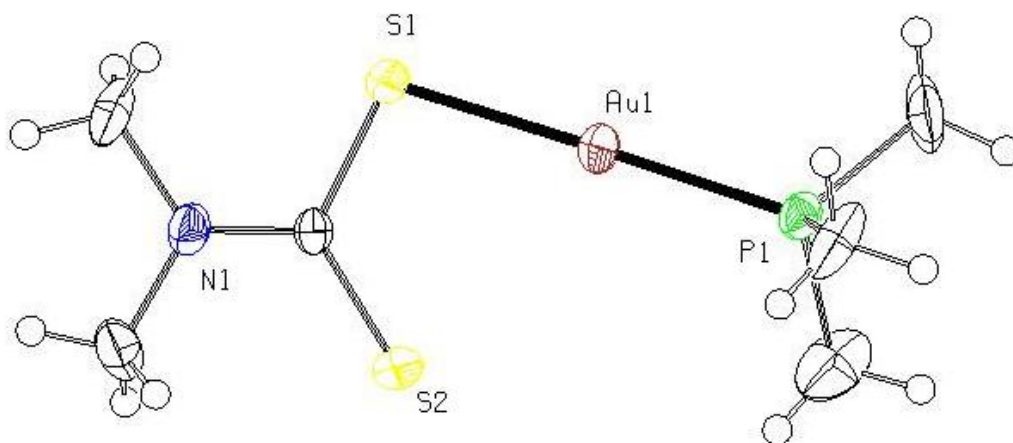


Figure 5.70A view of the molecular structure of complex (70), with partial atom labelling scheme and displacement ellipsoids are drawn at 50% probability level.

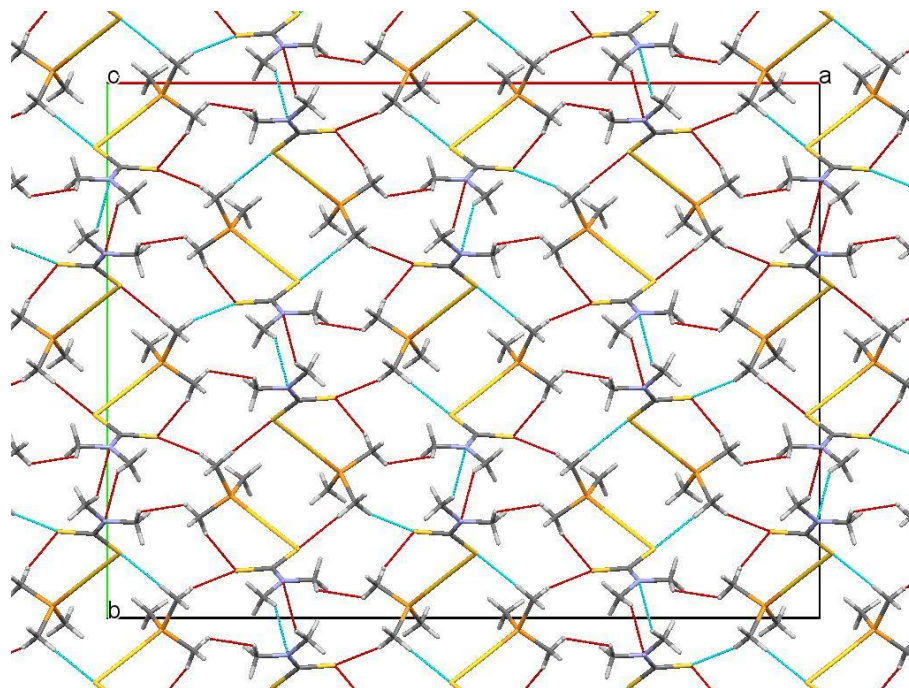


Figure 5.71 View of the crystal packing diagram of compound (70) along plane *c*-axis of the unit cell. Blue and red dotted lines show short contacts between different functional groups of molecules.

Table 5.43 Summary of crystal data and details of the structure refinement for compound (70)

Compound	70
Empirical formula	$C_6H_{15}Au_1N_1P_1S_2$
Formula weight	393.27
Crystal size/mm	<u>0.15</u> × <u>0.3</u> × <u>0.09</u>
Wavelength/Å	<u>0.71073</u>

Temperature/K	<u>173 (2)</u>
Crystal symmetry	Orthorhombic
Space group	Fdd2
$a/\text{\AA}$	32.075 (2)
$b/\text{\AA}$	24.0898 (14)
$c/\text{\AA}$	6.1700 (3)
$V/\text{\AA}^3$	4767.4 (5)
Z	8
$D_c/\text{Mg m}^{-3}$	2.192
$\mu(\text{Mo-K}\alpha)/\text{mm}^{-1}$	12.78
$F(000)$	2944
θ Limits/ $^\circ$	<u>2.1–25.7</u>
Collected reflections	8135
Unique reflections(R_{int})	2123 (0.082)
Observed reflections[$F_o > 2\sigma(F_o)$]	2175
Goodness of fit on F^2	1.08
$R_1(F)$, ^a [$I > 2\sigma(I)$]	0.043
$wR_2(F^2)$, ^b [$I > 2\sigma(I)$]	0.120
Largest diff.peak, hole/ $e \text{\AA}^{-3}$	1.40, -3.10

Table 5.44 Selected bond lengths and bond angles in compound (70)

Compound 1			
Bond Length (\AA)		Bond Angles ($^\circ$)	
Au1—P1	2.249 (3)	P1—Au1—S1	176.88 (13)
Au1—S1	2.326 (3)	C1—P1—C2	103.7 (10)
P1—C1	1.775 (16)	C1—P1—C3	104.1 (9)
P1—C2	1.792 (14)	C2—P1—C3	105.0 (8)
P1—C3	1.797 (15)	C1—P1—Au1	117.5 (6)
S1—C4	1.758 (12)	C2—P1—Au1	113.1 (6)

CHAPTER 6

SUMMARY AND CONCLUSIONS

This work reports the synthesis of gold(III) and gold(I) complexes based on 1,2-diaminocyclohexane, *n,n'*-dialkyldithiocarbamate, ammonium dithiocarbamate (1-16), 2-mercaptobenzimidazole (**17-23**) and chloridetrialkylphosphane gold(I) (**24-35**).

Various new series of gold(III) 1,2-diaminocyclohexane complexes (**36-53**) with general formula, [(1,2-DACH)AuCl₂]Cl, [(1,2-DACH)₂Au]Cl₃, [(1,2-DACH)Au(en)]Cl₃, [(1,2-DACH)Au(pn)]Cl₃, [(1,2-DACH)₂Au]Cl₃, [(1,2-DACH)Au(NH₃)Cl]Cl₂ and [(1,2-DACH)Au(NH₃)]Cl₃ have successfully been synthesized and characterized by using various analytical and spectroscopic techniques.

A novel series of gold(III) complexes (**54-69**) based on ammonium dithiocarbamate with general formula [(ADTC)AuCl₂]Cl are reported here that were characterized by using various analytical and spectroscopic techniques. In addition to the synthesis of gold(III) complexes, a series of gold(I) complexes (**70-93**) of the type [(R)₃PAu(MDTC)] and [(R)₃PAu(EDTC)] based on mixed ligands of trialkylphosphane and *n,n'*-dialkyldithiocarbamate have successfully been synthesized and characterized by using various analytical and spectroscopic techniques.

Moreover, various series gold(I) complexes (**94-129**) based on mixed ligands of 2-mercaptobenzimidazole of the type, [(2-MBI)AuP(R)₃], [(2-MBI)Au(carbene)] and [(2-

MBI)Au₂(L)] (L= 1,3-bis(diphenylphosphino)methane), were also prepared and characterized by various analytical and spectroscopic techniques

These gold complexes were characterized using CHN analysis, UV-Vis, mid-FTIR, Far-FTIR spectroscopy, solution and solid-state NMR and X-ray crystallography. Analytical data showed strong support for the formation of the proposed complexes. The coordination geometry around the gold(III) and gold(I) ions is pseudo-square planar and linear, respectively, as indicated by X-ray crystallography analysis. According to the biological assays, all (1,2-DACH) gold(III) chloride complexes are promising candidates as anti-cancer agents with [(*cis*-(1,2)-DACH)₂Au(III)]Cl₃ is the most active agent. Stability study of these bis-amine gold(III) complexes in physiological buffer solution studied by UV-Vis and cyclic voltammetry (CV) showed fair stability. According to IC₅₀ data, all (1,2-DACH) gold(III) chloride complexes show cytotoxicity better or comparable to cisplatin, towards SGC7019 prostate cancer cells.

6.1 Future Studies

- In the same line of Au(III) diamine complexes, Au(III) bipyridine and Au(III) phenanthroline complexes can also be synthesized and evaluated *in vitro* for potential anticancer activity.
- As *in vitro* anticancer activity of [(en)Au(1,2-DACH)]Cl₃ and its derivatives was significantly promising towards some cancer cell line, further *in vivo* anticancer evaluation would be worth-while.
- With same frame of mind, ammonium dithiocarbamate ligands can also be used to synthesize a new series of complexes with different metals and evaluated *in-vitro* for potential anticancer activity.

Appendix A -List of Publications

1. **S.S. Al-Jaroudi**, M. Fettouhi, M.I.M. Wazeer, A.A. Isab, S. Altuwaijri, “*Synthesis, characterization and cytotoxicity of new gold(III) complexes with 1,2-diaminocyclohexane: Influence of stereochemistry on antitumor activity*”, **Polyhedron**50 (2013) 434-442.
2. **S.S. Al-Jaroudi**, M. Monim-ul-Mehboob, M. Altaf, M. Fettouhi, M.I.M Wazeer, S. Altuwaijri and A.A. Isab “*Synthesis, spectroscopic characterization, X-ray structure and electrochemistry of new bis(1,2-diaminocyclohexane)gold(III) chloride compounds and their anticancer activities against PC3 and SGC7901 cancer cell lines*”**New Journal of Chemistry**, 2014, 38, 3199-3211.
3. **S.S. Al-Jaroudi**, M. Altaf, A.A. Al-Saadi, M.I.M. Wazeer, S. Altuwaijri and A.A. Isab “*Synthesis, spectroscopic characterization, electrochemical behavior and computational analysis of mixed diamine ligand gold(III) complexes: antiproliferative and in vitro cytotoxic evaluations against human cancer cell lines*” **Biomaterials** 2014, DOI 10.1007/s10534-014-9771-2.
4. **S.S. Al-Jaroudi**, M. Altaf, A.A. Al-Saadi, M.I.M. Wazeer, S. Altuwaijri and A.A. Isab “*Synthesis, spectroscopic characterization and electrochemistry of 1,2-Diaminocyclohexane1,3-Propylenediamine Gold(III) Chloride Complexes and Influence of Stereochemistry on Cytotoxicity and Antitumor Activity*” Submitted.
5. A.A. Isab, M.I.M. Wazeer, **S.S. Al-Jaroudi**, , S.Altuwaijri “Cytotoxic Compounds for Treating Cancer” **USA Patent Application**, USPTO Serial Number **13/944761**, filed on July 17, 2013.

Appendix B -Conference Presentations

1. **Said Al-Jaroudi** and Anvarhusein A. Isab, *Anti-cancer activity of new gold(III) complexes of [(1,2-DACH)AuCl₂]Cl against human prostate and gastric cancer cell lines*, Poster presentation in **244th ACS National Meeting 2012, USA**.

References

- [1] D.M. Parkin, P. Pisani, J. Ferlay, *CA Cancer, J. Clin.*, 49, 1999, 33.
- [2] D.M. Parkin, F. Bray, J. Ferlay, P. Pisani, *Int. J. Cancer*, 94, 2001, 153.
- [3] Rosenberg B., Van Camp L., Krigas T., *Nature* 1965, 205, 698.
- [4] J. Reedijk, *Eur. J. Inorg. Chem.* (2009) 1303–1312.
- [5] Gumus F., Algul O., Eren G., Eroglu H., *Eur. J. Med. Chem* 2003, 38, 473.
- [6] Jamieson E. R., Lippard S. J., *Chem. Rev.* 1999, 99, 2467.
- [7] Wong E., Giandomenico C. M., *Chem Rev.* 1999, 99, 2451.
- [8] Marzano C., Trevisan A., Giovagnini L., Fregona D., *Toxicology in Vitro*, 2002, 16, 413.
- [9] Kelland L. R., Sharp S. Y., O'Neill C. F., Raynaud F. I., Beale P. J., Judson I. R., *Inorg. Biochem.*, 1999, 77, 111.
- [10] Cadron I., Leunen K., Amant F., Van Gorp T., Neven P., Vergote I., *Gynecol. Oncol.*, 2007, 106, 354.
- [11] Holford J. Sharp S. Y., Murrer B. A., Abrams M., Kelland L. R., *Br. J. Cancer*, 1998, 77, 366.
- [12] S. Ahmad, A.A. Isab, S. Ali, A.R. Al-Arfaj, *Perspectives in bioinorganic chemistry of some metal based therapeutic agents*, *Polyhedron*. 25 (2006) 1633–1645.
- [13] S. Ahmad, *The chemistry of cyano complexes of gold(I) with emphasis on the ligand scrambling reactions*, *Coord. Chem. Rev.* 248 (2004) 231–243.
- [14] C.F. Shaw III, *Gold-based therapeutic agents.*, *Chem. Rev.* 99 (1999) 2589–600.
- [15] S.J. Berners-Price, P.J. Sadler, *Coordination chemistry of metallodrugs: insights into biological speciation from NMR spectroscopy*, *Coord. Chem. Rev.* 151 (1996) 1–40.
- [16] C.K. Mirabelli, R.K. Johnson, D.T. Hill et al., *Correlation of the in vitro cytotoxic and in vivo antitumor activities of gold(I) coordination complexes*, *J. Med. Chem.*, 29 (1986), pp. 218–223.
- [17] P.C.A. Bruijninx, P.J. Sadler, *Curr. Opin. Chem. Biol.* 12 (2008) 197.
- [18] M. Jakupec, B.K. Keppler, in: A. Sigel, H. Sigel, *Metal Ions in Biological Systems*, vol. 42, Marcel Dekker Inc., 2004.
- [19] S. Nobili, E. Mini, I. Landini, C. Gabbiani, A. Casini, L. Messori, *Med. Res. Rev.* 30 (2010) 550.
- [20] Morelle Negom Kouodom, Giulia Boscutti, Marta Celegato, Marco Crisma, Sergio Sitran, Donatella Aldinucci, Fernando Formaggio, Luca Ronconi, Dolores Fregona. *Journal of Inorganic Biochemistry* 117 (2012) 248–260.
- [21] Monica Carreira, Rubén Calvo-Sanjuán, Mercedes Sanaú, Xiangbo Zhao a, Richard S. Magliozzo, Isabel Marzo, María Contel, *Journal of Inorganic Biochemistry* 116 (2012) 204–214.
- [22] Janet B. Foley, Angela Herring, Bo Li, Evgeny V. Dikarev. *Inorganica Chimica Acta* 392 (2012) 300–310.
- [23] L. Canovese et al., *Inorganica Chimica Acta* 391 (2012) 141–149.

- [24] T. V. Segapelo et al., *Polyhedron* 36 (2012) 97–103.
- [25] Štěpnička Petr, Císařová Ivana. *Journal of Organometallic Chemistry* 716 (2012) 110-119.
- [26] H. Zhao, L. Zhou, *Computational and Theoretical Chemistry* 979 (2012) 22–32
- [27] Giulia Boscutti, Lisa Feltrin, Debora Lorenzon, Sergio Sitran, Donatella Aldinucci,
- [28] Luca Ronconi, Dolores Fregona, *Inorganica Chimica Acta* 393 (2012) 304–317.
- [29] Chiara Gabbiani, Maria Agostina Cinellu, Laura Maiore, Lara Massai, Federica Scaletti
- [30] Luigi Messori, *Inorganica Chimica Acta* 393 (2012) 115–124.
- [31] P.J. Barnard, S.J. Berners-Price, *Coord. Chem. Rev.* 251 (2007) 1889–1902.
- [32] M.J. McKeage, S.J. Berners-Price, P. Galettis, R.J. Bowen, W. Brouwer, L. Ding, L. Zhuang, B.C. Baguley, *Cancer Chemother. Pharmacol.* 46 (2000) 343–350.
- [33] J. D. Chaves, F. Neumann, T. M. Francisco , C. C. Corrêa , M. T. P. Lopes , H. Silva , A. P. S. Fontes , M. V. Almeida, *Inorganica Chimica Acta* 414 (2014) 85–90.
- [34] K. N. Kouroulis, S. K. Hadjidakou, N. Kourkoumelis, M. Kubicki, L. Male, M. Hursthouse, S. Skoulika, A. K. Metsios, V. Y. Tyurin, A. V. Dolganov, E. R. Milaeva and N. Hadjiliadis, *Dalton Trans.*, 2009, 10446–10456.
- [35] L. Cattaruzza, D. Fregona, M. Mongiat, M. Ronconi, A. Fassina, A. Colombatti, D. Aldinucci, *Int. J. Cancer* 128 (2010) 206–215.
- [36] L. Ronconi, D. Aldinucci, Q.P.D. Dou, *Anticancer Agents Med Chem.* 10 (2010) 283–292.
- [37] V. Milacic, D. Chen, L. Ronconi, K.R. Landis-Piwowar, D. Fregona, Q.P. Dou, *Cancer Res.* 66 (2006) 10478–10486.
- [38] Y.F. To, R.W.Y. Sun, V.S.F. Chen, W.Y. Chan, P.K.H. Yu, C.M. Tam, C. Che, L.S. Lin, *Int. J. Cancer* 124 (2009) 1971–1979.
- [39] R.W.Y. Sun, C.M. Che, *Coord. Chem. Rev.* 253 (2009) 1682–1691 and refs. therein.
- [40] Y. Wang, Q.Y. He, R.W.Y. Sun, C.M. Che, J.F. Chiu, *Cancer Res.* 65 (2005) 11553–11564.
- [41] K.H.M. Chow, R.W.Y. Sun, J.B.B. Lam, C.K.L. Li, A.M. Xu, D.L. Ma, R. Abagyan, Y. Wang, C.M. Che, *Cancer Res.* 70 (2010) 329–337.
- [42] D. Saggioro, M.P. Rigobello, L. Paloschi, A. Folda, S.A. Moggach, S. Parsons, L. Ronconi, D. Fregona, A. Bindoli, *Chem. Biol.* 14 (2007) 1128–1139.
- [43] X. Zhang, M. Frezza, V. Milacic, L. Ronconi, Y. Fan, C. Bi, D. Fregona, Q.P. Dou, *J. Cell Biochem.* 109 (2010) 162–172.
- [44] L. Giovagnini, L. Ronconi, D. Aldinucci, D. Lorenzon, S. Sitran, D. Fregona, *J. Med. Chem.* 48 (5) (2005) 1588.
- [45] A. Casini, M.A. Cinellu, G. Minghetti, C. Gabbiani, M. Coronello, E. Mini, L. Messori, *J. Med. Chem.* 49 (18) (2006) 5524.
- [46] D. Aldinucci, D. Lorenzon, L. Stefani, L. Giovagnini, A. Colombatti, D. Fregona, *Anti-Cancer Drug* 18 (3) (2007) 323.

- [47] M. Coronello, G. Marcon, S. Carotti, B. Caciagli, E. Mini, T. Mazzei, P. Orioli, L. Messori, *Oncol. Res.* 12 (2001) 361.
- [48] L. Ronconi, L. Giovagnini, C. Marzano, F. Bettio, R. Graziani, G. Pilloni, D. Fregona, *Inorg. Chem.* 44 (2005) 1867.
- [49] A. Bindoli, M.P. Rigobello, G. Scutari, C. Gabbiani, A. Casini, L. Messori, *Coord. Chem. Rev.* 253 (2009) 1692.
- [50] L. Ronconi, C. Marzano, P. Zanello, M. Corsini, G. Miolo, C. Macca, A. Trevisan, D. Fregona, *J. Med. Chem.* 49 (2006) 1648.
- [51] L. Ronconi, L. Giovagnini, C. Marzano, F. Bettio, R. Graziani, G. Pilloni, D. Fregona, *Inorg. Chem.* 44 (2005) 1867.
- [52] D.L. Bodenner, P.C. Dedon, P.C. Keng, R.F. Borch, *Cancer Res.* 46 (1986) 2745.
- [53] R.F. Borch, P.C. Dedon, A. Gringeri, T.J. Montine, in: M. Nicolini (Ed.), *Platinum and Other Metal Coordination Compounds in Cancer Chemotherapy*, Martinus Nijhoff, Boston, 1988.
- [54] H. Huang, L. Zhu, B.R. Reid, G.P. Drobny, P.B. Hopkins, *Science* 270 (1995) 1842.
- [55] Z. Huanzi and N. Yuantao, *Gold Bull.* 34 (2001), p. 24.
- [56] C. Orvig and M.J. Abrams, *Chem. Rev.* 99 (1999), p. 2201.
- [57] Kostova, *Anticancer Agents Med. Chem.* 6 (2006), p. 19.
- [58] B. Rosenberg, L. Vancamp, T. Krigas, Inhibition of Cell Division in *Escherichia coli* by Electrolysis Products from a Platinum Electrode, *Nature.* 205 (1965) 698–699.
- [59] B. Rosenberg, L. Vancamp, J.E. Trosko, V.H. Mansour, *Platinum Compounds: a New Class of Potent Antitumour Agents*, *Nature.* 222 (1969) 385–386.
- [60] D. Carpenter, *Reputation and Power: Organizational Image and Pharmaceutical Regulation at the FDA (Princeton Studies in American Politics: Historical, International, and Comparative P...)*, Princeton University Press, 2010.
- [61] B. Rosenberg, L. VanCamp, The successful regression of large solid sarcoma 180 tumors by platinum compounds., *Cancer Res.* 30 (1970) 1799–1802.
- [62] A. Dorcier, W.H. Ang, S. Bolaño, L. Gonsalvi, L. Juillerat-Jeannerat, G. Laurency, et al., In Vitro Evaluation of Rhodium and Osmium RAPTA Analogues: The Case for Organometallic Anticancer Drugs Not Based on Ruthenium, *Organometallics.* 25 (2006) 4090–4096.
- [63] E. Wong, C.M. Giandornenico, Current status of platinum-based antitumor drugs, *Chem. Rev.* 99 (1999) 2451–2466.
- [64] K.R. Koch, New chemistry with old ligands: N-alkyl- and N,N-dialkyl-N'-acyl(aryl)thioureas in co-ordination, analytical and process chemistry of the platinum group metals, *Coord. Chem. Rev.* 216-217 (2001) 473–488.
- [65] P.M. Takahara, C.A. Frederick, S.J. Lippard, Crystal Structure of the Anticancer Drug Cisplatin Bound to Duplex DNA, *J. Am. Chem. Soc.* 118 (1996) 12309–12321.
- [66] S. Ahmad, A.A. Isab, S. Ali, A.R. Al-Arfaj, Perspectives in bioinorganic chemistry of some metal based therapeutic agents, *Polyhedron.* 25 (2006) 1633–1645.

- [67] Chu G., *J. Biol. Chem.*, 1994, 269, 787.
- [68] Jordan P., Carmo-Fonseca M., *Cell Mol. Life Sci.*, 2000, 57, 1229.
- [69] Zamble D. B., Mu D., Reardon J. T., Sancer A., Lippard S. J., *Biochemistry*, 1996, 35, 10004.
- [70] Zlatanova J., Yaneva J., Leuba S. H., *FASEB J*, 1998, 12, 791.
- [71] T.S.L. Vincent, T. Devita, S.A. Rosenberg, *Cancer: Principles and Practice of Oncology*, in: Lippincott Williams and Wilkins, 2008: pp. 419–426.
- [72] A.K. Godwin, A. Meister, P.J. O'Dwyer, Chin Shiou Huang, T.C. Hamilton, M.E. Anderson, High resistance to cisplatin in human ovarian cancer cell lines is associated with marked increase of glutathione synthesis, *Proc. Natl. Acad. Sci. U. S. A.* 89 (1992) 3070–3074.
- [73] P.C.A. Bruijninx, P.J. Sadler, New trends for metal complexes with anticancer activity, *Curr. Opin. Chem. Biol.* (2008).
- [74] V. Milacic, D. Chen, L. Ronconi, K.R. Landis-Piwowar, D. Fregona, Q.P. Dou, A novel anticancer gold(III) dithiocarbamate compound inhibits the activity of a purified 20S proteasome and 26S proteasome in human breast cancer cell cultures and xenografts., *Cancer Res.* 66 (2006) 10478–86.
- [75] K. Palanichamy, A.C. Ontko, Synthesis, characterization, and aqueous chemistry of cytotoxic Au(III) polypyridyl complexes, *Inorganica Chim. Acta.* 359 (2006) 44–52.
- [76] P. Shi, Q. Jiang, Y. Zhao, Y. Zhang, J. Lin, L. Lin, et al., DNA binding properties of novel cytotoxic gold(III) complexes of terpyridine ligands: the impact of steric and electrostatic effects., *J. Biol. Inorg. Chem.* 11 (2006) 745–52.
- [77] E.R.T. Tiekink, Anti-cancer potential of gold complexes., *Inflammopharmacology.* 16 (2008) 138–42.
- [78] I. Kostova, Gold coordination complexes as anticancer agents., *Anticancer. Agents Med. Chem.* 6 (2006) 19–32.
- [79] X. Wang, Z. Guo, Towards the rational design of platinum(II) and gold(III) complexes as antitumour agents., *Dalton Trans.* (2008) 1521–32.
- [80] M.J. McKeage, L. Maharaj, S.J. Berners-Price, Mechanisms of cytotoxicity and antitumor activity of gold(I) phosphine complexes: the possible role of mitochondria, *Coord. Chem. Rev.* 232 (2002) 127–135.
- [81] M.J. McKeage, Gold opens mitochondrial pathways to apoptosis, *Br. J. Pharmacol.* 136 (2002) 1081–1082.
- [82] V. Parish, B.P. Howe, J.P. Wright, J. Mack, R.G. Pritchard, R.G. Buckley, et al., *Chem.* 35 (1996) 1659–1666.
- [83] I. Ott, X. Qian, Y. Xu, D.H. Vleck, I.J. Marques, D. Kubat, J. Will, W.S. Sheldrick, P. Jesse, A. Prokop, C.P. Bagowski, *Angew. Chem. Int. Ed.* 48 (2009) 1160.
- [84] M.F. Brana, A. Ramos, *Curr. Med. Chem. Anticancer Agents* 1 (2001) 237.
- [85] M. Deponte, S. Urig, L.D. Arscott, K. FritzWolf, R. Reau, C. HeroldMende, S. Konkarevic, M. Meyer, E. DavioudCharvet, D.P. Ballou, C.H. Williams, K. Becker, *J. Biol. Chem.* 280 (2005) 20628.
- [86] S. Urig, K. FritzWolf, R. Reau, C. HeroldMende, K. Toth, E. DavioudCharvet, K. Becker, *Angew. Chem. Int. Ed.* 45 (2006) 1881.

- [87] S.J. BernersPrice, R.J. Bowen, P. Galettis, P.C. Healy, M.J. McKeage, *Coord. Chem. Rev.* 186 (1998) 823.
- [88] J.L. Liu, P. Galettis, A. Farr, L. Maharaj, H. Samarasinha, A.C. McGechan, B.C. Baguley, R.J. Bowen, S.J. BernersPrice, M.J. McKeage, *J. Inorg. Biochem.* 102 (2008) 303.
- [89] A.S. Humphreys, A. Filipovska, S.J. BernersPrice, G.A. Koutsantonis, B.W. Skelton, A.H. White, *Dalton Trans.* 43 (2007) 4943.
- [90] O. Rackham, S.J. Nichols, P.J. Leedman, S.J. BernersPrice, A. Filipovska, *Biochem. Pharmacol.* 74 (2007) 992.
- [91] F. Caruso, M. Rossi, J. Tanski, C. Pettinari, F. Marchetti, *J. Med. Chem.* 46 (2003) 1737.
- [92] F. Caruso, R. Villa, M. Rossi, C. Pettinari, F. Paduano, M. Pennati, M.G. Daidone, N. Zaffaroni, *Biochem. Pharmacol.* 73 (2007) 773.
- [93] F. Caruso, C. Pettinari, F. Paduano, R. Villa, F. Marchetti, E. Monti, M. Rossi, *J. Med. Chem.* 51 (2008) 1584.
- [94] N. Pillarsetty, K.K. Katti, T.J. Hoffman, W.A. Volkert, K.V. Katti, H. Kamei, T. Koide, *J. Med. Chem.* 46 (2003) 1130.
- [95] M.L. Higginbotham, C.J. Henry, K.V. Katti, S.W. Casteel, P.M. Dowling, N. Pillarsetty, *Vet. Ther.* 4 (2003) 76.
- [96] E. Barreiro, J.S. Casas, M.D. Couce, A. Sanchez, A. SanchezGonzalez, J. Sordo, J.M. Varela, E.M.V. Lopez, *J. Inorg. Biochem.* 102 (2008) 184.
- [97] J.S. Casas, E.E. Castellano, M.D. Couce, O. Crespo, J. Elena, A. Laguna, A. Sanchez, J. Sordo, C. Taboada, *Inorg. Chem.* 46 (2007) 6236.
- [98] J.S. Casas, E.E. Castellano, M.D. Couce, J. Ellena, A. Sanchez, J. Sordo, C. Taboada, *J. Inorg. Biochem.* 100 (2006) 1858.
- [99] D. deVos, S.Y. Hoo, E.R.T. Tiekink, *Bioinorg. Chem. Appl.* 2 (2004) 141.
- [100] D. Suresh, M.S. Balakrishna, K. Rathinasamy, D. Panda, S.M. Mobin, *Dalton Trans.* (2008) 2812.
- [101] L. Messori, F. Abbate, G. Marcon, P. Orioli, M. Fontani, E. Mini, T. Mazzei, S. Carotti, T. O'Connell, P. Zanello, *J. Med. Chem.* 43 (2000) 3541.
- [102] C.M. Che, R.W. Sun, W.Y. Yu, C.B. Ko, N. Zhu, H. Sun, *Chem. Commun.* (2003) 1718.
- [103] Y. Wang, Q.Y. He, R.W. Sun, C.M. Che, J.F. Chiu, *Cancer Res.* 65 (2005) 11553.
- [104] Y. Wang, Q.Y. He, C.M. Che, J.F. Chiu, *Proteomics* 6 (2006) 131.
- [105] Y. Wang, Q.Y. He, R.W. Sun, C.M. Che, J.F. Chiu, *Eur. J. Pharmacol.* 554 (2007) 113.
- [106] Y. Wang, Q.Y. He, C.M. Che, S.W. Tsao, R.W.Y. Sun, J.F. Chiu, *Biochem. Pharmacol.* 75 (2008) 1282.
- [107] C.T. Lum, Z.F. Yang, H.Y. Li, R. WaiYin Sun, S.T. Fan, R.T. Poon, M.C. Lin, C.M. Che, H.F. Kung, *Int. J. Cancer* 118 (2006) 1527.
- [108] B. Bertrand, L. Stefan, M. Pirrotta, D. Monchaud, E. Bodio, P. Richard, P. Le Gendre, E. Warmerdam, M. H. de Jager, G. M. M. Groothuis, M. Picquet, A. Casini, *Inorg. Chem.* 2014, 53, 2296–2303.

- [109] L. Messori; L. Marchetti; L. Massai; F. Scaletti; A. Guerri; I. Landini; S. Nobili; G. Perrone; E. Mini; P. Leoni; M. Pasquali; C. Gabbiani; *Inorg. Chem.* 2014, 53, 2396-2403.
- [110] L. Maiore, M.A. Cinellu, S. Nobili, I. Landini, E. Mini, C. Gabbiani, et al., Gold(III) complexes with 2-substituted pyridines as experimental anticancer agents: solution behavior, reactions with model proteins, antiproliferative properties., *J. Inorg. Biochem.* 108 (2012) 123–7.
- [111] K. Palanichamy, N. Sreejayan, A.C. Ontko, Overcoming cisplatin resistance using gold(III) mimics: anticancer activity of novel gold(III) polypyridyl complexes., *J. Inorg. Biochem.* 106 (2012) 32–42.
- [112] C. Gabbiani, M.A. Cinellu, L. Maiore, L. Massai, F. Scaletti, L. Messori, Chemistry and biology of three representative gold(III) compounds as prospective anticancer agents, *Inorganica Chim. Acta.* 393 (2012) 115–124.
- [113] M.N. Kouodom, G. Boscutti, M. Celegato, M. Crisma, S. Sitran, D. Aldinucci, et al., Rational design of gold(III)-dithiocarbamate peptidomimetics for the targeted anticancer chemotherapy., *J. Inorg. Biochem.* 117 (2012) 248–60.
- [114] J.A. Lessa, K.S.O. Ferraz, J.C. Guerra, L.F. de Miranda, C.F.D. Romeiro, E.M. Souza-Fagundes, et al., Spectroscopic and electrochemical characterization of gold(I) and gold(III) complexes with glyoxaldehyde bis(thiosemicarbazones): cytotoxicity against human tumor cell lines and inhibition of thioredoxin reductase activity., *Biometals.* 25 (2012) 587–98.
- [115] Hogarth G, Ebony-Jewel, Rainford-Brent., Shariff E Kabir, Richards James D.E.T. Wilton-Ely, Zhang Q., *Inorganica Chimica Acta*, 362 (2009) 2026.
- [116] Pandeya K B, Singh R P, Mathur K, Singh R P, *Transition Met. Chem* 11 (1986) 340.
- [117] Milacic V, Chen D, Giovagnini L, Diez A, Fregona D, Dou Q. P. , *Toxicology and Applied Pharmacology* 231(2008) 24.
- [118] Malaguarnera L, Pilastro MR, DiMarco R, Scifo C, Renis M, Mazzarino MC, Messina A, *Apoptosis* 8 (2003) 539-545.
- [119] Schreck R, Meier B, Mannel DN, Droge W, Baeuerle PA, *J Exp Med*, 175(1992)1181-1194.
- [120] Critchfield, F.E.; Johnson, J.B. *Anal. Chem.* 1956, 28, 430-436.
- [121] Sassaman, M.B.; Giovanelli, J.; Sood, V.K.; Eckelman, W.C. *Bioorg. Med. Chem.* 1998, 6, 1759-1766.
- [122] Sztanke, K.; Pasternak, K.; Sidor-Wojtowicz, A.; Truchlińska, J.; Józwiak, K. *Bioorg. Med. Chem.* 2006, 14, 3635-3642.
- [123] Wong, R.; Dolman, S.J. *J. Org. Chem.* 2007, 72, 3969-3971.
- [124] Pérez R., Reyes O., Suarez M., Garay H.E., Cruz L.J., Rodríguez H., Molero-Vilchez M.D., Ochoa C., *Tetrahedron Lett.* 2000, 41, 613-616.
- [125] Azizi, N.; Ebrahimi, F.; Aakbari, E.; Aryanasab, F.; Saidi, M.R., *Synlett.* 2007, 2797-2800.
- [126] Yavari, I.; Seyfi, S.; Hossaini, Z.; Sabbaghan, M.; Shirgahi-Talari, F., *Monatsh. Chem.* 2008, 139, 1479-1482.
- [127] Erian, A.W.; Sherif, S.M., *Tetrahedron* 1999, 55, 7957-8024.
- [128] Beji, M.; Sbihi, H.; Baklouti, A.; Cambon, A., *Molecules* 16 (2011) 6311.

- [129] Goel, A.; Mazur, S.J.; Fattah, R.J.; Hartman, T.L.; Turpin, J.A.; Huang, M.; Rice, W.G.; Appella, E.; Inman, J.K., *Bioorg. Med. Chem. Lett.* 2002, 12, 767-770.
- [130] Mizuno, T.; Nishiguchi, I.; Okushi, T.; Hirashima, T., *Tetrahedron Lett.* 1991, 32, 6867-6868.
- [131] Rafin, C.; Veignie, E.; Sancholle, M.; Postal, D.; Len, C.; Villa, P.; Ronco, G., *J. Agric. Food Chem.* 2000, 48, 5283-5287.
- [132] Len, C.; Postal, D.; Ronco, G.; Villa, P.; Goubert, C.; Jeufrault, E.; Mathon, B.; Simon, H., *J. Agric. Food Chem.* 1997, 45, 3-6.
- [133] Morf, P.; Raimondi, F.; Nothofer, H.G.; Schnyder, B.; Yasuda, A.; Wessels, J.M.; Jung, T.A., *Langmuir* 2006, 22, 658-663.
- [134] McClain, A.; Hsieh, Y.L., *J. Appl. Polym. Sci.* 2004, 92, 218-225.
- [135] Dunn, A.D.; Rudorf, W.D., Ellis Horwood: Chichester, UK, 1989; pp. 226-367.
- [136] Ronconi, L.; Marzano, C.; Zanello, P.; Corsini, M.; Miolo, G.; Macca, C.; Trevisan, A.;
- [137] Fregona, D., *J. Med. Chem.* 2006, 49, 1648-1657.
- [138] Elgemeie, G.H.; Sayed, S.H., *Synthesis* 2001, 1747-1771.
- [139] L. Ronconi, D. Fregona, *Dalton Trans.* (2009) 10670–10680.
- [140] L. Ronconi, D. Aldinucci, Q.P. Dou, D. Fregona, *Anti-Cancer Agents Med. Chem.* 10 (2010) 283–292.
- [141] M.H. Hanigan, P. Devarajan, *Cancer Ther.* 1 (2003) 47–61.
- [142] N. Pabla, Z. Dong, *Kidney Int.* 73 (2008) 994–1007.
- [143] X. Wang, Z. Guo, *Anti-Cancer Agents Med. Chem.* 7 (2007) 19–34.
- [144] S. Yee, M. Fazekas-May, E.M. Walker, D. Montague, S. Stern, K.W. Heard, *Arch. Otolaryngol. Head Neck Surg.* 120 (1994) 1248–1252.
- [145] N. Segovia, G. Crovetto, P. Lardelli, M. Espigares, *J. Appl. Toxicol.* 22 (2002) 353–357.
- [146] U. Koelle, A. Laguna, *Inorg. Chim. Acta* 290 (1999) 44–50.
- [147] A. Ya Yakubovitch and V.A. Klimova, *J. Gen. Chem. U.S.S.R., Eng. Transl.*, 9, 1777 (1939).
- [148] S. U. Deshmukh, Zaheeruddin, B. Rajeeva, S. M. Shantakumar, R. K. Putta, *Journal of Biomedical and Pharmaceutical Research* 1 (3) 2012, 126-133.
- [149] S. J. Berners-Price, C. K. Mirabelli, R. K. Johnson, M. R. Mattern, F. L. McCabe, L. F. Faucette, C. M. Sung, S. M. Mong, P. J. Sadler, S. T. Crooke, *Cancer Research* 46, 5486-5493, November 1986.
- [150] S. Zhu, W. Gorski, D.R. Powell, J.A. Walmsley, *Inorg. Chem.*, 45 (2006) 2688-2694.
- [151] B. P. Block, J. C. Bailar, *J. Am. Chem. Soc.* 73 (1951) 4722-4725.
- [152] D. Saggioro, M.P. Rigobello, L. Paloschi, A. Folda, S.A. Moggach, S. Parsons, L. Ronconi, D. Fregona, A. Bindoli, *Chem. Biol.* 14 (2007) 1128–1139
- [153] A. K. Al-Sa'ady, C. A. McAuliffe, R. V. Parish and J. A. Sandbank, *Inorg. Synth.*, 1985, 23, 191–194.
- [154] K. N. Kouroulis, S. K. Hadjidakou, N. Kourkoumelis, M. Kubicki, L. Male, M. Hursthouse, S. Skoulika, A. K. Metsios, V. Y. Tyurin, A. V. Dolganov, E. R. Milaevag and N. Hadjiliadis, *Dalton Trans.*, 2009, 10446–10456.

- [155] R. Ellson, R. Stearns, M. Mutz, C. Brown, B. Browning, D. Harris, S. Qureshi, J. Shieh, D. Wold, *Comb Chem High Throughput Screen*, 2005 Sep;8(6):489-98.
- [156] SMART APEX Software (5.05) for SMART APEX Detector, (2001).
- [157] SAINT Software (5.0) for SMART APEX Detector, (2001).
- [158] G.M. Sheldrick, SADABS Program for Empirical Absorption correction of Area detector Data, (1996).
- [159] G.M. Sheldrick, SHELXTL V5.1 Software, (1997).
- [160] G.M. Sheldrick, SHELXTL 97, (1997).
- [161] L.J. Farrugia, ORTEP-3 for windows - A version of ORTEP-III with a graphical user interface (GUI), *J. Appl. Crystallogr.* 30 (1997).
- [162] C.F. Macrae, I.J. Bruno, J.A. Chisholm, P.R. Edgington, P. McCabe, E. Pidcock, et al., Mercury CSD 2.0 – new features for the visualization and investigation of crystal structures, *J. Appl. Crystallogr.* 41 (2008) 466–470.
- [163] Stoe, Cie, X-Area V1.35 and X-RED32 V1.31 Software, Stoe and Cie GmbH, Darmstadt, Germany, 2006.
- [164] A.L. Spek, *Acta Crystallogr., Sect. D* 65 (2009) 148.
- [165] M.J. Frisch, G.W. Trucks, H.B. Schlegel, G.E. Scuseria, M.A. Robb, J.R. Cheeseman, et al., GAUSSIAN03, Revision B.04, (2003).
- [166] N.U. Zhanpeisov, M. Matsuoka, H. Yamashita, M. Anpo, Cluster quantum chemical ab initio study on the interaction of NO molecules with highly dispersed titanium oxides incorporated into silicalite and zeolites, *J. Phys. Chem. B.* 102 (1998) 6915–6920.
- [167] A. Nicklass, M. Dolg, H. Stoll, H. Preuss, Ab initio energy-adjusted pseudopotentials for the noble gases Ne through Xe: Calculation of atomic dipole and quadrupole polarizabilities, *J. Chem. Phys.* 102 (1995) 8942–8952.
- [168] A. Nicklass, M. Dolg, H. Stoll, H. Preuss, Ab initio energy-adjusted pseudopotentials for the noble gases Ne through Xe: Calculation of atomic dipole and quadrupole polarizabilities, *J. Chem. Phys.* 102 (1995) 8942–8952.
- [169] J. Hans, A. Beckmann, H.-J. Kruiger, *Eur. J. Inorg. Chem.* (1999) 163-172.
- [170] M.J. Stewart, I.D. Watson, Standard units for expressing drug concentrations in biological fluids, *Br. J. Clin. Pharmacol.* 16 (1983) 3–7.
- [171] R.V. Parish, J.P. Wright, R.G. Pritchard, *J. Organomet. Chem.* 596 (2000) 165-176.
- [172] P.A. Bonnardel, R.V. Parish, R.G. Pritchard, *J. Chem. Soc., Dalton Trans.* (1996) 3185-3193.
- [173] W. Beck, W.P. Fehlhammer, P. Pollmann, E. Schuierer, K. Feldl, *Chem. Ber.* 100 (1967) 2335-2361.
- [174] K. Esumi, M. Nawa, N. Aihara, K. Usui, *New J. Chem.* 20(2), (1998) 719-720.
- [175] I. Haruko, F. Junnosuke and S. Kazuo, *Bull. Chem. Soc Jpn.*, 40 (1967) 2584-2591.
- [176] S. Zhu, W. Gorski, D. R. Powell, J. A. Walmsley. *Inorg. Chem.* 45 (2006) 2688-2694.
- [177] D. M. Motley, J. A. Walmsley, J. Zukerman-Schpector, E. R. T. Tiekink. *J. Chem. Cryst.* 39 (2009) 364-367.
- [178] F. H. Allen, *Acta Cryst., B*58 (2002) 380-388.

- [179] E. V. Makotchenko, I. A. Baidina. *J. Struct. Chem.*, 52 (2011), 572-576.
- [180] S.S. Al-Jaroudi, M.Fettouhi, M.I.M. Wazeer, A.A. Isab, S.Altuwaijri, *Polyhedron* 50 (2013) 434-442.
- [181] E. Kimura.; Y. Kurogi, T. Takahashi, *Inorg. Chem.* 1991, 30, 4117-4121.
- [182] M. Monim-ul-Mehboob, M. Altaf, M. Fettouhi, A. A. Isab, M. I. M. Wazeer, M. Nasiruzzaman Shaikh, S. Altuwaijri, *Polyhedron* 61 (2013) 225–234.
- [183] A.A. Isab, M.N. Shaikh, M. Monim-ul-Mehboob, B.A. Al-Maythalony, M.I.M. Wazeer, S. Altuwaijri, *Spectrochimica Acta Part A* 79 (2011) 1196– 1201.
- [184] F. H. Allen, O. Kennard, D. G. Watson, L. Brammer, A. G. Orpen. Tables of bond Lengths determined by X-Ray and Neutron Diffraction. Part 1. Bond Lengths in Organic Compounds. *J. Chem. Soc. Perkin Trans. II* 1987, S1-S19.
- [185] B.A.Al-Maythalony, M.I.M. Wazeer, A.A. Isab, *Inorganica Chimica Acta* 362 (2009) 3109–3113.
- [186] C.F. Macrae, P.R. Edgington, P. McCabe, E. Pidcock, G.P. Shields, R. Taylor, M. Towler, J. van de Streek, *J. Appl. Crystallogr.* 39 (2006) 453.
- [187] S.Y. Ho, E.R.T. Tiekink, *Z. Kristallogr.* 220 (2005) 342–344.
- [188] I. Sanger, H.W. Lerner, T. Sinke, M. Bolte, *Acta Cryst.* E68 (2012) m708.
- [189] P. Lu, T. C. Boorman, A.M.Z. Slawin, I. Larrosa, *J. Am. Chem. Soc.* 132 (2010) 5580-5581.
- [190] R. E. Marsh, *Acta Cryst.* B58 (2002) 893–899.
- [191] H. Schmidbaur, B. Brachthiuser, O. Steigelmann, H. Beruda, *Chem. Ber.* 125(1992) 2705–2710.

Vitae

Name :Said Salman Al-Jaroudi

Nationality :Saudi

Date of Birth :12/08/1388 H

Email :said.jaroudi@hotmail.com

Address :Tanajib 31311, Saudi Aramco, P. O. Box 65

Carrier Experience

2008-2014

Laboratory Supervisour

Northern Area Production Operation Engineering division,
NAP Laboratory Unit, Saudi Aramco, Tanajib

2005-2008

Lead Scientist

Northern Area Production Operation Engineering division,
NAP Laboratory Unit, Saudi Aramco, Tanajib

2003-2005

LabScientist

Northern Area Production Operation Engineering division,
NAP Laboratory Unit, Saudi Aramco, Tanajib

1997-2003

Scientist II

Central Analytical Laboratories & Materials
characterization Laboratories (CAL/MCL), Research
Institute, King Fahd University of Petroleum & Minerals,
Dhahran, Saudi Arabia

1999-2003

Lecturer B

Chemistry Department, King Fahd University of Petroleum
& Minerals, Dhahran, Saudi Arabia

Academic Background

2009-2014

PhD in Chemistry with specialization in Inorganic
Chemistry, King Fahd University of Petroleum and
Minerals (KFUPM), Dhahran-Saudi Arabia with minor in
Inorganic Chemistry

1993-1996

M.Sc. in Chemistry with specialization in Organic
Chemistry, King Fahd University of Petroleum and
Minerals (KFUPM), Dhahran-Saudi Arabia

1988-1993

B.S. in Industrial Chemistry, King Fahd University of
Petroleum and Minerals (KFUPM), Dhahran-Saudi Arabia

Publication

Patent

1. **Said S. Al-Jaroudi**, Rashed A. Hadi, Amer A. Al-Shahri. Optical Method for Determination of the Total Suspended Solids in Jet Fuel. **USA Patent**. 2011; Patent number: 7889337.
2. A patent on the invention entitled "Cytotoxic Compounds for Treating Cancer" **USA Patent Office**, USPTO Serial Number **13/944761**, filed on July 17, 2013.
3. A patent on the invention entitled "Synthesis of new bis(1,2-diaminocyclohexane)gold(III) chloride compounds and their anticancer activities against cancer cell lines" has been prepared and submitted to **USA Patent Office**.

Journals

1. **Said S. Al-Jaroudi**, Herman P. Perzanowski, Mohammed I. Wazeer and Sk. Asrof Ali. 1,3-Dipolar cycloaddition reaction of 1-aza-cyclooctene 1-oxide. **Tetrahedron**. 1997; 53(15): 5581-5592.
2. **Said S. Al-Jaroudi**, Sk. Asrof Ali, Herman P. Perzanowski and Mohammed I. Wazeer. A NMR study of the nitrogen inversion process in 1-oxa-11-azabicyclo[6,3,0]undecanes. **Canadian J. Analytical Science and Spectroscopy**. 1997; 42(6): 161-165.
3. Herman P. Perzanowski, **Said S. Al-Jaroudi**, Mohammed I. Wazeer and Sk. Asrof Ali. Cyclic nitrene-ethene cycloaddition reactions. **Tetrahedron**. 1997; 53(34): 11869-11880.
4. Abdullah J. Al-Hamdan, **Said S. Al-Jaroudi**. Reaction of aminonaphthoquinone with aldehyde. **Arab Journal for Science and Engineering**. 2003; 28: 51-60.
5. A. Ul-Hamid, A., H. M. Tawancy, A. I. Mohammed, **S. S. Al-Jaroudi** and N. M. Abbas. Cyclic oxidation behavior of ni-mo-cr alloy at 800 °C. **Anti-Corrosion Methods and Materials**. 2004; 51(5): 339-347.
6. A. Ul-Hamid, A., H. M. Tawancy, A. I. Mohammed, N. M. Abbas and **S. S. Al-Jaroudi**. Failure of ethylene furnace outlet transfer line due to overheating. **Journal of Failure Analysis and Prevention**. 2005; 5(4):54-61.
7. A. Ul-Hamid, H. M. Tawancy, A. R. I. Mohammed, **S. S. Al-Jaroudi**, N. M. Abbas. Quantitative WDS analysis using electron probe micro-analyzer. **Journal of Materials Characterization**. 2006; 56: 192-199.

8. A. Ul-Hamid, H. M. Tawancy, **S. S. Al-Jaroudi**, A. R. I. Mohammed, N. M. Abbas. Hydrogen-induced cracking of a stainless-steel dryer support component in a petrochemical plant. **Corrosion Prevention & Control**. 2005; 52(4): 131-135.
9. A. Ul-Hamid, H. M. Tawancy, **S. S. Al-Jaroudi**, A. R. I. Mohammed, N. M. Abbas. Carburisation of Fe-Ni-Cr alloys at high temperatures. **Materials Science-Poland**. 2006; 24(2/1): 319-331.
10. A. Ul-Hamid, H. M. Tawancy, **S. S. Al-Jaroudi**, A. R. I. Mohammed, N. M. Abbas. Evolution of oxide scale on a Ni-Mo-Cr alloy at 900°C. **Materials Characterization**. 2007; 58(1): 13-23.
11. **S. S. Al-Jaroudi**, A. Ul-Hamid, A. R. I. Mohammed, S. Saner. Use of X-ray powder diffraction for quantitative analysis of carbonate rock reservoir samples. **Power Technology**. 2007; 175(3): 115-121.
12. **Said S. Al-Jaroudi**, Anwar Ul-Hamid, Jamal A. Al-Matar. Prevention of failure in a desalination unit exhibiting extensive scale formation. **Desalination**. 2010; 260:119-128.
13. **S. S. Al-Jaroudi**, **A. Ul-Hamid**, M. M. Al-Gahtani. Failure of crude oil pipeline due to microbiologically induced corrosion. **Corrosion Engineering Science and Technology**. 2011; 46(4):568-579.
14. **S. S. Al-Jaroudi**, M. Fettouhi, M. I.M. Wazeer, A. A. Isab, S. Altuwaijri. Synthesis, characterization and cytotoxicity of new gold(III) complexes with 1,2-diaminocyclohexane: Influence of stereochemistry on antitumor activity. **Polyhedron**. 2013; 50(1): 434-442.
15. **S. S. Al-Jaroudi**, M. Monim-ul-Mehboob, M. Altaf, M. Fettouhi, M. I. M. Wazeer, S. Altuwaijri and A. A. Isab. Synthesis, spectroscopic characterization, X-ray structure and electrochemistry of new bis(1,2-diaminocyclohexane)gold(III) chloride compounds and their anticancer activities against PC3 and SGC7901 cancer cell lines. **New J. Chem**. 2014; 38: 3199-3211.
16. **S. S. Al-Jaroudi**, M. Monim-ul-Mehboob, M. Altaf, A. A. Al-Saadi, M. I. M. Wazeer, S. Altuwaijri and A. A. Isab. Synthesis, spectroscopic characterization, electrochemical behavior and computational analysis of mixed diamine ligand gold(III) complexes: antiproliferative and in vitro cytotoxic evaluations against human cancer cell lines. **Biomaterials**. 2014 July, DOI 10.1007/s10534-014-9771-2.

17. **S. S. Al-Jaroudi**, A. Ul-Hamid, M. A. Al-Moumen. Premature Failure of Tubing Joint used in a Crude Oil Production Well. **Engineering Failure Analysis**. 2014, In Press, Accepted Manuscript

Conference

1. **Said Al-Jaroudi** and Anvarhusein A. Isab, *Anti-cancer activity of new gold(III) complexes of [(1,2-DACH)AuCl₂]Cl against human prostate and gastric cancer cell lines*, Poster presentation in **244th ACS National Meeting 2012, USA**.
2. **Said Al-Jaroudi**. Optical Method for Determination of the Total Suspended Solids in Jet Fuel. Chemistry in industry (**CHEMINDIX 2007**), Manama, Bahrain (March 26-28, 2007).
3. A. Ul-Hamid, A., H. M. Tawancy, A. I. Mohammed, **S. S. Al-Jaroudi** and N. M. Abbas. Cyclic oxidation behavior of ni-mo-cr alloy at 800 °C. **Pittcon 2005**, USA, Orlando (Feb. 28-March 3, 2005).